PREPARATION AND APPLICATION OF MULTI-WALLED CARBON NANOTUBES/POLY(VINYLIDENE FLUORIDE-CO-HEXAFLUROPROPYLENE) COMPOSITE MEMBRANES FOR FILTRATION AND ADSORPTION OF CONTAMINANTS IN WATER

by

LUTENDO EVELYN MACEVELE

[redacted]

RESEARCH THESIS

Submitted in fulfilment of the requirements for the degree of

DOCTOR OF PHILOSOPHY

in

CHEMISTRY

in the

FACULTY OF SCIENCE AND AGRICULTURE

(School of Physical and Mineral Sciences)

at the

UNIVERSITY OF LIMPOPO

SUPERVISOR: Prof T Magadzu

CO-SUPERVISOR: Dr KLM Moganedi

2019

DEDICATION

I dedicate this work to the Almighty God for his love, grace, protection and leadership through all my life; and to my loving husband for his love, care, patience and support throughout my studies.

DECLARATION

I declare that PREPARATION AND APPLICATION OF MULTI-WALLED CARBON NANOTUBES/POLY(VINYLIDENE FLUORIDE-CO-HEXAFLUROPROPYLENE) COMPOSITE MEMBRANES FOR FILTRATION AND ADSORPTION OF CONTAMINANTS IN WATER is my own work and that all the sources that I have used or quoted have been indicated and acknowledged by means of complete references and that this work has not been submitted before for any other degree at any other institution.

....Lutendo Evelyn Macevele.... …….08/04/2019.....

Full names **Date**

ACKNOWLEDGEMENTS

My sincere gratitude goes to my creator God, for the life, wisdom, strength, encouragement and guidance in my life. I will continue to trust in His word which say that, “Trust in the LORD with all thine heart; and lean not unto thine own understanding. In all thy ways acknowledge him, and he shall direct thy paths. Be not wise in thine own eyes: fear the LORD, and depart from evil” Proverbs 3:5-7.

I am indeed grateful to my loving husband Mr Paul Mehleketo Macevele for allowing me to spend much time towards my studies with much support and patience; men like you are rare and I will forever be grateful to God for joining us together. “What therefore God has joined together, let no man put asunder” Mark 10:9.

I would like to thank my supervisor Prof T Magadzu for giving me the greatest opportunity and all the support I ever needed to accomplish this research. I acknowledge your guidance, supervision, effort and time towards the success of this work. It was a greatest pleasure working with you.

I would also like to thank my hard-working co-supervisor Dr KLM Moganedi for her support, assistance, patience and guidance throughout all my studies especially in the microbial studies.

I also acknowledge the department of Chemistry for granting me an opportunity to pursue my PhD, and for their support throughout my studies.

I would like to acknowledge the Chemistry head of department Dr MS Thomas and the School of Physical and Mineral Sciences Director, Prof TT Netshisaulu for their support in my studies and for granting me the study leave to finalise my work.

I would also like to appreciate the executive dean, Prof H Siweya for funding my sample analysis at University of Johannesburg and CSIR and also for giving me time and space to work. Without your support, this would not have been possible.

I would also like to thank the research office director, Dr T Mabila and his office for their financial support, both in purchasing instruments and paying for my sample analysis.

The financial support from the National Research Foundation, is also greatly appreciated for the success of this work.

I would like to acknowledge my parents' Dr Ntshengedzeni Collins Rananga and Mrs Namadzavho Esther Rananga for their encouragement, love and support during the course of my studies.

My siblings Seani, Apfaho and Unarine Rananga are all acknowledged for their love and encouragement in my studies and in my life.

I also appreciate my in-laws Kokwane Nwa-Risenga Lucia Mhlava Hlongwane, Mr Holman Macevele, Esther Macevele and Mr Maxwell Chauke, for their love and support throughout my studies.

I also thank Mr Bernard Rananga, Vho-Tshinakaho Tshifularo, Vho-Sophia Rananga, Vho-Elisa Sikhipha, Nkhensani Chauke and Gundo Mapholi for their love, support and encouragement during the course of my studies.

PUBLICATION AND PRESENTATIONS

PUBLICATIONS

1. **L.E. Macevele**, K.L.M Moganedi and T Magadzu. Investigation of Antibacterial and Fouling Resistance of Silver and Multi-Walled Carbon Nanotubes Doped Poly(Vinylidene Fluoride-co-Hexafluoropropylene) Composite Membrane. Membranes 2017, 7, 35; doi:10.3390/membranes7030035
2. **L.E. Macevele**, K.L.M Moganedi and T Magadzu. Poly-amidoamine (PAMAM) dendrimeric/ Multi-walled carbon nanotubes for adsorption of cadmium (II) ions from water samples. To be submitted for publication to Journal of nanomaterials.

CONFERENCE PRESENTATIONS

1. **L.E. Macevele**, K.L.M Moganedi and T. Magadzu. Investigation of Antibacterial and Fouling Resistance of Silver and Multi-Walled Carbon Nanotubes Doped Poly(Vinylidene Fluoride-co-Hexafluoropropylene) Composite Membrane. Presented at the 9th International conference of the African Materials Research Society (AMRS 2017) conference, Botswana, Gaborone International Conference Centre, December, 2017.
2. **L.E. Macevele**, K.L.M Moganedi and T. Magadzu. Ag-MWCNTs doped poly (vinylidene fluoride-co-hexafluoropropene) nanocomposite membranes for water purification. Presented at the 6th Annual Gauteng Nanosciences Young researcher's symposium at Mintek Conference Centre, Randburg, Johannesburg, November, 2016.
3. **L.E Macevele** and T Magadzu. Preparation of MWCNTs doped PVDF-HFP nanocomposite membranes for water purification. Presented at the Applied Nanotechnology and Nanoscience International Conference (ANNIC 2016), Spain, Barcelona, November, 2016.

ABSTRACT

This work presents the synthesis, characterisation and application of poly(vinylidene fluoride-co-hexafluropropylene) (PVDF-HFP) membrane prepared using a phase-inversion method. PVDF-HFP was blended with either functionalised multi-walled carbon nanotubes (MWCNTs), poly-amidoamine (PAMAM) dendrimeric MWCNTs or silver (Ag) nanoparticles and their combinations. Nanocomposite blends such as MWCNTs/PVDF-HFP, PAMAM-MWCNTs/PVDF-HFP, Ag-MWCNTs/PVDF-HFP and Ag-PAMAM-MWCNTs/PVDF-HFP were synthesised successfully.

A variety of PVDF-HFP composite membranes prepared were characterised by X-ray powder diffraction (XRD), fourier transform infrared (FTIR), thermogravimetric analysis (TGA), Brunauer-Emmett-Teller (BET), scanning electron microscopy (SEM) and contact angle. The fMWCNTs, Ag-MWCNTs, PAMAM-MWCNTs and Ag-PAMAM-MWCNTs nanocomposites were further characterised by Transmission electron microscopy (TEM) and energy dispersive X-ray (EDX). FTIR spectra of PAMAM-MWCNTs confirmed the formation of functional groups such as COOH, NCO, NH_2 and PAMAM dendrimer.

XRD analysis demonstrated that the crystallite sizes of the silver nanoparticles were larger (8.4 nm) than those of Ag-MWCNTs (7.8 nm) and Ag-PAMAM/MWCNTs (6.4 nm) nanocomposites. These findings were further confirmed by TEM analysis which showed Ag nanoparticles, Ag-MWCNTs and Ag-PAMAM/MWCNTs having diameters of silver particles between 9 to 20 nm, 5 to 10 nm and 4 to 8 nm respectively. The reduced Ag particle sizes was due to the complexation of MWCNTs and PAMAM-MWCNTs with Ag metal ions, which correlates with an enhanced surface area in the nanocomposite membranes, leading to good filtration and antibacterial properties.

TGA studies demonstrated that the thermal stability of PVDF-HFP composite membrane was greatly enhanced by the addition of PAMAM-MWCNTs. However, the composite membranes consisting of both Ag nanoparticles and MWCNTs on PVDF-HFP did not improve the structural stability of PVDF-HFP. All composite membranes have shown stability up to 400 ^{o}C. The contact angle, porosity, swellability and water content measurements of the composite membranes were improved showing enhanced hydrophilicity due to addition of MWCNTs, PAMAM-MWCNTs and/or Ag nanoparticles.

The scanning electron microscopy (SEM) images have depicted the formation of microporous structure, with few MWCNTs on the surface strongly interacting with PVDF-HFP as demonstrated by TGA, XRD and FTIR data. SEM cross-sections of PVDF-HFP composite membranes showed a mixture of fingure-like microvoids with a membrane diameter of approximately 180 μm. The BET data showed an improved surface area, pore volume and pore sizes of PVDF-HFP composite membranes when blended with fMWCNTs and PAMAM. These membranes also showed high fouling resistance, good desalination and high Cd(II) ions rejections during permeability studies. *E. coli* filtration studies indicated that 2.5 wt.% Ag-MWCNTs/PVDF-HFP and 1.8 wt.% Ag-PAMAM-MWCNTs/PVDF-HFP composite membranes displayed good microbial load reduction (100%) and excellent antibacterial properties as evidenced by the bacterial growth on the edges of the membranes.

The microbial, physicochemical and chemical analysis of surface water samples from Sekhukhune area showed that the water was contaminated with *Enterobacteriaeceae*, *E. coli*, total coliform with high turbidity and total suspended solids above the South African national standard (SANS 241) water guidelines. After filtration with 1.8 wt.% Ag-MWCNTs/PVDF-HFP composite membrane, turbidity was reduced to 4 Nephelometric turbidity units (NTU), total suspended solids to 1 mg/L while *Enterobacteriaeceae, E. coli* and total coliform were undetectable and complied with SANS 241 limits. Chromium concentration levels were reduced from 0.194 to 0.0138 mg/L, after filtration with 1.8 wt.% Ag-PAMAM-MWCNTs/PVDF-HFP composite membrane also within acceptable SANS 241 limits.

Adsorption studies of all composite membranes demonstrated that the adsorption processes of Cd(II) ions was well conformed to Freundlich model (R^2 = 0.999), which suggests that the sorption process met heterogeneous adsorption. However, for Cr(VI) ions studies, the adsorption process was conformed to both Langmuir (R^2 = 0.999) and Freundlich (R^2 = 0.998) model which suggest that that the adsorption process meet both monolayer and heterogeneous adsorption. The maximum adsorption capacity fitted by Langmuir isotherm was 166.7 and 9.72 mg/g for Cd(II) ions (at optimum pH 6.5) and Cr(VI) ions (at optimum pH 2.5) respectively, using 1 wt.% PAMAM-MWCNTs/PVDF-HFP composite membrane. The adsorption capacities of Cd(II) ions were higher than those of Cr(VI) ions, which is thought to be due to the properties of the composite membrane material. According to the thermodynamic

parameters, the Cd(II) and Cr(VI) ions adsorption process was spontaneous and endothermic. Reusability studies showed that PVDF-HFP composite membranes can be reused at least 4 times with an adsorption loss of only 5% for 1 wt.% PAMAM-MWCNTs/PVDF-HFP composite membrane, confirmed by TGA and ICP-OES analysis. The 1 wt.% PAMAM-MWCNTs-PVDF-HFP composite membrane exhibited a higher selectivity towards Cd(II) over Cu(II), Zn(II) and Ni(II) in binary and quaternary metal adsorption studies.

TABLE OF CONTENTS

LIST OF FIGURES

LIST OF TABLES

LIST OF ABBREVIATIONS

AAS	Atomic absorption spectroscopy
Ag-MWCNTs	Silver multi-walled carbon nanotubes
BET	Brunauer-Emmett-Teller
BOD	Biochemical oxygen demand
DBPs	Disinfection by-products
DMAc	Dimethyl acetamide
EC	Electrical conductivity
EDX	Energy dispersive x-ray
E.coli	*Escherichia coli*
FIB-SEM	Focused Ion Beam Scanning electron microscopy
fMWCNTs	Functionalised multi walled carbon nanotubes
FTIR	Fourier transform infrared
HAAs	Haloacetic acids
ICP-OES	Inductively coupled plasma Optical Emission Spectroscopy
MWCNTs	Multi walled carbon nanotubes
NF	Nanofiltration
NOM	Natural organic matter
NTU	Nephelometric turbidity units
PAMAM	Poly(amidoamine)
PEG	Polyethylene glycol
PVDF	Poly(vinylidene fluoride)
PVDF-HFP	Poly(vinylidene fluoride-co-hexafluropropylene)

PVP	Polyvinylpyrrolidone
RO	Reverse osmosis
SANS	South African national standard
SEM	Scanning electron microscopy
SDS	Sodium dodecyl sulphate
SWCNTs	Single walled carbon nanotubes
TDS	Total dissolved solids
TEM	Transmission electron microscopy
TFC	Thin film composite
TGA	Thermogravimetric analysis
TSS	Total suspended solids
UF	Ultrafiltration
WHO	World health organization
XRD	X-ray powder diffraction

THESIS OUTLINE

This thesis is divided into five chapters. A brief synopsis of each chapter is given below:

Chapter 1 focuses on the background, aims, objectives of the study and thesis outline.

In **Chapter 2**, the literature and information to establish the thrust of this research is presented. Different water pollutants, water purification principles, current and potential methods of water purification are outlined and discussed in detail. The above topics were reviewed with relevance to the work of preparing membranes for water purification.

In **Chapter 3**, the experimental methodologies used for preparing nanocomposites, PVDF-HFP nanocomposite membranes are included in this chapter. Characterisation of nanocomposites and nanocomposite membranes using techniques such as SEM, XRD, TGA, SEM, BET, TEM, EDX and contact angle is presented. A detailed description of synthetic methods and phase inversion technique used for the preparation of PVDF-HFP composite membrane materials is included in this chapter. The water analysis methods for filtration and adsorption of heavy metals are also outlined in this chapter.

Chapter 4 focusses on the results and discussions of the work undertaken. The interpretation of the characterisation results is included in this chapter. The effects of PVDF-HFP nanocomposites membranes during filtration, fouling adsorption studies are outlined. Salt rejection, filtrate flux, leaching, fouling and adsorption studies using nanocomposite membranes were discussed in detail in this chapter.

Chapter 5 presents the conclusions and recommendations obtained from the results presented in subsequent chapters.

CHAPTER 1

INTRODUCTION

1.1 BACKGROUND

Membrane technology has become a popular filtration technique worldwide and is very important in removing organic and inorganic pollutants [1]. Membrane technologies for water treatment should focus on improving the effectiveness and competence of membranes to selectively eradicate targeted contaminants in water. The most significant purpose in this regard, is to attain control of membrane structure and thus membrane performance [2]. This is not easy to accomplish since membrane structure and performance depend on various factors. These factors include the type of polymer used, the coagulating solvent, conditions for synthesis such as temperature, time and doping materials [2].

The non-solvent induced phase-inversion process has been extensively implemented as a reliable method for preparing or modifying asymmetric membranes [3,4]. This method is used to produce a wide range of membranes types including mixed-matrix by varying the composition and properties of the polymer solution. The temperature and composition of the precipitation solution can also be enhanced to obtain the desired results. In phase-inversion, a more volatile solvent is often introduced to the polymer solution to adjust the solvent evaporation and the polymer coagulation [5]. Most common water-miscible solvents used in hydrophobic asymmetry are dimethyl formamide, Dimethyl acetamide dimethyl sulfoxide, N-Methyl Pyrrolidone, dimethyl acetamide, and many more [4,6]. A more volatile solvent is expected to exhibit good miscibility with water. However, a good water-miscible solvent usually has a high degree of polarity and hydrogen bonding that is able to suppress the solvent volatility. Hence, the outermost surface of the membrane generates a high polymer concentration as a more volatile solvent is removed during the evaporation process. The more co-solvent evaporated, the thicker the concentrated polymer region which leads to a thicker selective layer of the membrane. This concentrated polymer region thus leads to a reduction in permeation rate [6].

A significant number of studies on membrane nanotechnology have focused on doping nanomaterials into polymeric or inorganic membranes. Nanomaterials used for such

applications include hydrophilic metal oxide nanoparticles, antimicrobial nanoparticles such as nano-Ag and MWCNTs) [7]. Current application of nanocomposite membranes is in selective permeation of natural organic matter, humic acid and inorganic salts and microbial contaminants [8-10]. In order to improve nanocomposite membranes, for pervaporation, several researchers are now using MWCNTs and the functionalised MWCNTs in membrane materials. CNTs strongly adsorb many polar organic compounds due to the diverse contaminant CNT interactions including hydrophobic effect, pep interactions, hydrogen bonding, covalent bonding, and electrostatic interactions [11]. Addition of CNTs in to the polymeric membranes improves the hydrophilicity, electrical, mechanical and thermal properties of polymers significantly. Furthermore, CNTs additions are beneficial to enhance the dielectric constant and electrical conductivity of polymers [12].

1.2 PROBLEM STATEMENT

Clean drinking water availability is a major problem for developing countries [13]. Scarcity of safe drinking water remains a global problem and is expected to rise with increasing population growth and environmental changes [14]. Drinking polluted water can cause serious health problems; for example, cholera and diarrheal diseases cause many deaths of children in developing countries [15,16]. The World Health Organization (WHO) recommends that any water intended for drinking should contain faecal and total coliform counts of 0.00 in any 100 mL sample [17]. When bacteria are encountered in water samples, immediate investigative action should be taken [17].

Various methods of water treatment have been used in the past, such as sedimentation, flocculation, disinfection and filtration [18]. Conventional disinfection methods, such as ozonation, and UV light have been used, and are both good disinfectants but their running and maintenance cost are too high to sustain [18]. Ozonation also partially oxidises natural organic matter to produce smaller toxic compounds. Chlorination is a good disinfectant and affordable method. However, it degrades some of the organic contaminants into more harmful by-products such as trihalomethanes, polychlorinated biphenyls and trihaloacetic acids which are known to be either endocrine disruptors or carcinogenic [19].

Membrane technology has become a popular separation technology and it plays a big role in separation of unwanted constituents such as organic pollutants, inorganic pollutants and desalination of sea-water. Examples of membrane processes include microfiltration (MF) ultrafiltration (UF), nanofiltration (NF) and reverse osmosis (RO). However, the key challenges for membrane separation technologies include maintaining selectivity, flux and durability, cost, pressure, fouling and membrane lifetime. Membrane fouling adds to the energy consumption and the complexity of the process design and operation. Furthermore, it reduces the lifetime of membranes and membrane fouling [1].

It remains a challenge to researchers to produce a membrane that has high rejection capability and high water permeability. On the other hand, thinner porous membranes provide higher flux but poorer rejection due to structural stability problems [20]. The membrane performance thus should be adjusted such that other advantageous structures of the membrane can be improved. It is also important to study the fundamentals of membrane-formation processes and relate them to the performance. The method of the membrane preparation has a significant effect on the membrane performance and therefore a good method should be developed [20].

Polysulfone membranes are the most common membranes used in ultrafiltration of wastewater due to its mechanical robustness and structural and chemical stability. Unfortunately, polysulfone is a hydrophobic material, making its surface prone to fouling due to adsorptive mechanism [21]. Poly(vinylidene fluoride) (PVDF) is also one of the most commonly used membrane materials for water treatment application because of its high strength, good thermal stability and good resistance to solvents, acids, and bases [22]. However, PVDF membranes have a relatively low surface energy and high hydrophobicity, which makes PVDF membranes susceptible to fouling especially when treating aqueous influents containing organic fouling and biofouling, such as protein, oil [23]. Unfortunately, PVDF-based composites suffer from its poor interfacial stability [24-25].

1.3 MOTIVATION

Although various types of membranes have been developed, the focus is on developing nanocomposite membranes with high selectivity, rejection and permeability fabricated from compatible and cheap precursor materials using superficial and environmentally friendly synthesis method [8]. The addition of functional groups into the membrane leads to hydrophilic surfaces which prevent the membrane from being easily fouled. Novel reactions can be accomplished at the nanoscale due to an increase in the number of surface energy, which is not possible with the analogous bulk material. Among various membrane compositions, very few studies considered doping nanomaterials such as silver and CNTs on poly(vinylidene fluoride-co-hexafluoropropene) (PVDF-HFP) for water treatment purposes [26,27]. This polymeric membrane possesses a high dielectric constant and good mechanical properties [28]. It is a chemically inert fluoropolymer, with lower crystallinity compared with PVDF [29]. This is due to the combination of an amorphous phase of hexafluropropylene (HFP) into the vinylidene fluoride (VDF) blocks, which aids in higher ionic conduction of the polymer, whereas the crystalline phase acts as a mechanical support for the polymer [30].

Studies have shown that addition of MWCNTs improves the electrical, mechanical and thermal properties of polymers [31,32]. MWCNTs are preferred during the preparation of polymeric membranes over single walled CNTs because of their high mechanical properties, electrical and chemical stability [31]. This provides opportunity to modify the structure and to optimise solubility and dispersion, allowing innovative applications in materials, electronics, chemical processing and energy management as observed in literature [32]. This carbon nano-material was further reported to inactivate bacteria upon direct contact [33,34]. Silver (Ag) nanoparticles have been extensively researched, due to their high antibacterial activity [35-37] etc. For example, Ag loaded membranes displayed an improved surface hydrophilicity [38] and good antibacterial activity [39]. Dendrimers show a large range of possible applications because of their tunable physical and chemical properties. Dendritic materials such as poly-amidoamine (PAMAM) can be used to enhance the CNT dispersion properties due to their abundant amino groups; resulting in an increase in adsorption capacity and filtration properties [40]. The addition of functional materials such as PAMAM, Ag and

MWCNTs in their combinations into PVDF-HFP polymer can lead to hydrophilic surfaces which prevent the membrane from being easily fouled.

To the best of our knowledge, no attempts have been made thus far to incorporate functionalised MWCNTs and Ag-PAMAM dendrimers into the PVDF-HFP polymer for water filtration and heavy metal adsorption.

1.3.1 Membranes and membrane processes.

Membrane filtration describes a family of separation methods. Membranes provide a physical barrier for constituents based on their size, allowing use of unconventional water sources. The membrane acts as a filter that allows water flow through, while removing suspended solids and other substances. Membrane process can be pressure driven or dependent on electrical potential gradients, concentration gradients, or other driving forces [41]. Pressure-driven membrane processes include microfiltration (MF) ultrafiltration (UF), nanofiltration (NF) and reverse osmosis (RO). MF and UF are characterized by their ability to remove suspended or colloidal particles via a sieving mechanisms based on the size of the membrane pores relative to that of the particulate matter. NF and RO constitute the class of membrane processes that is most often used in applications that require the removal of dissolved contaminants, as in the case of softening or desalination [41].

As the key components of water treatment and reuse, membranes provide high level of automation, require less land and chemical use, and the modular configuration allows flexible design [1]. A major challenge of the membrane technology is the inherent trade-off between membrane selectivity and permeability. The high energy consumption is an important barrier to the wide application of pressure driven membrane processes. Membrane fouling adds to the energy consumption and the complexity of the process design and operation. Furthermore, it reduces the lifetime of membranes and membrane modules [42]. The performance of membrane systems is largely decided by the membrane material. Incorporation of functional nanomaterials into membranes offers a great opportunity to improve the membrane permeability,

fouling resistance, mechanical and thermal stability, as well as to render new functions for contaminant degradation and self-cleaning [42].

1.3.2 Poly (vinylidene fluoride) (PVDF)

Poly (vinylidene fluoride) (PVDF) membrane is used in the field of municipal, industrial wastewater and potable water treatment [43,44]. However, the main problem of PVDF membrane focuses on vulnerable membrane fouling and contamination by proteins, other impurities and/or microorganism in water due to its hydrophobic nature [45]. This leads to an enormous decrease of permeability, and therefore frequently chemical or physical cleaning of membrane modules. And bacteria, as one of the most important microorganisms, usually cause serious fouling for membranes so that the membrane performance is irreversibly reduced [46]. To fight against the membrane fouling and water contamination caused by bacteria in membrane separation processes, it is necessary to endow the membrane with a property of inhibiting the growth and reproduction of bacteria and the development of bacteria film.

As an alternative polymer for PVDF, poly(vinylidenefluoride-hexafluoropropylene) (PVDF-HFP) has drawn the attention of many researchers because of its higher dielectric constant and mechanical properties [28,32]. This is due to the combination of an amorphous phase of hexafluropropylene (HFP) into the vinylidene fluoride (VDF) blocks. This polymer also comprises of both amorphous and crystalline phase; the amorphous phase of the polymer helps for higher ionic conduction, whereas the crystalline phase acts as a mechanical support for the polymer electrolyte. PVDF-HFP is a chemically inert fluoropolymer, it has lower crystallinity compared with PVDF, it has good mechanical strength, can tolerate high-temperature feed solutions, and is a hydrophobic material. PVDF-HFP polymers can be used in the preparation of membrane for water purification [28].

1.3.3 Nanocomposite membranes

Studies on membrane nanotechnology have focused on addition nanomaterials into polymeric or inorganic membranes. Nanomaterials used for such applications include

hydrophilic metal oxide nanoparticles, antimicrobial nanoparticles and (photo) catalytic nanomaterials. The addition of metal oxide nanoparticles to polymeric ultrafiltration membranes has been shown to increase membrane surface hydrophilicity, water permeability, or fouling resistance [46]. These inorganic nanoparticles also help enhance the mechanical and thermal stability of polymeric membranes, reducing the negative impact of compaction and heat on membrane permeability [39]. Antimicrobial nanomaterials such as nano-Ag and CNTs can reduce membrane biofouling. Nano-Ag has been doped or surface grafted on polymeric membranes to inhibit bacterial attachment and biofilm formation [46] on the membrane surface as well as inactivate viruses [38]. However, its long-term efficacy against membrane biofouling has not been reported.

The superior properties of MWCNTs, especially its high intrinsic mechanical properties and electrical conductivity, make them attractive for many applications [32]. CNTs inactivate bacteria upon direct contact (Brady-Estevez et al., 2008). High bacterial inactivation (>90%) has been achieved using polyvinyl-N-carbazole-SWCNT nanocomposite at 3 wt% of SWCNT [34,40]. As CNTs are insoluble in water and not consumed, there is no need for replenishment. However, as direct contact is required for inactivation, long term filtration experiments are needed to determine the impact of fouling on the antimicrobial activity of CNTs. Addition of oxidized MWCNT at low weight percentage (up to 1.5 wt%) also increases the hydrophilicity and permeability of polysulfone membranes [24]. By incorporating MWCNTs in a PVDF matrix, a nanocomposite material with a low-electric percolation threshold is obtained, which also exhibit the piezoelectric properties of beta-phase PVDF and the electric properties of MWCNTs [26].

1.4. AIM AND OBJECTIVES

AIM

The aim of the study was to prepare, characterise and investigate the properties of PVDF-HFP nanocomposites as membranes and adsorbents for drinking water treatment.

OBJECTIVES

The specific objectives of the project were as follows:

i. To synthesise and characterise Ag nanoparticles, fMWCNTs, and PAMAM-MWCNTs nanocomposites.
ii. To prepare PVDF-HFP polymer nanocomposites using various dosages of Ag-PAMAM, MWCNTs and Ag-PAMAM/MWCNTs nanomaterials.
iii. To characterise nanocomposite membranes using FTIR, TGA, XRD, SEM, contact angle and BET.
iv. To investigate the performance of the PVDF-HFP nanocomposite membranes for filtration of surface and ground water samples, cadmium and chromiummetals, sodium chloride salt, and microbial contaminants such as *E. Coli* and coliform.
v. To investigate the nanocomposite membrane performance on adsorption of cadmium and chromium metals.

1.5. SCIENTIFIC CONTRIBUTION

Modification of PVDF-HFP membranes will result in new membrane architectures with novel properties. It is envisaged that the nanocomposite membranes will have improved hydrophilicity, permeability, fouling resistance, mechanical and thermal stability. The outcome of this project will potentially assist industries such as mining, recycling wastewater, pharmaceutical as well as municipalities in their quest to solve the problem of water contamination. This will furthermore improve health of numerous nations.

1.6. ETHICAL CONSIDERATIONS

No specimens of human or animal origin will be used in this study; hence no ethical clearance was necessary.

1.7. REFERENCES

1. Qu, XL., Brame, J., Li, Q. and Alvarez, JJP. 2013. Nanotechnology for a safe and sustainable water supply: enabling integrated water treatment and reuse. *Accounts of chemical research*, 46 (3), 834-843.

2. Ahmad, N.K., Goh, P.S., Karim, Z.A. and Ismail, A.F. 2018Thin film composite membrane for oily waste water treatment: recent advances and challenges. *Membranes*, 8, 86.

3. Uekama, K. 2002. Recent aspects of pharmaceutical application of cyclodextrins. *Journal of Inclusion Phenomena and Macrocyclic Chemistry*, 44 (1-4), 3-7.

4. Strathmann, H. and Kock, K. 1996. Recent advances in the formation of phase inversion membranes made from amorphous or semi-crystalline polymers. *Journal of membrane science*, 113, 361-371.

5. Jung, J.T., Kim, J.F. and Wang, H.H. 2016. Understanding the non-solvent induced phase separation (NIPS) effect during the fabrication of microporous PVDF membranes via thermally induced phase separation (TIPS). *Journal of membrane science,* 15, 250-263.

6. Lafta, J.G. 2015. Analysis of Water Quality using chemical physical biological parameters of the kinds of water used for drinking in the Baghdad province- Al Adhamiya City Jassam. *Chemistry and Materials Research*, 7 (12), 1-4.

7. De Gusseme, B., Hennebel, T., Christiaens, E., Saveyn, H., Verbeken, K., Fitts, J.P., Boon, N. and Verstraete, W. 2011. Virus disinfection in water by biogenic silver immobilized in polyvinylidene fluoride membranes. *Water research,* 45(4), 1856-1864.

8. Ursino, C., Castro-Munoz, R., Drioli, E., Gzara, L., Albeirutty, M.H. and Figoli, A. 2018. Progress of nanocomposite membranes for water treatment. *Membranes*, 8, 2

9. Ali, S., Rehman, S.A.U., Luan, H-Y., Farid, M.U. and Huang, H. 2019. Challenges and opportunities in functional carbon nanotubes for membrane-based water treatment and desalination. *Science of the environment*, 646, 1, 1126-1139.

10. Ekambaram, K. and Doraisamy, M. 2016. Study on the fabrication, characterization and performance of PVDF/ calcium stearate composite nanofiltration membranes. *Desalination*, 385, 24-38.

11. Ozdemir, K. and Gungor, O. Monitoring of trihalomethanes removal in chlorinated drinking water sources with carbon nanomaterials. *Karaelmas science and engineering journal*, 8, 121-125.

12. Shakoor, A., Niaz, A., Khan, W., Asghar, G., Khalid, N.R., Rehman, M.N., Bashir, T., Anwer, N. and Rizvi, T.Z. Dielectric properties of polypyrrole multi-walled carbon nanotubes nanocomposites. Digest journal of nanomaterials and biostructures, 11 (4), 1145-1153.

13. Kummu, M., Guillaume, J.H.A., Moel, H., Eisner, S., Florke, M., Porkka, M., Siebert, S., Veldkamp, T.I.E. and Ward, P.J. 2016. The world's road to water scarcity: shortage and stress in the 20th century and pathways towards sustainability. *Scientific reports*, 6: 38495.

14. Falkenmark, M. 2013. Growing water scarcity in agriculture: future challenge to global water security. Philosophical transactions of the royal society *A: Mathematical, physical and engineering sciences,* 371.

15. Chan, C.L., Zalifah, M.K., Norrakiah, A.S. 2007. Microbiological and physiochemical quality of drinking water. *Malaysian journal of analytical sciences*, 11, 414-420.

16. Abdel-Moety, N.M., Al-Fassi, F.A. and Ali, M.A. Health aspects of virological water quality: An overview review. *Journal of applied sciences*. 2008, 4, 1205-1215.

17. Havelaar, A. and Bartram, J. 1996. World health organization: guidelines for drinking water quality. *World health organisation*, 2, 29-31.

18. Almeida, C.R., Spiandorello, F.B., Giroldo, D. and Yunes, J.S. 2016. The effectiveness of conventional water treatment in removing Ceratium furcoides (Levander) Langhans, Microcystis sp. and microcystins. *Water SA*, 42 (4).

19. Sharma, S. and Bhattacharya, A. 2017. Drinking water contamination and treatment techniques. *Applied water science*, 7(3), 1043-1067.

20. Giwa, A., Akther, N., Dufour, V. and Hasan, S.H. 2016. A critical review on recent polymeric and nanoenhanced membranes for reverse osmosis. *RSC Advances*, 6, 8134

21. Richards, H.L., Baker, P.G.L. and Iwuoha, E. 2012. Metal Nanoparticle Modified Polysulfone Membranes for Use in Wastewater Treatment: A critical review. *Journal of surface engineered materials and advanced technology*, 2, 183-193.

22. H, Wu, J. Mansouri, V. 2013. Chen, Silica nanoparticles as carriers of antifouling ligands for PVDF ultrafiltration membranes. *Journal of membrane science,* 433, 135-151.

23. Li, G, Shen L, Luo Y and Zhang S. The effect of silver-PAMAM dendrimer nanocomposites on the performance of PVDF membranes. 2014. *Desalination* 338. 115-120.

24. Wang, T., Song, B., Qiao, K., Huang, Y. and Wang, L. Effect of dimensions and agglomerations of carbon nanotubes on synchronous enhancement of mechanical and damping properties of epoxy nanocomposites. Nanomaterials, 8, 10. 3390.

25. Chi, Q.G., Ma, T. and Zhang, Y. 2017. Excellent energy storage of sandwich-structured PVDF-based composite at low electric field by introduced the hybrid CoFe2O4@BZT-BCT nanofibers. *ACS sustainable chemistry & engineering*, 10.1021.

26. Liu, F., Hashim, N.A., Liu, Y., Abed, M.R.M. and Li, K. 2011. Progress in the production and modification of PVDF membranes. *Journal of membrane science*, 375, 1-27.

27. Shi, H., Liu, F. and Xue, L. 2013. Fabrication and characterisation of antibacterial PVDF hollow fibre membrane by doping Ag-loaded zeolites. *Journal of membrane science*, 437, 205-215.

28. Stephan, A.M., Kumar, S.G., Renganathan, N.G. and Kulandainathan, M.A. 2005. Characterization of poly(vinylidene fluoride-hexafluoropropylene) (PVdF-HFP) electrolytes complexed with different lithium salts. *European polymer journal*, 41, 15-21.

29. Salazar, H., Nunes-Pereira, J., Correia, D.M., Cardoso, V.F., Goncalves, R., Martins, P.M., Ferdov, S., Martins, M.D., Botelho, G. and Lanceros-Mendez, S. 2016. Poly(vinylidene fluoride-hexafluoropropylene)/bayerite composite membranes for efficient arsenic removal from water. *Materials chemistry and physics,* 183, 430-438.

30. Shi, L., Wang, R., Cao, Y., Liang, D.T. and Tay, J.H. 2007. Fabrication of poly(vinylidene fluoride-co-hexafluropropylene) (PVDF-HFP) asymmetric microporous hollow fiber membranes. *Journal of membrane science*, 305, 215-225.

31. Choi, H.J., Jegal, J.J. and Kim, W.N. 2006. Fabrication and characterization of multi-walled carbon nanotubes/polymer blend membranes. *Journal of membrane science*, 284, 406-415.

32. Su, F. and Miao, M. 2014. Effect of MWCNT dimension on the electrical percolation and mechanical properties of poly(vinylidenefluoride-hexafluoropropylene) based nanocomposite. *Synthetic metals*, 191, 99-103.

33. Brady-Estevez, A.S., Kang, S. and Elimelech, M. 2008. A single-walled-carbon-nanotube filter for removal of viral and bacterial pathogens. *Small*, 4, 481-484.

34. Ahmed, F., Santos, C.M., Vergara, R. and Tria, M.C.R. 2012. Antimicrobial applications of electroactive PVK-SWNT nanocomposites. *Environmental science & technology*, 46, 1804-1810.

35. Rananga, L.E. and Magadzu, T. 2014. Interaction of silver doped carbon nanotubes-cyclodextrin nanocomposites with Escherichia coli bacteria during water purification. *Water science and technology*, 14, 367-375.

36. Panacek, Ales., Kvitek, Libor., Smekalová, Monika., Vecerova, Renata., Kolar, Milan., Roderova, Magdalena., Dycka, Filip., Sebela, Marek., Prucek, Robert., Tomanec, Ondrej. and Zboril, Radek. 2017. Bacterial resistance to silver nanoparticles and how to overcome it. *Nature nanotechnology*,13, 10.

37. Wang, L., Hu, C. and Shao, L. 2017. The antimicrobial activity of nanoparticles: present situation and prospects for the future. *International journal of nanomedicine,* 12, 1227-1249.

38. Li, J.H., Shao, X.S., Zhou, Q., Li, M.Z. and Zhang, Q.Q. 2013. The double effects of silver nanoparticles on the PVDF membrane: Surface hydrophilicity and antifouling performance. *Applied surface science*, 265, 663-670.

39. Sawada, I., Fachrul, R., Ito, T., Ohmukai, Y., Maruyama, T. and Matsuyama, H. 2012. Development of a hydrophilic polymer membrane containing silver nanoparticles with both organic antifouling and antibacterial properties. *Journal of membrane science*, 387-388, 1-6.

40. Hayati, B., Maleki, A., Najafi, F., Gharibi, F., McKay, G., Gupta, V.K., Puttaiah, S.H. and Marzban, N. 2018. Heavy metal adsorption using PAMAM/CNT nanocomposite from aqueous solution in batch and continuous fixed bed systems. *Chemical engineering journal,* 346, 258-270.

41. Tansel, B. 2008. New Technologies for Water and Wastewater Treatment: A Survey of Recent Patents. *Recent patents on chemical Engineering* 1, 17-26.

42. Le, N.L. and Nunes, S.P. 2016. Materials and membrane technologies for water and energy sustainability. *Sustainable materials and technologies*, 7, 1-28.

43. Sukitpaneenit, P. and Chung, T.S. 2011. Molecular design of the morphology and pore size of PVDF hollow fibre membranes for ethanol-water separation employing the modified pore-flow concept. *Journal of membrane science,* 374, 67-82.

44. Wang, Q., Wang, Z. and Wu, Z. 2012. Effects of solvent compositions on physicochemical properties and anti-fouling ability of PVDF microfiltration membranes for waste water treatment. *Desalination,* 297, 79-86.

45. Feng, C., Khulbe, K.C., Matsuura, T., Gopal, R., Kaur, S., Ramakrishna, S. and Khayet, M. 2008. Production of drinking water from saline water by air-gap membrane distillation using polyvinylidene fluoride nanofiber membrane, *Journal of membrane science,* 311, 1-6.

46. Mansouri, J., Harrisson, S. and Chen, V. 2010. Strategies for controlling biofouling in membrane filtration systems: challenges and opportunities. *Journal of materials chemistry*, 20, 4567.

47. Pan B., Cui D., Gao F. and He R. 2006. Growth of multi-amine terminated poly(amidoamine) dendrimers on the surface of carbon nanotubes. *Nanotechnology* 17, 2483-2489.

48. Yuan W., Giang G., Che J., Qi X., Xu R., Chang M.W., Chen Y., Lim S.Y., Dai J, and Chan-Park M.M. 2008. Deposition of silver nanoparticles on multi-walled carbon nanotubes grafted with hyper-branched poly(amidoamine) and their antimicrobial effects. *Journal of physical chemistry C, 112,* 18754-18759.

49. Wongchitphimon, S., Wang, R., Jiraratananon, R., Shi, L. and Loh, C.H. 2011. Effect of polyethylene glycol (PEG) as an additive on the fabrication of polyvinylidene fluoride-co-hexafluropropylene (PVDF-HFP) asymmetric microporous hollow fiber membranes. *Journal of membrane science*, 369, 329-338.

CHAPTER 2

LITERATURE REVIEW

2.1 WATER POLUTION

Safe drinking-water is a basic need for the development, health and well-being of humans. Safe drinking-water is therefore an internationally accepted human right [1,2]. Water that does not meet accepted drinking water standards should be treated to ensure that the health of the consumer or community is not compromised through exposure to toxic pollutants [3]. Drinking polluted or contaminated water can cause serious health problems; for example, cholera and diarrheal diseases cause many deaths of children in developing countries [4,5]. Microorganisms are accountable for many diseases initiated by consumption of contaminated water [6,7].

The domestic waste and agricultural wastewater contaminate water sources of surrounding area and ultimately affect human health [7,8]. Natural bodies of water are not absolutely pure as various organic compounds and inorganic elements remain in dissolved form. Chemical contamination of drinking-water is often considered a lower priority than microbial contaminants, because adverse health effects from chemical contaminants are generally associated with long-term exposures, whereas the effects from microbial contaminants are usually immediate. Nonetheless, chemicals in water supplies can cause very serious problems [3,7-8]

2.1.1 Chemical contamination of natural water sources

2.1.1.1 Arsenic

Arsenic (As) is a naturally occurring chemical which is responsible for severe health effects due to exposure through drinking-water in numerous countries. In water, arsenic has no taste, smell, or colour; as a result, it can only be detected through a chemical test [9]. Its distribution in groundwater is extensive and their possible presence in surface water should not be ruled out, because groundwater discharge is frequently a major contributor to surface water bodies [8]. When absorbed by living organisms, arsenic is excreted slowly, and hence accumulation easily occurs. Ingestion of arsenic in drinking water is most likely to lead to chronic effects, principally

different types of skin lesions. Once absorbed, arsenic is not readily lost and accumulates in the body; therefore, a single, once-off exposure to a high concentration of arsenic can have serious effects [10].

2.1.1.2 Lead

High concentrations of lead (Pb) in drinking-water can cause severe health effects. The presence of Pb in drinking-water is primarily a consequence of Pb plumbing and Pb-containing metal fittings in buildings. Risks posed by Pb in drinking-water should be assessed in localities where lead has been extensively used in plumbing materials, particularly if the water supplied is corrosive or is likely to dissolve Pb [8]. If Pb concentrations significantly exceed guideline values (≤ 10 µg/L), it may be appropriate to apply mitigating measures, such as corrosion control or replacement of pipes and plumbing materials [11].

2.1.1.3 Cadmium

Cadmium (Cd) is a soft, bluish-white metal, chemically similar to zinc and highly toxic to living organisms. The presence of Cd in the aquatic environment and in drinking water is of concern because it bioaccumulates [12]. Exposure of Cd has been associated with cancer of the lung, breast, pancreas, kidney and urinary bladder. An excessive level of cadmium ions in the water can affect the bio-systems and be a threat to human beings [13,14]. Conventional methods such as flocculation, precipitation, and ion exchange are used to remove Cd from water at low concentrations. These methods however are found to be inefficient and expensive [14]. Hence the removal of Cd ions from the water and wastewater is highly important, since it can be potentially dangerous to human health.

2.1.1.4 Chromium (IV)

Chromium (VI) is a highly oxidised state of metallic chromium (Cr) and occurs as the yellow coloured dichromate salt under neutral or alkaline conditions and as the orange-

coloured chromate salt under acidic conditions [15]. Cr(VI) is highly water soluble at all pH values, with the reduced forms of chromium, namely, Cr(II) and Cr(III), being less soluble. The reduced forms have much lower toxicity indices than Cr(VI), and do not constitute as serious a health hazard [16]. Occupational exposure to Cr(VI) is associated with the occurrence of nasal septum and skin ulcers, as well as with the occurrence of lung cancer and gastrointestinal cancer [17].

Several methods, such as adsorption, reduction, solvent extraction, precipitation, reverse osmosis have been used for removal of Cr(VI) from industrially polluted wastewaters [18]. However, most of these techniques have several limitations and drawbacks; such as the need of high energy or massive use of reducing agents. Of particular importance, adsorption is considered to be simple, economical, and remains one of the most attractive approaches for treating Cr(VI) [19].

2.1.1.5 Copper

Copper (Cu) is an essential trace element to plants, animals and humans and occurs in three oxidation states, namely metallic Cu (0), Cu(I) and (II). A significant source of Cu in domestic water arises from the dissolution of copper from plumbing systems in areas with soft or low pH values [20]. Cu concentrations in drinking-water vary widely as a result of variations in water characteristics such as pH, hardness and copper availability in the distribution system. Ingestion of high concentrations of copper results in gastrointestinal disturbances and possible liver, kidney and red blood cell damage [9].

2.1.1.6 Iron

Pure iron (Fe) is silvery in colour but usually appears as greyish black or brown deposits as a result of oxidation. Iron is found in three oxidation states, namely, 0, II and III of which the Fe(III) oxidation state is the most common. In water, iron can be present as dissolved ferric iron, Fe(III), as ferrous iron, Fe(II) or as suspended iron hydroxides [21]. High concentrations of iron in water are predominantly an aesthetic concern since ferrous salts are unstable under the pH conditions prevailing in drinking

water and precipitate as insoluble ferric hydroxide, which settles out as a rust-coloured silt [22].

Iron in the distribution system promotes proliferation of iron-oxidising bacteria which oxidise Fe(II) to Fe(III), and manifest as slimy coatings in plumbing when the iron concentration of the water in the distribution system approaches 0.3 mg/L. Fe complexed with humic acid, a natural water constituent in certain regions, causes a brown discolouration of water at high concentrations. This may be aesthetically unacceptable, but has no adverse health implications [20].

2.1.1.7 Nickel

Nickel (Ni) is an abundant element on Earth, most notably the planet's iron/nickel core [23]. When ingested through water, in small amounts, it is harmless to humans and in fact necessary in our diet. Inhalation of Ni is the greatest risk of developing health problems, as it becomes highly carcinogenic [24]. Nickel can be found in drinking-water as a consequence of its presence in alloys used in contact with drinking-water, chromium or nickel plating of fittings, or its presence in water sources, usually as a consequence of dissolution from naturally occurring nickel-bearing strata in groundwater. Conventional surface water treatment, comprising chemical coagulation, sedimentation, and filtration, can achieve 35-80% removal of nickel [25]. For waters containing low concentrations of suspended, the addition of powdered activated carbon has been used to enhance Ni removal [26]. However, another study has reported that Ni is rather poorly adsorbed on activated carbon [27].

2.1.1.8 Cobalt

Cobalt (Co) is found throughout the environment and critical exposure to high levels of Co by inhalation in humans and animals results in respiratory effects, such as a significant decrease in ventilatory function, congestion, oedema, and haemorrhage of the lung [28]. Cobalt can enter the aquatic environment from a number of sources, both natural and anthropogenic. Natural sources include volcanic emissions, the weathering of rocks by the action of water, and decomposition of plant waste [29].

2.1.1.9 Zinc

The stable oxidation states of metallic zinc are (0) and (II), of which (II) is the form found in nature. The presence of zinc in domestic water arises mainly from the leaching of galvanised plumbing and fittings [9]. Zn is an essential nutritional trace element for plants and animals. Humans have a high tolerance level to elevated zinc concentrations, while fish are highly susceptible to poisoning. Zn strongly interacts with cadmium; to which it is chemically very similar and at concentrations sufficient to cause gastrointestinal disturbances, zinc imparts a bitter astringent taste, and a milky appearance to water [21].

2.1.2 Microbial contamination of natural water sources

2.1.2.1 Faecal coliform and Escherichia coli

Faecal coliforms are bacteria that are associated with human or animal waste. Coliform bacteria are unlikely to cause illness; however, their presence in drinking water indicate that disease-causing organisms (pathogens) could be in the water system. Most pathogens that can contaminate water supplies come from the faeces of humans or animals [30].

Escherichia coli (E. coli) is a Gram-negative, rod-shaped bacterium commonly found in the intestines of animals and humans. The presence of *E. coli* in water is a strong signal of recent sewage or animal waste contamination. Sewage may contain many types of disease-causing organisms [31]. The presence of *E. coli* is used as an indicator to monitor the possible presence of other more harmful microbes, such as *Cryptosporidium, Shigella,* and *norovirus*. Diseases acquired from contact with contaminated water can cause gastrointestinal illness, skin, ear, respiratory, eye, neurologic, and wound infections. The most commonly reported symptoms are stomach cramps, diarrhoea, nausea, vomiting, and low-grade fever [32].

2.1.3 Physicochemical indicators of non-potable water

2.1.3.1 pH

The pH of a solution is a measure of the acidity or basicity of water and it ranges from 0 - 14, with pH of less than 7 indicating acidity, 7 being neutral, and pH greater than 7 indicating basicity [33]. A pH measures the relative amount of free hydrogen and hydroxyl ions in the water. The pH of most water sources lies within the range of 6.5 - 8.5, and it is an important indicator of the chemical changes in a water system. The pH of natural waters is influenced by various factors and processes, including temperature, acid mine drainage, acidic precipitation, runoff and microbial activity [34].

The taste of water, its corrosivity and the solubility and speciation of metal ions are all influenced by pH; and at low pH water may taste sour, while at high pH water tastes bitter or soapy [2]. The potential toxicity of metal ions and chemicals which can be protonated, for example ammonia, is influenced by pH. Changes in pH affect the degree of dissociation of weak acids and bases. This effect is of special importance because the toxicity of many compounds is affected by their degree of dissociation [35].

2.1.3.2 Colour

Water is transparent, and thus aquatic plants can live within the water because sunlight can reach them. True colour is the colour of a water sample from which the turbidity has been removed and apparent colour includes the colour and appearance of suspended matter [36]. True colour is described by the dominant wavelength or the degree of brightness or luminance and the saturation or purity of the colour. Colour in domestic water may be due to natural sources of coloured organic matter like humic and fulvic acids and it is strongly influenced by the presence of iron, manganese and certain other metals either as natural impurities or corrosion products [36]. There are no direct health effects from the presence of colour in drinking water except when colourants are toxic. Aesthetic effects are mainly visual but some colourants may stain or otherwise affect household appliances, for example, iron or manganese. For drinking purposes, small amounts of water can be treated using domestic water purifiers/ filters [20].

2.1.3.3 Turbidity

Turbidity is a measure of the light-scattering ability of water and is indicative of the concentration of suspended matter in water [36]. Micro-organisms are often associated with turbidity; hence low turbidity reduces the potential for transmission of infectious diseases. Turbidity also affects the aesthetic quality of water [22]. Turbidity in water is caused by the presence of suspended matter which usually consists of a mixture of inorganic matter, such as clay, soil particles and organic matter. The consumption of turbid water does not have any direct health effects, but associated effects can be due to microbial contamination [20].

2.1.3.4 Conductivity

Electrical conductivity (EC) is a measure of the ability of water to conduct an electrical current. This ability is a result of the presence of ions in water such as carbonate, bicarbonate, chloride, sulphate, nitrate, sodium, potassium, calcium and magnesium, all of which carry an electrical charge [37]. Most organic compounds dissolved in water do not dissociate into ions, consequently they do not affect the EC. Pure water has a low electrical conductivity, but this increases significantly with the dissolution of a small amount of ionic material such as sodium chloride [38].

In many cases, conductivity is linked directly to the total dissolved solids (TDS). The taste threshold for dissolved salts in water is in the region of 45 mS/m (300 mg/L TDS), hence a slight salty taste may be detected above this concentration. The threshold varies according to the salt composition. Water with extremely low TDS concentrations may be distasteful because of its flat, bland taste.

2.1.3.5 Total dissolved solids

The total dissolved solids (TDS) are a measure of the amount of various inorganic salts dissolved in water and it is directly proportional to the electrical conductivity (EC) of water [36]. The properties of TDS are governed by the characteristics of the constituent inorganic salts dissolved in water, and TDS is closely related to other water quality constituents such as the total hardness, the corrosion and scaling potential of

water [35]. Low concentrations of particularly calcium and magnesium salts have nutritional value, although water with an extremely low TDS concentration may be objectionable because of its flat bland taste, in contrast, high concentrations of salts impart an unpleasant taste to water and may also adversely affect the kidneys [2]. Health effects related to TDS are minimal at concentrations below 1200 mg/L [11].

2.1.3.6 Total hardness

Total hardness is defined as the sum of the calcium and magnesium concentrations, expressed as mg/L of calcium carbonate. Other metals such as strontium, iron, aluminium, zinc and manganese may occasionally contribute to the hardness of water, but the calcium and magnesium hardness usually predominates [35]. Temporary hardness is due to the presence of bicarbonates of calcium and magnesium and can be removed by boiling, whereas permanent hardness is attributed to other salts such as sulphate and chloride salts, which cannot be removed by boiling. Excessive hardness of water can give rise to scaling in plumbing and household heating appliances and hence has adverse economic implications. It also poses an irritation in personal hygiene. Total hardness of water varies and ranges from 0-1 000 mg $CaCO_3$ /L [2].

2.2 WATER PURIFICATION PRINCIPLES

The guidelines below are used to regulate water standards in South Africa. Potable water should comply with the microbiological, physical, aesthetic and chemical numerical limits for lifetime consumption specified in table 2.2.1 & 2.

Table 2.2.1 Microbiological determinands [11]

Determinand	**Risk**	**Unit**	**Standard limits**
E. coli or faecal coliforms	Acute health	Count per 100 mL	Not detected

Protozoan parasites Cryptosporidium species *Giardia* species	 Acute health Acute health	 Count per 10 L Count per 10 L	 Not detected Not detected
Total coliforms	Operational	Count per 100 mL	≤ 10
Heterotrophic plate count	Operational	Count per mL	≤ 1 000
Somatic coliphages	Operational	Count per 10 mL	Not detected

Table 2.2.2: Physical, aesthetic, operational and chemical determinands [2]

Determinand	Risk	Unit	Standard limits
Physical and aesthetic determinands			
Colour	Aesthetic	mg/L	≤ 15
Conductivity at 25 °C	Aesthetic	mS/m	≤ 170
Total dissolved solids	Aesthetic	mg/L	≤ 1 200
Turbidity	Operational	NTU	≤ 1
	Aesthetic	NTU	≤ 5
pH at 25 °C	Operational	pH units	≥ 5 to ≤ 9,7
Chemical determinands — macro-determinands			
Free chlorine as Cl_2	Chronic health	mg/L	≤ 5
Monochloramine	Chronic health	mg/L	≤ 3
Nitrate as N	Acute health	mg/L	≤ 11
Nitrite as N	Acute health	mg/L	≤ 0,9
Combined nitrate plus nitrite	Acute health		≤1
Sulfate as SO_4^{2-}	Acute health	mg/L	≤ 500
	Aesthetic	mg/L	≤ 250
Fluoride as F^-	Chronic health	mg/L	≤ 1,5
Ammonia as N	Aesthetic	mg/L	≤ 1,5
Chloride as Cl^-	Aesthetic	mg/L	≤ 300
Sodium as Na	Aesthetic	mg/L	≤ 200
Zinc as Zn	Aesthetic	mg/L	≤ 5

Chemical determinands — micro-determinands			
Antimony as Sb	Chronic health	µg/L	≤ 20
Arsenic as As	Chronic health	µg/L	≤ 10
Barium as Ba	Chronic health	µg/L	≤ 700
Boron as B	Chronic health	µg/L	≤ 2 400
Cadmium as Cd	Chronic health	µg/L	≤ 3
Total chromium as Cr	Chronic health	µg/L	≤ 50
Copper as Cu	Chronic health	µg/L	≤ 2 000
Cyanide (recoverable) as CN^-	Acute health	µg/L	≤ 200
Iron as Fe	Chronic health	µg/L	≤ 2 000
	Aesthetic	µg/L	≤ 300
Lead as Pb	Chronic health	µg/L	≤ 10
Manganese as Mn	Chronic health	µg/L	≤ 400
	Aesthetic	µg/L	≤ 100
Mercury as Hg	Chronic health	µg/L	≤ 6
Nickel as Ni	Chronic health	µg/L	≤ 70
Selenium Se	Chronic health	µg/L	≤ 40
Uranium as U	Chronic health	µg/L	≤ 30
Aluminium as Al	Operational	µg/L	≤ 300
Chemical determinands — organic determinands			
Total organic carbon as C	Chronic health	mg/L	≤ 10
Trihalomethanes Chloroform Bromoform Dibromochloromethane Bromodichloromethane	 Chronic health Chronic health Chronic health Chronic health	 µg/L µg/L µg/L µg/L	 ≤ 300 ≤ 100 ≤ 100 ≤ 60
Combined trihalomethane	Chronic health		≤ 1
Total microcystin	Chronic health	µg/L	≤ 1
Phenols	Aesthetic	µg/L	≤ 10

2.3 CURRENT AND POTENTIAL METHODS USED IN WATER PURIFICATION

2.3.1 Chlorination

Although several methods eliminate disease-causing microorganisms in water, chlorination is the most commonly used. Chlorination is effective against many pathogenic bacteria, but at normal dosage rates it does not kill all viruses, cysts, or worms [39]. Chlorine however oxidizes organic matter in wastewater, sometimes creating compounds that could be harmful to humans and the environment and certain types of microorganisms have shown resistance to low doses of chlorine [40]. When chlorine is added to water, it reacts with organic substances that occur naturally in the water which forms disinfection by-products. The amount formed depends on the amount of chlorine used and contact time between the organic substances and the chlorine. Some studies of human health effects from exposure to chlorinated water show increased risk to cancer and reproductive and developmental effects [41].

2.3.2 Ozonation

Ozonation is a chemical water treatment technique based on the infusion of ozone into water. Ozone gas is one of the most powerful oxidants composed of three oxygen atoms (O_3), which is involved in the production of very reactive oxygen species able to attack a wide range of organic compounds and microorganisms [42]. The treatment of water with ozone is efficient for disinfection as well as for the degradation of organic and inorganic pollutants. Ozone is produced with the use of energy by subjecting oxygen (O_2) to high electric voltage or to UV radiation. The required amounts of ozone can be produced at the point of use but the production requires a lot of energy and is therefore costly [43].

2.3.3 Adsorption

Adsorption technology is widely recognised as one of the most powerful methods for heavy metal ions and dye removals from water. However, the development of efficient inexpensive adsorbent materials remains an ongoing challenge.

2.3.3.1 Metal and carbon-based adsorbents

Nanostructured carbon materials such as carbon nanotubes and graphene are currently attracting immense interest as promising new class of adsorbent because of their large surface area and exceptional physicochemical properties [44]. Carbon based adsorbents are usually used for removal of heavy metals and organic contaminants. Carbon nanotubes (CNTs) have shown higher efficiency on adsorption of various organic chemicals [45]. CNTs have much higher adsorption capacity for some bulky organic molecules because of their larger pores in bundles and more accessible sorption sites [46]. CNTs strongly adsorb many polar organic compounds due to the diverse contaminant-CNT interactions including hydrophobic effect, π-π interactions, hydrogen bonding, covalent bonding, and electrostatic interactions [47]. Oxidized CNTs have high adsorption capacity than activated carbon for metal ions such as Cu^{2+}, Pb^{2+} and Zn^{2+}. The surface functional groups (e.g., carboxyl, hydroxyl, and phenol) of CNTs are the major adsorption sites for metal ions, mainly through electrostatic attraction and chemical bonding [47].

Lakshmanan *et al*. [48] studied the effect of magnetic iron oxide nanoparticles in surface water treatment (Trace minerals and microbes). Their study focused on the efficiency of micro emulsion prepared magnetic iron oxide nanoparticles (ME-MIONs) and protein-functionalized nanoparticles (MOCP + ME-MIONs) in water treatment. Their results imparted that ME-MIONs could reduce the water turbidity even in low turbid water samples. They observed reduction of microbial content (98%) at 37 ^{o}C, more than 90% reduction at room temperature when compared to untreated samples from lake Orlangen. They also observed the reduction of copper and phosphate when using ME-MIONs in simulated water [48].

Ganesan *et al*. [49] reported on the cost-effective fabrication of novel functional hybrid composed of graphene oxide (GO)-wrapped magnetite (Fe_3O_4) nanoclusters (Fe_3O_4@GO) by electrostatically driven co-assembly for fast and highly efficient removal of organic dyes from wastewater. Their results showed that the adsorption kinetics and the equilibrium adsorptions were well-fitted with pseudo-second order kinetic model and Langmuir isotherm model, respectively. They observed the maximum adsorption capacities for MB, RhB and MO to be 131.10, 34.50 and 39.95 mg/g respectively at 303 K. The Fe_3O_4@GO adsorbent exhibited rapid magnetic

separation, easy regeneration, excellent stability, and good sustainability in removal efficiency even after continued recycling. Their results demonstrated that Fe_3O_4@GO composite possess great potential as an efficient and recyclable adsorbent for the removal of both cationic and anionic dye pollutants in environmental remediation [49].

The adsorption properties of carbon nanotubes were studied by Li *et al*. [50]. They investigated the adsorption properties of carbon nanotubes to a series of toxic agents, such as lead, cadmium and 1,2-dichlorobenzene. Their results showed that carbon nanotubes are excellent and effective adsorbent for eliminating these harmful media in water. They also found that Cd(II) adsorption capacity increased up to 11.0 mg/g at a Cd (II) equilibrium concentration of 4 mg/L [50].

In 2016 Sambaza *et al*. [51] synthesised Polyethyleneimine-carbon nanotube polymeric nanocomposite adsorbents (PEI-MWCNT) for the removal of Cr(VI) ions from water. Their batch adsorption studies showed that PEI-MWCNT nanocomposite materials were more efficient in the removal of Cr(VI) ions solution from water samples at an optimum pH of 4. The kinetic adsorption data obtained for Cr(VI) solution followed pseudo-second order model and their results also showed that the adsorption of Cr(VI) solution reached equilibrium within 60 min of contact time, with a removal above 80%. [51].

2.3.3.2 Polymeric adsorbents

Dendrimers are custom-made adsorbents that are capable of removing both organics and heavy metals. Their interior shells can be hydrophobic for sorption of organic compounds while the exterior branches can be tailored for adsorption of heavy metals. The sorption can be based on complexation, electrostatic interactions, hydrophobic effect, and hydrogen bonding [52]. A dendrimer-ultrafiltration system was designed to recuperate metal ions from aqueous solutions. The system achieved almost complete removal of Cu^{2+} ions, with initial concentration of 10 ppm Cu^{2+} ions to PAMAM dendrimer-NH_2 ratio of 0.2. After adsorption, the metal ion laden dendrimers were recovered by ultrafiltration and regenerated by decreasing pH to 4 [53].

Chitosan beads were modified, in a novel way, using sodium dodecylsulfate (SDS), a well-known anionic surfactant by Pal and Pal *et al*. [54]. The surfactant-modified

chitosan beads synthesised were used for Cd(II) ions adsorption and the maximum adsorption capacity obtained was 125 mg/g at a dosage of 0.45 g/L and pH of 7 [55]. Chitosan and epichlorohydrin cross-linked chitosan/eggshell composite for cadmium adsorption was studied by Rahmi [55]. His studies showed that the optimum pH of adsorption was pH = 6.0 and the equilibrium time of adsorption was 40 min. Langmuir isotherm indicated the maximum adsorption capacity of Cd(II) ions onto composite was 11.765 mg/g and this value was more than ten times larger than maximum adsorption capacity of Cd(II) ions onto chitosan. Regeneration studies performed also showed that the adsorbents can be used several times for adsorption of Cd(II) ions [55].

The removal of Cd(II) ions from water using natural phosphate as adsorbent was studied by Yaacuobi *et al*. [56]. Their results showed that natural phosphate had the monolayer adsorption capacity to 26 mg/g at pH of 5.0. Their adsorption measurements show that the process is very fast and physical in nature and their results showed that natural phosphate is a good adsorbent for cadmium from aqueous solutions and could be used as a purifier for water and wastewater [56].

In 2015, Wang *et al*. [57] studied the Adsorption and removal of malachite green from aqueous solution using magnetic β-cyclodextrin-graphene oxide (Fe_3O_4/β-CD/GO) nanocomposites as adsorbents. Their results indicated that the Fe_3O_4/β-CD/GO nanocomposites had good adsorption ability at 45 ^oC and pH 7. In addition, they also investigated the thermodynamic parameters which indicated that the adsorption process was spontaneous and endothermic in nature [57].

2.3.4 Membrane filtration

Membranes are used for removal of infectious microbial species, reducing turbidity, hardness, natural organic matter, and improving the taste and odour. Different treatment needs membranes of different pore diameters [45]. Membrane filtration is a vital resource for the treatment and reuse of municipal water and wastewater. Membrane filtration process can be pressure driven or dependent on electrical potential gradients, concentration gradients, or other driving forces [58]. Pressure-driven membrane processes include microfiltration, ultrafiltration, nanofiltration and

reverse osmosis [58]. The chart below (figure 2.1) summarises various separation processes relative to common materials that would be filtered out through each process.

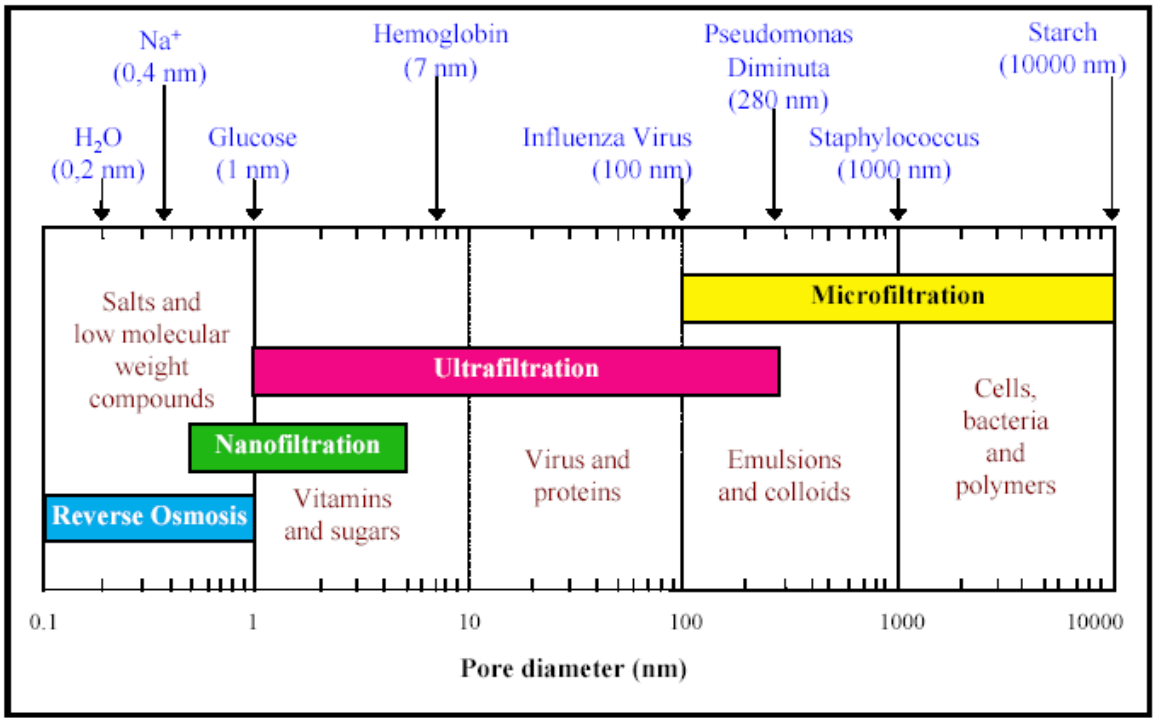

Figure 2.1: Separation processes of different membranes [59].

A microfiltration filter has a pore size of about 0.1 µm, and thus removes many microorganisms from water except viruses. Microfiltration has significant applications in simple dead-end filtration for water, sterilisation of beverages, in aseptic pharmaceuticals and operates at relatively low pressures [60]. Ultrafiltration (UF) is a type of membrane filtration in which hydrostatic pressure forces a liquid through a semipermeable membrane. An ultrafiltration filter has a pore size of around 0.01 µm [61]. UF excels at the clarification of solutions containing suspended solids, bacteria, and high concentrations of macromolecules, including oil and water, pharmaceuticals, potable water, and tertiary wastewater. UF is also increasingly applied in production of drinking water and reclamation of wastewater in recent years [61]. However, several studies have shown that natural organic matter is one of the major fouling materials during the UF process [62-64]

Nanofiltration (NF) is a filtration technique pore sizes around 0.001 µm, functioning in a similar way as reverse osmosis, although it's normally targeted to remove only divalent and larger ions. NF removes most organic molecules, nearly all viruses, most of the NOM and a range of salts. NF removes divalent ions, which make water hard, and it is often used to soften hard water and in desalination [65]. In water treatment, NF membranes are used for hardness removal, pesticide elimination, and colour reduction [66].

Reverse osmosis (RO) is a water purification technology process by which a solvent pass through a porous membrane in the direction opposite to that for natural osmosis when subjected to a hydrostatic pressure greater than the osmotic pressure. Reverse osmosis filters have a pore size around 0.0001 µm [65]. Reverse osmosis can remove many types of dissolved and suspended species from water, including viruses, bacteria, organic molecules and its used in both industrial processes and the production of potable water. One of its common applications is seawater desalination, in which pure water is produced from a highly saline feed stream, similar to evaporation with far better economy. Because the osmotic pressure of many process streams is quite high, RO membranes must operate at pressures of 400-1,200 psi (29-83 bars), which restricts available membrane geometries [67].

Drawbacks of membrane filtration

A major challenge of the membrane technology is its fouling, which adds to the energy consumption and the complexity of the process design and operation [45]. Membrane fouling includes inorganic fouling/scaling, organic fouling, particulate/colloidal fouling and biofouling. The most common categories of membrane fouling mechanisms are [68,69]:

- Formation of a cake layer on the top surface of the membrane.
- Adsorption of solid matter on the surface and within the pores of the membrane.
- Accumulation of solid substances within the membrane pores.
- Accumulation of rejected solutes within the membrane.
- Biofouling phenomena because of the presence of micro-organisms

Biofouling has been known as a contributing factor to more than 45% of all membrane fouling and has been reported as a major problem in membrane filtration [70,71]. Biofouling can have numerous adverse effects on membrane systems such as membrane flux decline, membrane biodegradation and increased energy consumption [87]. Incorporation of functional nanomaterials into membranes offers a great opportunity to improve the membrane permeability, fouling resistance, mechanical and thermal stability, as well as to render new functions for contaminant degradation and self-cleaning [60,69].

2.3.4.1 Nanocomposite membranes

A significant number of studies on membrane nanotechnology have focused on doping nanomaterials into polymeric or inorganic membranes. Nanomaterials used for such applications include hydrophilic metal oxide nanoparticles, antimicrobial nanoparticles (e.g., nano-Ag and CNTs), and (photo) catalytic nanomaterials. However, its long-term efficacy against membrane biofouling has not been reported [72].

In 2014 Adams *et al*. [89] prepared polysulfone/cyclodextrin mixed-matrix membranes for application in the removal of natural organic matter from water. In their studies, the pure water flux of the membranes improved from 12 to 137 l/m^2 h when the applied pressure was increased from 0.62 to 2.41 MPa and the highest NOM removal efficiency achieved was 69% [73].

Graphene oxide nanosheets were synthesised and employed in the adsorption of Cd(II) in acidic aqueous solutions by Xue *et al.* [74]. Their adsorption data results were revealed to fit well in pseudo-second-order kinetics and Langmuir isotherm model, with the maximum Cd(II) adsorption capacity recorded to be about 44.64 mg/g with 0.50 g/L of adsorbent dosage. They also found that ion-exchange, electrostatic attraction and physical adsorption were found to be involved in the adsorption mechanisms of the adsorption process [74]. An aluminium oxide-impregnated carbon nanotube membrane was developed via a novel approach and used in the removal of toxic metal cadmium ions, Cd(II) by Ihsanullah *et al*. [75]. Their filtration system removed 84% of the Cd(II) ions at pH 7 using CNT membrane with 10 wt.% Al_2O_3 loading. They observed a maximum adsorption capacity of 54 mg/g as predicted by the Langmuir

isotherm model for the CNT membrane with 10 wt.% Al_2O_3 loading. This high adsorption capacity observed indicated that adsorption was the main mechanism involved in the removal of Cd(II) ions [75].

Ekambaram *et al*. [76] fabricated hydrophobic nanofiltration membranes by blending polyvinylidene fluoride (PVDF) and calcium stearate through nonsolvent induced phase inversion process. Their filtration performances of the membranes were examined by determining molecular weight cut off, porosity, and water uptake rate. Their results showed that the inorganic salts were highly rejected by these membranes in the following sequence Na_2SO_4 > $MgSO_4$ > $MgNO_3$ > LiCl > NaCl. They also used humic acid as the model foulant to account for the antifouling property and the flux recovery ratio was high, ensuring excellent irreversible fouling. Their results showed that the highly hydrophobic nanofiltration composite membranes prepared exhibited superior irreversible fouling property, good stability and durability using humic acid as the model foulant [76].

2.3.4.2 Thin film nanocomposite membranes

Development of thin film nanocomposite membranes mainly focuses on incorporating nanomaterials into the active layer of thin film composite (TFC) membranes via doping in the casting solutions or surface modification. Nanomaterials that have been researched for such applications include nano-zeolites, nano-Ag, nano-TiO_2, and CNTs. The impact of nanoparticles on membrane permeability and selectivity depends on the type, size and percentage weight of nanoparticles added. Nano-zeolites are the most frequently used dopants in TFN and have shown potential in enhancing membrane permeability [77,78].

Thin film nanocomposite (TFN) membranes containing MCM-41 silica nanoparticles (NPs) were synthesized by Kadhom *et al*. [79] using the interfacial polymerization (IP) process. In their study, an m-phenylenediamine aqueous solution and an organic phase with trimesoyl chloride dissolved in isooctane were used in the IP reaction, occurring on a nanoporous polysulfone support layer [79]. Their results showed that doping with MCM-41 silica nanoparticles yielded slightly improved and more stable results than adding them to a trimesoyl chloride solution. With 0.02% MCM-41 silica

nanoparticles in the m-phenylenediamine solution, they observed that the water flux rate was increased from 44.0 to 64.1 L/m^2.h, while the rejection virtually remained the same at 95% (2000 ppm NaCl saline solution, 25 ^oC, 2068 kPa (300 psi) [79].

In 2014, Pala *et al*. [80] investigated the possibility of using new generated potassium lanthanum titanates ($K_2La_2Ti_3O_{10}$, KLTO) photocatalyst thin films and CeO_2 buffer layer produced using sol–gel method to remove cyanide from wastewater. In their study, the degradation experiments were fitted to first order kinetic model and the maximum degradation efficiency of cyanide was found to be 99.87% at pH of 10 and light intensity of 750W/m^2 by using 100 mg/l cyanide initial concentration after 5 h irradiation [80].

2.3.5 Polymeric membranes

2.3.5.1 Poly (vinylidene fluoride) (PVDF)

Poly (vinylidene fluoride) (PVDF) is a semi crystalline thermoplastic having excellent thermal stability, good chemical resistance, good mechanical strength, unique piezoelectric characteristics. It is known to exhibit at least four different polymorphic structures, namely α, β, λ and δ. The most stable is the non-polar α-phase which forms upon crystallisation of PVDF from the melt. In particular, PVDF membrane is used in the field of municipal, industrial wastewater and potable water treatment [81,82]. The main problem of PVDF membrane is its vulnerability to fouling and contamination by proteins, other impurities and/or microorganism in water [83]. This is due to its hydrophobic nature, which leads to an enormous decrease of permeability of membrane [84]. To fight against the membrane fouling and water contamination caused by bacteria in membrane separation processes, it is necessary to endow the membrane with a property of inhibiting the growth and reproduction of bacteria and the development of bacteria film [85].

2.3.5.2 Poly(vinylidene fluoride-cohexafluoropropylene)

As an alternative polymer for PVDF, poly(vinylidenefluoride-hexafluoropropylene) (PVDF-HFP) has drawn the attention of many researchers because of its higher

dielectric constant and mechanical properties [86,87]. This is due to the combination of an amorphous phase of hexafluropropylene (HFP) into the vinylidene fluoride (VDF) blocks. This polymer also comprises of both amorphous and crystalline phase; the amorphous phase of the polymer helps for higher ionic conduction, whereas the crystalline phase acts as a mechanical support for the polymer electrolyte. PVDF-HFP is a chemically inert fluoropolymer, it has lower crystallinity compared with PVDF, it has good mechanical strength, can tolerate high-temperature feed solutions, and is a hydrophobic material. PVDF-HFP polymers can be used in the preparation of membrane for water purification [88].

2.35.3 Polysulfone

Polysulfones are a class of polymers with high thermal, oxidative and hydrolytic stability and they are amorphous, transparent thermoplastics that can be molded, extruded, or thermoformed into a wide variety of shapes [89]. The high thermal stability is provided by the diphenylene sulfone group which also imparts high strength, high resistance to oxidation, and excellent flame retardancy, which makes the polymer rigid. Flexibility in the backbone of the polymer is provided by ether linkages and these ether linkages also add to the thermal stability [90]. Polysulfones are highly resistant to aqueous mineral acids, bases, and oxidizing agents and are fairly resistant to many non-polar solvents. However, polysulfones are not resistant to low polar solvents, such as esters, ketones, aromatic and chlorinated hydrocarbons [91]. Polysulfone membranes are the most common membranes used in ultrafiltration of wastewater due to its mechanical robustness and structural and chemical stability. Unfortunately, polysulfone is a hydrophobic material, making its surface prone to fouling due to adsorptive mechanism [92].

2.3.5.4 Cellulose

Cellulose is a polysaccharide consisting of a linear chain of several hundreds to over ten thousand β-(1→4)-linked D-glucose units with the formula $(C_6H_{10}O_5)n$. Being a carbohydrate polymer the molecular structure of cellulose possesses a large number of hydroxyl groups (three per anhydroglucose unit), which forms vast intra- and

intermolecular hydrogen bonds [93]. Cellulose is odourless, nontoxic, hydrophilic and biodegradable. Cellulose is widely available in nature and closely relevant to people's daily life in the form of paper, textiles etc. [94]. In nature, cellulose does not appear as an isolated individual molecule, but it is built up of self-assembled individual cellulose chain forming fibres. Cellulose has a hierarchical structure from the nano-scale building up to the micro scale by nature [95].

Nanocellulose, which offers a combination of biosorption, nano dimensions and unique cellulosic nature, has a tremendous potential for a new and green route to solve the current heavy metal pollution problems [96]. High specific area of nanocellulose is expected to provide large number of active sites on the surface of biosorbent to immobilize metal ions. The specific surface area of cellulose nanofiber prepared using a supercritical drying process, can be as high as 480 m^2/g [97]. It has shown fabrication of hybrid composite membranes having nanocellulose as functional material within chitosan matrix for the adsorption of dyes from model wastewater [98].

2.3.6 Nanocomposite and nanoparticles doping materials

Studies on membrane nanotechnology have focused on doping nanomaterials into polymeric or inorganic membranes. Nanomaterials used for such applications include hydrophilic metal oxide nanoparticles, antimicrobial nanoparticles and (photo) catalytic nanomaterials. The main goal of adding hydrophilic metal oxide nanoparticles is to reduce fouling by increasing the hydrophilicity of the membrane.

2.3.6.1 Metal oxides

The addition of metal oxide nanoparticles to polymeric ultrafiltration membranes has been shown to increase membrane surface hydrophilicity, water permeability, or fouling resistance [99]. These inorganic nanoparticles also help enhance the mechanical and thermal stability of polymeric membranes, reducing the negative impact of compaction and heat on membrane permeability [100]. Several metal oxide nanomaterials including nanosized magnetite and TiO_2 have shown arsenic adsorption performance superior to activated carbon [101]. Metal hydroxide

nanoparticles can be impregnated onto the skeleton of activated carbon or other porous materials to achieve simultaneously removal of arsenic and organic co-contaminants, which favours point-of use (POU) applications [102].

2.3.6.2 Silver nanoparticles

The antibacterial activities of silver ions and silver nanoparticles have been researched extensively [103,104]. A review by Ahamed *et al*. [105] has indicated that Ag nanoparticles are toxic to a variety of organs including the lung, liver, brain, vascular system and reproductive organs. They further suggested that Ag nanoparticles-induced toxicity includes induction of oxidative stress, DNA damage and apoptosis [106]. Such health and environmental hazards of nanoparticles can be greatly reduced if they can be either enclosed in or strongly attached to bigger structures. Tran *et al*. [107] suggested that a new approach would be to develop a hybrid nanostructure between carbon-based nanomaterials such as carbon nanotubes or graphene and Ag nanoparticles. By decorating Ag nanoparticles on carbon nanomaterials, the toxicity of Ag nanoparticles will be reduced, thus helping in preventing potential human hazards and contamination to the environment [107,108].

2.3.6.3 Poly-amidoamine

Dendrimers are highly branched, well defined, synthetic macromolecules possessing a globular structure with a high density of functional groups on their periphery. The size and shape of dendrimers depend on their number of branched units (*i.e.*, generation) and their backbone constituents. Dendrimers accommodate small molecules and nanoparticles in their interior through electrostatic or hydrophobic interactions to form host-guest complexes [109]. The surface of dendrimers also binds guest molecules through electrostatic binding because polar functionalities, such as amine and carboxyl groups, are located at the dendrimers periphery.

Poly-amidoamine (PAMAM) dendrimers are monodisperse macromolecules with highly branched three-dimensional architecture, which can act as templates for metal nanoparticles since they have internal cavity capable of encapsulating the metal

particles [110]. In addition, their pocket structure has a high number of amide groups. These functional groups have great efficiency to remove heavy metals via coordination and chelation linkages [110]. PAMAM dendrimer due to their abundant amino groups can be used to enhance the CNT dispersion properties resulting in an increase in the adsorption capacity [111]. PAMAM dendrimers have terminal amine groups and a high specific surface area; consequently, they are a good choice for complexation with metal ions and carbon materials [112-114].

2.3.6.4 Polyethylene glycol and polyvinylpyrrolidone additives

Additives or pore formers are often used to balance or improve the permeation performance of the final membrane through adjusting the membrane structure in the phase inversion process. Polyethylene glycol (PEG) is one of the additives used to promote pore formation in the polymeric membranes and it has been used as a pore former to enhance the permeation properties for hydrophilic polymeric membranes [115]. Polyvinylpyrrolidone (PVP) is among the most commonly used additive in membrane fabrication as an effective method to produce highly porous membranes [116]. PVP is hydrophilic in nature, thus the presence of this polymer could enhance the liquid-liquid demixing process during precipitation of the dope solution since they are miscible with water. Due to its hydrophilic nature, the addition of PVP promotes the non-solvent influx upon immersion in the coagulation bath, thus favouring the formation of large finger-like macrovoids in PVDF hollow fibre membranes [117].

2.4 PREPARATION OF MEMBRANES

During the three decades of thorough membrane preparation research, different techniques have been proposed to generate selective and permeable films. The most utilised and thus important class of techniques is called phase inversion techniques. The term phase inversion is used to describe the formation of porous polymeric membranes, it refers to a process during which a homogeneous, polymer solution is converted into two phases, i.e. a solid polymer rich phase forming the rigid membrane structure and a polymer lean phase representing the liquid filled pores [118].

The non-solvent induced phase-inversion process has been widely adopted as a reliable method for preparing or modifying asymmetric membranes [119]. This method is used to produce a wide range of membranes types including mixed-matrix by varying the composition and properties of the polymer solution. The temperature and composition of the precipitation solution can also be enhanced to obtain the desired results. In phase-inversion, a more volatile solvent is often introduced to the polymer solution to adjust the solvent evaporation and the polymer coagulation [118]. Most common water-miscible solvents used in hydrophobic asymmetry are dimethyl formamide, Dimethyl acetamide dimethyl sulfoxide, N-Methyl Pyrrolidone, dimethyl acetamide, and many more [118,119]. A more volatile solvent is expected to exhibit good miscibility with water.

2.6 REFERENCES

1. Momba, M.N.B. and Broukavert, B.M. 2005. Water problems. *WRC report TT*, 5, 249.

2. WHO. 2001. Water health and human rights, World water day 2001. Available online at http://www.worldwaterday.org/thematic/hmnrights.html#n4

3. Reddy, C.D. and Voortman, W.J. 2005. Package water treatment plant selection. *Water Research Commission Report,* 450, 3-7.

4. Chan, C.L., Zalifah, M.K. and Norrakiah, A.S. 2007. Microbiological and physiochemical quality of drinking water. *Malaysian journal of analytical sciences*, 11, 414-420.

5. Abdel-Moety, N.M., Al-Fassi, F.A. and Ali, M.A. 2008. Health aspects of virological water quality: An overview review. *Journal of applied sciences research,* 4, 1205-1215.

6. Shannon, M.A., Bohn, P.W., Elimelech, M. Georgiadis, J.G., Mariñas, B.J. and Mayes, A.M. 2008. Science and technology for water purification in the coming secades. Nature, 452, 301-310.

7. Lafta, J.G. 2015. Analysis of Water Quality using chemical physical biological parameters of the kinds of water used for drinking in the Baghdad province- Al Adhamiya City Jassam. *Chemistry and Materials Research*, 7 (12), 1-4.

8. WHO. 2004. Guidelines for drinking-water quality, 3rd ed., World health organization, Geneva.

9. Berman, E. 1980. Toxic Metals and their Analysis. Heyden, London.

10. Kempster, P.L. and H.R. Van Vliet. 1991. Water quality fitness for use curves for domestic water.

11. SANS 241-1. 2015. Drinking water, Part 1: Microbial, physical, aesthetic and chemical determinants. South African bureau of standards (SABS), Pretoria.

12. Guo, H.R., Wang, N.S. and Monson, R.R. 2004. Cell type specificity of lung cancer associated with arsenic ingestion. Cancer epidemiology, biomarkers & prevention, 13 (4), 638-643.

13. Mohan, D. and Singh, K. P. 2002. Single- and multi-component adsorption of cadmium and zinc using activated carbon derived from bagasse – an agricultural waste. *Water research*, 36, 2304-2318.

14. Fu, F.L. and Wang, Q. 2011. Removal of heavy metal ions from wastewaters: a review, *Journal of Environmental Management*, 92, (3),407-418

15. Khezami, L. and Capart, R. 2005. Removal of chromium (VI) from aqueous solution by activated carbons: kinetic and equilibrium studies. *Journal of hazardous materials*, 123 (1-3), 223-231.

16. Guo, X., Fei, G.K., Su, G.T.H. Zhang, L.D. 2011. High-performance and reproducible polyaniline nanowire/tubes for removal of Cr(VI) in aqueous solution. *Journal of physical chemistry C*, 115 (5), 1608-1613.

17. Gimenez, J.A., Aguado, M.A. and Cervera-March S.1996. Photocatalytic reduction of chromium(VI) with titania powders in a flow system. Kinetics and catalyst activity. *Journal of molecular catalysis A*, 105 (1), 67-78.

18. Chon, K, Kim, S.J. and Cho, J. 2012. Combined coagulation-disk filtration process as a pre-treatment of ultrafiltration and reverse osmosis membrane for wastewater reclamation: an autopsy study of a pilot plant. *Water research*, 46 (6).1803-1816.

19. Zhu, J.H., Yan, K.L., Liu, Y. and Zhang, B. 2006. Improving alachlor biodegradability by ferrate oxidation. *Journal of hazardous materials*, 135 (1-3), 94-99.

20. WORLD HEALTH ORGANIZATION. 1993. Guidelines for Drinking Water Quality, 2nd Edition, Volume 1: Recommendations. Geneva.

21. Bowen, H.J.M. 1979. Environmental chemistry of the elements. Academic Press, London.

22. Aucamp, P.J. and Viviers, F.S. 1990. Water quality criteria in South Africa. Technology SA, 21-30.

23. Morgan, L.G., Flint, G.N. 1989. Nickel alloys and coatings: release of nickel. In: Maibach HI, Menné T, eds. Nickel and the skin: immunology and toxicology. Boca Raton, FL, CRC Press, 45-54.

24. Rodriguez, R.E., Misra, M., Diwan, B.A., Riggs, C.W. and Kasprzak, K.S. 1996. Relative susceptibility of C57BL6, (C57BL6×C3HHe)F_1, and C3HHe mice to acute toxicity and carcinogenicity of nickel subsulfide. *Toxicology*, 107 (2),131-140.

25. Duguet, J.P. and Rizet M. 1996. Traitement du nickel dans la préparation des eaux de consommation. Techniques, Sciences, Méthodes, 91(10), 712–715.

26. Welté B. 2002. Le nickel: 4 Partie. Treatment techniques, sciences, méthodes, 97(5), 61-66.

27. Seco, A., Marzal, P., Gabaldon, C. and Ferrer, J. 1997. Adsorption of heavy metals from aqueous solutions onto activated carbon in single Cu and Ni systems and in binary Cu–Ni, Cu–Cd and Cu–Zn systems. *Journal of chemical technology and biotechnology*, 68(1), 23-30.

28. Parametrix. 2009. Cobalt concentrations in drinking, ground, and surface waters of the United States and Canada. Prepared by Parametrix, Albany, Oregon. CI study 50.

29. Kim, D.H., Kim, K.W. and Cho, J. 2006. Removal and transport mechanisms of arsenics in UF and NF membrane processes. *Journal of water and health*, 4 (2), 215-223.

30. Todar, K. Pathogenic *E. coli*. Online textbook of bacteriology. University of Wisconsin–Madison department of bacteriology. Retrieved 2018-01-12.

31. Edberg, S.C., Rice, E.W., Karlin, R.J. and Allen, M.J. 2000. *Escherichia coli*: the best biological drinking water indicator for public health protection. *Journal of applied microbiology*, 88, 106-116.

32. Gaffield, S., Goo, R., Richards, L. and Jackson, R. 2003. Public health effects of inadequately managed storm water runoff. *American journal of public health,* 93(9), 1527-1533.

33. Bates, R.G. 1973. Determination of pH: theory and practice. 2nd Edition, John Wiley & Sons, New York, London, Sydney, Toronto.

34. Covington, A. K., Bates, R. G. and Durst, R.A. 1985. Definitions of pH scales, standard reference values, measurement of pH, and related terminology. *Pure and applied chemistry*, 57 (3), 531-542.

35. McKee, J.E. and H.W. Wolf.1963. Water quality criteria, 2nd edition. California state water resources control board, publication no. 3-A. California.

36. APHA 1992. Standard Methods for the Examination of Water and Waste Water, 18th Edition. American Public Health Association, American Water Works Association, Water Environment Federation. Published by the American Public Health Association, Washington DC, USA.

37. Gray, J.R. 2004. Conductivity Analyzers and Their Application. Environmental Instrumentation and Analysis Handbook. Wiley. pp. 491-510.

38. Bockris, J.O.M., Reddy, A.K.N. and Gamboa-Aldeco, M. 1998. Modern electrochemistry, 2nd. Ed., Springer. ISBN 0-306-45555-2.

39. Koski, T.A., Stuart, L.S. and Ortenzio, L.F. 1966. Comparison of chlorine, bromine, iodine as disinfectants for swimming pool water. *Applied microbiology*, 14 (2), 276-279.

40. Connell, D. 1999. Introduction to ecotoxicology. *Blackwell science*. 68-70.

41. Gribble, G.W.1998. Naturally occurring organohalogen compounds. *Accounts of chemical research journal*, 31. 141-152.

42. Gunten, U. 2003. Ozonation of Drinking Water: Part II. Disinfection and by-products formation in the presence of bromide, iodide or chlorine. *Water research* 37, 1469-1487.

43. Margot, J., Magnet, A., Thonney, D., Chevre, N., Alencastro, F., Kienle, C., Abeggien, C., Barry, D.A. and Rossi, L. 2011. Elimination of micropollutants in wastewater treatment plants: ozonation or activated carbon? conclusions of a one-year pilot project. In: SETAC Europe 21st Annual meeting, Milano, Italy.

44. Chowdhury, S., Balasubramanian, R. and Das, P. 2015. Novel carbon-based nanoadsorbents for removal of synthetic textile dyes from wastewaters. *Green chemistry for dyes removal from wastewater*, 35-82.

45. Qu, X.L., Brame, J., Li, Q. and Alvarez, J.J.P. 2013. Nanotechnology for a safe and sustainable water supply: enabling integrated water treatment and reuse. *Accounts of Chemical Research* 46 (3), 834-843.

46. Lin, D.H. and Xing, B.S. 2008. Adsorption of phenolic compounds by carbon nanotubes: role of aromaticity and substitution of hydroxyl groups. *Environmental science and technology* 42(19), 7254-7259.

47. Rao, G.P., Lu, C. and Su, F. 2007. Sorption of divalent metal ions from aqueous solution by carbon nanotubes: a review. *Separation and purification technology* 58 (1), 224-231.

48. Lakshmanan, R., Okoli, C., Boutoneet, M., Jaras, S. and Rajarao, GK. 2013. Effect of magnetic iron oxide nanoparticles in surface water treatment: Trace minerals and microbes. *Bioresource technology,* 129, 612-615

49. Ganesan, V., Louis, C. and Damodaran, S.P. 2018. Graphene oxide-wrapped magnetite nanoclusters: A recyclable functional hybrid for fast and highly efficient removal of organic dyes from wastewater. *Journal of environmental chemical engineering*, 6, 2176-2190.

50. Li, Y.H., Zhao, Y.M., Hu, W.B., Ahmad, I., Zhu, Y.Q. and Pend, X.J. 2007. Carbon nanotubes - the promising adsorbent in wastewater treatment. *Journal of physics: conference series*, 61, 698-702.

51. Sambaza, S.S., Masheane, M.L., Malinga, S.P., Nxumalo, E.N. and Mhlanga, S.D. 2017. Polyethyleneimine-carbon nanotube polymeric nanocomposite adsorbents for the removal of Cr^{6+} from water. *Physics and chemistry of the earth, parts A/B/C,* 100, 236-246.

52. Crooks, R.M., Zhao, M., Sun, L., Chechik, V. and Yeung, L.K. 2001. Dendrimer-encapsulated metal nanoparticles: synthesis, characterization, and applications to catalysis. *Accounts of chemical research*, 34(3), 181-190

53. Diallo, M.S, Christie, S., Swaminathan, P., Johnson, J.H Jr. and Goddard, W.A 3rd. 2005. Dendrimer enhanced ultrafiltration. 1. Recovery of Cu(II) from aqueous solutions using PAMAM dendrimers with ethylene diamine core and terminal NH_2 groups. *Environmental science & technology* 39,1366-1377.

54. Pal. P. and Pal A. 2017. Surfactant-modified chitosan beads for cadmium ion adsorption. *International journal of biological macromolecules,* 104, 1548-1555.

55. Rahmi, M.N. 2018. Comparison of cadmium adsorption onto chitosan and epichlorohydrin crosslinked chitosan/eggshell composite. IOP Conf. Series: *Materials science and engineering,* 352.

56. Yaacoubi, H., Zidani, O., Mouflih, M., Gourai, M. Sebti, S. 2014. Removal of cadmium from water using natural phosphate as adsorbent. *Procedia engineering*, 83, 386- 393.

57. Wang, D., Liu, L., Jiang, X., Yu, J. and Chen, X. 2015. Adsorption and removal of malachite green from aqueous solution using magnetic β-cyclodextrin-graphene oxide nanocomposites as adsorbents. *Colloids and surfaces A: physicochemical and engineering aspects*, 466, 166-173.

58. Tansel, B. 2008. New technologies for water and wastewater treatment: a survey of recent patents. *Recent patents on chemical engineering* 1, 17-26.

59. Mulder M. 1996. Basic principles of membrane technology. kluwer academic publishers, Netherlands.

60. Choi, J.H., Jegal, J., Kim, W.N., 2006. Fabrication and characterization of multi-walled carbon nanotubes/polymer blend membranes. *Journal of membrane science* 284 (1-2), 406-415.

61. Song, H., Shao, J., Wang, J. and Zhong, X. 2014. The removal of natural organic matter with LiCl–TiO_2-doped PVDF membranes by integration of ultrafiltration with photocatalysis. *Desalination,* 344, 412-421.

62. Mallevialle, J. Anselme, C. and Marsigny, O. 1996. Effect of humic substances on membrane process. Aquatic humic substances, proceedings of the 193rd meeting of the *American chemical society*, Denver, CO., 749-767.

63. Maartens, A. Swart P. and Jacobs, E.P. 1998. Humic membrane foulants in natural brown water: characterization and removal. *Desalination*, 153. 215-227.

64. Schafer, A.I. Fane A.G. and Waite, T.D. 2000. Fouling effect on rejection in the membrane filtration of natural waters. *Desalination*, 131. 215-224.

65. Tang, S. Wang, Z. Wu, Z. and Zhou, Q. 2010. Role of dissolved organic matters (DOM) in membrane fouling of membrane bioreactors for municipal wastewater treatment. *Journal of hazardous materials*, 178, 377-384.

66. Fan, L., Harris, J.L., Roddick, F.A. and Booker, N.A. 2001. Influence of the characteristics of natural organic matter on the fouling of microfiltration membranes. *Water research*, 35, 4455-4463.

67. Cloete, T.E., Kwaadsteniet, M., Botes, M. and Lopez-Romero, J.M., 2010. Nanotechnology in water treatment applications. Caister academic press.

68. Zhang, T.C. 2012. Environmental, water resources institute. membrane technology task, c., and American society of civil, e., membrane technology and environmental applications, Reston, VA: American society of civil engineers.

69. Mohanty, K. and Purkait, M.K. (2010), Membrane technologies and applications, Boca Raton FL: CRC Press. USA.

70. Ridgway, H.F. and Safarik, J. 1991. Biofouling of reverse osmosis membranes. In biofouling and biocorrosion in industrial water system; Flemming, H.C., Geesey, G.G., Ed. Springer Verlag: Heidelberg, Germany, 81-111.

71. Kramer, J.F and Tracey, D.A. 1995. The solution to reverse osmosis biofouling. In proceedings of IDA world congress on desalination and water use, Abu Dhabi, Saudi Arabia, 4, 33-44.

72. De Gusseme, B., Hennebel, T., Christiaens, E., Saveyn, H., Verbeken, K., Fitts, J.P., Boon, N. and Verstraete, W. 2011. Virus disinfection in water by biogenic silver immobilized in polyvinylidene fluoride membranes. *Water research,* 45(4), 1856-1864.

73. Adams, FV., Nxumalo, EN., Krause, RWM., Hoek, EMV. And Mamba, BB. 2014. Application of polysulfone/cyclodextrin mixed-matrix membranes in the removal of natural organic matter from water. *Physics and chemistry of the earth* 67-69, 71-78.

74. Xue, X., Xu, J., Baig, S.A. and Xu, X. 2016. Synthesis of graphene oxide nanosheets for the removal of Cd(II) ions from acidic aqueous solutions. *Journal of the Taiwan institute of chemical engineers*, 59, 365-372.

75. Ihsanullah., Patel, F., Khraisheh, M., Atieh, M.A. and Laoui, T. 2017. Novel aluminum oxide-impregnated carbon nanotube membrane for the removal of cadmium from aqueous solution. *Materials*, 10, 1144.

76. Ekambaram, K. and Doraisamy, M. 2016. Study on the fabrication, characterization and performance of PVDF/ calcium stearate composite nanofiltration membranes. *Desalination*, 385, 24-38.

77. Lind, M.L., Ghosh, A.K., Jawor, A., Huang, X.F., Hou, W., Yang, Y. and Hoek, E.M.V. 2009. Influence of zeolite crystal size on zeolite polyamide thin film nanocomposite membranes. *Langmuir* 25 (17), 10139-10145.

78. Jeong, B.H., Hoek, E.M.V., Yan, Y.S., Subramani, A., Huang, X.F., Hurwitz, G., Ghosh, A.K. and Jawor, A. 2007. Interfacial polymerization of thin film nanocomposites: a new concept for reverse osmosis membranes. *Journal of membrane science,* 294(1-2), 1-7.

79. Kadhom, M., Yin, J. and Deng, B. 2016. A thin film nanocomposite membrane with MCM-41 silica nanoparticles for brackish water purification. *Membranes*, 6, 50.

80. Pala, A., Politi, RR., Kursun, G., Erol, M., Bakal, F., Oner, G. and Celik, E. 2015. Photocatalytic degradation of cyanide in wastewater using new generated nano-thin film photocatalyst. *Surface & coatings technology,* 271, 207-216

81. Sukitpaneenit, P. and Chung, T.S. 2011. Molecular design of the morphology and pore size of PVDF hollow fibre membranes for ethanol-water separation employing the modified pore-flow concept. *Journal of membrane science,* 374, 67-82.

82. Wang, Q., Wang, Z. and Wu, Z. 2012. Effects of solvent compositions on physicochemical properties and anti-fouling ability of PVDF microfiltration membranes for waste water treatment. *Desalination,* 297, 79-86.

83. Feng, C., Khulbe, K.C., Matsuura, T., Gopal, R., Kaur, S., Ramakrishna, S. and Khayet, M. 2008. Production of drinking water from saline water by air-gap membrane distillation using polyvinylidene fluoride nanofiber membrane, *Journal of membrane science,* 311, 1-6.

84. Mansouri, J., Harrisson, S. and Chen, V. 2010. Strategies for controlling biofouling in membrane filtration systems: challenges and opportunities. *Journal of materials chemistry*, 20, 4567.

85. Shi, H., Liu, F. and Xue, L. 2013. Fabrication and characterization of antibacterial PVDF hollow fibre membrane by doping Ag-loaded zeolites. *Journal of membrane science*, 437, 205-215.

86. Stephan, A.M., Kumar, S.G., Renganathan, N.G. and Kulandainathan, M.A. 2005. Characterization of poly(vinylidene fluoride-hexafluoropropylene) (PVdF-

HFP) electrolytes complexed with different lithium salts. *European polymer journal*, 41, 15-21.

87. Su, F. and Miao, M. 2014. Effect of MWCNT dimension on the electrical percolation and mechanical properties of poly(vinylidenefluoride-hexafluoropropylene) based nanocomposites. *Synthetic metals, 191*, 99-103.

88. Tian, X. and Jiang, X. 2008. Poly(vinylidene fluoride-co-hexafluoropropene) (PVDF-HFP) membranes for ethyl acetate removal from water. *Journal of hazardous materials*, 153, 128-135.

89. Zhang, Y., Jin, Z., Shan, X., Sunarso, J. and Cui, P. 2011. Preparation and characterization of phosphorylated Zr-doped hybrid silica/PSF composite membrane. *Journal of hazardous materials,* 186, 390-395.

90. Zhang, Y., Shana, L., Tua, Z. and Zhang. Y. 2008. Preparation and characterization of novel Ce doped nonstoichiometric nanosilica/polysulfone composite membranes. *Separation and purification technology*, 63, 207-212.

91. Saha, N.K., Balakrishnan, M. and Ulbricht, M. 2009. Fouling control in sugarcane juice ultrafiltration with surface modified polysulfone and polyethersulfone membranes. *Desalination,* 249, 1124-1131.

92. Richards, H.L., Baker, P.G.L. and Iwuoha, E. 2012. Metal Nanoparticle Modified Polysulfone Membranes for Use in Wastewater Treatment: A critical review. *Journal of surface engineered materials and advanced technology*, 2, 183-193.

93. Updegraff, D.M. 1969. Semimicro determination of cellulose in biological materials. *Analytical biochemistry*, 32, 420-424.

94. Smook, G.A. 2003. Handbook for pulp & paper technologists, 3rd Ed. Angus wilde publications.

95. Habibi, Y. 2014. Key advances in the chemical modification of nanocelluloses. *Chemical society reviews,* 43,1519-1542.

96. Sehaqui, H., Zhou, Q., Ikkala, O. and Berglund, L.A. 2011. Strong and tough cellulose nanopaper with high specific surface area and porosity. *Biomacromolecules*. 12, 3638-3644.

97. Carpenter, A.W., De Lannoy, C. and Wiesner, M.R. 2015. Cellulose nanomaterials in water treatment technologies. E*nvironmental science & technology*, 49, 5277-5287.

98. Karim, Z., Mathew, A.P., Grahn, M., Mouzon, J. and Oksman, K. 2014. Nanoporous membranes with cellulose nanocrystals as functional entity in chitosan: Removal of dyes from water. *Carbohydrate polymers,* 112, 668-676.

99. Sotto, A., Kim, J., Arsuaga, J.M., de Rosario, G., Martinez, A., Nam, D., Luis, P. and Van der Bruggen, B. 2014. Binary metal oxides for composite ultrafiltration membranes. *Journal of materials chemistry* A, , 2, 7054-7064.

100. Pendergast, M.T.M., Nygaard, J.M., Ghosh, A.K. and Hoek, E.M.V. 2010. Using nanocomposite materials technology to understand and control reverse osmosis membrane compaction. *Desalination,* 261(3), 255-263.

101. Mayo, J.T., Yavuz, C., Yean, S., Cong, L., Shipley, H., Yu, W., Falkner, J., Kan, A., Tomson, M. and Colvin, V.L. 2007. The effect of nanocrystalline magnetite size on arsenic removal. *Science and technology of advanced materials,* 8 (1-2), 71-75.

102. Hristovski, K.D., Westerhoff, P.K., Moller, T. and Sylvester, P. 2009. Effect of synthesis conditions on nano-iron hydroxide impregnated granulated activated carbon. *Chemical engineering journal,* 146 (2), 237-243.

103. Liao, C., Yu, P., Zhao, J., Wang, L. and Luo, Y. 2011. Preparation and characterization of NaY/PVDF hybrid ultrafiltration membranes containing silver ions as antibacterial materials. *Desalination,* 272, 59-65.

104. Sawada, I., Fachrul, R., Ito, T., Ohmukai, Y., Maruyama, T. and Matsuyama, H. 2012. Development of a hydrophilic polymer membrane containing silver nanoparticles with both organic antifouling and antibacterial properties. *Journal of membrane science*, 387-388, 1-6.

105. Ahamed, M., AlSalhi, M. and Siddiqui, M. K. J. 2010. Silver nanoparticle applications and human health. *Clinica chimica acta,* 411, 1841-1848.

106. Karumuri, A.K., Oswal, D.P., Hostetler, H.A. and Mukhopadhyay, S.M. 2013. Silver nanoparticles attached to porous carbon substrates: robust materials for chemical-free water disinfection. *Materials letters 109,* 83-87.

107. Rananga, L.E. and Magadzu T. 2014. Interaction of silver doped carbon nanotubes-cyclodextrin nanocomposites with Escherichia coli bacteria during water purification. *Water science & technology: water supply* 14.3. 367 - 373.

108. Tran, Q. H., Nguyen, V. Q. & Le, A. 2013. Silver nanoparticles: synthesis, properties, toxicology, applications and perspectives. Advances in natural sciences: nanoscience and nanotechnology 4, 033001.

109. Sato, K. and Anzai, J. 2013. Dendrimers in layer-by-layer assemblies: synthesis and applications. *Molecules*, 18, 8440-8460.

110. Hayati, B., Mahmoodi, N.M. and Maleki A. 2015. Dendrimer-titania nanocomposite: synthesis and dye-removal capacity. *Research on chemical intermediates,* 41, 3743-3757.

111. Hayati, B., Arami, M., Maleki, A. and Pajootan, E. 2015. Thermodynamic properties of dye removal from colored textile wastewater by poly (propylene imine) dendrimer. *Desalination and water treatment*, 56, 97-106.

112. Maleki, A., Jebelli, M.A., Hayati, B., Daraei, H. and Gharibi, F. 2015. Antimicrobial effect of poly(amidoamine)-G2 and G4 dendrimers on some bacteria in water resources, *Journal of Mazandaran university of medical sciences*, 25.

113. Grossiord, N., Loos, J., van Laake, L., Maguey M, Zakri, C., Koning, CE., Hart, A.J. 2008. High-conductivity polymer nanocomposites obtained by tailoring the characteristics of the carbon nanotube fillers. *Advanced functional materials*, 18, 3226-3234.

114. Hamwi A, Alvergnat H, Bonnamy S, Beguin F. 1997. Fluorination of carbon nanotubes. *Carbon*, 35, 723-728.

115. Wongchitphimon, S., Wang, R., Jiraratananon, R., Shi, L. and Loh, C.H. 2011. Effect of polyethylene glycol (PEG) as an additive on the fabrication of polyvinylidene fluoride-co-hexafluropropylene (PVDF-HFP) asymmetric

microporous hollow fiber membranes. *Journal of membrane science*, 369, 329-338.

116. Liu, F., Hashim, N.A., Liu, Y., Abed, M.R.M. and Li, K. 2011. Progress in the production and modification of PVDF membranes. *Journal of membrane science*, 375, 1-27.

117. Wang, D. Li, K. Teo, W. 1999. Preparation and characterization of polyvinylidene fluoride (PVDF) hollow fiber membranes, *Journal of membrane science,* 163, 211-220.

118. Strathmann, H. and Kock, K. 1996. Recent advances in the formation of phase inversion membranes made from amorphous or semi-crystalline polymers. *Journal of membrane science*, 113, 361-371.

119. Uekama, K. 2002. Recent aspects of pharmaceutical application of cyclodextrins. *Journal of Inclusion Phenomena and Macrocyclic Chemistry*, 44 (1-4), 3-7.

CHAPTER 3

METHODOLOGY

3.1 MATERIALS

All chemicals were of analytical reagent grade and were used as received, whilst some were further purified when required. Sodium dodecyl sulphate (SDS), hydrazine hydrate, MWCNTs (>95% purity), poly(vinylidene fluoride-co-hexafluoropropene), N,N-dimethylacetamide (DMAc), calcium sulphate, silver nitrate, sodium citrate, nitric acid, sulphuric acid, polyethylene glycol (PEG), polyvinylpyrrolidone (PVP), toluene 2,4-diisocyanate, ethylenediamine, methyl acrylate (MA), methanol and ethanol were all purchased from Sigma Aldrich. *Escherichia coli* (*E. coli),* ATCC 25922 bacteria, bacteriological agar and nutrient broth were purchased from Merck.

3.2 ACID TREATMENT OF CARBON NANOTUBES

Acid treated MWCNTs and Ag-MWCNTs were prepared following a method described elsewhere [1]. Approximately 1 g of MWCNTs was sonicated at 25 ^{o}C in a 1:3 (v/v) mixture of each HNO_3:H_2SO_4. After 3 h of sonication, the functionalised MWCNTs were diluted with 200 mL of distilled water and filtered through a 0.45 µm pore sized nylon membrane. The fMWCNTs were then washed thoroughly with distilled water until a neutral pH is reached, and then dried at room temperature overnight.

3.3 PREPARATION OF Ag NANOPARTICLES AND Ag-MWCNTs

For the synthesis of silver nanoparticles, sodium dodecyl sulphate (SDS) (0.1 g) was added into a solution of silver nitrate (50 ml, 0.1 M). Silver nitrate was used as a metal precursor and SDS as a stabilizing agent [2]. A 1:1 solution of hydrazine hydrate (25 mL) and sodium citrate (25 mL, 0.1M) was added drop-wise to a mixture of SDS, MWCNTs and $AgNO_3$ for 2 h while stirring at room temperature. The mixture was left to stir for an additional 48 h, after which the precipitates were filtered and washed with distilled water, acetone and ethanol. Hydrazine hydrate solution was used as reducing agents while Sodium citrate was also used both as reducing agent and stabilizing

agent at room temperature [1]. To prepare Ag-MWCNTs, the same procedure described above was followed wherein $AgNO_3$ (50 mL, 0.01 M) and SDS (0.1 g) was added to a round bottom flask containing 0.2 g MWCNTs.

3.4 PREPARATION OF DENDRITIC MULTI-WALLED CARBON NANOTUBES

Anhydrous acetone used was prepared as follows: About 10 g of calcium sulphate was added to a 1 L bottle followed by addition of 1000 mL acetone (98%). The bottle was well shaken and left to settle for 24 h, allowing the salt to sink to the bottom, which was done to get rid of water in the acetone. Anhydrous methanol was also prepared following the same procedure. The same method can be performed using magnesium sulphate instead of calcium sulphate.

3.4.1 Preparation of MWCNTs functionalised with the NCO group

About 2 g of fMWCNTs was dispersed in anhydrous acetone (20 mL) under stirring for 30 minutes. This was followed by drop-wise addition of 4 mL toluene 2,4-diisocyanate, under dry nitrogen atmosphere at 25 °C for 1 h. The mixture was allowed to stir for an additional 23 h, after which the MWCNTs-NCO was washed with anhydrous acetone to completely remove the residuals, filtered and left to dry at room temperature overnight [3].

3.4.2 Preparation of MWCNTs-NH_2 initiator from MWCNTs-NCO

Approximately 0.5 g of produced MWCNTs-NCO was dispersed in 20 mL of anhydrous acetone under sonication for 30 minutes, and then an excess amount of ethylenediamine was added drop-wise while stirring for 1 h at 25 °C under a nitrogen atmosphere. The reaction was allowed to continue for 24 h. The resulting solid was washed with anhydrous methanol, filtered and dried overnight under vacuum, generating MWCNT-NH_2 [4].

3.4.3 Preparation of poly (amidoamine) dendrimer on the MWCNTs surface initiated by MWCNTs-NH_2

Michael addition of methyl acrylate (MA) to peripheral amino groups was carried out following a procedure described by Yuan *et al*., 2008: Briefly, approximately 0.3 g of MWCNTs-NH_2 was dispersed in methanol (20 mL) under stirring and then added to 40 mL of methanol/MA solution (1:1). The mixture was allowed to react for 48 h at 30 °C under nitrogen atmosphere. The resulting solid was filtered, washed with distilled water and dried; yielding functionalised MWCNTs containing the “first generation” ester group (MWCNTs-$G_{0.5}$-$COOCH_3$).

The amidation of the terminal groups of MWCNTs-$COOCH_3$ was carried out by the same procedure as discussed above using EDA instead of MA. About 0.2 g of MWCNTs-$G_{0.5}$-$COOCH_3$ was dispersed in methanol (20 mL) under stirring and then added to 40 mL of methanol/EDA solution (1:1). The mixture was allowed to react for 48 h at 30 °C. The resulting solid was washed with methanol, filtered, and dried; yielding functionalised MWCNTs containing the “first generation” amino groups (MWNTs-G_1-NH_2) [5].

3.4.4 Preparation of PAMAM-MWCNTs-Ag nanoparticles

For the synthesis of PAMAM-Ag nanocomposites, SDS (0.1 g) was added into a solution of silver nitrate (50 mL, 0.1 M) and 1:1 solutions of hydrazine hydrate (25 mL, 0.1 M) and sodium citrate (25 mL, 0.1 M) were added drop-wise to a round bottom flask containing 0.5 g PAMAM-MWCNTs mixture, SDS and $AgNO_3$ for 2 h while stirring at room temperature. The mixture was left to stir for an additional 46 h, after which the precipitates were filtered and washed with distilled water, acetone and ethanol.

3.5 PREPARATION PVDF-HFP NANOCOMPOSITE MEMBRANES

3.5.1 Preparation of PVDF-HFP membranes

PVDF-HFP membranes were prepared by a phase inversion process described in literature [6]. Approximately 2.0 g of PVDF-HFP was dissolved in 15 mL of DMAc at

80 ^{o}C to form a polymer solution. To this solution, about 0.62 g of PVP was added (to enhance pore formation) and the reaction mixture was stirred for 2 h at 80 ^{o}C. The mixture was allowed to stir for an additional 1 h and then hand cast into a glass plate using a casting knife (Elcometer 3580 adjustable bird film applicator, BAMR, Cape Town, South Africa) of 180 µm thickness. The prepared membranes were first dried in a vacuum oven at 80 ^{o}C (for 30 s) for solvent pre-evaporation and then coagulated using distilled water (at 5 ^{o}C) as the anti-solvent. After complete coagulation, the membranes were dried on plain sheets of paper at room temperature.

3.5.2 Preparation of MWCNTs/PVDF-HFP nanocomposite membranes

The polymer solution was prepared by heating and dissolving PVDF-HFP (2 g) in 15 ml DMAc at 80 ^{o}C to form a polymer solution. To this solution, about 0.62 g of PVP was added and the reaction mixture was stirred for 2 h at 80 ^{o}C. Separately 0.021 g fMWCNTs were also sonicated in 5 ml DMAc for 30 minutes. The final mixture was prepared by adding the sonicated fMWCNTs to the PVDF-HFP solution. The resultant mixture was left to stir for another 1 h, and afterwards hand cast into a glass plate using a casting knife (Elcometer 3580 adjustable bird film applicator) of 180 µm thickness. The membrane was first dried in a vacuum oven at 50 ^{o}C (for 30 s) for solvent pre-evaporation and then coagulated using distilled water (at 5 ^{o}C) as the anti-solvent. After complete coagulation, the membranes were dried on plain sheets of paper towel at room temperature. The same procedure was repeated to prepare 1.5 wt.% MWCNTs/PVDF-HFP, wherein 0.03 g of fMWCNTs was used.

3.5.3 Preparation of Ag/PVDF-HFP nanocomposite membrane

Approximately 2.0 g of PVDF-HFP was dissolved in 15 mL of DMAc at 80 ^{o}C to form a polymer solution. To this solution, about 0.62 g of PVP was added and the reaction mixture was stirred for 2 h at 80 ^{o}C. Separately 0.1 g Ag nanoparticles were also sonicated in 5 ml DMAc for 30 minutes. The final mixture was prepared by adding sonicated Ag to the PVDF-HFP solution. The resultant mixture was left to stir for another 1 h, and then hand cast into a glass plate using a casting knife (Elcometer 3580 adjustable bird film applicator) of 180 µm thickness. The membrane was first

dried in a vacuum oven at 50 ^{o}C (for 30 s) for solvent pre-evaporation and then coagulated using distilled water (at 5 ^{o}C) as the anti-solvent. After complete coagulation, the membranes were dried on plain sheets of paper towel at room temperature.

3.5.4 Preparation of Ag-MWCNTs/PVDF-HFP nanocomposite membranes

About 2 g of PVDF-HFP was dissolved in 15 ml DMAc at 80 ^{o}C to form a polymer solution. To this solution, about 0.62 g of PVP was added and the reaction mixture was stirred for 2 h at 80 ^{o}C. Separately 0.052 g of Ag-MWCNTs was also sonicated in 5 ml DMAc for 30 minutes. The final mixture was prepared by adding sonicated Ag-MWCNTs to the PVDF-HFP solution. The resultant mixture was left to stir for another 1 h and afterwards hand cast into a glass plate using a casting knife (Elcometer 3580 adjustable bird film applicator) of 180 µm thickness. The membrane was first dried in a vacuum oven at 50 ^{o}C (for 30 s) for solvent pre-evaporation and then coagulated using distilled water (at 5 ^{o}C) as the anti-solvent. After complete coagulation, 2.5% Ag-MWCNTs/PVDF-HFP membranes were dried on plain sheets of paper towel at room temperature. The same procedure was repeated to prepare 3 wt.% Ag-MWCNTs/PVDF-HFP membrane.

3.5.5 Preparation of Ag-PAMAM-MWCNTs/PVDF-HFP nanocomposite membranes

Approximately 2 g of PVDF-HFP was dissolved in 15 ml DMAC at 80 ^{o}C to form a polymer solution. To this solution, about 0.62 g of PVP was added and the reaction mixture was stirred for 2 h at 80 ^{o}C. Separately 0.037 g of Ag-PAMAM-MWCNTs was sonicated in 5 ml DMAC for 30 minutes. The final mixture was prepared by adding sonicated Ag-PAMAM-MWCNTs to the PVDF-HFP solution. The resultant mixture was left to stir for another 1 h then hand cast into a glass plate using a casting knife (Elcometer 3580 adjustable bird film applicator) of 200 µm thickness. The membrane was first dried in a vacuum oven at 50 ^{o}C (for 30s) for solvent pre-evaporation and then coagulated using distilled water (at 5 ^{o}C) as the anti-solvent. After complete

coagulation, the membranes were dried on plain sheets of paper towel at room temperature.

3.6 CHARACTERISATION OF MEMBRANES

3.6.1 X-Ray powder diffraction

X-Ray powder diffraction patterns of the synthesised nanomaterials and PVDF-HFP composite membranes were determined on a Philips x-ray diffractometer PW 1830 which is a bench-top type with high intensity Cu-Kα radiation (λ = 1.54 Å) and a graphite monochrometer at a scanning rate of 0.02 s^{-1} ranging from 10 to 80^{o}. The diffractometer was operated at 30 kV and 10 mA current.

3.6.2 Scanning electron microscopy

A Focused Ion Beam Scanning electron microscopy (FIB-SEM) (Auriga Zeiss-39-42 SEM with Germini FE-SEM column) was used to investigate the morphology the PVDF-HFP membrane. The FIB-SEM was operated at accelerating velocities of 15 kV and 17 kV. The polymeric membranes were placed on a carbon tape, stuck to an aluminium stud and coated with gold and palladium (1:1) to provide a reflective surface for the SEM imaging. Membrane cross sections were prepared by dropping them in liquid nitrogen followed by sectioning them before putting them on a carbon tape. The EDX of membranes was also done from the same instrument for elemental analysis.

3.6.3 Transmission Electron Microscope

A JEOL, JEM-2100 Transmission Electron Microscope was used to observe the internal structure of the samples. The microscope had accelerating voltage from 80 to 200 kV and standard magnification from 5000 to 300000 x. Images were acquired using a peltier-cooled CCD camera KeenView. The EDX of nanoparticles was also done from the same instrument for elemental analysis.

3.6.4 Fourier-transform infrared spectroscopy

Agilent Cary 600 series FTIR spectrophotometer was used in these studies. The instrument was calibrated by running the background first, followed by collecting the sample which was loaded as received on the sampling plate. The results obtained were exported and then plotted using Origin 6.1 software program. FTIR spectra were collected and recorded with characteristic peaks in wavenumbers from 650 to 4000 cm^{-1}.

3.6.5 Thermogravimetric analysis

Thermogravimetric analysis was carried out in a TGA Q500 (V20.13 Build 19 software used) heating at a range of 30 ^{o}C to 900 ^{o}C in oxygen and nitrogen gas. The samples were degassed with nitrogen.

3.6.6 Brunauer-Emmett-Teller analysis

Brunauer-Emmett-Teller analysis was carried out on a Micromeritics ASAP 2020 instrument. A sample of about 200 to 300 mg was degassed at 150 ^{o}C for 3 hours under vacuum. Nitrogen was used as the probe gas.

3.6.7 Contact angle (Sessile-drop method)

The wettability and surface hydrophilicity of the PVDF-HFP membranes and MWCNTs were evaluated by the DATA Physics optical contact angle SCA 20 (version 4.1.12 build 1019 software) using the sessile drop measurement method. A 1 µL drop of deionised (DI) water was placed on a flat membrane surface using a Gilmont syringe. Droplets were contacted with the membrane at 5 different locations on each membrane sample taking data at each point. All measurements were carried out at room temperature. Generally, a small angle is associated with higher hydrophilicity and vice versa.

3.7 PERMEATION TESTS

3.7.1. Swellability tests

The membranes were first weighed and then soaked in distilled water for 7 h after which they were weighed again in the balance [7].

3.7.2. Water content and porosity measurements

The membranes where immersed in distilled water for 24 h after which, the weight of the wet membrane (W_0) was obtained. The wet membrane was then dried in an oven at 80 ºC for 24 h after which it was weighed (W_1) to obtain the dry weight [8,9].

3.8. SALT REJECTION TESTS AND FOULING TEST STUDIES

Desalination test using composite membranes were carried out for 120 minutes. All the membranes had an effective area of 0.00126 m^2. The pervaporation desalination performance of PVDF-HFP membranes was evaluated by measuring water flux and salt rejection. The water flux (J) was determined from permeate volume (V) measured in (L), the effective membrane area (A) and the time (t) necessary for the volume to be collected [10,11].

3.9 MICROBIAL STUDIES AND ANTIBACTERIAL APPLICATION IN WATER TREATMENT

3.9.1 Preparation of culture media

Nutrient broth and nutrient agar media were prepared according to the manufacturer's instructions. Briefly, about 6.2 g bacteriological agar was added in 200 mL of distilled water. The solution was then heated while stirring until it completely dissolved. The resulting clear solution was autoclaved for 30 min, poured into sterile petri-dishes and allowed to set in the laminar flow.

3.9.2 Resuscitation of the test culture

Escherichia coli (ATCC 25922) was used as a test organism in this study. The glycerol stock culture of *E. coli* was revived in nutrient broth solution in a shaking incubator (New Brunswick G 25 Shaker Incubator) at 200 rpm for 24 h at 37 ^{o}C.

3.9.3 Antibacterial and entrapment analysis

3.9.3.1 Antibacterial and entrapment analysis of *E. coli* spiked water

Hundred millilitres of sterilised deionised water were spiked with an overnight culture of *E. coli*. This was followed by vacuum-filtration through the prepared PVDF-HFP based membranes. The filter membranes were then placed on nutrient agar plates and incubated for 24 h at 37 ^{o}C. Following incubation, the plates were observed for growth on and around the filter membranes for antibacterial and leaching properties. Antibacterial activity was further confirmed by placing a piece of the used membrane in nutrient broth and observed for growth following an overnight incubation at 37 ^{o}C. All experimental procedures were performed in triplicates. A sterile membrane (MF-Millipore™ membrane filter, 0.45 µm pore size) was used as control. Bacterial enumeration was performed before and after filtration to evaluate the entrapment ability of the membranes. Hundred fold serial dilutions of the spiked water samples (100 µL) were spread plated on nutrient agar before filtration treatment, followed by plating 100 µL of the filtrate. Bacterial counts were expressed as colony forming units per millilitres (CFU/ mL).

3.9.3.2 Antibacterial and entrapment analysis of surface and ground water

Surface water samples were collected from Olifants River next to Flag Boshielo dam, Makotswane dam, and Apel cross furrow in the Sekhukhune district, Limpopo province (figure 3.1). Borehole water samples were collected from three areas in Jerome, Malamulele and Shigalo village in Vhembe district, also in Limpopo province. All the water samples were collected into sterile bottles (2.5 L) and microbial analysis was performed within 6 hours of sampling. Both the ground and surface water were

sampled from water resources which are used by surrounding communities for domestic purposes.

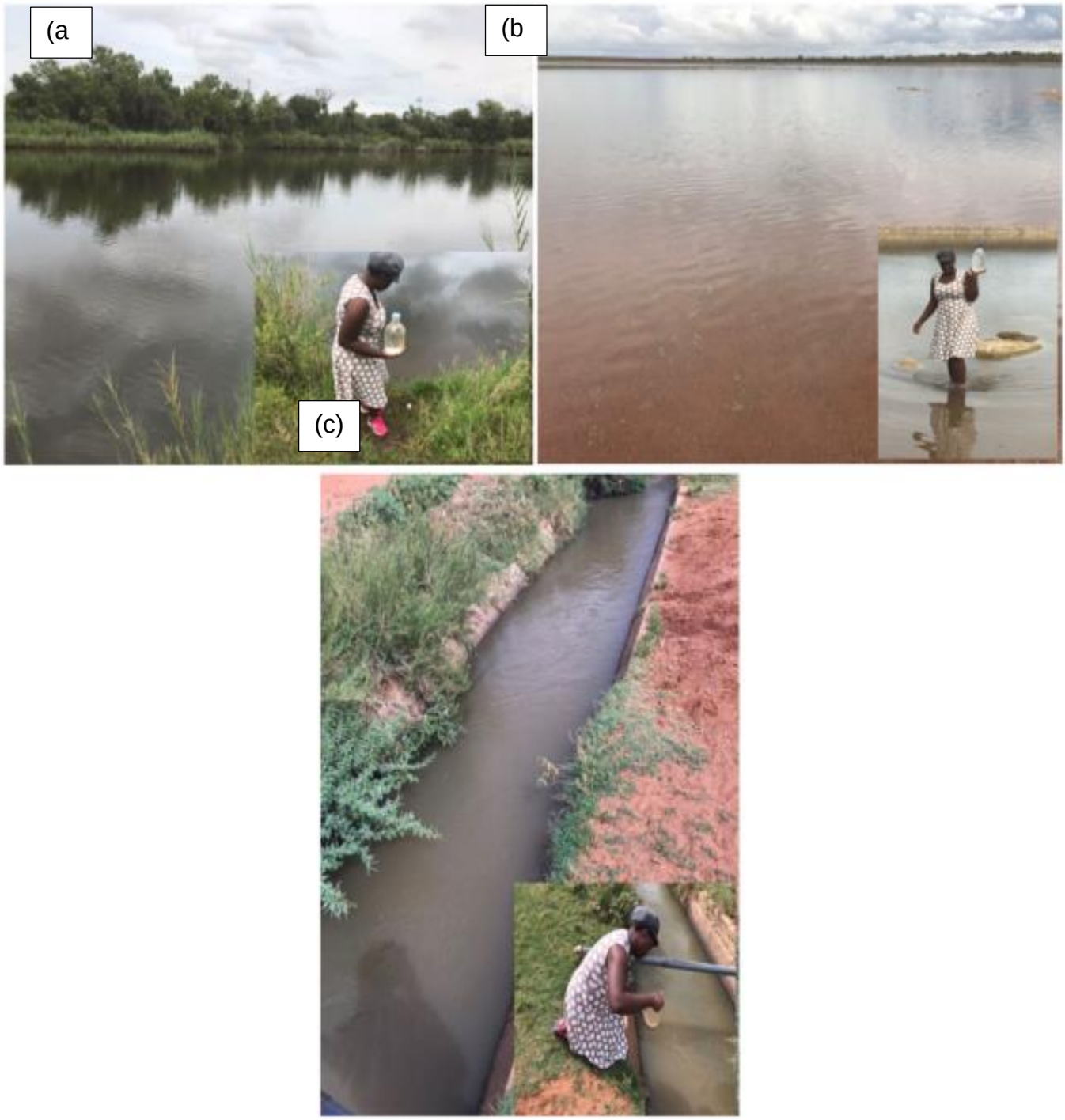

Figure 3.1: Sample water collection done at (a) Olifants river, (b) Makotswane dam and (c) Apel cross furrow

For microbial analysis, 10 mL of water was added to 100 mL of buffered peptone water. The mixture was shaken for 20 seconds using a stomacher. After shaking, 0.1 mL of the mixture was added into 3.9 mL of liquid media TEMPO AC used for enumeration of aerobic bacteria. A Tempo card was inserted into the liquid media containing the water sample, and was inserted into the Tempo filler. Inside the filler, the mixture of the media together with the samples was sucked from the bottle into the card. The cards were then removed from the filler and were incubated at 37 ^{o}C for 48 h. Following incubation, the cards were read using the Tempo reader; the colonies were enumerated as CFU/mL.

For enumeration of total coliforms and *E. coli* the same procedure was followed however, 1 mL of the mixture was added into 3 mL of the media and the incubation period was 24 hours.

3.9.4 Physical parameters

3.9.4.1 Conductivity

Conductivity was measured directly by placing the multi-parameter analyser (HI 991300 pH/EC/TDS meter) into the water samples. Conductivity was measured in µS/cm.

3.9.4.2 Colour and Turbidity

Turbidity, and colour was measured using UV/Vis NANOCOLOR® UV/vis spectrophotometer (Macherey-Nagel) at a wavelength of 620 nm. The apparent colour was determined by directly measuring the absorbance of the collected water samples and the true water colour was determined by measuring the absorbance of the water samples after filtering the water with glass fibre membranes. The test method number used for colour was Test 1-39, and the method used for measuring turbidity was Test 1-92 according to manufacturer's instruction.

3.9.4.3 Total suspended solids

Total suspended solids (TSS) (mg/L) were determined using the gravimetric method, in which initially the glass fibre membrane was weighed and the weight was recorded. For each test water sample, 100 mL was filtered through a pre-weighed glass membrane, the filter was dried at 105 ^{o}C until completely dry and the weight was recorded. This was done in duplicates and the average was calculated.

3.9.5 Chemical parameters

3.9.5.1 Total dissolved solids

Total dissolved solids (mg/L) were determined by using APHA 2540 method in which a dry glass beaker was initially weighed and the weight was recorded, then 100 mL of each sample was evaporated at 80 ^{o}C until the beaker was dry. The beaker was allowed to cool and the weight of the beaker was measured and recorded. This was done in duplicates and the average was calculated.

3.9.5.2 pH

The pH was measured directly by placing the multi-parameter analyser (HI 991300 pH/EC/TDS meter) into the water samples.

3.9.5.3 Hardness

Water hardness (mg/L) was measured with a UV/Vis NANOCOLOR® spectrophotometer (Macherey-Nagel) at wavelength of 620 nm. For total hardness, the total hardness nanokit was used following the manufacturer's instructions. For carbonate hardness the cuvette used for measuring total hardness was placed in the spectrophotometer and adjusted to zero. To determine the carbonate hardness, the Test 0-15 method was used according to manufacturer's instruction.

3.9.5.4 Biochemical oxygen demand (BOD)

Preparation of aerating water

To prepare aerating water, about 4 L of distilled water was added into an aerating bottle and aerated for 6 hours in the dark according to the manufacturer's instructions (Test no: 8221). Thereafter it was left for 1 hour to prevent oversaturated with oxygen. The pH of the water was maintained between 6 and 8 and the concentration of dissolved oxygen in the diluting water was 8 mg/L O_2.

Preparation of the control

To prepare the control, about 500 mL of aerated water was added to 1 L laboratory flask. 2.5 mL nutrient according to manufactures instruction (Test no: 8221) was added in the flask containing aerated water after which the flask was closed and shaken vigorously to prepare the control mixture. The same mixture was added into the Winkler oxygen flask and filled to the brim without air bubbles and incubated in a water bath at 20 ^oC for 5 days in the dark. The control mixture was added to the test tube which was measured immediately using a UV/Vis NANOCOLOR® spectrometer as control.

Preparation of the test sample

About 475 mL of aerated water was mixed with 25 mL of kitchen waste water. The same procedure was followed for preparing bath wastewater. The sample mixtures were then added into the Winkler oxygen flask and filled to the brim without air bubbles and incubated in a water bath at 20 ^oC for 5 days in the dark. Sample mixtures were also added to the test tubes which were measured immediately using a UV/Vis NANOCOLOR® UV/vis spectrometer as control.

Measurement of dissolved oxygen after 5 days

After 5 days of incubation, the test samples and control were each added in the test tubes and filled to the brim. 2 drops of BOD5 R 1 and R 2 nutrients were added to each test tube according to the manufacturer's instruction. The test tubes were closed,

shaken and left to settle for 2 minutes after which 5 drops of BOD5, R 3 was added to each test tube according to the manufacturer's instruction. The test tubes were closed tightly without air bubbles and shaken to dissolve the flakes after which the concentration of dissolved oxygen was measured for each test tube in the UV-Vis nanocolor spectrometer.

3.10 ADSORPTION STUDIES

The procedures described below were used to study Cadmium (II) and Chromium (VI) adsorption.

3.10.1 Effect of pH

The effect of pH on the adsorption capacity was examined by varying the initial pH of the solution. Approximately, 50 mL of metal standard solution (100 ppm) with different pH (4, 5, 5.5, 6, 6.5, 7 and 8) were prepared in glass vials and the membrane dosage of 0.5 g/L (i.e. 10 mg mass of the sample/20 mL volume of the solution) was added. About 0.1 M nitric acid (HNO_3) and 0.1 M sodium hydroxide (NaOH) were both used to adjust the pH of metal solutions. The Erlenmeyer flaks containing the metal solutions and the membranes were placed on a rotary shaker and shaken at room temperature (25 °C) for 48 hrs. At the end of 48 h, the residual metal concentration was measured using the Atomic Absorption Spectrophotometer (AAS). The amount of metal ions adsorbed in milligram per gram and percentage removal of Cd(II) ions were determined using the mass balance the equations below [12,13]:

$$q_e = \frac{(C_o - C_e)V}{m}$$

$$\%\ \text{removal} = \frac{(C_o - C_e}{C_o}\ \text{x}\ 100$$

where q_e is the equilibrium adsorption amount (mg/g), C_o is the initial concentration of metals in solution (mg/L), C_e is the equilibrium concentration of the metal adsorbed in solution (mg/L), m is the mass of adsorbent (g), and V is the volume of solution (L) [13].

The effect of adsorbent dosage for Chromium studies was also done. The adsorbent dosage is a key parameter for determining the adsorbent capacity for a given initial concertation [12,13]. The effect of the adsorbent dosage on the adsorption of Cr(VI) ions (100 ppm) was studied by varying the membrane dosage from 0.5 g/L to 10 g/L at a pH of 2.5 for 48 h.

3.10.2 Batch adsorption experiments

Adsorption studies were carried out by batch process. In batch process, PVDF-HFP composite membranes (10 mg) were placed in Erlenmeyer flasks containing Cd(II) solutions (20 mL) with different initial concentrations (20-100 mg/L). The membrane dosage was 0.5 g/L and the pH values of solutions were adjusted to 6.5 by 0.1 M nitric acid or sodium hydroxide solution. The Erlenmeyer flaks containing the metal solutions and the membranes were placed on a rotary shaker and shaken at different temperatures (15 °C, 25 °C, 35 °C and 45 °C) for 48 h. At the end of 48 h, the residual Cd(II) ions concentration was measured using AAS. For Chromium studies, an adsorption dosage of 5 g/L and the pH was 2.5. The experimental data was fitted to both Langmuir and Freundlich isotherms. The thermodynamics parameters were also evaluated

3.10.2.1 Adsorption kinetics

For kinetics studies, the Erlenmeyer flaks containing metal (100 mg/L) solutions and PVDF-HFP composite membranes (0.5 g/L) were placed on a rotary shaker and shaken at 25 °C while varying the contact time from 0 to 1600 minutes. At predetermined times, the flasks were withdrawn from the shaker and the reaction mixtures were measured using AAS. Experimental data were fitted to empirical kinetic models by nonlinear regression analyses to obtain the kinetic parameters for each of the systems studied at different temperatures. Lagergren's pseudo-first-order and a pseudo-second-order model were used to fit the data [14].

Lagergren's pseudo-first-order model and its linearised form are expressed in the equations below [15]:

$q_t = q_e(1 - e^{-k1t})$

In ($q_e - q_t$) = In$q_e - k_1 t$

The pseudo-second-order model is as follows:

$$\frac{t}{q_t} = \frac{1}{K_2 q_e^2} + \frac{t}{q_e}$$

where q_e (mg/g) and q_t (mg/g) are the concentrations of Cd(II) ions adsorbed at equilibrium and at time t respectively. k_1 (min^{-1}) is the pseudo-first-order kinetic constant (min^{-1}) and k_2 is the pseudo-second-order rate constant of sorption (g/mg·min).

3.10.2.2 Langmuir and Freundlich isotherms

The Langmuir isotherm and Freundlich isotherm model was used to fit the isotherm data.

The Langmuir isotherm and its linearised form are expressed in the equations below [15,16]:

$$q_e = \frac{q_{max} b C_e}{1 + b C_e}$$

$$\frac{1}{q_e} = \frac{1}{q_{max}} + \frac{1}{b q_{max} C_e}$$

where q_e is the equilibrium adsorption amount (mg/g), C_e (mg/L) is the equilibrium concentration of metal adsorbed in the solution, q_{max} (mg/g) represents the maximum adsorption capacity or the theoretical monolayer saturation capacity and b (L/mg) is the Langmuir equilibrium constant.

The essential features of the Langmuir isotherm indicating the favourability of the adsorption (R_L, also called equilibrium parameter) is expressed by equations below [15,17]:

$$R_L = \frac{1}{1 + b C_o}$$

where C_o (mg/L) is the initial metal concentration and b is Langmuir equilibrium constant for adsorption (L/mg). The value of R_L indicates the type of Langmuir isotherm to either be unfavourable adsorption (R_L>1), linear (R_L = 1), favourable (0 < R_L < 1) or irreversible (R_L = 0).

The Freundlich model and its linearised form are expressed in the equations below [17]:

$$q_e = K_f C_e^{1/n}$$

$$\ln q_e = \ln K_f + \frac{1}{n} \ln C_e$$

where q_e is the equilibrium adsorption amount (mg/g), C_e (mg/L) is the equilibrium concentration of metal adsorbed in the solution. K_f ($mg^{1-1/n}$ $L^{1/n}$ g^{-1}) and n (dimensionless) are Freundlich constants which correspond to adsorption capacity and adsorption intensity, respectively.

3.10.2.3 Thermodynamics parameters

Thermodynamic parameters were evaluated from the following equations [18]:

$$\Delta G^o = -RT \ln K_c$$

$$\ln K_c = \frac{\Delta S^\circ}{R} - \frac{\Delta H^\circ}{RT}$$

$$K_c = \frac{C_{ad}}{C_e}$$

where C_e (mg/L) is the equilibrium concentration of metal adsorbed in the solution and C_{ad} is the concentration of the metal in the adsorbent at equilibrium (mg/L). ΔG^o, ΔH^o and ΔS^o are changes in the standard Gibbs free energy (kJ/mol), standard enthalpy (kJ/mol) and standard entropy (J/mol/K). R is the gas constant (8.314 J/mol.K). The values of ΔH^o and ΔS^o are determined from the slope and the intercept from the plot of $\ln K_c$ versus 1/T.

3.10.3 Reusability studies

Reusability studies of the three PVDF-HFP composite membranes were performed by following the Cd(II) ions adsorption-desorption studies for four cycles. In order to study the reusability of the adsorbents, PVDF-HFP composite membranes (0.5 g/L) were contacted with 20 mL of Cd(II) solution (100 ppm) for 48 h at 25 ^{o}C. After 48 hours, the solution was analysed and the final concentration of Cd(II) ions was determined using the AAS. The PVDF-HFP composite membranes were recycled by immersing them separately into 50 mL of 0.5 M HNO_3 solutions for 1 h (for desorption to occur), and finally the adsorbents were washed thoroughly with distilled water and bicarbonate solution to remove HNO_3. The membranes were added again into another Cd(II) solution to start a new adsorption batch. The adsorption process was repeated 4 times to test the reusability of the adsorbents.

3.10.4 Selectivity studies

To evaluate the selectivity of the 1 wt.% PAMAM-MWCNTs/PVDF-HFP composite membrane, the following procedure was followed: An Erlenmeyer flask containing a mixture of Cd(II) solution (100 mg/L) and 1 wt.% PAMAM-MWCNTs/PVDF-HFP composite membranes (0.5 g/L) at a pH of 6.5, were placed on a rotary shaker for 48 h at 25 °C. The selectivity coefficient $K_{Cd/X}$ for the 1 wt.% PAMAM-MWCNTs/PVDF-HFP membrane was obtained using the following equations [19]:

$$k_{Cd/X} = \frac{K_d[Cd]}{K_d[X]}$$

$$K_d = \frac{q_e}{C_e}$$

where K is the selectivity coefficient, X represent the competing ions of Cu(II), Zn(II) and Ni(II), K_d is the distribution coefficient (L/g), q_e is the amounts of metal adsorbed by the membrane (mg/g) in solution and C_e (mg/L) is the concentration of the metal at equilibrium.

3.11 REFERENCES

1. Rananga, L.E. and Magadzu, T. 2014. Interaction of silver doped carbon nanotubes-cyclodextrin nanocomposites with *Escherichia coli* bacteria during water purification. *Water science and technology*, 14(3), 367-375.

2. Guzman, M.G., Dille, J. and Godet, S. 2008. Synthesis of silver nanoparticles by chemical reduction method and their antibacterial activity. *Chemical*, *molecular, nuclear, materials and metallurgical engineering*. 2, 91-98.

3. Zhao C., Ji L., Liu H., Hu G., Zhang s., Yang M. and Yang Z., 2004, Functionalized carbon nanotubes containing isocyanate groups. *Journal of solid state chemistry,* 177, 4394-4398.

4. Pan B., Cui D., Gao F. and He R. 2006. Growth of multi-amine terminated poly(amidoamine) dendrimers on the surface of carbon nanotubes. *Nanotechnology* 17, 2483-2489.

5. Yuan W., Giang G., Che J., Qi X., Xu R., Chang M.W., Chen Y., Lim S.Y., Dai J, and Chan-Park M.M. 2008. Deposition of silver nanoparticles on multi-walled carbon nanotubes grafted with hyper-branched poly(amidoamine) and their antimicrobial effects. *Journal of physical chemistry C, 112,* 18754-18759.

6. Wongchitphimon, S., Wang, R., Jiraratananon, R., Shi, L. and Loh, C.H. 2011. Effect of polyethylene glycol (PEG) as an additive on the fabrication of polyvinylidene fluoride-co-hexafluropropylene (PVDF-HFP) asymmetric microporous hollow fiber membranes. *Journal of membrane science*, 369, 329-338.

7. Bessadok, A., Marais, S., Gouanve, F., Colasse, L., Zimmerlin, I., Roudesli, S. and Metayer M. 2007. Effect of chemical treatments of Alfa (Stipa tenacissima) fibres on water-soption properties. *Composites science and technology*, 67(3-4), 685-697.

8. Liang, H., Wan, L. and Xu, Z. 2016. Poly(vinylidene fluoride) Separators with Dual-asymmetric Structure for High-performance Lithium Ion Batteries. *Chinese Journal of polymer science*, 12, 1423-1435.

9. Zheng, Q.Z., Wang, P., Yang, Y.N. and Cui, D.J. 2006. The relationship between porosity and kinetics parameter of membrane formation in PSf ultrafiltration membrane. *Journal of membrane science*, 286, 7-11.

10. Adams, F.V., Nxumalo, E.N., Krause, R.W.M., Hoek, E.M.V. and Mamba, B.B. 2014. Application of polysulfone/cyclodextrin mixed-matrix membranes in the removal of natural organic matter from water. *Physics and chemistry of the earth,* 67-69, 71-78.

11. Kasim, N., Mohammad, A.W. and Abdullah, S.R.S. 2016. Performance of membrane filtration in the removal of iron and manganese from Malaysia's groundwater. *Membrane water treatment*, 7(4), 277-296.

12. Tohdee, K., Kaewsichan, L. and Asadullah. 2018. Enhancement of adsorption efficiency of heavy metal Cu(II) and Zn(II) onto cationic surfactant modified bentonite. *Journal of environmental chemical engineering*, 6, 2821-2828.

13. Ahmad, A., Razali, M.H., Mamat, M., Mehamod, F.S.B. and Amin, K.A.M. 2017. Adsorption of methyl orange by synthesized and functionalized-CNTs with 3-aminopropyltriethoxysilane loaded TiO_2 nanocomposites. *Chemosphere*, 168 474-482.

14. Ganesan, V., Louis, C. and Damodaran, S.P. 2018. Graphene oxide-wrapped magnetite nanoclusters: A recyclable functional hybrid for fast and highly efficient removal of organic dyes from wastewater. *Journal of environmental chemical engineering*, 6, 2176-2190.

15. Bhatt, A.S., Sakaria, P.L., Vasudevan, M., Pawar, R.R., Sadheesh, N., Bajaj, H.C. and Mody, H, M. 2012. Adsorption of an anionic dye from aqueous medium by organ clays: equilibrium modelling, kinetic and thermodynamic exploration. *RSC advances*, 2, 8663-8671.

16. Wang, X., Chen, C. and Wang, X. 2015. Ozone degradation of 1-naphthol on multiwalled carbon nanotubes/iron oxides and recycling of the adsorbent. *Chemical engineering journal* 262, 1303-1310.

17. Rahman, M., Gul, S., Ajmal, M., Iqbal, A. and Achakzai, A.K.K. 2014. Removal of cadmium from aqueous solutions using excised leaves of quetta pine (pinus halepensis mill.). *Bangladesh journal of botany*, 43(3), 277-28.

18. Nthumbi, R.M. Adelodun, A.A. and Ngila, J.C. 2017. Electrospun and functionalized PVDF/PAN composite for the removal of trace metals in contaminated water. *Physics and chemistry of the earth,* 100, 225-235.

19. Zhao, D., Ju, Y. and Chen, J.P. 2016. Treatment of lead contaminated water by a PVDF membrane that is modified by zirconium, phosphate and PVA. *Water research*, 101, 564-573.

CHAPTER 4

RESULTS AND DISCUSSIONS

4.1 CHARACTERISATION OF SYNTHESISED NANOMATERIALS AND NANOCOMPOSITE MEBRANES

4.1.1 Fourier transform infrared (FTIR) results

4.1.1.1 FTIR spectra of raw MWCNTs, and functionalised MWCNTs

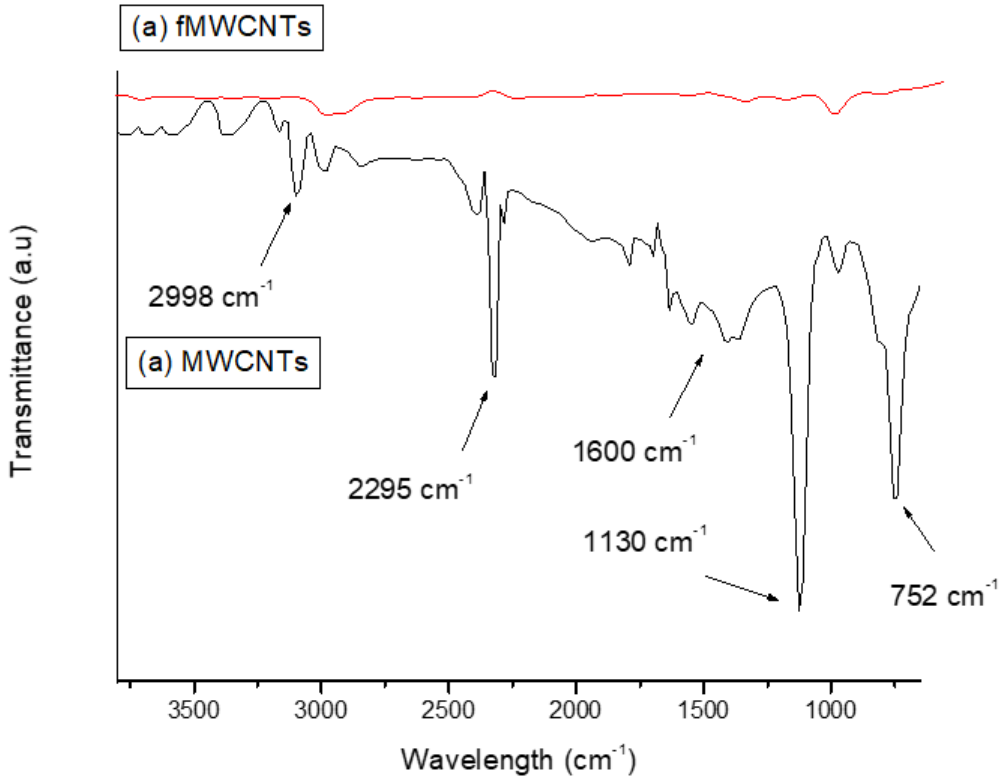

Figure 4.1: FTIR spectra of (a) raw and (b) fMWCNTs

Figure 4.1 show the FTIR spectra of raw and functionalized MWCNTs. In the FTIR spectrum of MWCNTs-COOH, the peaks at 2998 and 1600 cm^{-1} can be attributed to the stretching vibrations of O-H and C=O of carboxyl groups, respectively. In addition, the peak at 1130 cm^{-1} is assigned to the C-O stretching vibration. The increase in the peak intensity of the C-H stretching mode at 2295 cm^{-1} suggests that oxidation of the MWCNTs successfully introduced the carboxylic group (-COOH) on the walls of carbon nanotubes. Similar results have been reported in literature [1,2].

4.1.1.2 FTIR spectra of NCO-MWCNTs, NH_2-MWCNTs and PAMAM-MWCNTs

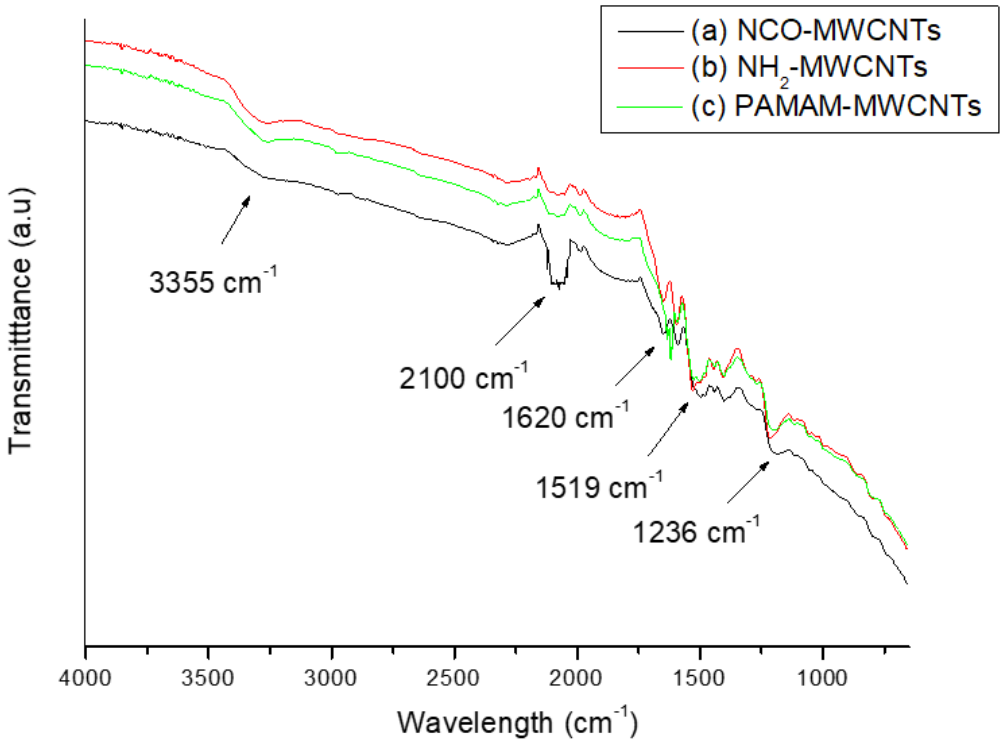

Figure 4.2: FTIR spectra of (a) NCO-MWCNTs, (b) NH_2-MWCNTs and (c) PAMAM-MWCNTs

Figure 4.2 show the FTIR spectra of NCO-MWCNTs, NH_2-MWCNTs and PAMAM-MWCNTs. The strong absorption band at 2100 cm^{-1} (figure 4.1.2) is due to the out-of-phase stretching of the N=C=O bonds showing the presence of the NCO group on the MWCNTs-COOH. The two broad bands at 3355 and 1620 cm^{-1} (slightly intense) is attributed to the NH_2 stretching vibration and N-H bending modes of the free NH_2 group in figure 4.2b and c respectively. Bands at 1519 cm^{-1} (figure 4.2c) are characteristic of amide (-CO-NH), stretching vibration of the C=N group of the imine and C=C backbone, indicating that the PAMAM dendrimer was bound to fMWCNTs. The intense peak at 1620 cm^{-1} (figure 4.2c) also represent the amide group (CO-NH) of type I and type II, which proves the existence of a dendrimer of polyamidoamine structure on the surface of carbon nanotubes as observed by Zhang *et al*. [3] and Fan *et al*. [4].

4.1.1.3 FTIR spectra of PVDF-HFP, 1 wt.% MWCNTs and 1 wt.% PAMAM-MWCNTs composite membranes

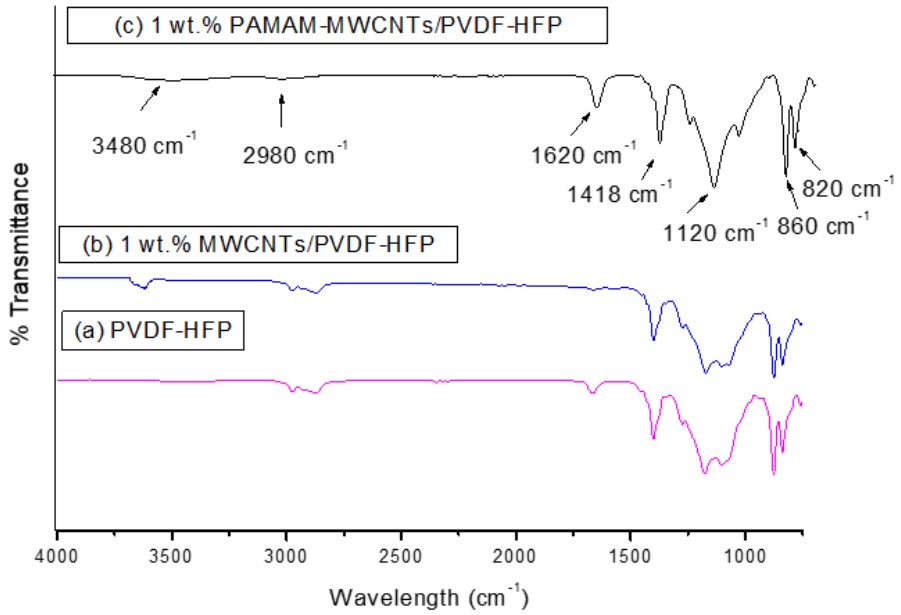

Figure 4.3: FTIR spectra of (a) PVDF-HFP, (b) 1 wt.% and (c) 1 wt.% PAMAM-MWCNTs/PVDF-HFP composite membranes

Figure 4.3 show the FTIR spectra of PVDF-HFP, 1 wt.% MWCNTs/PVDF-HFP and 1 wt.% PAMAM-MWCNTs/PVDF-HFP composite membranes. The peak intensities at 1418, 1120, 860 and 820 cm^{-1} (figure 4.3.c) confirm the γ-phase crystalline structure of the PVDF-HFP polymer, which is present in all composites membranes. The FTIR spectra at 3480 cm^{-1} appearing on 1 wt.% MWCNTs-PVDF-HFP, is due to an O-H stretching mode of MWCNTs and this peak appears to be broader on 1 wt.% PAMAM-MWCNTs-PVDF-HFP as result of PAMAM dendrimer attached to the -OH of the carboxylic groups on the walls of MWCNTs [5]. Band at 1620 cm^{-1} is a characteristic of amide (-CO-NH-) I and II bonds, respectively, indicating that the PAMAM dendrimer was bound to fMWCNTs. Similar results were observed by Fan *et al*. [4].

4.1.2 XRD Results

4.1.2.1 XRD patterns of raw MWCNTs, fMWCNTs and PAMAM-MWCNTs

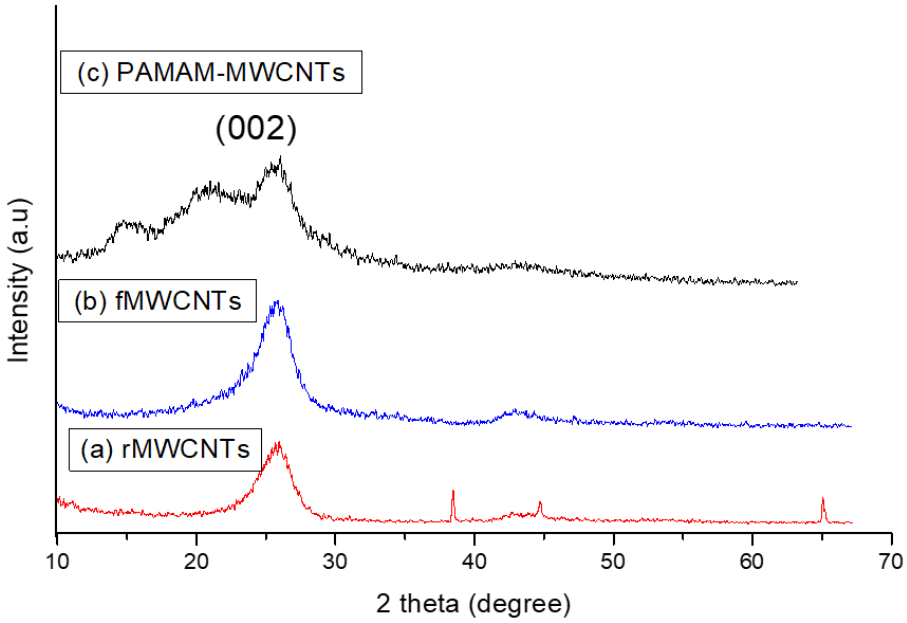

Figure 4.4: XRD patterns of (a) rMWCNTs, (b) fMWCNTs, and (C) PAMAM-MWCNTs

Figure 4.4 show the XRD patterns of raw MWCNTs, functionalised MWCNTs and PAMAM-MWCNTs. All the three nanomaterials revealed a significant diffraction pattern which appeared at $2\theta = 26.01^{o}$ corresponding to the hexagonal graphite structure support [5]. The intensity of the diffraction peak at (002) plane in functionalised MWCNTs (Figure 4.4a) was increased as compared to the raw MWCNTs (Figure 4.4b). This was an indication of the carbon nanotubes purity after acid treatment [6]. The diffraction peak in the XRD pattern of raw MWCNTs shows the presence of carbon along with other peaks due to the metallic impurities. The removal of metallic impurities was observed in the XRD pattern after acid treatment (figure 4.4b). The interlayer peak of PAMAM-MWCNTs (figure 4.4c) indicate that the functional materials do affect the crystallinity of the MWCNTs. A similar behaviour was reported by Yuan *et al*. [8]

4.1.2.2 XRD patterns of Ag nanoparticles, Ag-MWCNTs, and Ag-PAMAM/MWCNTs

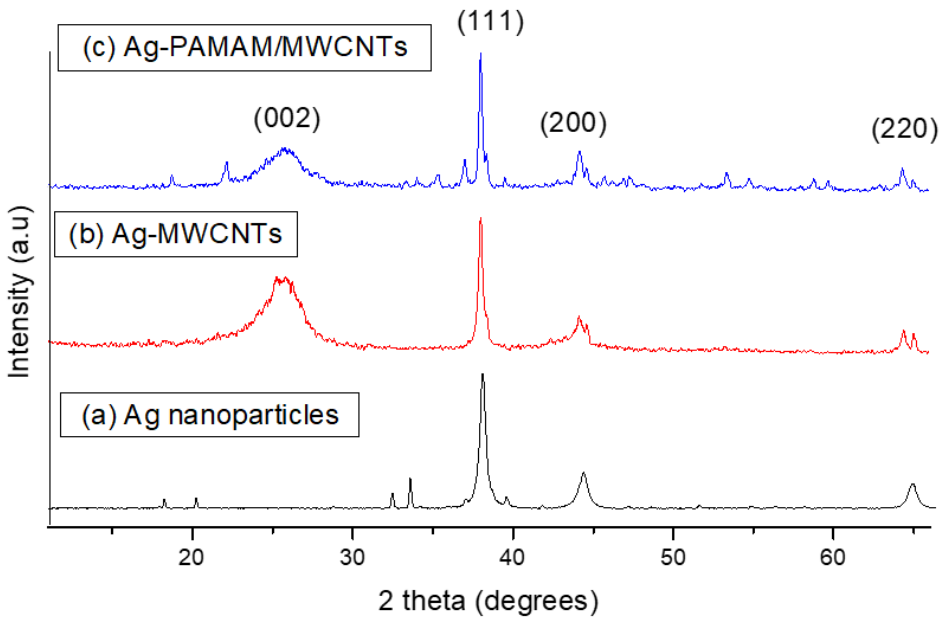

Figure 4.5: XRD patterns of (a) Ag nanoparticles, (b) Ag-MWCNTs, and (c) Ag-PAMAM/MWCNTs

Figure 4.5 shows the XRD pattern of Ag nanoparticles, Ag-MWCNTs, and Ag-PAMAM/MWCNTs. The diffraction peaks on silver nanoparticles pattern at 2θ of 38.20º, 44.4º and 64.86º (figure 4.5) correspond to the (111), (200) and (220) planes, which can be indexed to a face-centred cubic symmetry. The XRD pattern (Figure 4.5) thus clearly shows that the silver nanoparticles are crystalline in nature [9]. The characteristic diffraction peak of fMWCNTs at 2θ = 26.01º is still present in the Ag-fMWCNTs and Ag-PAMAM/MWCNTs patterns but with diminished intensity. As shown from Figure 4.5b and c, the characteristic diffraction peak at 26º 2θ of MWCNTs decreased in both Ag-MWCNTs and Ag-PAMAM/MWCNTs due to high intense peaks generated from strongly attached Ag nanoparticles to the surface of fMWCNTs as compared to raw and functionalised MWCNTs in figure 4.4. A similarity in the peak intensity decrease was noticed by Haider *et al*. [10] on the preparation and characterization of multi walled carbon nanotubes/Ag nanoparticles hybrid materials. The unassigned noisy peaks on figure 4.5c could be due to the amorphous impurities encountered during the formation of the composite.

The estimated crystallite size of the silver nanocrystals using the (111) peak by the Scherrer equation is 8.6, 7.8 and 6.4 nm for Ag nanoparticles, Ag-MWCNTs and Ag-PAMAM/MWCNTs respectively. The results correspond with the TEM analysis in section 4.1.4.2 as observed by Shi *et al*. [11].

4.1.2.3 XRD patterns of PVDF-HFP, 1 wt.% MWCNTs/PVDF-HFP and 1 wt.% PAMAM-MWCNTs/PVDF-HFP composite membranes

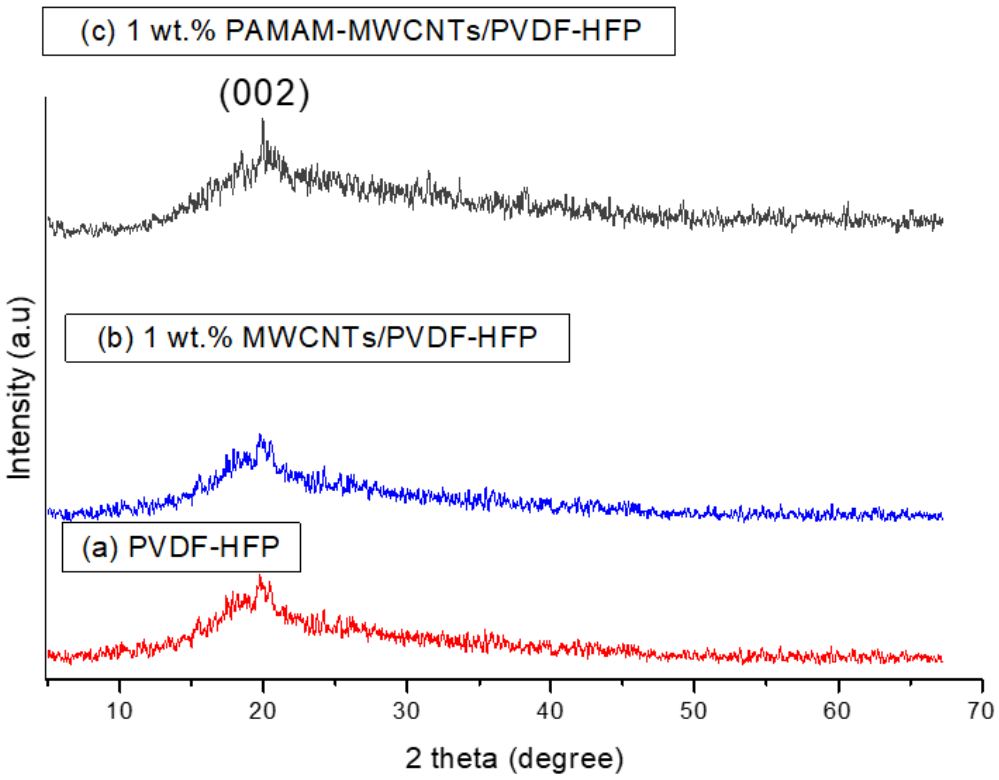

Figure 4.6: XRD patterns of PVDF-HFP, 1 wt.% MWCNTs/PVDF-HFP and 1 wt.% PAMAM-MWCNTs/PVDF-HFP composite membranes

XRD patterns of PVDF-HFP, 1 wt.% MWCNTs/PVDF-HFP, 1.5 wt.% MWCNTs/PVDF-HFP and 1 wt.% PAMAM-MWCNTs/PVDF-HFP composite membranes are shown in figure 4.6. The XRD profile of as-prepared PVDF-HFP shows a noisy hump appearing at $2\theta = 20^{o}$. The broad peak indexed to (002) crystal plane is ascribed to PVDF-HFP. This peak usually appears at $2\theta = 26.01^{o}$ for MWCNTs [12], however even on figure 4.6 b and c, the peak has shifted in the presence of PVDF-HFP. The broad peak for

PVDF-HFP broadened upon addition of 1 wt.% MWCNTs into PVDF-HF and the 1 wt.% PAMAM-MWCNTs/PVDF-HFP composite membrane showed an undistorted broad peak compared to that of figure 4.6 (b) and (c).

4.1.2.4 XRD patterns of 5 wt.% Ag-PVDF-HP, 2.5 wt.% Ag-MWCNTs/PVDF-HFP and 1.8 wt.% Ag-PAMAM-MWCNTs/PVDF-HFP

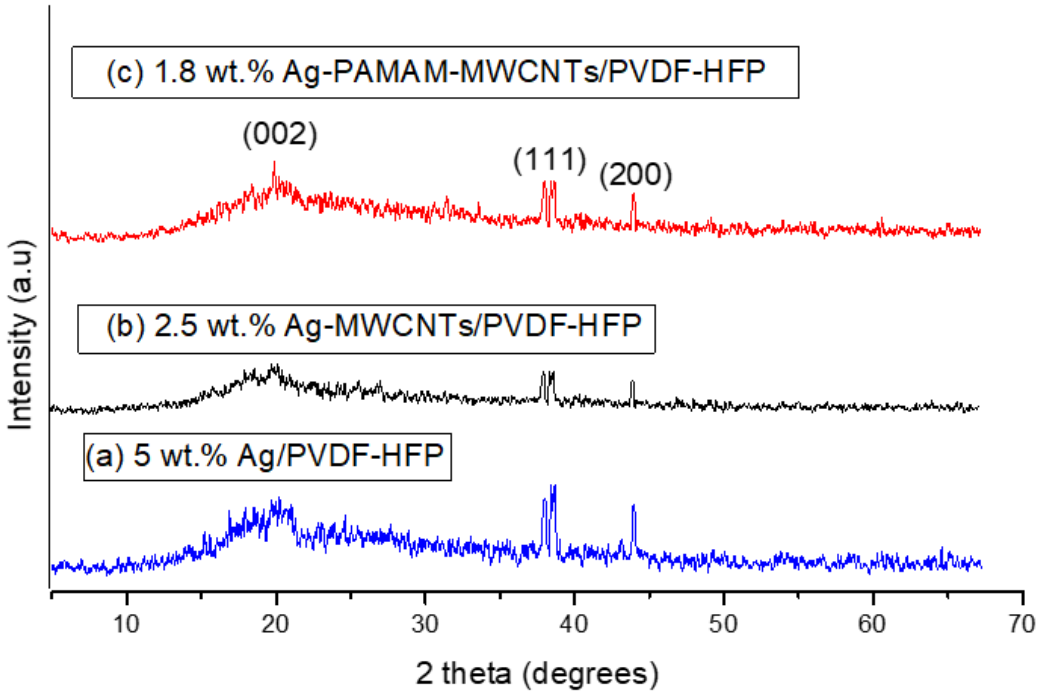

Figure 4.7: XRD patterns of (a) 5 wt.% Ag-PVDF-HFP, (b) 2.5 wt.% Ag-MWCNTs/PVDF-HFP, and (c) 1.8 wt.% Ag-PAMAM-MWCNTs/PVDF-HFP composite membranes

XRD patterns of 5 wt.% Ag-PVDF-HFP, 2.5 wt.% Ag-MWCNTs/PVDF-HFP and 1.8 wt.% Ag-PAMAM-MWCNTs/PVDF-HFP composite membranes are shown in figure 4.7. The noisy hump appearing at $2\theta = 20^{o}$ for PVDF-HFP and MWCNTs appear in all patterns. The two sharp peaks seen also in all the XRD profiles in figure 4.7, are indexed to a (111) and (200) planes, confirming the presence of Ag nanoparticles.

4.1.3 Thermogravimetric analysis results

4.1.3.1 TGA results of raw MWCNTs, fMWCNTs, PAMAM-MWCNTs, Ag-MWCNTs and Ag-PAMAM/MWCNTs

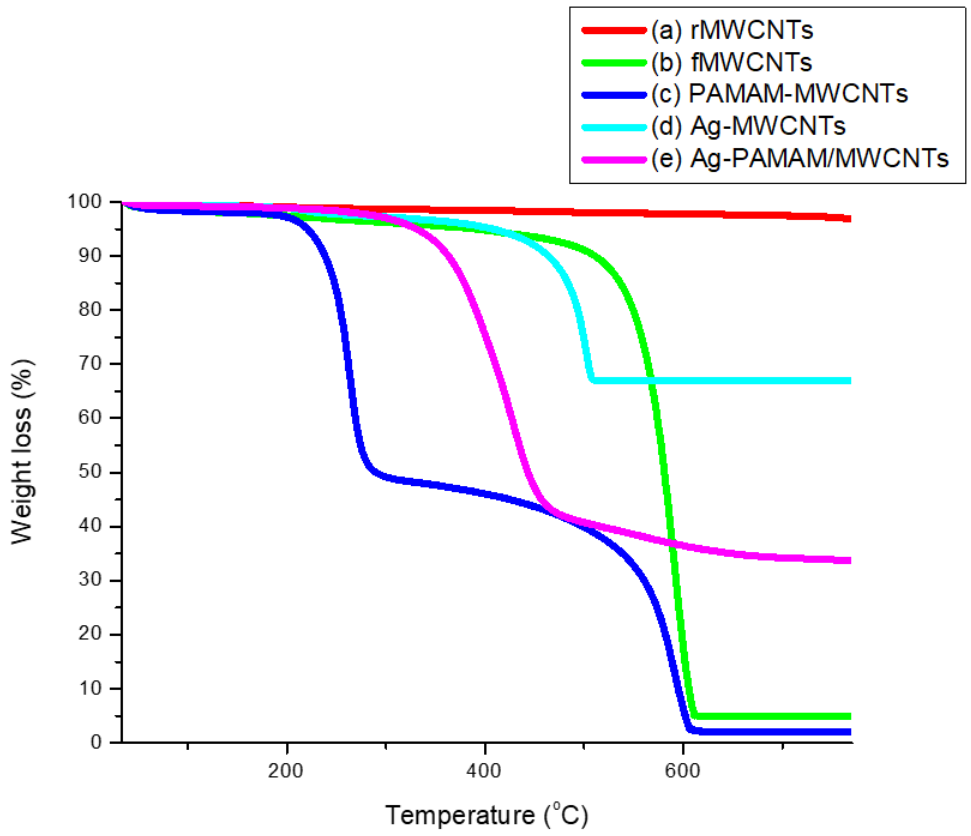

Figure 4.8: TGA curves of (a) raw MWCNTs, (b) fMWCNTs and (c) PAMAM-MWCNTs, (d) Ag-MWCNTs and (e) Ag-PAMAM/MWCNTs

Figure 4.8 shows the TGA curves of raw MWCNTs, fMWCNTs, PAMAM-MWCNTs, Ag-MWCNTs and Ag-PAMAM/MWCNTs. The raw MWCNTs (figure 4.8a) weight decreased with increasing temperature, but this weight loss was insignificant (less than 3%), compared with the rest of the nanomaterials in figure 4.8. The weight loss of fMWCNTs started at temperatures above 500 ^{o}C, and it's attributed to the loss of the oxygen-containing functional groups (carboxylic acid) of MWCNTs, as observed by Watts et al. [13]. The MWCNTs started to decompose at about 430 ^{o}C, in the early stage when compared to fMWCNTs due to the catalytic effects of Ag nanoparticles on the thermolysis of carbon nanotubes [14,15]. The TGA profiles of PAMAM-MWCNTs

shows a 50% weight loss from 240 to 290 ^{o}C, which can easily be attributed to the decomposition of PAMAM organic moiety substituent. The weight loss PAMAM-MWCNTs after 300 ^{o}C is attributed to the thermal decomposition of the defect sites of PAMAM-MWCNTs. This TGA results indicated that the structure of PAMAM-MWCNTs composite is composed of 50% PAMAM by weight. Similar weight percentages were observed by Salam and Burk [16]. In the case of Ag-PAMAM/MWCNTs composite, the primary and secondary weight loss at 220 ^{o}C and 500 ^{o}C are due to the decompositions of the polyamidoamine moiety and carbon nanotube body, respectively [14]. It was clearly observed that Ag nanoparticles contributed to the thermal stability of both Ag-MWCNTs and Ag-PAMAM/MWCNTs, with the latter more stable up to 600 ^{o}C. The enhanced stability of Ag-PAMAM/MWCNTs composite was also noted compared to PAMAM-MWCNTs due to the presence of Ag nanoparticles. The total mass loss of Ag/MWCNTs and Ag-PAMAM/MWCNTs were decreased to 68% and 45% till above 700 ^{o}C respectively, which indicate that the loading percentages of silver are respectively about 32% and 45%. Similar results were recorded in literature, on the synthesis and characterization of multi-walled carbon nanotubes modified with octadecylamine and polyethylene glycol [16]. In general, all the nanocomposites were stable up to 280 ^{o}C.

4.1.3.2 TGA results of PVDF-HFP, 1 wt.% MWCNTs-PVDF-HFP, 1 wt.% PAMAM-MWCNTs/PVDF-HFP, 2.5 wt.% Ag-MWCNTs/PVDF-HFP, and 1.8 wt.% Ag-PAMAM-MWCNTs/PVDF-HFP composite membranes

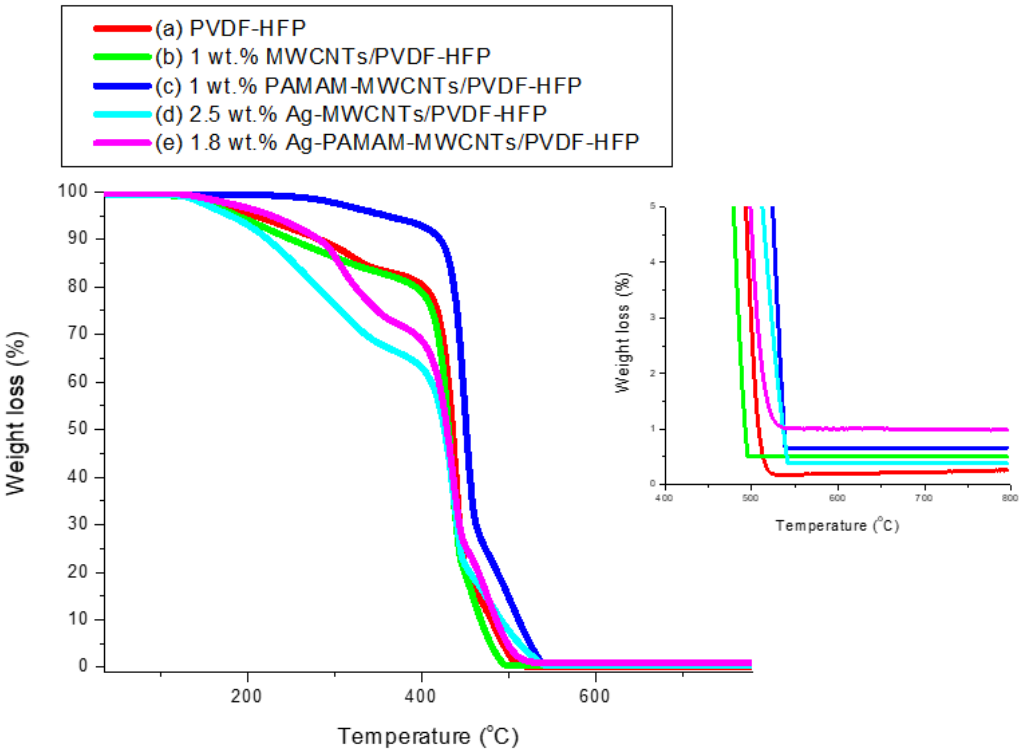

Figure 4.9: TGA curves of (a) PVDF, (b) 1 wt.% MWCNTs/PVDF-HFP, (c) 1 wt.% PAMAM-MWCNTs/PVDF-HFP, (d) 2.5 wt.% Ag-MWCNTs/PVDF-HFP and (e) 1.8 wt.% Ag-PAMAM-MWCNTs/PVDF-HFP composite membranes; and the insert showing the thermograms between 500 to 800 ^{o}C

Figure 4.9 shows the thermogravimetric analysis curves (TGA) of PVDF-HFP, 1 wt.% MWCNTs/PVDF-HFP, 1 wt.% PAMAM-MWCNTs/PVDF-HFP, 2.5 wt.% Ag-MWCNTs/PVDF-HFP and 1.8 wt.% Ag-PAMAM-MWCNTs/PVDF-HFP composite membrane. The TGA of PVDF-HFP in figure 4.9a shows that the material decomposed at around 430 ^{o}C. The TGA curve of 1wt.% MWCNTs-PVDF-HFP (Figure 4.9b) shows that fMWCNTs did not improve the stability PVDF-HFP as they were seen to decompose just almost at the same temperatures with PVDF-HFP. The 1 wt.% PAMAM-MWCNTs/PVDF-HFP composite membrane retained stability up to 500 ^{o}C, due to the presence of PAMAM, with only less than 10% weight loss at 600 ^{o}C. The data indicates that PAMAM/MWCNTs does improve the structural stability of PVDF-

HFP membrane, as the structure remained stable even at high temperatures when compared to the rest of the PVDF-HFP composite membranes. The showed that Ag did not improve the structural stability of PVDF-HFP. Interestingly, the TGA of 2.5 wt.% Ag-MWCNTs/PVDF-HFP and 1.8 wt.% Ag-PAMAM-MWCNTs/PVDF-HFP composite membrane collapsed with a weight loss of 40% from 170 to 450 ^{o}C. It was noted that Ag does not improve the structural stability of PVDF-HFP although 1.8 wt.% Ag-PAMAM-MWCNTs/PVDF-HFP was slightly better due to the presence of PAMAM.

The insert figure represents a closer look of the TGA curves between 500 and 800 ^{o}C. A closer look on the insert figure at temperatures above 450 ^{o}C, shows that all the weight percentages of the composite membranes were view to be approximately 98%. Only 99.8% loss was viewed for PVDF-HFP. The rest of the PVDF-HFP based composite membranes still maintained a 1% weight suggesting that MWCNTs were still present in the composite membrane (only 1% MWCNTs was used during the synthesis process) and that they were not completely decomposed. This also shows that the MWCNTs have noticeable thermal stability. Similar results were recorded in literature [16], on the as-prepared composites of multi-walled carbon nanotubes modified with octadecylamine and polyethylene glycol. However, all composites have shown stability up to 300 ^{o}C. Similar behaviour in terms of structural instability of polymeric membranes (in the presence of dopants) is comparable to the work reported in literature [17,18].

4.1.4 Transmission Electron Microscope results

4.1.4.1 TEM images of raw MWCNTs, fMWCNTs and PAMAM-MWCNTs

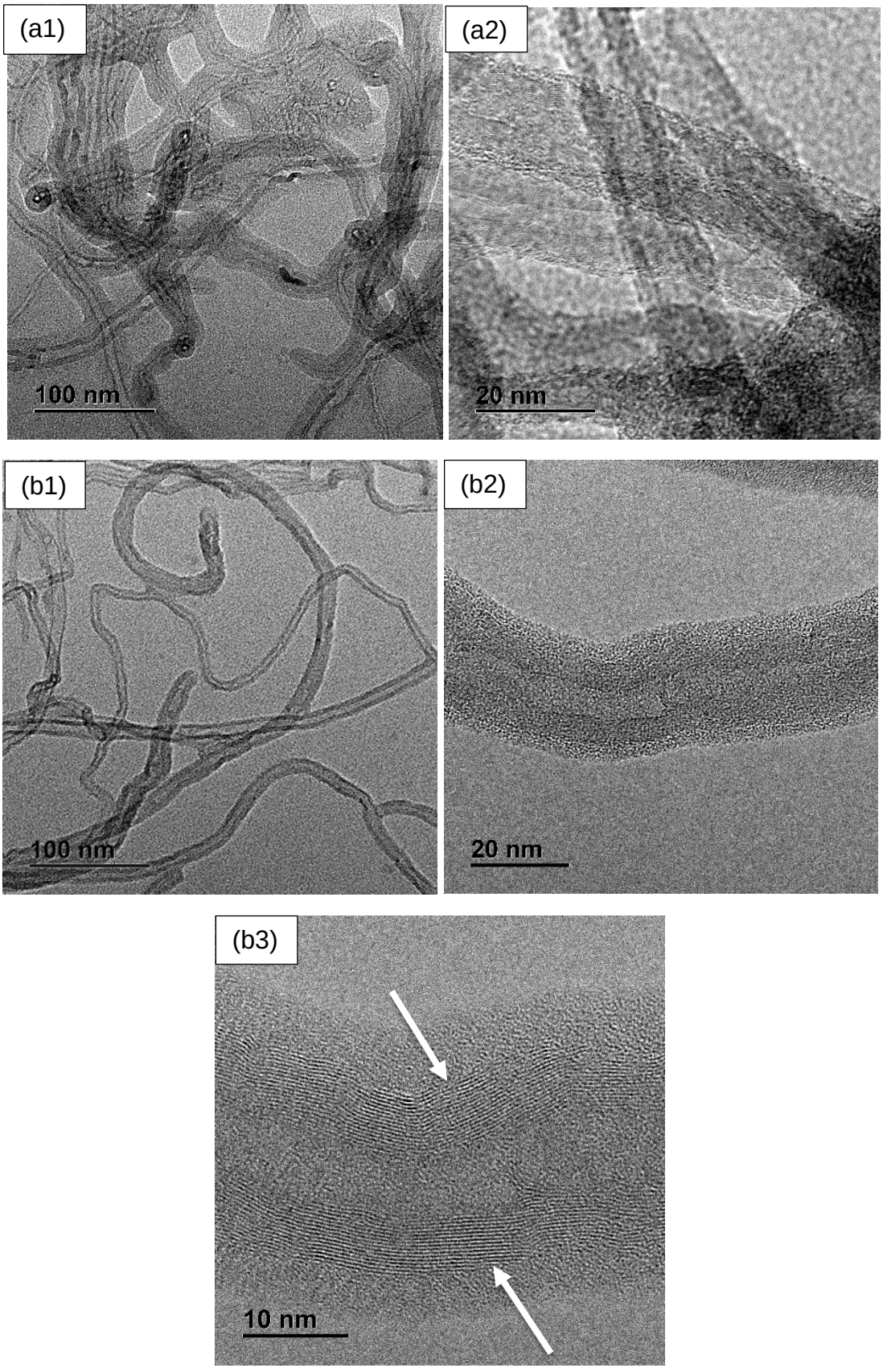

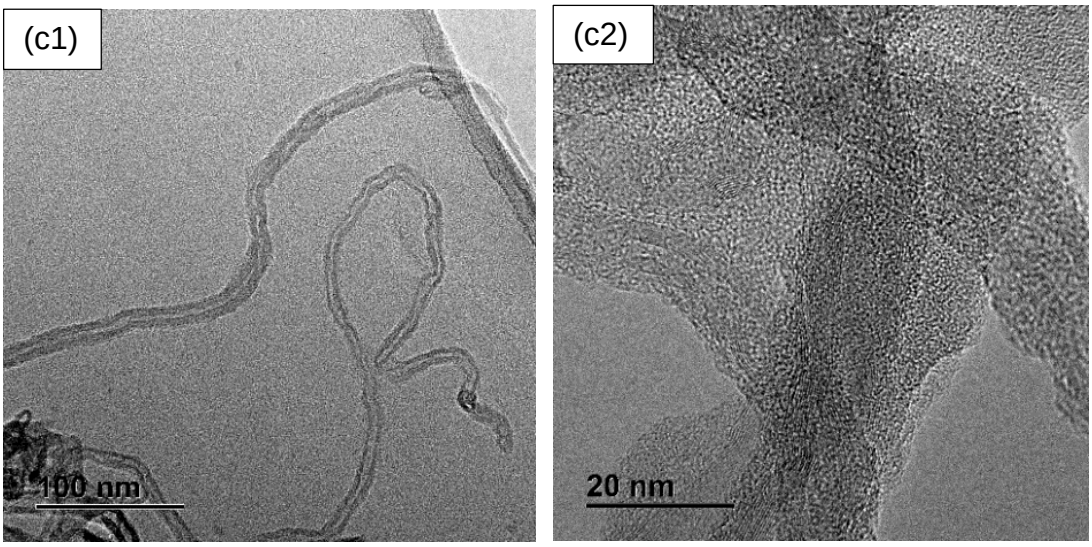

Figure 4.10: TEM images of (a1&2) raw MWCNTs, (b1,2&3) fMWCNTs and (c1&2) PAMAM-MWCNTs

Figure 4.10 show the TEM images of raw MWCNTs, fMWCNTs and PAMAM-MWCNTs obtained during the morphological analysis of the composite materials. Functionalised MWCNTs (figure 4.10 b1 and c1) showed better dispersion in comparison with the raw MWCNTs (figure 4.10a). The TEM images of MWCNTs after acid treatment, also showed reduced thickness of amorphous carbon layer on the walls of the MWCNTs, better observed at high magnification. The TEM image in figure 4.10b shows the presence of multiple graphene layers that form on the walls of the nanotubes, with an average diameter of 20 nm. In figure 4.10b3, the arrows indicate the multi- walled surface of CNTs (which is clearly visible under high magnification) [19-21].

The morphology of the MWCNTs revealed both open and closed tubes (figure. 4.10b). Similar observations have been made by Kim *et al*. [22] on this type of CNTs. In Figure 4.10c, the surface of the PAMAM-MWCNTs seems amorphous at higher magnification due to the dendrimer molecules attached on the surfaces of MWCNTs.

4.1.4.2 TEM images EDX of Ag nanoparticles, 2.5 wt.% Ag-MWCNTs and 1.8 wt.% Ag-PAMAM/MWCNTs

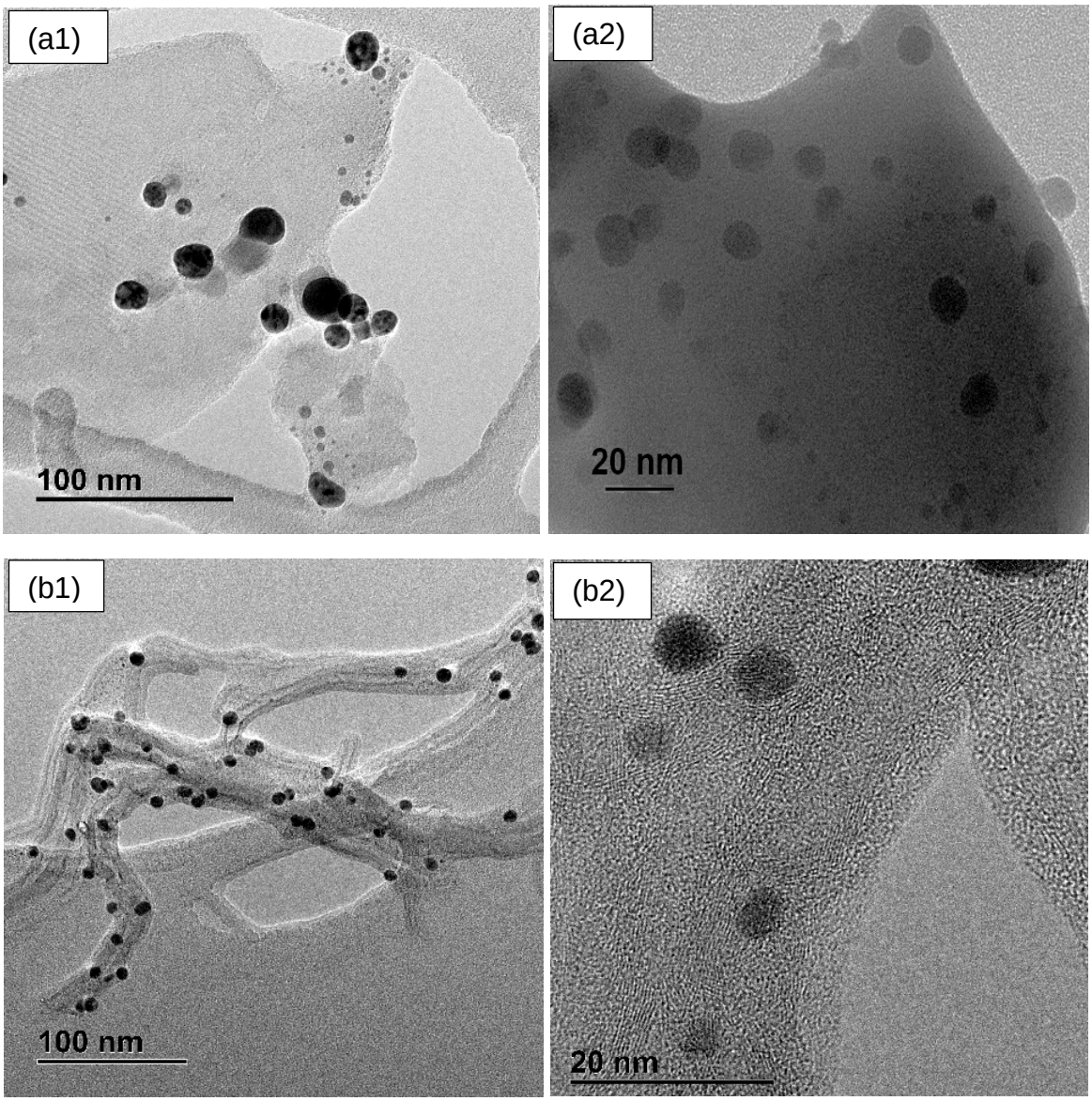

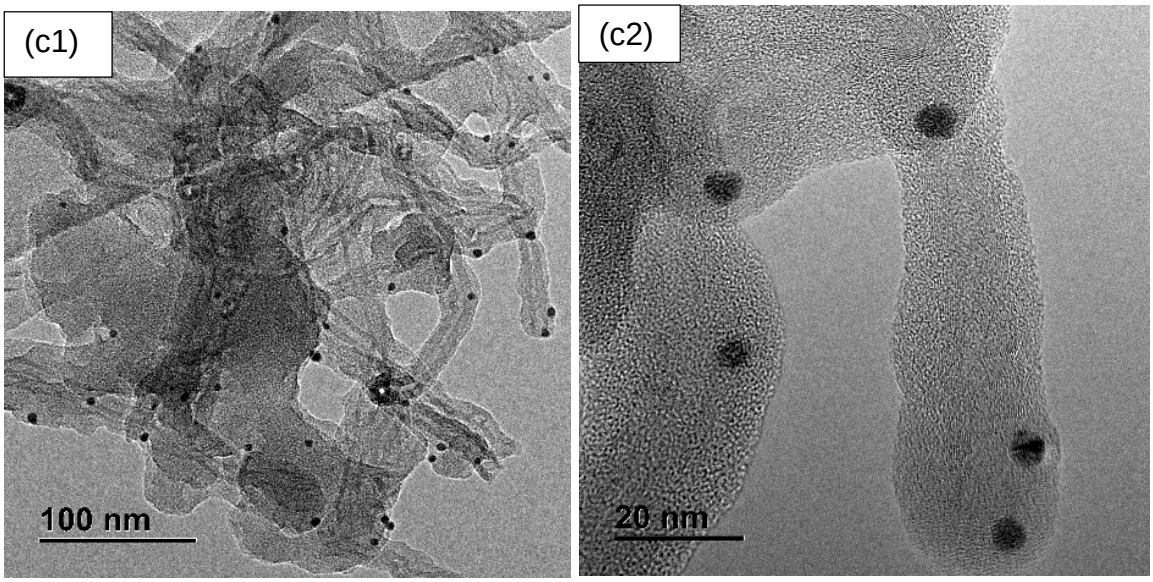

Figure 4.11: TEM images of (a) Ag nanoparticles (b) Ag-MWCNTs and (b) Ag-PAMAM/MWCNTs nanocomposites

Figure 4.11 show the TEM images of Ag nanoparticles, Ag-MWCNTs and Ag-PAMAM/MWCNTs. TEM studies confirmed successful decoration of silver nanoparticles on the surface and within MWCNTs. TEM analysis showed dark spherical spots corresponding to Ag nanoparticles (figure 4.11a) and light tubes corresponding to MWCNTs. As shown in Figure 4.11 b&c), Ag nanoparticles are fairly homogeneously distributed on the PAMAM-MWCNTs as compared to their deposition on the MWCNTs surface (figure 4.11b). From the TEM images (figure 4.11), the diameter of the Ag nanoparticles was observed to be from 5 to 10 nm for Ag-MWCNTs and from 4 to 8 nm for Ag-PAMAM/MWCNTs. The findings are comparable to the work done by Larrude *et al*. [23] during the synthesis and characterisation of silver nanoparticle-MWCNT composites. The silver nanoparticles size further corresponds with the crystallite sizes calculated from XRD results in section 4.1.2.2. As described in the literature review (section 2.3.7), studies have shown that Ag loaded membranes displayed an improved surface membrane hydrophilicity [24] and good antibacterial activity [25,26]. PAMAM dendrimer due to their abundant amino groups can be used to enhance the CNT dispersion properties resulting in an increase in the adsorption capacity [27]. PAMAM dendrimers have terminal amine groups and a high specific surface area; consequently, they are a good choice for complexation with metal ions and carbon materials [28-30].

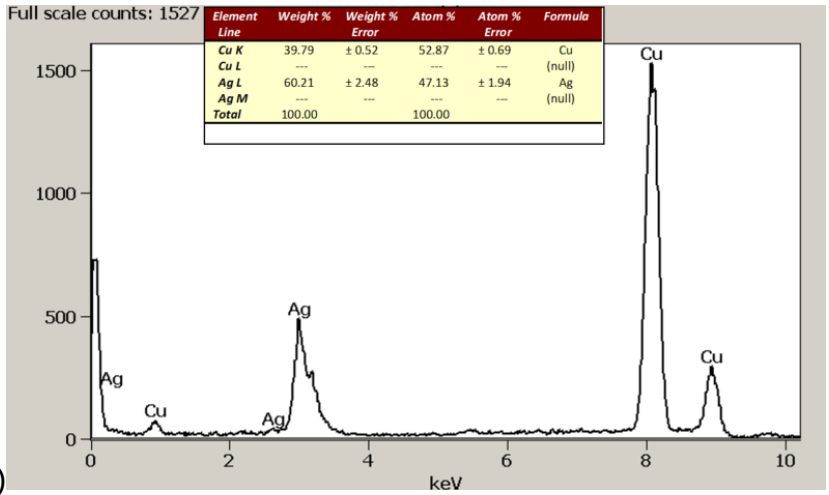

(a)

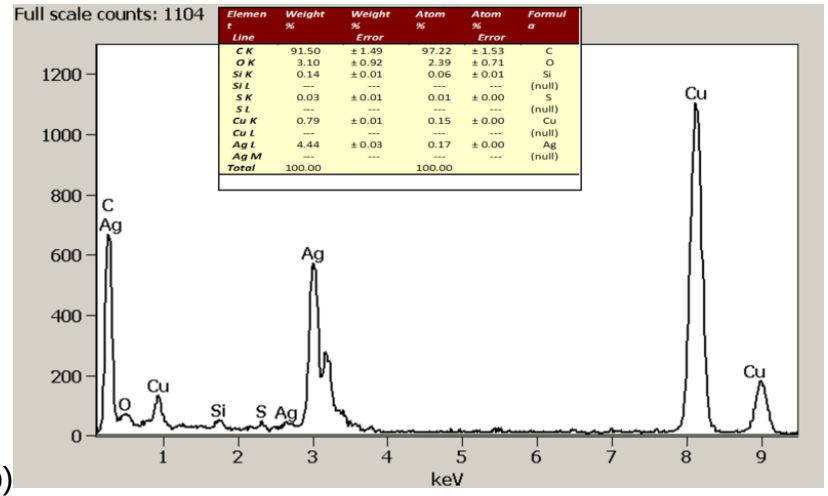

(b)

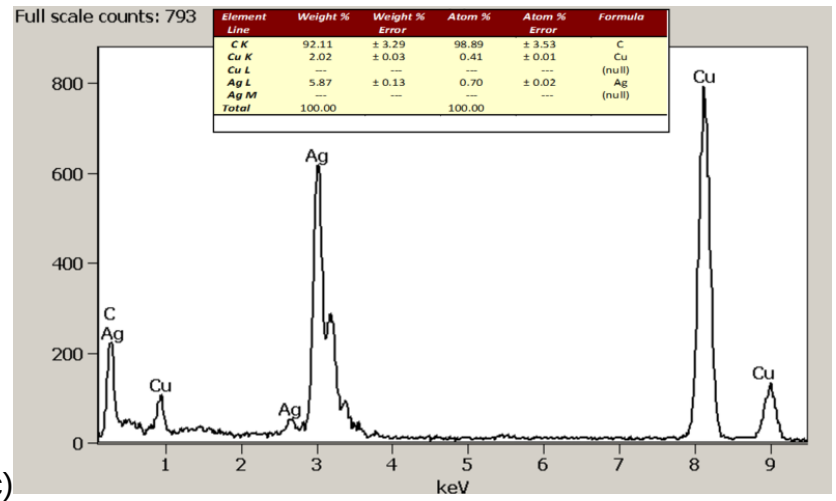

(c)

Figure 4.12: EDX of (a) Ag nanoparticles, (b) Ag-MWCNTs and (c) Ag-PAMAM/MWCNTs nanocomposites

Figure 4.12 show EDX of Ag nanoparticles, Ag-MWCNTs and Ag-PAMAM/MWCNTs nanocomposites. EDX showed 60%, 4.44% and 5.87% of Ag on Ag nanoparticles, Ag-MWCNTs and Ag-PAMAM/MWCNTs surfaces respectively. The peaks due to copper are from the copper grid used to place Ag nanoparticles for TEM analysis and are not part of the nanocomposites prepared. The oxygen and sulphur peaks noticed in figure 4.12b confirmed that the functionalisation of MWCNTs from HNO_3 and H_2SO_4 acids introduced the –OH group.

4.1.5 Scanning electron microscopy results

4.1.5.1 SEM images of PVDF-HFP, 1 wt.% MWCNTs-PVDF-HFP and 1 wt.% PAMAM-MWCNTs/PVDF-HFP composite membranes

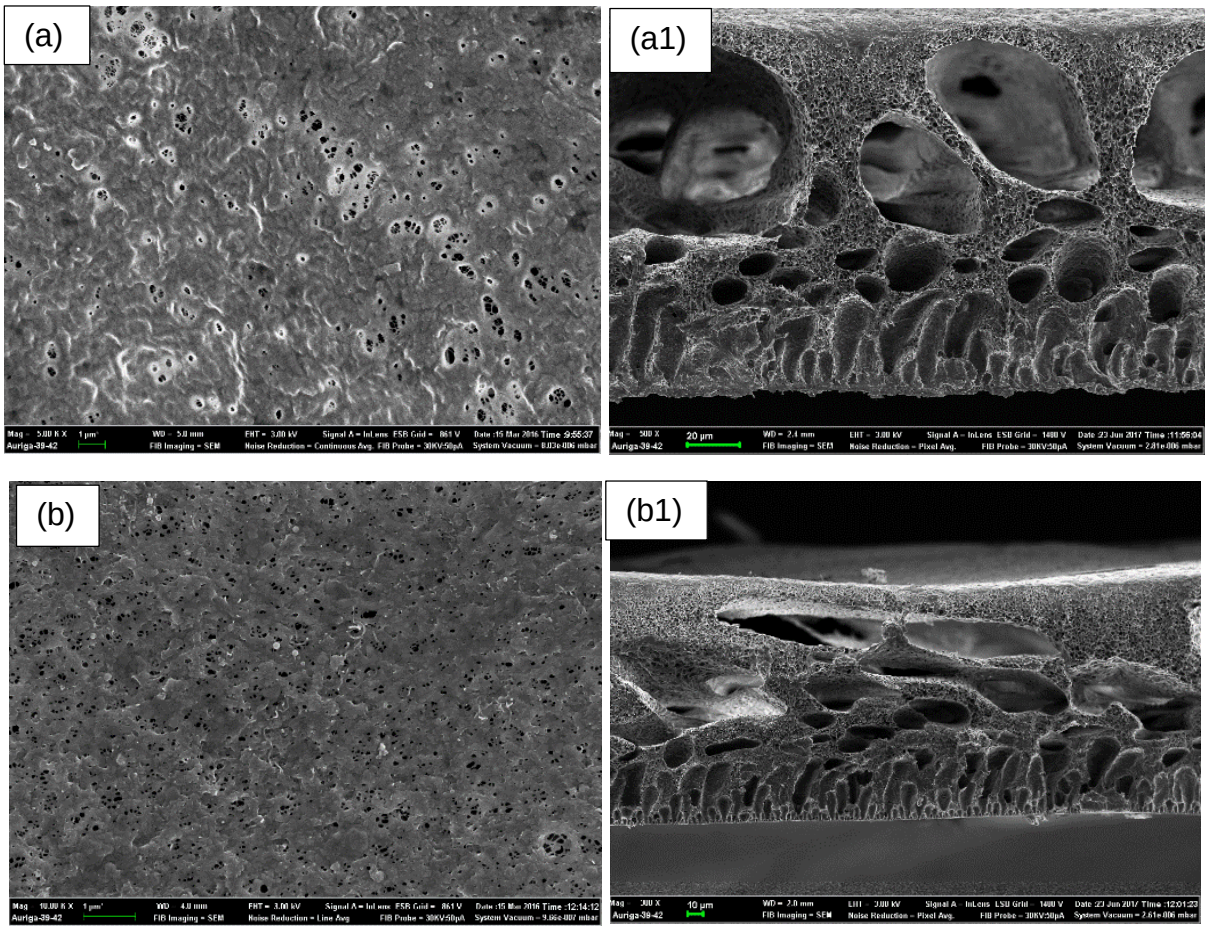

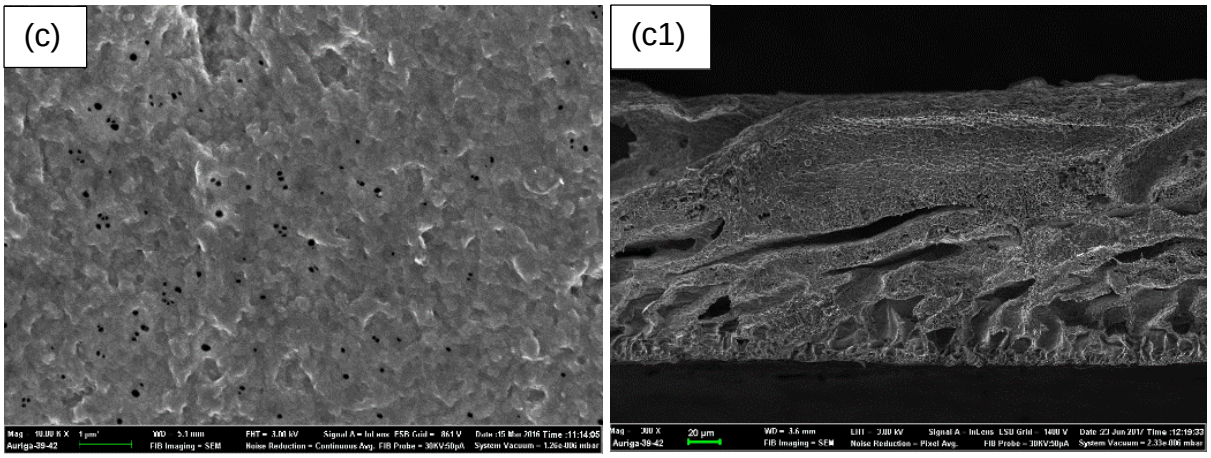

Figure 4.13: SEM images of: (a) PVDF-HFP, (b) 1 wt.% MWCNTs/PVDF-HFP and (c) 1 wt.% PAMAM-MWCNTs/PVDF-HFP composite membranes and their cross-sections (a1, b1 and c1)

The surface and cross-section morphologies of PVDF-HFP, 1 wt.% MWCNTs/PVDF-HFP and 1 wt.% PAMAM-MWCNTs/PVDF-HFP are shown in Figure 4.13. It can be observed in figure 4.13a that the pores were distributed uniformly on the surface of the PVDF-HFP composite membrane. As demonstrated in figure 4.13 (b and c), the surface structure of the membranes was significantly affected by the presence of MWCNTs and PAMAM. The cross sections of PVDF-HFP composite membranes showed a mixture of figure-like microvoids with a membrane diameter of approximately 180 μm. Similar behaviour was observed by Zhao *et al*. [31]. SEM cross sections images of the PVDF-HFP composite membranes in figure 4.13 (a), (b) and (c) show that the membranes exhibit a mixture of microvoids and spongy cross-section structure. The modified PVDF-HFP composite membranes (figure 4.13 b1 and c1) showed a decrease in the microvoids, with a high spongy surface which is good for heavy metal adsorption and desalination.

4.1.5.2 SEM images of 5 wt.% Ag/PVDF-HFP, 2.5 wt.% Ag-MWCNTs-PVDF-HFP and 1.8 wt.% Ag-PAMAM/PVDF-HFP composite membranes

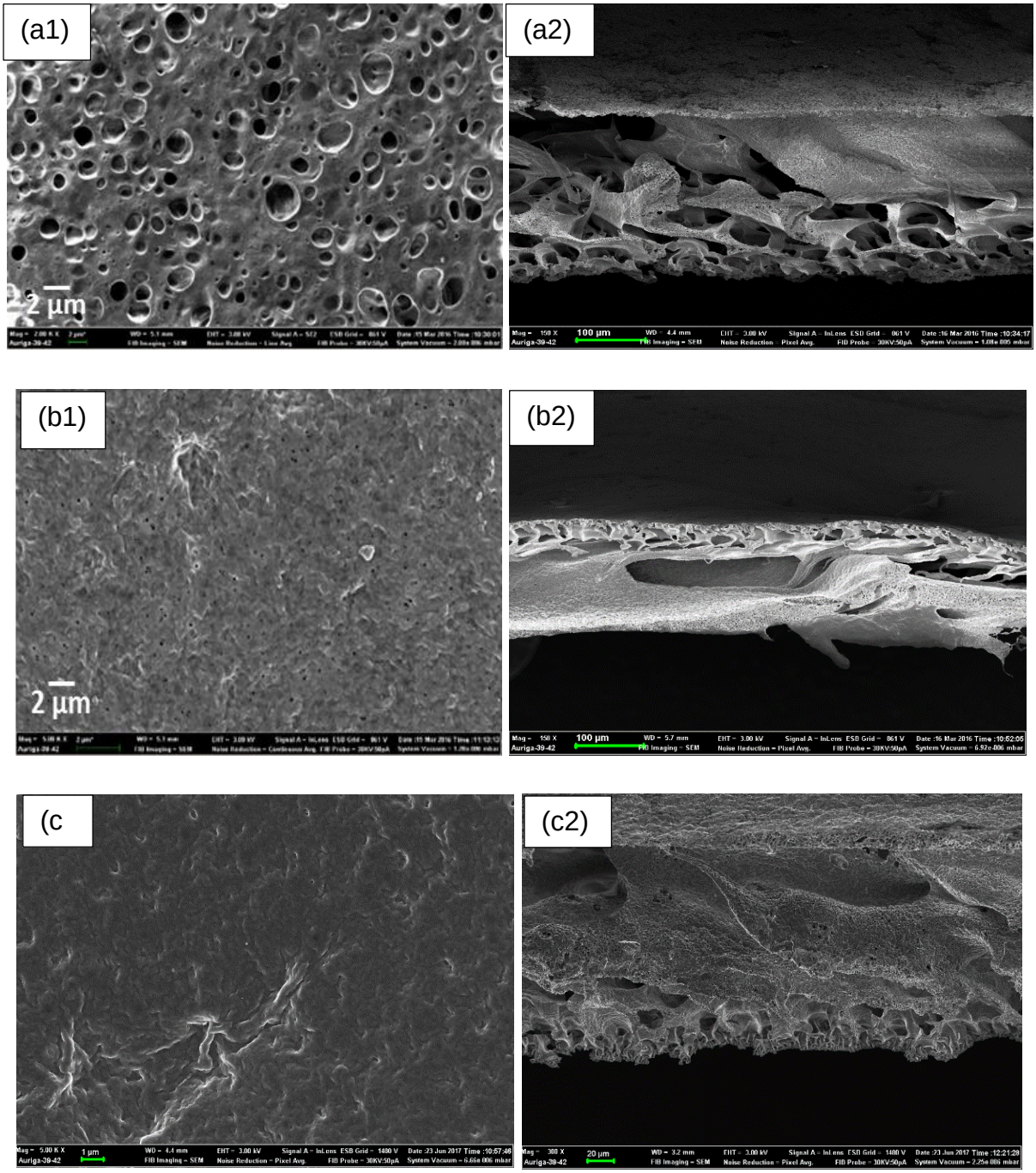

Figure 4.14: SEM images of (a) 5 wt.% Ag/PVDF-HFP, (b) 2.5 wt.% Ag-MWCNTs-PVDF-HFP, (c) 1.8 wt.% Ag-PAMAM/PVDF-HFP composite membranes and their cross-sections (a2, b2 & c2)

Figure 4.14 SEM images of 5 wt.% Ag/PVDF-HFP, 2.5 wt.% Ag-MWCNTs-PVDF-HFP, 1.8 wt.% Ag-PAMAM/PVDF-HFP membranes and their cross-sections. The addition of Ag nanoparticles changed the spongy surface layer of PVDF-HFP (Figure 4.14 a1) into highly porous structure. The cross-section clearly depicts a disappearance of dense layer of PVDF-HFP upon Ag loading (Figure 4.14 a2 & b2). This data is consistent with the improved permeability of the Ag/PVDF-HFP composite membrane (Table 4.2.1), and studies undertaken using on Ag/-PVDF composite membrane reported elsewhere [32]. However, the combined effects of Ag nanoparticles and MWCNTs or PAMAM-MWCNTs did not improve the porosity of PVDF-HFP, as evidenced by the formation of a dense surface layer (Figure 4.14 b1 and c1). These findings correspond with the porosity, water content and swellability data in table 4.2.1. This was further confirmed by an EDX data (Figure 4.15), which indicated the presence of Ag in all PVDF-HFP composite membrane.

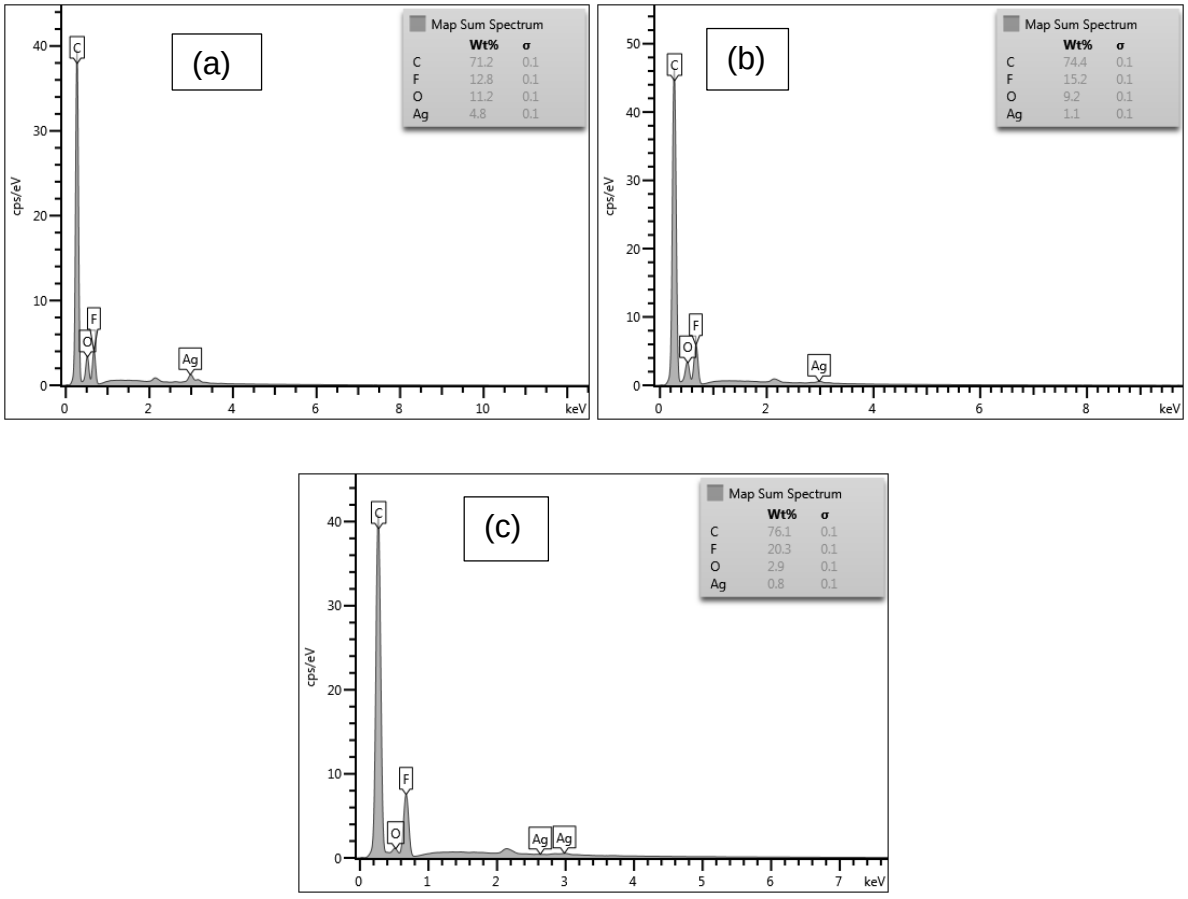

Figure 4.15: EDX results of (a) 5 wt.% Ag/PVDF-HFP, (b) 2.5 wt.% Ag MWCNTs-PVDF/HFP and (c) 1.8 wt.% PAMAM-MWCNTs/PVDF-HFP composite membranes

Figure 4.15 show the EDX results of 5 wt.% Ag/PVDF-HFP, 2.5 wt.% Ag MWCNTs-PVDF/HFP and 1.8 wt.% PAMAM-MWCNTs/PVDF-HFP composite membranes. EDX analysis confirmed that Ag nanoparticles were deposited on the PVDF-HFP based membranes, with oxygen introduced after functionalisation of MWCNTs by nitric and sulphuric acid while carbon and fluorine form part of the PVDF-HFP structure. The results also illustrate efficient interactions and compatibility between PAMAM, PAMAM-MWCNTs or Ag nanoparticles on PVDF-HFP leading to the presence of silver on the surfaces of the PVDF-HFP membranes.

4.1.6 BET Results

The surface area, average pore diameter, and average pore volume for fMWCNTs, PAMAM-MWCNTs, Ag nanoparticles, Ag-MWCNTs, PVDF-HFP, 1 wt.% MWCNTs-PVDF-HFP, 1 wt.% PAMAM-MWCNTs/PVDF-HFP, 2.5 wt.% Ag-MWCNTs/PVDF-HFP and 1.8 wt.% Ag-PAMAM-MWCNTs/PVDF-HFP are presented in Table 4.1.1. The BET data indicated that the surface area of fMWCNTs decreased when PAMAM was introduced in the MWCNTs while its pore volume increased. A similar trend was noticed when comparing the BET surface areas and pore volumes of Ag nanoparticles and Ag-MWCNTs. It is suggested that the observed decrease in surface area resulted from enhanced interfacial interactions between the functional groups on the MWCNTs surfaces and the PAMAM or Ag nanoparticles [33,34].

The BET data for composite membranes showed that the PVDF-HFP composite membranes have low surface area (3.608 m^2g^{-1}); however, after modification with MWCNTs, PAMAM-MWCNTs and Ag-MWCNTs, the surface area increased. The trend was as follows: 1 wt.% PAMAM-MWCNTs/PVDF-HFP > 1.8 wt.% Ag-PAMAM-MWCNTs/PVDF-HFP >1 wt.% MWCNTs-PVDF-HFP > 2.5 wt.% Ag-MWCNTs/PVDF-HFP > PVDF-HFP. According to Li et al. [35], hydrogen bonds develop between the OH of the COOH groups of the functionalized CNTs and the carbonyl groups of the ester linkages of the PVDF-HFP polymer. Thus, the increase in surface area and pore volume of modified PVDF-HFP nanocomposite membranes can be attributed to the crosslinking of MWCNTs and the hydrophobic nature long chain of PVDF-HFP moiety as reported by Kahu et al. [36] on the modified Chitosan.

Table 4.1.1 BET data of fMWCNTs, PAMAM-MWCNTs, Ag nanoparticles, Ag-MWCNTs, PVDF-HFP, 1 wt.% MWCNTs-PVDF-HFP, 1 wt.% PAMAM-MWCNTs/PVDF-HFP, 2.5 wt.% Ag-MWCNTs/PVDF-HFP and 1.8 wt.% Ag-PAMAM-MWCNTs/PVDF-HFP

Sample name	BET surface area (m^2g^{-1})	Pore volume (cm^3g^{-1})	Pore size (nm)
fMWCNTs	239.8	1.797	36.95
PAMAM-MWCNTs	87.71	0.6687	42.79

Ag nanoparticles	339.0	1.113	4.269
Ag-MWCNTs	172.13	1.523	28.59
PVDF-HFP	3.608	0.09436	14.78
1 wt.% MWCNTs-PVDF-HFP	3.772	0.09508	15.51
1 wt.% PAMAM-MWCNTs/PVDF-HFP	3.975	0.1199	19.17
2.5 wt.% Ag-MWCNTs/PVDF-HFP	3.714	0.1075	20.87
1.8 wt.% Ag-PAMAM-MWCNTs/PVDF-HFP	3.822	0.148	21.34

4.2 WATER FILTRATION AND FOULING STUDIES

4.2.1. Physical properties of composite membranes

Table 4.2.1 shows the effects of Ag nanoparticles and MWCNTs on swellability, and water content of PVDF-HFP membrane. The data indicates an increase in porosity (resulting in higher swellability, and water content) of the composite membranes with addition of MWCNTs and/or Ag nanoparticles, showing an improved hydrophilicity. Similar behaviour was reported elsewhere, wherein Ag nanoparticles improved the hydrophilicity of PVDF membrane [37]. It is worth noting that MWCNTs doped PVDF-HFP had higher porosity as compared to a PVDF-HFP composite containing both Ag nanoparticles and MWCNTs. This is thought to be due to the presence of reactive functional groups on the surface of MWCNTs [38], with the later possessing smaller pores due to occupation by Ag nanoparticles. Hydrophilicity of the membranes was further confirmed by contact angle measurements.

Table 4.2.1 Structural features and fouling resistance rate of PVDF-HFP based composite membranes

Type of membrane [a]	Swellability (%)	Water content (%)	Porosity (%)	Fouling resistance rate ($Lm^{-2}min^{-2}$)[b]
PVDF-HFP	12	61	70	0.0233 ± 0.006
5 wt.% Ag/PVDF-HFP	13	67	82	0.0257 ± 0.0032
1 wt.% MWCNTs/PVDF-HFP	22	89	92	0.0467 ± 0.003
1.5 wt.% MWCNTs/PVDF-HFP	20	86	91	0.0455 ± 0.009
2.5 wt.% Ag-MWCNTs/PVDF-HFP	17	88	87	0.0385 ± 0.0043
3 wt.% Ag-MWCNTs/PVDF-HFP	16	87	85	0.0376 ± 0.005
1 wt.% PAMAM-MWCNTs/PVDF-HFP	25	92	94	0.0486 ± 0.004

1.8 wt.% Ag-PAMAM-MWCNTs/PVDF-HFP	18	89	90	0.0393 ± 0.0056

[a]Thickness of all membranes is 180 µm, with an estimated surface area of 0.00126 m^2. [b] Fouling resistance rates were calculated from the gradient of curves in Figure 4.2.1.

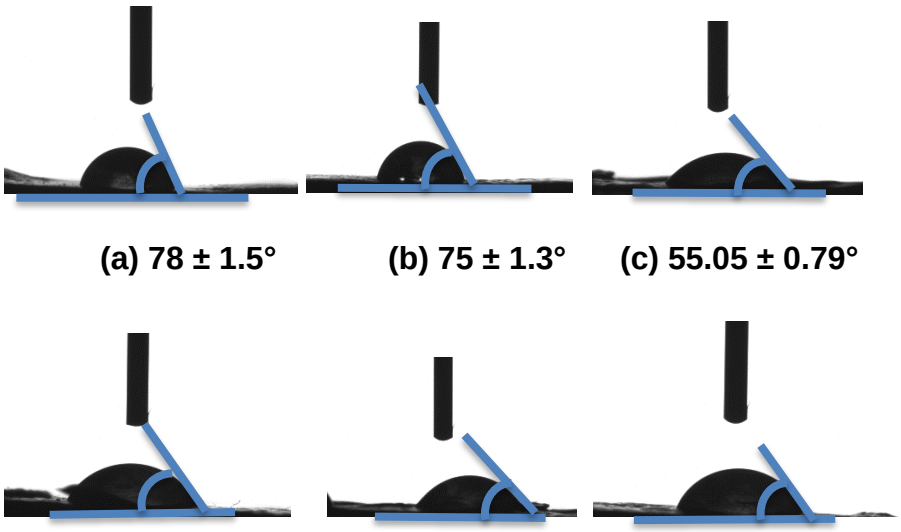

(a) 78 ± 1.5° **(b) 75 ± 1.3°** **(c) 55.05 ± 0.79°**

(d) 66.76 ± 2.21° **(e) 44.98 ± 2.1°** **(f) 64.11 ± 1.6°**

Figure 4.16: Contact angle measurements of (a) PVDF-HFP, (b) 5 wt.% Ag/PVDF-HFP, (c) 1 wt.% MWCNTs/PVDF-HFP, (d) 2.5 wt.% Ag-MWCNTs/ PVDF-HFP, (e) 1 wt.% PAMAM-MWCNTs/PVDF-HFP and (f) 1.8 wt.% Ag-PAMAM-MWCNTS/PVDF-HFP composite membranes

Figure 4.16 shows the contact angles of PVDF-HFP, 5 wt.% Ag/PVDF-HFP, 1 wt.% MWCNTs/PVDF-HFP, 2.5 wt.% Ag-MWCNTs/ PVDF-HFP, 1 wt.% PAMAM-MWCNTs/PVDF-HFP and 1.8 wt.% Ag-PAMAM-MWCNTS/PVDF-HFP membranes. PVDF-HFP membrane and 5 wt.% Ag/PVDF-HFP had the highest water contact angles as compared to the rest of the membranes. The data indicates that the hydrophobicity of PVDF-HFP polymeric membrane was reduced when Ag nanoparticles, PAMAM and MWCNTs were added separately. Surprisingly, the combined Ag and MWCNTs nanoparticles could not further lower the hydrophobicity of PVDF-HFP, but the contact angle was reduced in 1.8 wt.% Ag-PAMAM-MWCNTS/PVDF-HFP. These results correlate with BET results in table 4.1.1.

4.2.2. Water filtration studies

4.2.2.1. Pure water flux measurement and antifouling performance

Figure 4.17 (i & ii) shows the effects of filtrate flux and salt rejection for the water filtered through the PVDF-HFP, 1 wt.% MWCNTs/PVDF-HFP, 1.5 wt.% MWCNTs/PVDF-HFP, 1 wt.% PAMAM-MWCNTs/PVDF-HFP, Ag/PVDF-HFP, 2.5 wt.% Ag-MWCNTs/PVDF-HFP, 3 wt.% Ag-MWCNTs/PVDF-HFP and 1.8 wt.% Ag-PAMAM-MWCNTs/PVDF-HFP composite membranes. The permeation flow rate was measured using 2.0 g/L of an aqueous NaCl feed solution. The data in figure 4.17(i) indicates an initial rapid flux decline in all composite membranes, due to an increase in salt accumulation on the surface of the membranes. The flux decline is initially linked to pores blockage and later formation of a cake layer on the surface of membrane. Similar behaviour was reported elsewhere while monitoring the flux behaviour of bovine serum albumin (BSA) [39].

The salt rejection studies were undertaken by measuring conductivity of the permeate solution as time changes. As the NaCl was accumulating on the membrane surface during filtration, conductivity of the permeate solution decreased. The salt rejection (figure 4.17(ii)) showed the following trend, which correlated with the flux measurements: 1 wt.% PAMAM-MWCNTs/PVDF-HFP > 1 wt.% MWCNTs/PVDF-HFP > 1.5 wt.% MWCNTs/PVDF-HFP > 5 wt.% Ag-/PVDF-HFP > 1.8 wt.% Ag-PAMAM-MWCNTs/PVDF-HFP > 2.5 wt.% Ag-MWCNTs/PVDF-HFP > 3 wt.% Ag-MWCNTs/PVDF-HFP > PVDF-HFP. The results showed improved salt rejection compared to studies reported previously [40,41]. These results imply that the PVDF-HFP membrane modified with PAMAM, MWCNTs and Ag nanoparticles as dopants can be significant for sea water desalination. Salt rejection studies had no significant error bars meaning that the difference in the mean values of flux is not statistically significant. The studies show enhanced results compared to studies reported elsewhere using polyamide membrane and rejecting natural organic matter [42].

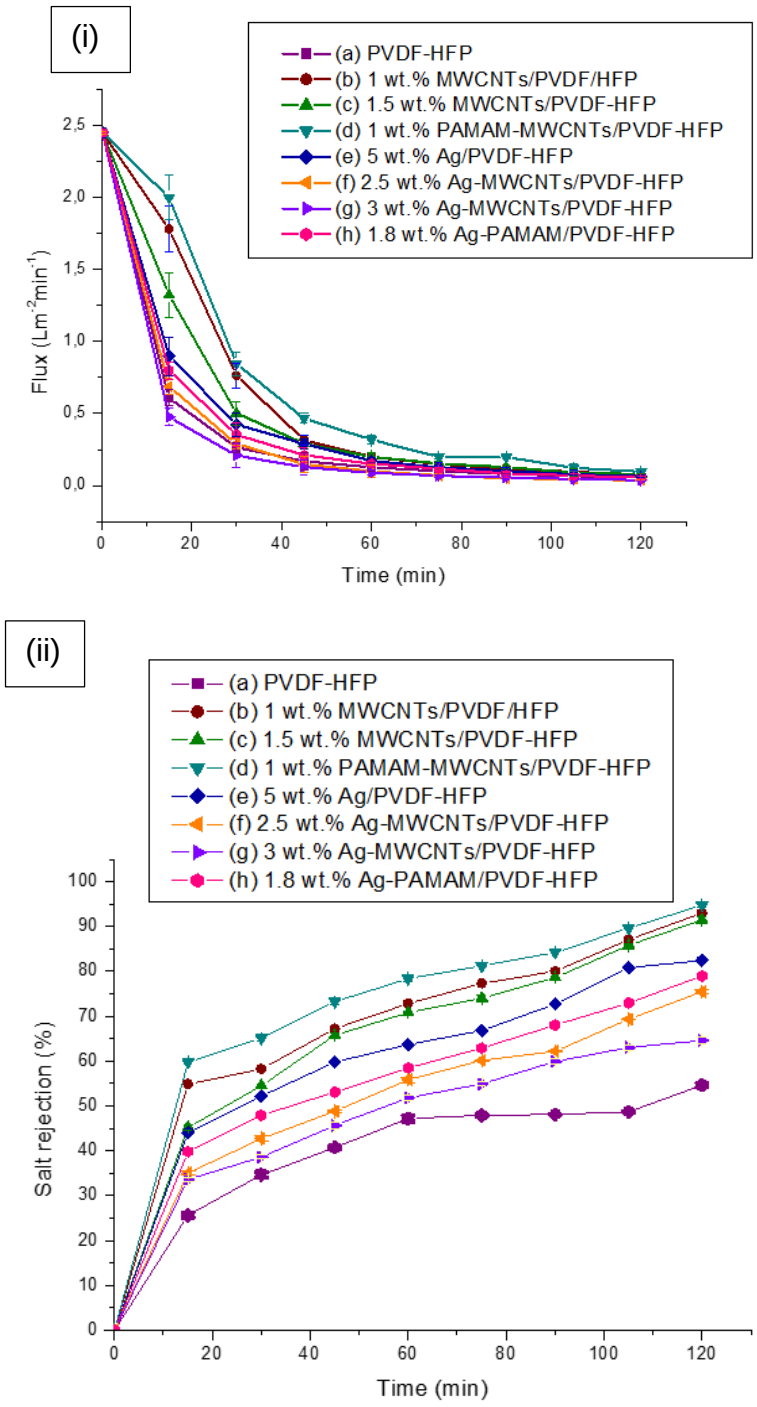

Figure 4.17: (i) Filtrate flux for salted water and (ii) the salt rejection tests filtered through the (a) PVDF-HFP, (b) 1 wt.% MWCNTs/PVDF-HFP, (c) 1.5 wt.% MWCNTs/PVDF-HFP, (d) 1 wt.% PAMAM-MWCNTs/PVDF-HFP, (e) 5 wt.% Ag/PVDF-HFP, (f) 2.5 wt.% Ag-MWCNTs/PVDF-HFP, (g) 3 wt.% Ag-MWCNTs/PVDF-HFP and (h) 1.8 wt.% Ag-PAMAM-MWCNTs/PVDF-HFP composite membranes

The fouling resistance rates of the composites increased as follows: PVDF-HFP < 5 wt.% Ag/PVDF-HFP < 3 wt.% Ag-MWCNTs/PVDF-HFP < 2.5 wt.% Ag-MWCNTs/PVDF-HFP < 1.8 wt.% Ag-PAMAM-MWCNTs/PVDF-HFP < 1.5 wt.% MWCNTs/PVDF-HFP < 1 wt.% MWCNTs/PVDF-HFP < 1 wt.% PAMAM-MWCNTs/PVDF-HFP (Table 4.2.1.1). The fouling resistance rate of 1 wt.% PAMAM-MWCNTs/PVDF-HFP (0.0467 ± 0.003 $L.m^{-2}.min^{-2}$) is higher than the pore blockage/cake filtration model membrane and nanofibrous composite-PVDF-hyper branched membrane (based on the flux rate decline, the filtration model and branched membrane gave values of 2.70 $x10^{-5}$ and 9.23 x 10^{-4} $L.m^{-2}.min^{-2}$, respectively, as calculated from the graph [43-45]. Interestingly, the addition of either Ag nanoparticles, PAMAM or MWCNTs increased the fouling resistance of the PVDF-HFP membrane, which correlate with both the pore sizes (Table 4.2.1) and contact angles of the composite. However, the combination of both Ag nanoparticles and MWCNTs did not further promote fouling resistance of PVDF-HFP membranes, which can be linked to pore blockage by Ag nanoparticles (See Table 4.2.1) and the observed water contact angle (Figure 4.16).

Although the Zeta potential measurements were not done, studies have shown that MWCNTs modified on the PDF-HFP membrane result in formation of conductive membrane materials which cause an increase in the negative charge of the surface of the membrane, as observed also from the contact angle studies [46]. This is usually due to the increased pore sizes (as observed from BET and porosity measurements in section 4.1.6 and section 4.2.2) or due to the electric conductance of MWCNTs and Ag nanoparticles [47,48]. This in turn contributes to the absorption and adsorption of heavy metals during filtration and heavy metal adsorption analyses.

4.2.3 Cadmium (II) and chromium (VI) filtration tests

Figure 4.18 shows the calibration curves of Cd(II) ions and Cr(VI) ions. The standard curves were obtained to calibrate the AAS before analysis of both Cd(II) and Cr(VI) ions was performed.

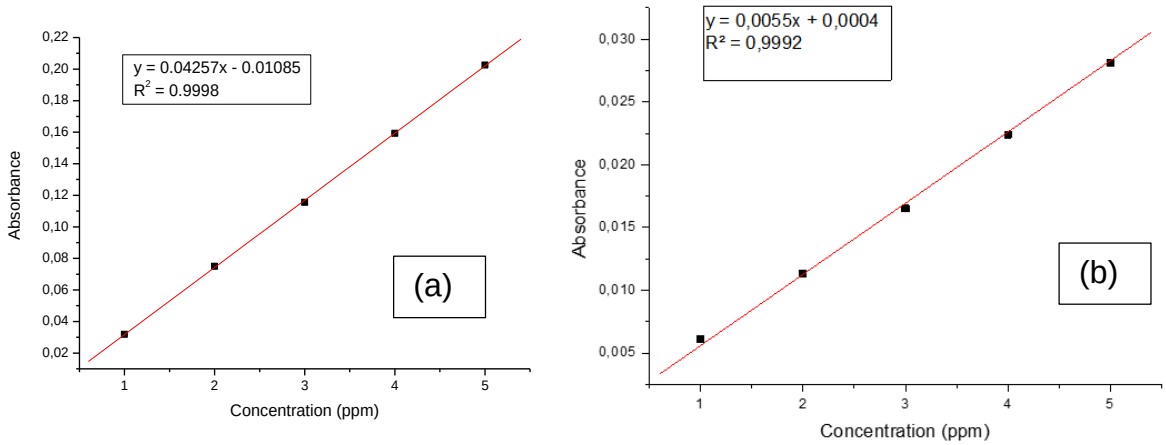

Figure 4.18: The standard curve of (a) Cd(II) ions at 228.3 nm and (b) Cr(VI) ions at 357.87 nm

Table 4.2.2: Cd(II) and Cr(VI) ions removal using PVDF-HFP based composite membranes

Membrane	Cd(II) (8 ppm)	Cr (VI) (8 ppm)
	Cd(II) ions rejection (%)	Cr(VI) rejection (%)
1 wt.% MWCNTs/PVDF-HFP	91	66
1.5 wt.% MWCNTs/PVDF-HFP	89	60
1 wt.% PAMAM-MWCNTs/PVDF-HFP	93	73
1.5 wt.% PAMAM-MWCNTs/PVDF-HFP	91	69
1 wt.% Ag-MWCNTs/PVDF-HFP	69	60
2 wt.% Ag-MWCNTs/PVDF-HFP	71	64
2.5 wt.% Ag-MWCNTs/PVDF-HFP	75	66
2.8 wt.% Ag-MWCNTs/PVDF-HFP	72	62
3 wt.% Ag-MWCNTs/PVDF-HFP	70	62

1.5 wt.% Ag-PAMAM-MWCNTs/PVDF-HFP	84	62
1.8 wt.% Ag-PAMAM-MWCNTs/PVDF-HFP	90	72
2.0 wt.% Ag- PAMAM-MWCNTs/PVDF-HFP	87	70

Table 4.2.2 shows the Cd(II) and Cr(VI) ions filtration results using a variety of PVDF-HFP composite membranes. Both Cd(II) and Cr(VI) ions rejection decreased with an increase in MWCNTs and PAMAM-MWCNTs doping on PVDF-HFP composite membrane. However, it was noted that the rejection was higher for 1 wt.% PAMAM-MWCNTs/PVDF-HFP than that of 1 wt.% MWCNTs/PVDF-HFP. The effect of Ag within the 2.5 wt.% Ag-MWCNTs/PVDF-HFP composite membrane is noted by the highest rejection of both Cd(II) and Cr(VI) ions.

When Ag-PAMAM was doped on PVDF-HFP, the best metal rejection was achieved with the 1.8 wt.% Ag-PAMAM-MWCNTs/PVDF-HFP composite material. The highest percentage rejection for both metals was obtained when using the 1 wt.% PAMAM-MWCNTs/PVDF-HFP followed by 1.5 wt.% PAMAM-MWCNTs/PVDF-HFP & 1 wt.% MWCNTs/PVDF-HFP, 1.8 wt.% Ag-PAMAM-MWCNTs/PVDF-HFP, 1.5 wt.% MWCNTs/PVDF-HFP, 2.0 wt.% Ag- PAMAM-MWCNTs/PVDF-HFP, 1.5 wt.% Ag-PAMAM-MWCNTs/PVDF-HFP, 2.5 wt.% Ag-MWCNTs/PVDF-HFP, 2.8 wt.% Ag-MWCNTs/PVDF-HFP, 2 wt.% Ag-MWCNTs/PVDF-HFP, 3 wt.% Ag-MWCNTs/PVDF-HFP and lastly 1 wt.% Ag-MWCNTs/PVDF-HFP. The high rejection correlated with high porosity and surface area, as confirmed by BET data for 1 wt.% PAMAM-MWCNTs/PVDF-HFP composite membrane. The same membrane later also showed good adsorption properties for cadmium (II) and chromium (VI) ions.

4.2.4 Filtration of *E. coli* spiked water with composite membranes

4.2.4.1 Effects of membrane compositions on filtration of *E. coli* bacteria

Table 4.2.3 shows the effects of various dopants on PVDF-HFP polymeric membrane on *E. coli* bacteria. Complete entrapment of bacteria (100% reduction) was observed with 2.5 wt.% Ag-MWCNTs/PVDF-HFP, 1 wt.% MWCNTs-PVDF-HFP, 1 wt.%

PAMAM-MWCNTs/PVDF-HFP and 1.8 wt. Ag-PAMAM-MWCNTs/PVDF-HFP composite membranes, whereas 5 wt.% Ag/PVDF-HFP showed 87% reduction followed by 67% microbial reduction with PVDF-HFP membrane (Table 4.2.3). It is evident from these results that the pore sizes of 2.5 wt.% Ag-MWCNTs/PVDF-HFP, 1 wt.% MWCNTs-PVDF-HFP, 1 wt.% PAMAM-MWCNTs/PVDF-HFP, and 1.8 wt.% Ag-PAMAM-MWCNTs/PVDF-HFP composite membranes were optimum for entrapment of bacteria while allowing water to easily pass through.

Table 4.2.3. Effects of membrane compositions on filtration of *E. coli*.

Membrane	**Pre-filtration colony count (CFU/100mL)**	**Post-filtration colony count (CFU/100mL)**	**% microbial load reduction**
PVDF-HFP	150	50	67
1 wt.% MWCNTs-PVDF-HFP	150	0	100
1 wt.% PAMAM-MWCNTs/PVDF-HFP	150	0	100
2.5 wt.% Ag-MWCNTs/PVDF-HFP	150	0	100
1.8 wt.% Ag-PAMAM-MWCNTs/PVDF-HFP	150	0	100
5 wt.% Ag/PVDF-HFP	150	20	87

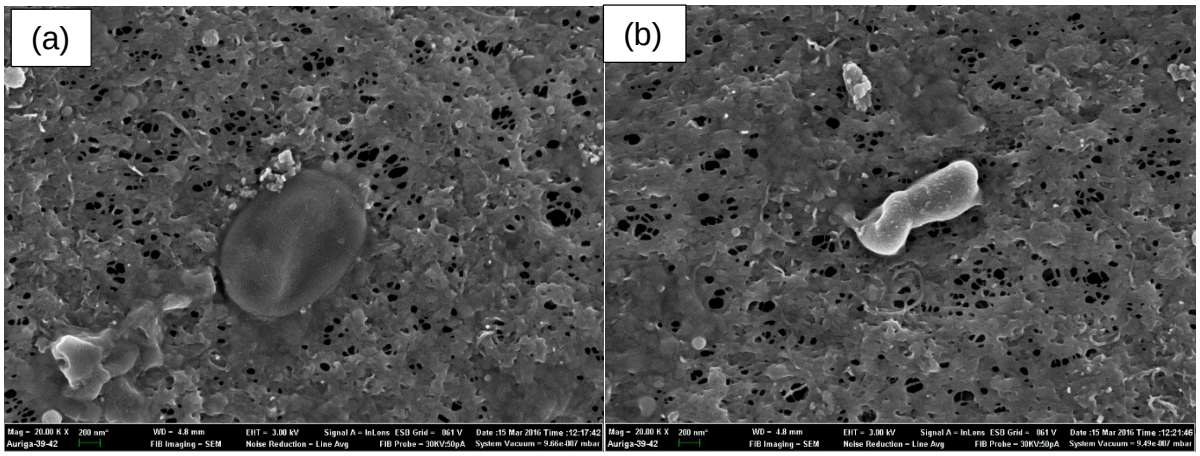

Figure 4.19: (a) 2.5 wt.% Ag-MWCNTs-PVDF-HFP and (b) 1.8 wt.% Ag-PAMAM-MWCNTs/PVDF-HFP after *E. coli* filtration

Figure 4.19 shows SEM results of 2.5 wt.% Ag-MWCNTs-PVDF-HFP and 1.8 wt.% Ag-PAMAM-MWCNTs/PVDF-HFP nanocomposite membranes after *E. coli* filtration tests. After filtration test, the membranes were sterilised to kill the bacteria, and allowed to dry at room temperature. The SEM data in figure 4.2.5, confirmed that *E. coli* (1.5 µm) was trapped on the surface of both 2.5 wt.% Ag-MWCNTs-PVDF-HFP and (b) 1.8 wt.% Ag-PAMAM-MWCNTs/PVDF-HFP composite membranes. It is also clear that the size of the bacteria was bigger than the pore sizes of the membrane pores.

4.2.4.2. Evaluation of antibacterial and non-leaching properties of PVDF-HFP composite membranes

The evaluation of the antibacterial activity of PVDF-HFP, 5 wt.% Ag/PVDF-HFP, 1 wt.% MWCNTs-PVDF-HFP, 2.5 wt.% Ag-MWCNTs-PVDF-HFP, 1 wt.% PAMAM-MWCNTs/PVDF-HFP and 1.8 wt.% Ag-PAMAM-MWCNTs/PVDF-HFP composite membranes. There was no bacterial growth on the top of 1.8 wt.% Ag-PAMAM-MWCNTs/PVDF-HFP and 2.5 wt.% Ag-MWCNTs-PVDF-HFP composite membrane following vacuum filtration of *E. coli* spiked water (Figure 4.20(d, e & f)). These findings can be attributed to the presence of Ag nanoparticles dispersed on the surface of MWCNTs. The Ag nanoparticles are not present on 1 wt.% MWCNTs-PVDF-HFP composite; hence confluent *E. coli* was observed in figure 4.20c.

Interestingly, the 1 wt.% PAMAM-MWCNTs/PVDF-HFP (figure 4.20e) composite membrane also did not have bacterial growth on the surface, which can be attributed to the properties of dendritic PAMAM attached on the walls of CNTs [8]. The PAMAM-MWNTs are more antimicrobial than MWCNTs-COOH due to PAMAM and MWCNTs bundle effects. MWCNTs are usually in the form of bundles and ropes because of their intrinsic van der Waals force attraction and high aspect ratio nature [8]. Functionalization of MWCNTs with PAMAM helps in debundling MWCNTs ropes and improves their dispersion. The bundle of PAMAM-MWNTs is likely to be smaller than that of fMWCNTs. Kang et al. [49] provided evidence that size (diameter) of CNTs is a key factor governing their antimicrobial activity, thus, compared with MWCNTs-COOH, the increased antimicrobial effect of d-MWCNTs may be attributed partially to their smaller bundle size. Furthermore, 2.5 wt.% Ag-MWCNTs/PVDF-HFP and 1.8 wt.% Ag-PAMAM-MWCNTs/PVDF-HFP membrane showed good non-leaching properties of the dopant materials (MWCNTs and Ag), as evidenced by bacterial growth on the edges of the membranes (Figure 4.20c, d & e).

The leaching studies of Ag were conducted on filtrates with an ICP-OES technique (after 2 h of filtration, collecting approximately 2 L of water), using silver doped membranes. Interestingly, the control tap water analysed contained 0.0228 ±0.013 mg/L of Ag, which is below permissible levels by WHO [44]. The filtrates of Ag/PVDF-HFP, 2.5 wt.% Ag-MWCNTs/PVDF-HFP and 1.8 wt.% Ag-PAMAM-MWCNTs/PVDF-HFP composite membranes contained 0.0275 ± 0.016, 0.0257 ± 0.015 and 0.0158 ± 0.011 mg/L of Ag, respectively. The results indicate that the membranes leach out very small amounts of Ag, as compared to the amount loaded on the membranes; and the leached amounts are still below the acceptable limits of WHO (i.e., 0.1 mg/L Ag in drinking water) [5]. These results contradicted the work reported in the literature [32,45] where in an inhibitory halo zone around the membrane was observed. This makes Ag-MWCNTs/PVDF-HFP and Ag-PAMAM-MWCNTs/PVDF-HFP composite membrane ideal water purification membranes wherein dopant materials do not leach out.

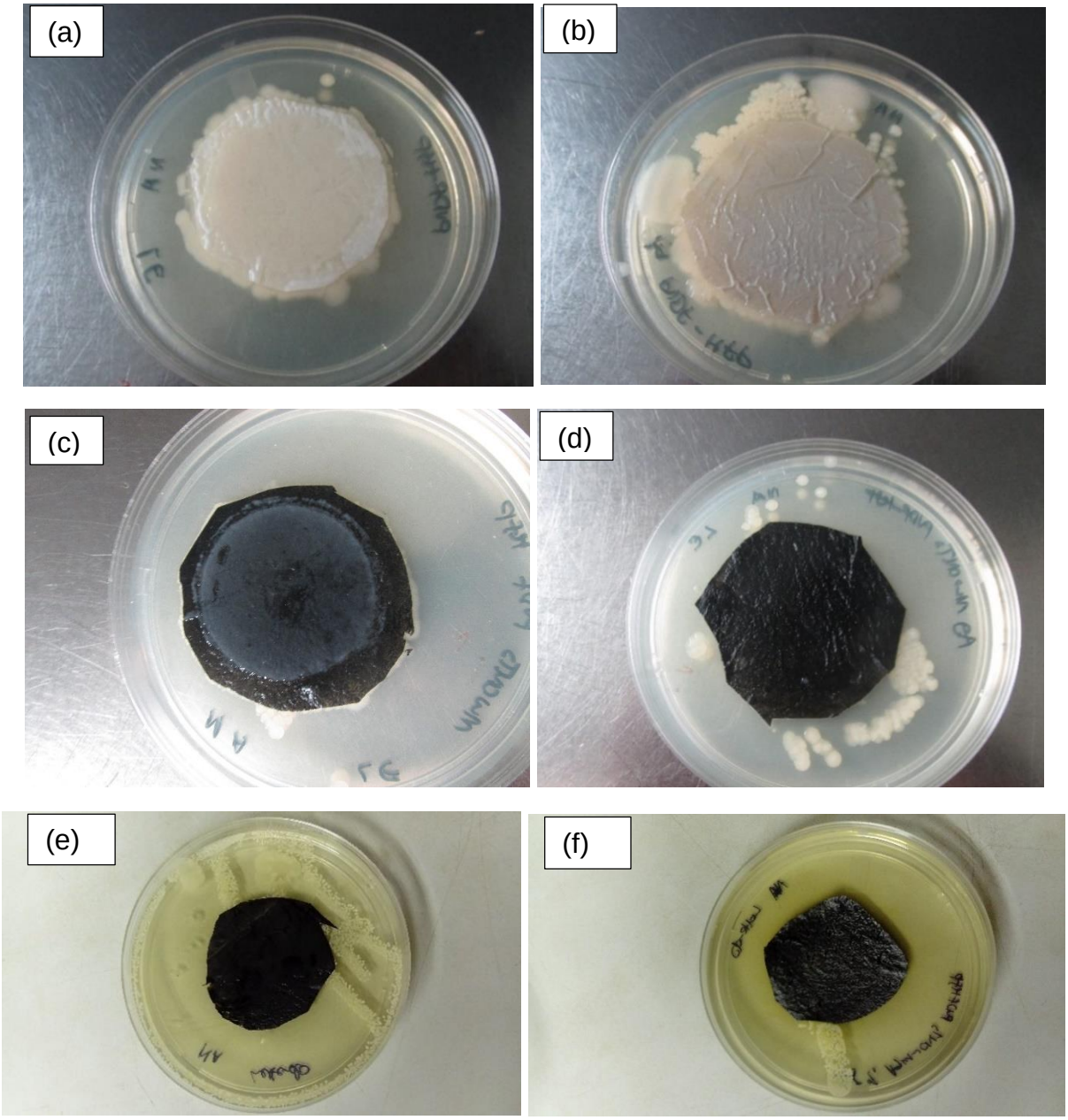

Figure 4.20: Evaluation of antibacterial activity of (a) PVDF-HFP, (b) 5 wt.% Ag/PVDF-HFP, (c) 1 wt.% MWCNTs-PVDF-HFP (d) 2.5 wt.% Ag-MWCNTs-PVDF-HFP, (e) 1 wt.% PAMAM-MWCNTs/PVDF-HFP and (f) 1.8 wt.% Ag-PAMAM-MWCNTs/PVDF-HFP composite membranes

The antibacterial activity of 2.5 wt.% Ag-MWCNTs/PVDF-HFP composite membrane was further confirmed by incubating the membrane in nutrient broth for 24 h (figure 4.21). No growth was observed as indicated by non-turbid broth media in the test sample (figure 4.21a), while growth was observed as cloudiness in the reference sample (figure 4.21b).

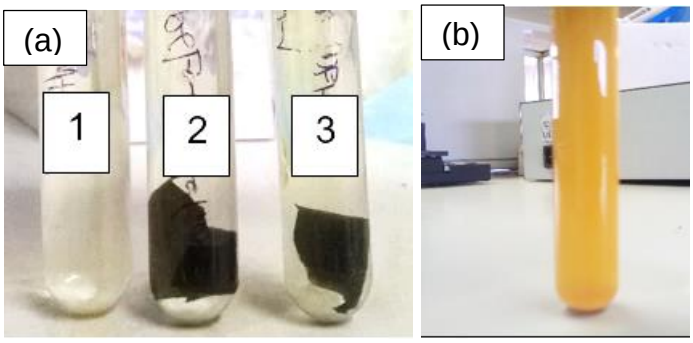

Figure 4.21: Demonstration of bactericidal property of Ag-MWCNTs/PVDF-HFP membrane in *nutrient* broth media and (b) growth of *E. coli* bacteria in nutrient broth medium.

4.2.5 Surface and ground water sample analysis

4.2.5.1 Physicochemical properties of collected surface and ground water samples

Table 4.2.4 shows the physicochemical properties of surface and ground water before and after analysis. The physical parameters are described in section 4.2.5.1.1 and the chemical parameters are described in section 4.2.5.1.2. As discussed in section 3.9.3.2, surface water samples were collected from Olifants River next to Flag Boshielo dam, Makotswane dam, and Apel cross furrow in the Sekhukhune district, Limpopo province. Borehole water samples were collected from three areas in Jerome, Malamulele and Shigalo village in Vhembe district, also in Limpopo province. Both the ground and surface water were sampled from water resources which are used by surrounding communities for domestic purposes. Hence it is important to analyse these water samples to assist the communities in case the water is not fit for human consumption prior purification or not, as well as to provide a better solution.

Table 4.2.4: Physicochemical analysis of surface and ground water samples before and after treatment

Sample names	Physical parameters					Chemical parameters		
	Conductivity (mS/m)	Colour (mg/L Pt)		Turbidity (NTU)	TSS (mg/L)	pH	TDS (mg/L)	Carbonate hardness (mg/L)
		Apparent colour	True colour					
SANS 241 standards	≤170	≤15	≤15	≤5	≤5	≥5 to ≤9.7	≤1200	≤150
WHO Standards	≤250	≤15	≤6	≤5	≤5	≥6.5 to ≤8.5	≤1000	≤100
Water samples analysed before membrane filtration								
Olifants river	62.5	8.5	0.7	58	26	7.78	313	8.5
Makotswane dam	85.5	0.4	0.5	5	18	8.55	428	14.7
Apel cross furrow	41.3	1.8	0.3	11	22	8.17	205	7.9
Pooled surface water	63.5	3.0	0.3	21	28	8.15	320	10.4
Borehole 1[a]	127.6	1.4	0.8	20	15	7.40	1276	18.1
Borehole 2[b]	140.7	0.9	0.6	46	6	7.24	1406	16.0
Borehole 3[c]	130.2	1.8	0.5	15	22	7.45	106	4.0
Pooled borehole	130.4	1.3	0.6	28	14	7.37	492	15.4

Water samples analysed after membrane filtration								
Sample names	**Physical parameters**					**Chemical parameters**		
	Conductivity (mS/m)	**Colour (mg/L Pt)**		**Turbidity (NTU)**	**TSS (mg/L)**	**pH**	**TDS (mg/L)**	**Carbonate hardness (mg/L)**
***Membrane 1 filtered pooled water**	15.1	0.3	0.2	4	1	7. 26	75	5.9
****Membrane 2 filtered pooled water**	24.2	0.6	0.6	7	8	7. 69	121	2.3
***Membrane 1 filtered pooled borehole water**	26.3	0.2	0.2	4	1	7.28	32	7.9
****Membrane 2 filtered pooled borehole water**	44.9	0.3	0.2	5	4	7.21	223	2.6

[a]Jerome borehole, [b]Malamulele borehole and [c]Shigalo borehole.

* **Membrane 1** is 1.8 wt.% Ag-PAMAM-MWCNTs/PVDF-HFP and ****Membrane 2** is 2.5 wt.% Ag-MWCNTs/PVDF-HFP composite membranes.

4.2.5.1.1 Physical parameters

Conductivity

Conductivity measurements were recorded in table 4.2.4. Conductivity measures the ability of water to conduct an electrical current as a result of the presence of ions in water such as carbonate, bicarbonate, chloride, sulphate, nitrate, sodium, potassium, calcium and magnesium (all of which carry an electrical charge) [50]. The data indicated that the conductivity measurements of ground water samples were greater than that of surface water samples. The conductivity measurements (table 4.2.4) of all the surface and borehole water were below the standard limit of 170 mS/m [41]. The conductivity of both pooled surface and borehole water were reduced after filtration with 1.8 wt.% Ag-PAMAM-MWCNTs/PVDF-HFP and 2.5 wt.% Ag-MWCNTs/PVDF-HFP composite membranes. The conductivity remained within the limits which is ≤ 170 mS/m as recommended by SANS 241 [51] and WHO.

Colour

Apparent colour and true colour measurements were recorded in table 4.2.4. Olifants river and borehole 3 (Shigalo borehole) had the highest apparent colour of 8.5 and 1.8 respectively, as compared to the rest of the water samples analysed. The apparent colour for both surface and borehole water samples (after filtration with 1.8 wt.% Ag-PAMAM-MWCNTs/PVDF-HFP and 2.5 wt.% Ag-MWCNTs/PVDF-HFP composite membranes) was comparable with the true colour determined after the glass fibre membrane filtration. This demonstrated that 1.8 wt.% Ag-PAMAM-MWCNTs/PVDF-HFP and 2.5 wt.% Ag-MWCNTs/PVDF-HFP composite membranes filters had significantly reduced the colour of water to more desirable colourless water. Borehole water samples were clearer than surface waters since ground water is not exposed to the environment. Colour also affects the acceptability of drinking water, which is the aesthetic property of drinking water.

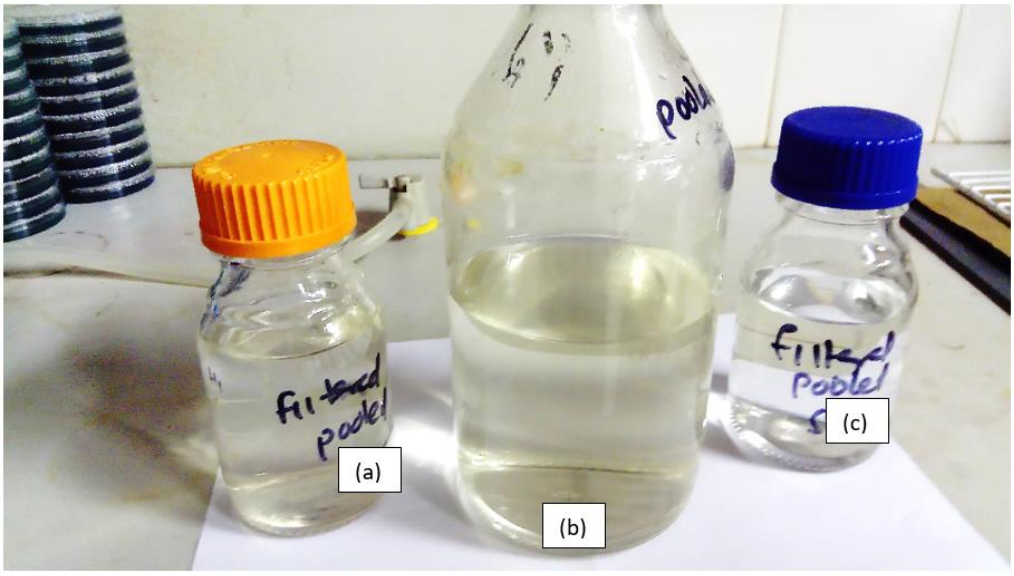

Figure 4.22: Surface water samples filtered with (a) 2.5 wt.% Ag-MWCNTs/PVDF-HFP, (b) pooled unfiltered water and (c) 1.8 wt.% Ag-PAMAM-MWCNTs/PVDF-HFP

The images of the surface water before and after filtering pooled water are shown in figure 4.22. The images are in agreement with the measured colour from the UV/Vis wherein the colour of the water filtered with 1.8 wt.% Ag-PAMAM-MWCNTs/PVDF-HFP membrane, was more improved as compared to the water filtered with 2.5 wt.% Ag-MWCNTs/PVDF-HFP and pooled unfiltered water. The analysis also correlates with the TSS results and surface area measurements.

Turbidity

Turbidity measurements were recorded in table 4.2.4. Turbidity in water is caused by the presence of suspended matter which usually consists of a mixture of inorganic matter, such as clay and soil particles, organic matter and microorganisms, hence Olifants river water samples showed highest turbidity. The turbidity for borehole and surface water reduced after membrane filtration, with 1.8 wt.% Ag-PAMAM-MWCNTs/PVDF-HFP composite membrane giving values within the allowable limits.

Total suspended solids

Total suspended solids (TSS) analysis results were recorded in table 4.2.4. TSS affect water clarity because the presence of suspended solids in water block light to pass through when measuring turbidity resulting in high value of turbidity. Figure 4.2.9 shows the TSS determination using glass fibre membranes after analysing pooled surface water filtered with 1.8 wt.% Ag-PAMAM-MWCNTs/PVDF-HFP and 2.5 wt.% Ag-MWCNTs/PVDF-HFP composite membrane filtered water samples. From figure 4.23 it can be clearly seen that the glass fibre membrane which was used to analyse the filtrates of 1.8 wt.% Ag-PAMAM-MWCNTs/PVDF-HFP composite membrane was more clean compared to the glass fibre membranes used to analyse the filtrates of 2.5 wt.% Ag-MWCNTs/PVDF-HFP composite membrane. The total suspended solids (TSS) for both surface and ground water were above the SANS 241 [51] limits of ≤5. TSS for both surface and ground water were reduced to acceptable limits after filtering with 1.8 wt.% Ag-PAMAM-MWCNTs/PVDF-HFP composite membranes.

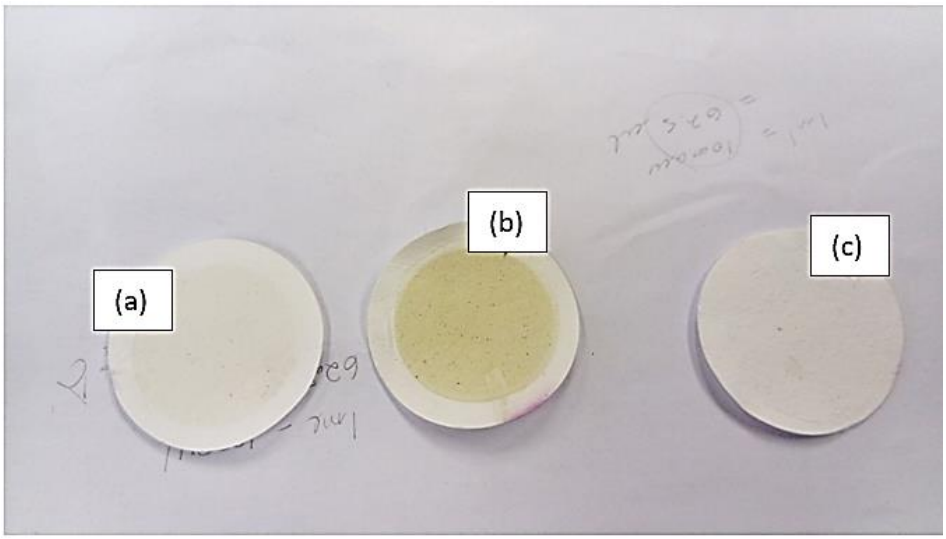

Figure 4.23: TSS determination using glass fibre membranes after analysing surface water (a) filtered with2.5 wt.% Ag-MWCNTs/PVDF-HFP, (b) pooled unfiltered water and (c) 1.8 wt.% Ag-PAMAM-MWCNTs/PVDF-HFP filtered water samples

4.2.5.1.2 Chemical parameters

pH

A pH value closer to the neutral is most desired for drinking water. The pH of the water samples was all within acceptable levels of ≥ 5 to ≤ 9.7 (see table 4.2.4) [31]. The pH of water from the three boreholes was neutral, as compared to the surface water with basic pH. The pH was reduced from 8.15 to 7.26 and 7.24 for pooled surface water samples and from 7.37 to 7.28 and 7.21 borehole water samples respectively after filtration with 1.8 wt.% Ag-PAMAM-MWCNTs/PVDF-HFP and 2.5 wt.% Ag-MWCNTs/PVDF-HFP composite membranes. The 1.8 wt.% Ag-PAMAM-MWCNTs/PVDF-HFP composite membranes showing the lowest pH. Water has positive H^+ ions and OH^- ions. When water is passed through a semi permeable membrane using pressure (like in the case of 1.8 wt.% Ag-PAMAM-MWCNTs/PVDF-HFP), many organic and inorganic compounds fail to pass through, however gases like carbon dioxide make it to the other side. CO_2 combines with the free OH^- ions in water to form acidic HCO_3, while the H^+ ions fail to find any substance to interact with as most of the impurities have been removed through the RO process. As a result, the water will have a positive balance of H^+ ion, and hence the pH gets lowered slightly [52].

Total dissolved solids

Total dissolved solids (TDS) measurements were recorded in table 4.2.4. As previously stated, TDS is directly proportional to the electrical conductivity of water [30], since the properties of the TDS are governed by the characteristics of the constituent inorganic salts dissolved in water. The total dissolved solids for the surface water were all at acceptable limits of ≤ 1 200 mg/L while the borehole 1 and 2 water samples showed limits above the SANS 241 [51], except for borehole 3. After filtration with 1.8 wt.% Ag-PAMAM-MWCNTs/PVDF-HFP and 2.5 wt.% Ag-MWCNTs/PVDF-HFP composite membranes, TDS was significantly reduced to acceptable limits for both ground and surface water with 1.8 wt.% Ag-PAMAM-MWCNTs/PVDF-HFP composite membranes showing better results.

Carbonate hardness

Carbonate hardness measurements were recorded in table 4.2.4. Borehole water samples had the high values of water hardness, this is because ground water is in constant contact with minerals in the soil and rocks; and as it flows through, these minerals are dissolved. The carbonate hardness of the water samples analysed were all within the acceptable limits according to SANS 241 [51] limits. The carbonate hardness was further reduced after both 1.8 wt.% Ag-PAMAM-MWCNTs/PVDF-HFP and 2.5 wt.% Ag-MWCNTs/PVDF-HFP composite membranes filtration for both surface and ground pooled water samples.

An evaluation of the physicochemical quality of water in the present study confirmed that the surface water and ground water can be greatly improved by filtration with the prepared 1.8 wt.% Ag-PAMAM-MWCNTs/PVDF-HFP and 2.5 wt.% Ag-MWCNTs/PVDF-HFP composite membranes. The 1.8 wt.% Ag-PAMAM-MWCNTs/PVDF-HFP composite membrane showed better results than the 2.5 wt.% Ag-MWCNTs/PVDF-HFP composite membrane for both ground water and surface water. These membranes also showed improved surface areas by BET (table 4.1.1), high hydrophilicity observed from contact angle measurements (figure 4.16), water content and porosity measurement. However, both the two membranes can still be used interchangeably.

4.2.5.2 Microbial analysis of the collected surface and ground water samples

4.2.5.2.1 Microbial analysis

Table 4.2.5 shows the microbial assay of surface and borehole water before and after analysis. The surface water microbiological study (table 4.2.5) confirmed that the selected water sources from Sekhukhune area are not suitable for consumption if not treated prior to consumption. For the microbial analysis in surface water, 1.8 wt.% Ag-PAMAM-MWCNTs/PVDF-HFP composite membrane showed better results, as no bacteria was observed after filtration. The same membranes had shown better physicochemical properties after filtration. There were also no bacteria observed in all the three borehole water samples before and after filtration, meaning that the water is relatively clean for microbial contamination.

Table 4.2.5: Enumeration of bacteria in surface and ground water samples before and after membrane filtration

Samples	***Enterobacteriaeceae*** **(CFU/mL)**	***E. coli*** **(CFU/ 100 mL)**	**Total Coliform (CFU/ 100 mL)**	**Aerobic Count (CFU/mL)**
SANS standard	Not mentioned	Not detected	≤10	≤ 1 000
WHO standard	Not mentioned	Not detected	≤200	≤ 1 000
Water samples analysed before membrane filtration				
Olifants	21	0	10	>4.9 x10 ^{5}
Makotswane dam	0	0	0	>4.9 x10 ^{5}
Apel cross furrow	1.1 x 10 ^{2}	10	2.1 x10 ^{2}	>4.9 x10 ^{5}
Pooled surface water	89	10	105	>4.9 x10 ^{5}
Borehole 1[a]	0	0	0	-
Borehole 2[b]	0	0	0	-
Borehole 3[c]	0	0	0	-
Pooled borehole	0	0	0	-
Water samples analysed after membrane filtration				
***Membrane 1 filtered pooled surface water**	0	0	0	0

****Membrane 2 filtered pooled surface water**	21	0	21	>4.9 x10 ^{5}
Membrane 1 filtered Pooled borehole water	0	0	0	-
Membrane 2 filtered Pooled borehole water	0	0	0	-

***Membrane 1** is 1.8 wt.% Ag-PAMAM-MWCNTs/PVDF-HFP and ****Membrane 2** is 2.5 wt.% Ag-MWCNTs/PVDF-HFP composite membranes. [a]Jerome borehole, [b]Malamulele borehole and [c]Shigalo borehole.

4.2.5.2.2 Biochemical oxygen demand

Table 4.2.6 shows the BOD for ground, surface and filtered water samples with 1.8 wt.% Ag-PAMAM-MWCNTs/PVDF-HFP and 2.5 wt.% Ag-MWCNTs/PVDF-HFP composite membranes. BOD is the amount of dissolved oxygen required to meet the metabolic needs of aerobic organisms in water rich in organic matter (WHO, 2004). It is a measure of the biochemically-mediated oxygen demand of water that is indicative of that portion of the organic carbon which is relatively easily oxidised by micro-organisms. The BOD of Apel cross and Olifants River were higher than that of Makotswane dam. All the BOD of surface water samples was also higher than the BOD of ground water, since surface water was more contaminated by microorganisms. The 1.8 wt.% Ag-PAMAM-MWCNTs/PVDF-HFP composite membrane showed the lowest BOD for both surface and ground water in day zero and after day 5.

Water sample with a 5-day BOD between 1 and 2 mg/L indicates very clean water, 3.0 to 5.0 mg/L indicates moderately clean water and above 8 mg/L indicates severely polluted water (for river water) [53]. The borehole water was moderately clean, even before filtration as compared to the surface water which is heavily polluted, and this

correlated with the results in table 4.2.5. The results indicate that the control water sample, pooled filtered surface and pooled filtered borehole water samples were clean after filtration by 1.8 wt.% PAMAM-MWCNTs/PVDF-HFP composite membrane.

Table 4.2.6 show BOD results for surface and ground water samples before and after treatment

Sample names	**Concentration measurements (mg/L)**		**Oxygen consumption (mg/L)**	**BOD_5 (mg/L O_5) = D x (O_s - O_s) +O_c**
	Day zero	**After 5 days**		
Water samples analysed before membrane filtration				
Control	11.6	9.9	1.7	1.7
Olifants river	27.8	11.6	16.2	16.2
Makotswane dam	26.0	12.7	13.3	13.3
Apel cross furrow	27.8	11.6	16.2	16.2
Pooled surface water	27.8	14.2	13.6	13.6
Borehole 1[a]	13.2	8.5	4.7	4.7
Borehole 2[b]	12.9	8.9	4.0	4.0
Borehole 3[c]	13.3	8.1	5.1	5.0
Pooled borehole	13.0	8.7	4.3	4.3
Water samples analysed after membrane filtration				
***Membrane 1 filtered Pooled surface water**	15.7	12.5	3.0	3.0
****Membrane 2 filtered Pooled surface water**	19.3	15.5	3.8	3.8
***Membrane 1 filtered Pooled borehole water**	8.9	6.2	2.7	2.7

[**]Membrane 2 filtered Pooled borehole water	10.8	6.7	4.1	4.1

[*]**Membrane 1** is 1.8 wt.% Ag-PAMAM-MWCNTs/PVDF-HFP and [**]**Membrane 2** is 2.5 wt.% Ag-MWCNTs/PVDF-HFP. [a]Jerome borehole, [b]Malamulele borehole and [c]Shigalo borehole.

4.2.5.3 Heavy metal analysis of the collected surface and ground water samples

The standard curves in figure 4.24 was obtained during the calibration of AAS for heavy metal analysis for the collected water samples. The R^2 values were all 0.999 and above, indicating good linear fit.

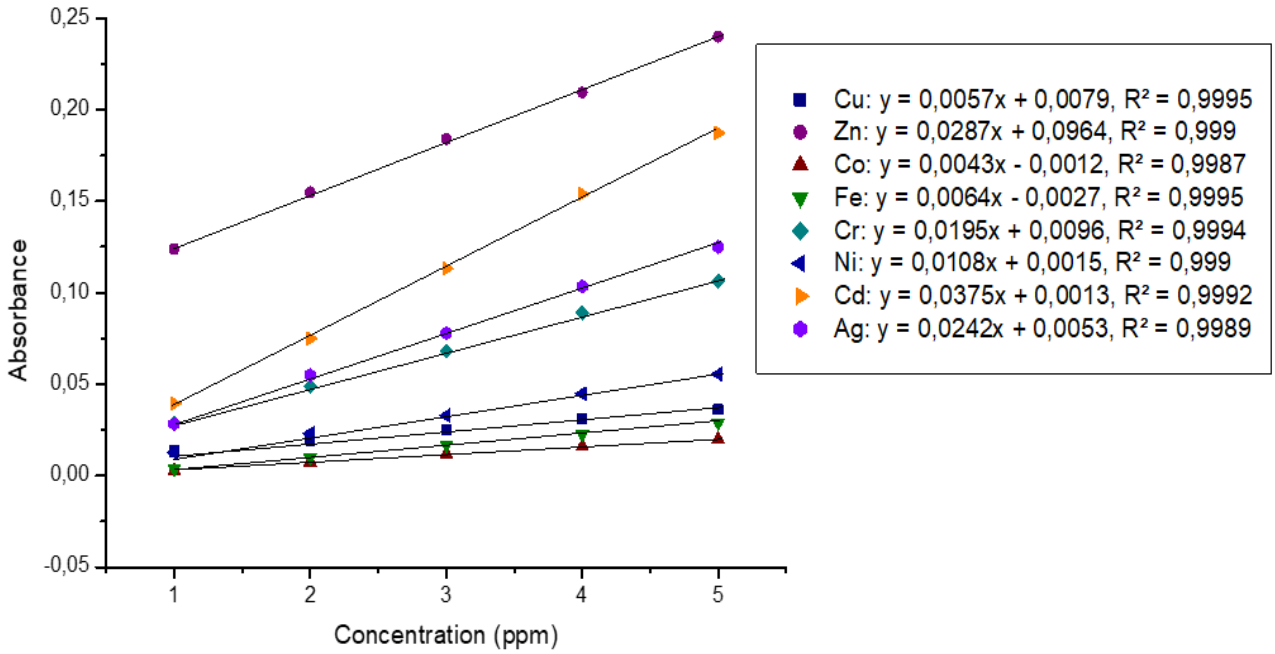

Figure 4.24: Standard curves of Cu, Cu, Zn, Co, Fe, Cr, Ni, Cd and Ag used for AAS calibration before water analysis.

Table 4.2.7: Atomic adsorption spectroscopy (AAS) elemental analysis for borehole, surface water and membrane filtered water.

Sample name	**Concentration (mg/L)**						
Determinand	Cu	Zn	Fe	Cr	Ni	Cd	Ag
SANS standards	≤2	≤5	≤2	≤0.05	≤0.07	≤0.003	≤
WHO standards	≤2	≤3	≤	≤0.05	≤0.02	≤0.003	≤0.1
Water samples analysed before membrane filtration							
Olifants river	0.057	0.000	0.347	0.204	0.120	0.026	0.046
Makotswane dam	0.003	0.000	0.199	0.198	0.132	0.032	0.035
Apel cross furrow	0.003	0.000	2.979	0.196	0.101	0.046	0.034
Pooled surface water	0.018	0.000	0.512	0.194	0.099	0.057	0.028
Borehole 1[a]	0.033	0.003	0.001	0.123	0.057	0.088	0.001
Borehole 2[b]	0.024	0.000	0.416	0.111	0.134	0.094	0.000
Borehole 3[c]	0.000	0.000	0.001	0.101	0.121	0.101	0.001
Pooled borehole water	0.015	0.000	0.000	0.081	0.148	0.095	0.000
Water samples analysed after membrane filtration							
[a]Membrane 1 filtered Pooled surface water	0.02	0.000	0.002	0.0138	0.015	0.0012	0.022
[b]Membrane 2 filtered Pooled surface water	0.011	0.000	0.003	0.0160	0.027	0.0028	0.010
[a]Membrane 1 filtered Pooled borehole water	0.005	0.000	0.000	0.012	0.0120	0.001	0.000

[b]**Membrane 2 filtered Pooled borehole water**	0.009	0.000	0.000	0.013	0.0128	0.001	0.000

[a]**Membrane 1** is 1.8 wt.% Ag-PAMAM-MWCNTs/PVDF-HFP and [b]**Membrane 2** is 2.5 wt.% Ag-MWCNTs/PVDF-HFP. [a]Jerome borehole, [b]Malamulele borehole and [c]Shigalo borehole.

Table 4.2.7 shows the atomic adsorption spectroscopy (AAS) elemental analysis for borehole, surface water and membrane filtered water. Zinc and cobalt were not detected in the borehole and surface water samples. Both copper and iron were detected at limits lower than 2 mg/L as recommended by SANS 241 [51]. The concentration further decreased after membrane filtration.

Chromium was detected at a higher concentration in surface water and slightly at lower concertation in borehole water, and all being higher than the recommended value of 0.05 mg/L in drinking water. Adverse health effects associated with Cr(VI) exposure include occupational asthma, eye irritation and damage, kidney damage, liver damage, pulmonary congestion and respiratory cancer, therefore it is important to reduce chromium levels in water [53]. After filtration, the concentration of chromium was reduced to allowable limits both for ground water and surface water, with membrane 1 showing the lowest concentration.

Nickel and cadmium were also detected at higher limits than the SANS 241 [51] limits which are 0.07 and 0.003 mg/L respectively; for both ground and surface water. Nickel when ingested through water, in large amounts it is carcinogenic, while cadmium health effects include nausea, diarrhoea, liver injury and kidney damage. After membrane filtration, these water samples had a significantly reduced concentration within the acceptable limits. Silver was also tested, and small amounts of silver below the recommended (0.1 mg/L) was detected. After membrane filtration, tiny amounts of silver remained in water, indicating the non-leaching properties of silver from the Ag-PAMAM-MWCNTs/PVDF-HFP and 2.5 wt.% Ag-MWCNTs/PVDF-HFP composite membranes.

An evaluation of the heavy metal analysis results indicates that surface water from Sekhukhune district is not suitable for consumption if not treated prior to consumption.

1.8 wt.% Ag-PAMAM-MWCNTs/PVDF-HFP composite membrane has shown better heavy metal reduction for both surface water and borehole water within SANS 241 and WHO standards of drinking water. These membranes had shown good antibacterial and non-leaching qualities during *E. Coli* studies in figure 4.2.6 and 4.2.7.

4.2.5.4 SEM and EDX analysis of the membranes after surface and borehole water samples filtration

The SEM and EDX of 2.5 wt.% Ag-MWCNTs/PVDF-HFP and 1.8 wt.% Ag-PAMAM-MWCNTs/PVDF-HFP membranes after filtration of surface and borehole water samples are shown in figure 4.25. In comparison with SEM of the membranes in section 4.1.6, the SEM images appeared rough with suspended solids clearly viewed on top of the membrane surfaces. More particles with sizes up to 10 µm were viewed in the membranes used for surface water filtration (figure 4.25 a &b) as compared to the water from boreholes. This is in agreement with the results recorded in table 4.2.4, since more suspended solids were perceived in surface water samples. It was also noticed that the EDX detected more metals on the membrane surfaces after surface water filtration, and the results correlates with the AAS results in table 4.2.7. A low concentration of metals was detected (table 4.2.7) in the pooled borehole water samples, hence the EDX could not detect any metals on the surface of the membranes used for borehole water filtration (figure 4.26 a &b).

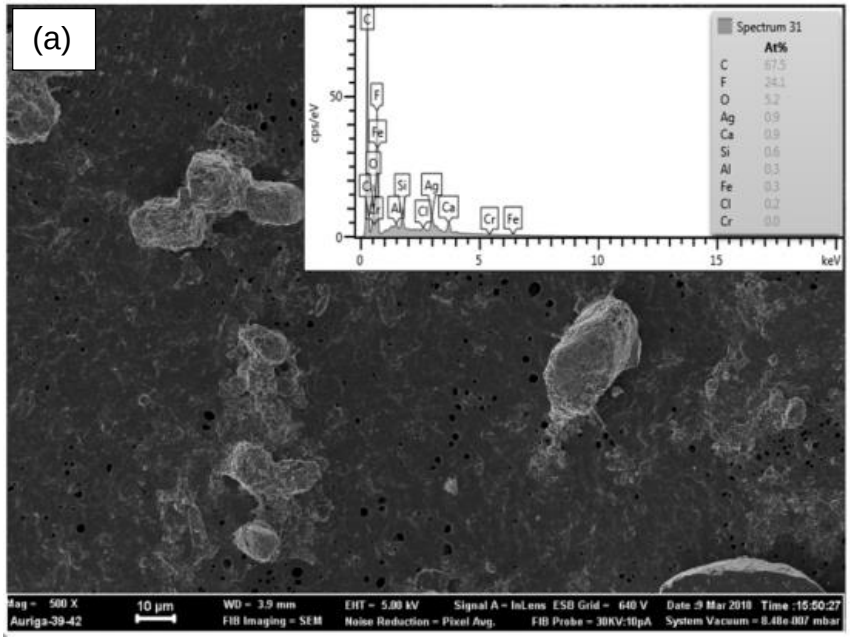

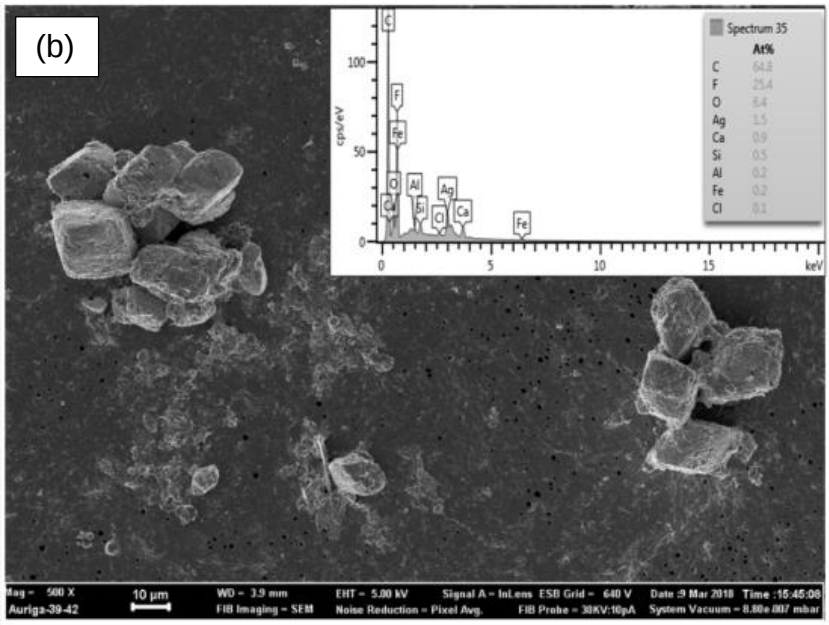

Figure 4.25: SEM and EDX of (a) 2.5 wt.% Ag-MWCNTs/PVDF-HFP and (b) 1.8 wt.% Ag-PAMAM-MWCNTs/PVDF-HFP composite membranes after filtering surface water samples

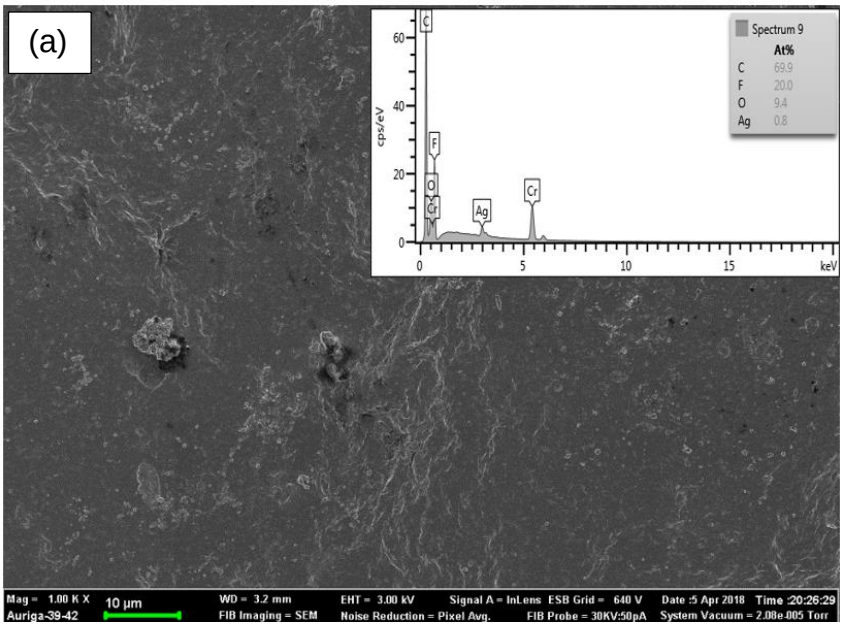

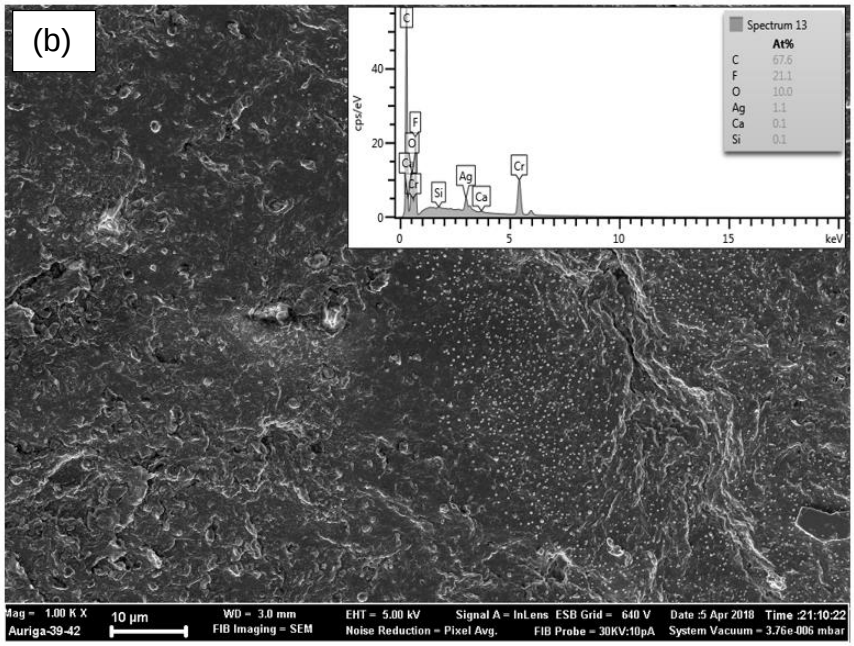

Figure 4.26: SEM and EDX of (a) 2.5 wt.% Ag-MWCNTs/PVDF-HFP and (b) 1.8 wt.% Ag-PAMAM-MWCNTs/PVDF-HFP composite membranes after filtering borehole water samples

4.3 ADSORPTION STUDIES

4.3.1 Batch Adsorption studies of Cadmium (II) ions

4.3.1.1 Effect of pH on Cd(II) ions removal by composite membranes

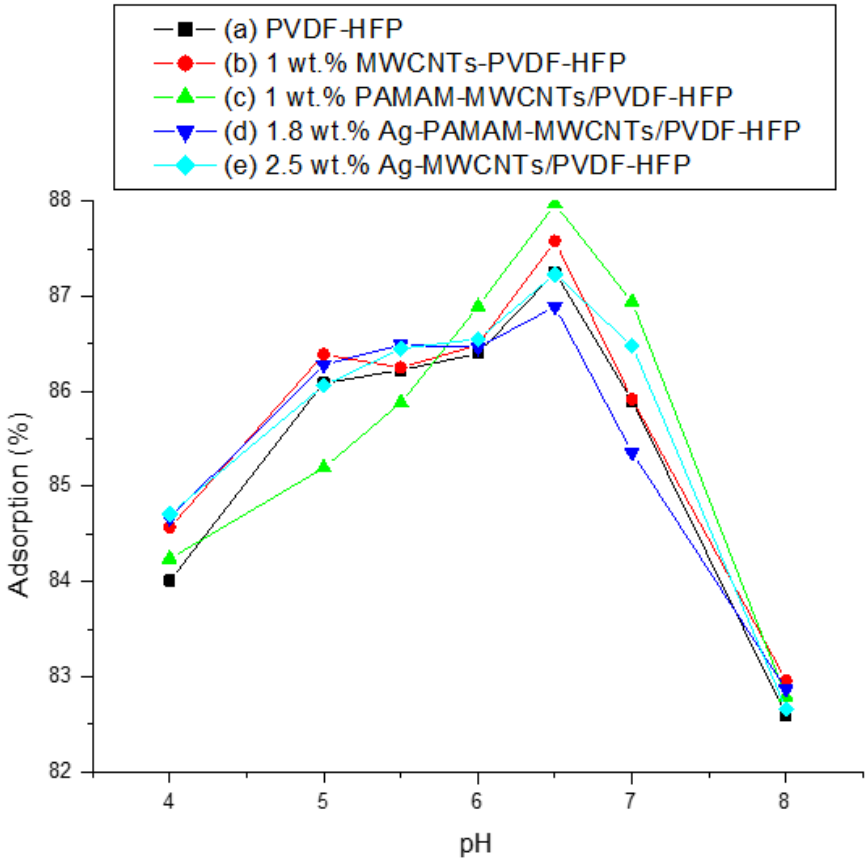

Figure 4.27: Effect of pH on the adsorption of cadmium on (a) PVDF-HFP (b) 1 wt.% MWCNTs/PVDF-HFP, (c) 1 wt.% PAMAM-MWCNTs/PVDF-HFP, (d) 1.8 wt.% Ag-PAMAM-MWCNTs/PVDF-HFP and (e) 2.5 wt.% Ag-MWCNTs/PVDF-HFP membrane membranes

Figure 4.27 shows the effect of pH on adsorption of Cd(II) ions by PVDF-HFP, 1 wt.% MWCNTs/PVDF-HFP, 1 wt.% PAMAM-MWCNTs/-PVDF-HFP, 1.8 wt.% Ag-PAMAM-MWCNTs/PVDF-HFP and 2.5 wt.% Ag-MWCNTs/PVDF-HFP composite membrane. The pH value is considered as one of the main parameters controlling the sorption of metals with adsorbent. The data shows that the adsorption of Cd(II) ions increased from 84.24 to 87.97% as the pH increases from 4 to 6.5, when using the 1 wt.% PAMAM-MWCNTs/PVDF-HFP composite membrane. However, at pH higher than

6.5, the Cd(II) ions adsorption decreased in a steep slope until pH 8 is reached. The optimum pH was further reaffirmed by the adsorption capacity of PVDF-HFP, 1 wt.% MWCNTs-PVDF-HFP, 1.8 wt.% Ag-PAMAM-MWCNTs/PVDF-HFP and 2.5 wt.% Ag-MWCNTs-PVDF-HFP as shown in figure 4.3.1. The decrease in adsorption of Cd(II) ions at higher pH is due to precipitation of cadmium hydroxides; forming white crystals [54]. At low pH values, H^+ ions occupy most of the adsorption sites on the membrane surface; hence less Cd(II) ions are adsorbed due to electric repulsion [55]. This study showed that the pH of 6.5 gave the best adsorption which is close to the neutral pH of water (6.8-7); hence, the pH value of 6.5 was selected for the remaining tests.

4.3.1.2 Effects of contact time on adsorption efficiency of composite membranes

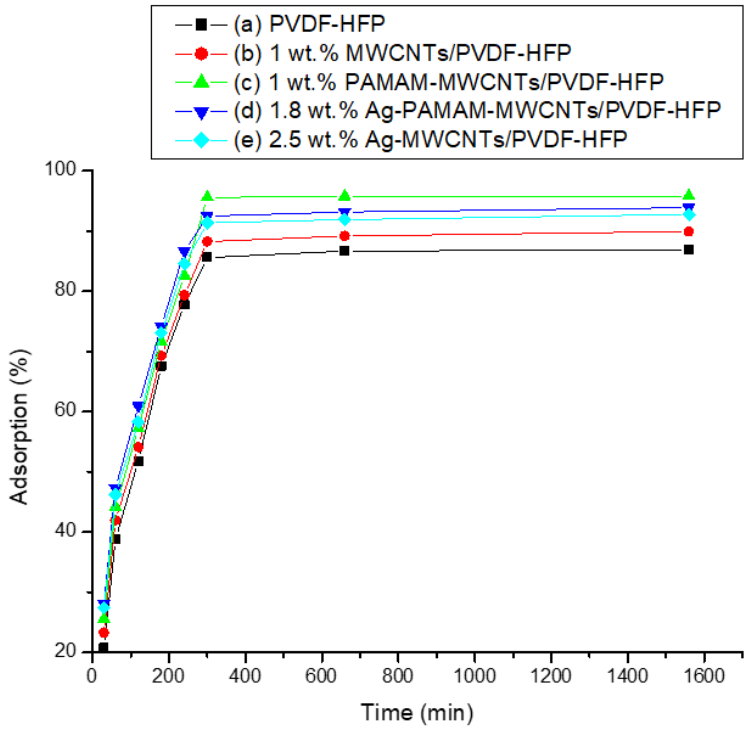

Figure 4.28: Effect of contact time on adsorption efficiency of Cd (II) ions on (a) PVDF-HFP (b) 1 wt.% MWCNTs-PVDF-HFP, (c) 1 wt.% PAMAM-MWCNTs-PVDF-HFP, (d) 1.8 wt.% Ag-PAMAM-MWCNTs-PVDF-HFP and (e) 2.5 wt.% Ag-MWCNTs-PVDF-HFP composite membranes

Figure 4.28 shows the effect of contact time on the percentage removal of Cd(II) ions on PVDF-HFP based membranes. During the first 180 minutes, adsorption of Cd(II) ions increased rapidly after which it became slow when the equilibrium point was reached after about 360 minutes. Such behaviour is typical due to the presence of several adsorption sites on the membrane surface in the initial stage of reaction, which gradually gets saturated with the metal as the contact time increases. Interestingly, a slight increase was observed when MWCNTs were added on PVDF-HFP. The highest adsorption of 96% was observed on 1 wt.% PAMAM-MWCNTS/PVDF-HFP, better than the adsorption percentage reported in literature [31,54].

4.3.1.3 Adsorption kinetics of Cd(II) ions removal by composites membranes

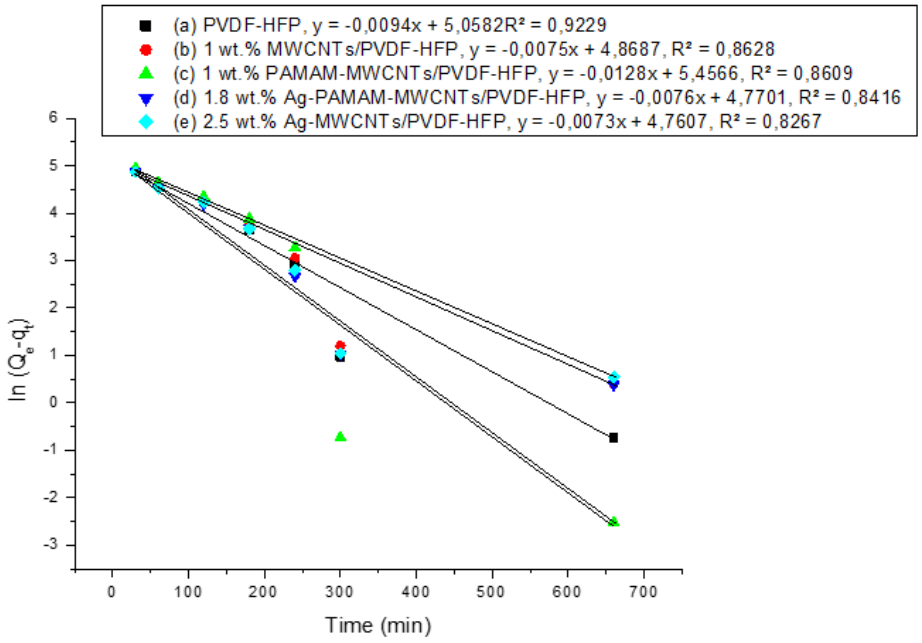

(i)

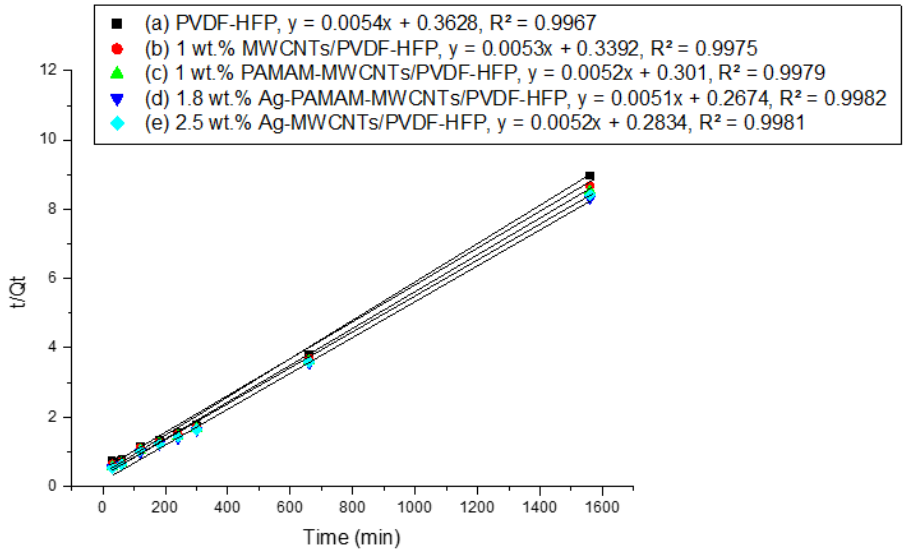

(ii)

Figure 4.29: (i) Pseudo-first order and (ii) Pseudo-second order kinetic model for adsorption of Cd (II) ions on (a) PVDF-HFP, (b) 1 wt.% MWCNTs-PVDF-HFP, (c) 1 wt.% PAMAM-MWCNTs-PVDF-HFP, (d) 1.8 wt.% Ag-PAMAM-MWCNTs-PVDF-HFP and (e) 2.5 wt.% Ag-MWCNTs-PVDF-HFP composite membranes

Table 4.3.1: Kinetics parameters for Cd(II) ions adsorption onto PVDF-HFP membranes

Membrane	Experimental q_e (mg g-1)	Pseudo-first order kinetic model			Pseudo-second order kinetic model		
		K_1	Q_e (mg g^{-1})	R^2	K_2	Q_e (mg g^{-1})	R^2
PVDF-HFP membrane	173.82	0.0094	157.3	0.923	8.04 x 10^{-5}	185.2	0.997
1 wt.% MWCNTs-PVDF-HFP	179.88	0.0075	130.2	0.863	8.28 x 10^{-5}	188.7	0.998
1 wt.% PAMAM-MWCNTs-PVDF-HFP	191.64	0.00128	234.3	0.861	8.98 x 10^{-5}	192.3	0.998

1.8 wt.% Ag-PAMAM-MWCNTs-PVDF-HFP	187.78	0.0076	117.9	0.842	9.73×10^{-5}	196.1	0.998
2.5 wt.% Ag-MWCNTs-PVDF-HFP	185.56	0.0073	116.82	0.826	9.54×10^{-5}	192.3	0.998

In order to describe the kinetic behaviour, pseudo-first-order, and pseudo-second-order, models were used. Figure 4.29 shows the linearized forms of the pseudo-first and pseudo-second order models of Cd(II) ions adsorption. The data (table 4.3.1) indicates that the kinetics of adsorption is better described as pseudo-second-order reaction (R^2 = 0.997-0.998) than the pseudo-first-order model (R^2 = 0.826-0.923). The data further shows large differences on average between experimental and calculated pseudo-first-order adsorption capacity values. The data in figure 4.29(i) at 300 minutes shows a noticeable deviation which makes it unfit for explaining the kinetic behaviour. Hence, a pseudo-first-order model was considered as an inappropriate model to explain the proposed adsorption behaviour. The Pseudo-second-order kinetic model is based on the assumption that the chemisorption is the rate limiting step [55]. Comparable results were reported by Tran *et al*., 2016 while studying the kinetics of Cd(II) ions on orange peels [56].

4.3.1.4. Adsorption isotherms

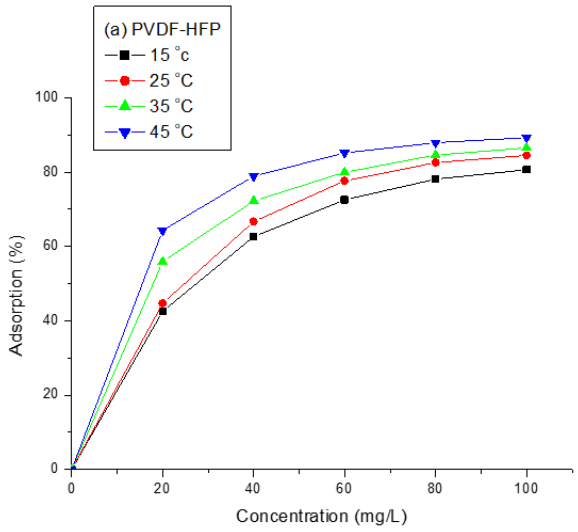

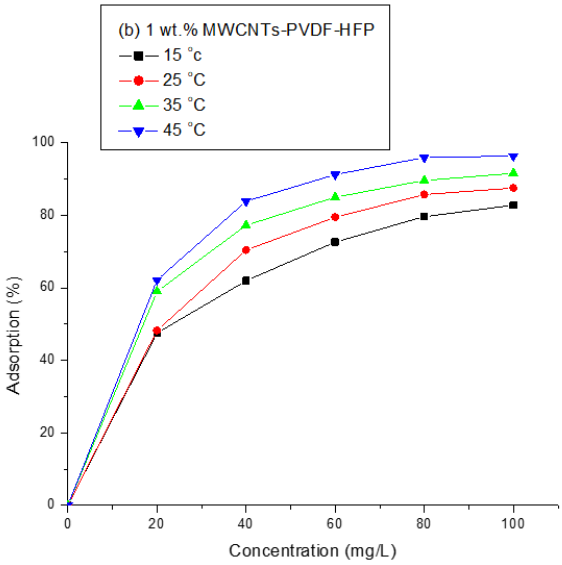

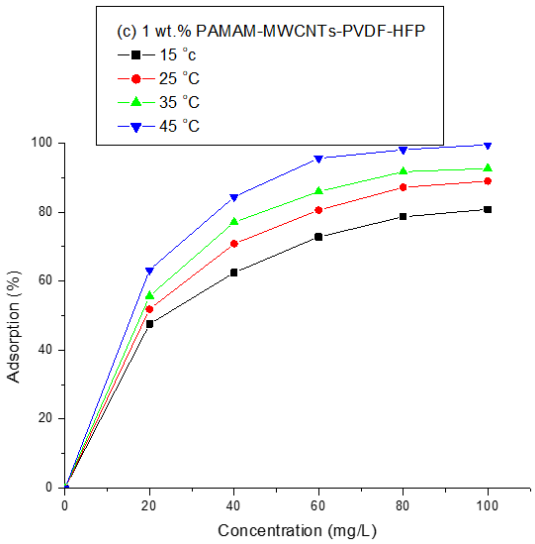

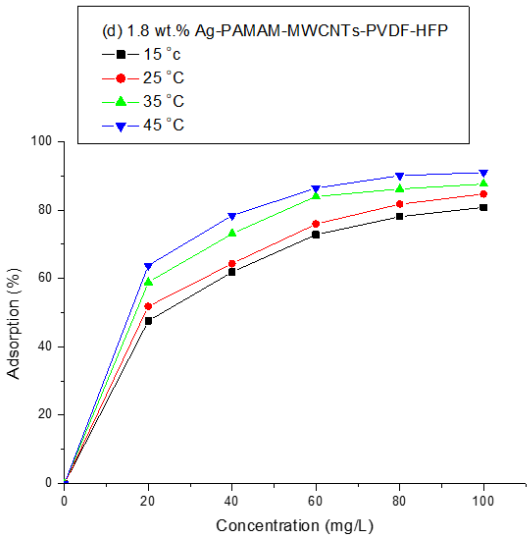

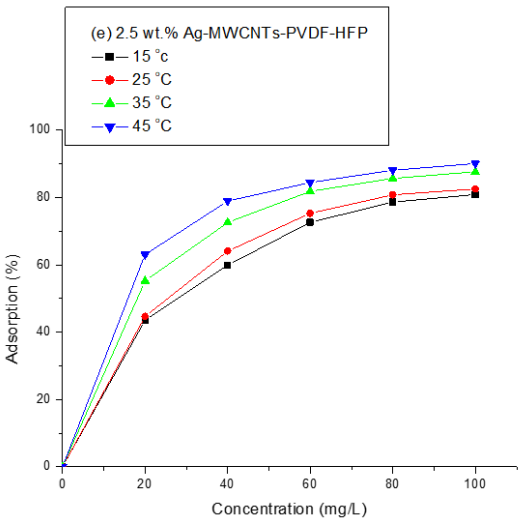

Figure 4.30: Effect of temperature on adsorption efficiency of Cd(II) ions on (a) PVDF-HFP, (b) 1 wt.% MWCNTs-PVDF-HFP, (c) 1 wt.% PAMAM-MWCNTs-PVDF-HFP, (d) 1.8 wt.% Ag-PAMAM-MWCNTs-PVDF-HFP, (e) 2.5 wt.% Ag-MWCNTs-PVDF-HFP composite membranes

The effect of temperature at 15 ^{o}C, 25 ^{o}C, 35 ^{o}C and 45 ^{o}C on the adsorption of Cd(II) ions using PVDF-HFP, 1 wt.% MWCNTs-PVDF-HFP, 1 wt.% PAMAM-MWCNTs-PVDF-HFP, 1.8 wt.% Ag-PAMAM-MWCNTs-PVDF-HFP and 2.5 wt.% Ag-MWCNTs-PVDF-HFP composite membranes is shown in figure 4.30. The results indicate an increase of the Cd(II) ions adsorption percentage with an increase of solution temperature and concentration. This may be due to an increase in thermal energy of the adsorbing material, which leads to higher adsorption and faster adsorption rate as observed by Li *et al*. [57]. An increase in the initial Cd(II) ions concentration also improves the interaction between the metal and the adsorbent, due to the increase in the driving force of the concentration gradient produced, which results in higher adsorption [55,58]. It was noticed that after 80 ^{o}C, the equilibrium state is reached wherein the adsorption percentage now remains constant. The highest percentage adsorption was in the following order: 1 wt.% PAMAM-MWCNTs/PVDF-HFP (99%) > 1 wt.% MWCNTs-PVDF-HFP (96%)> 1.8 wt.% Ag-PAMAM-MWCNTs-PVDF-HFP (92%) > 2.5 wt.% Ag-MWCNTs-PVDF-HFP (90%) > PVDF-HFP (88%). The results indicate that 1 wt.% PAMAM-MWCNTs/PVDF-HFP composite membrane had 99% adsorption at 45 ^{o}C, which correlate with high BET surface area data (table 4.1.1).

(i) Langmuir isotherm adsorption

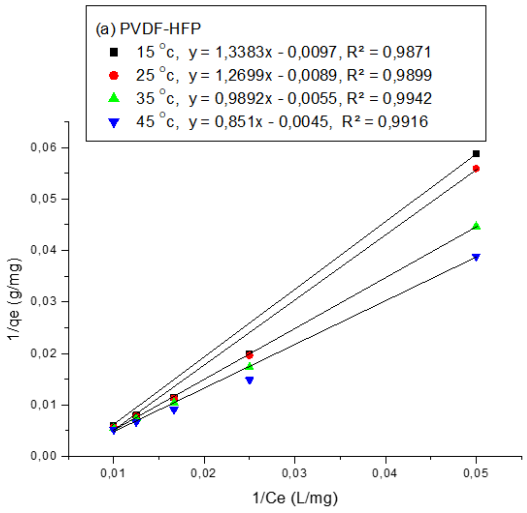

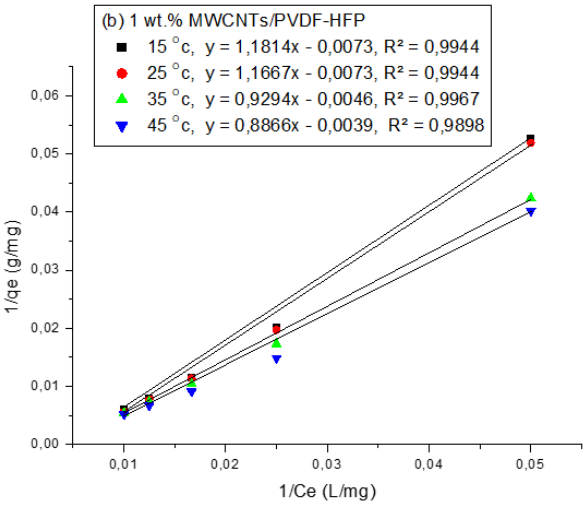

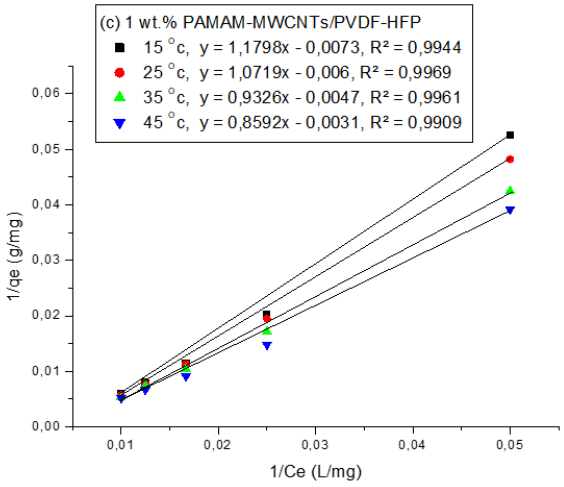

(ii) Freundlich isotherm adsorption

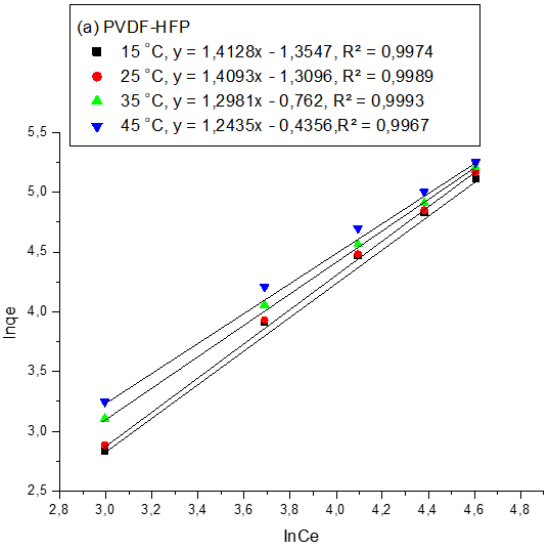

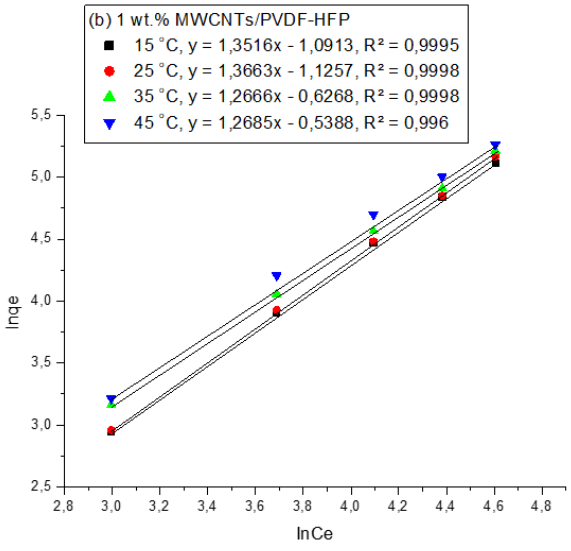

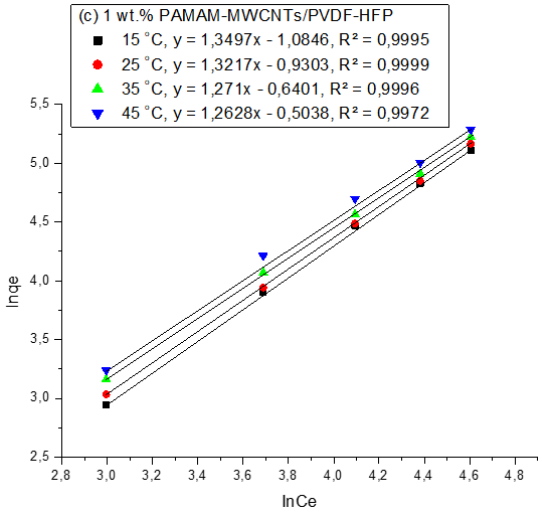

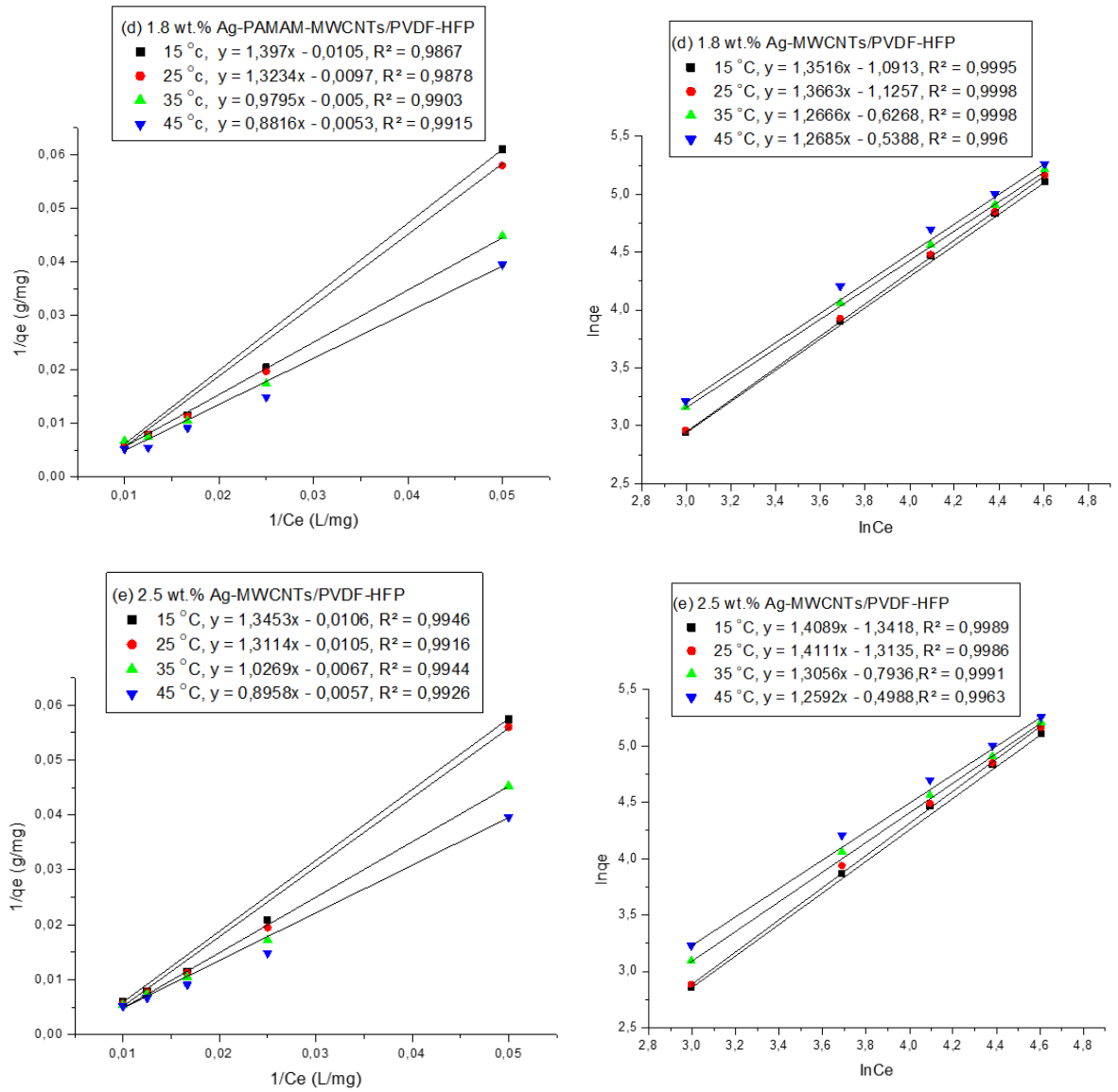

Figure 4.31: (i) Langmuir isotherm adsorption and (ii) Freundlich isotherm of Cd(II) ions on (a) PVDF-HFP, (b) 1 wt.% MWCNTs-PVDF-HFP, (c) 1 wt.% PAMAM-MWCNTs-PVDF-HFP, (d) 1.8 wt.% Ag-PAMAM-MWCNTs-PVDF-HFP, (e) 2.5 wt.% Ag-MWCNTs-PVDF-HFP composite membranes

Table 4.3.2: Parameters of Langmuir and Freundlich isotherm for cadmium adsorption by PVDF based composite membranes

Membrane	Temperature (°C)	Langmuir model			Freundlich model		
		q_m (mg/g)	b (L/mg)	R^2	K_f (mg/g)	n	R^2
PVDF-HFP	15	103.09	0.00725	0.9871	0.258	0.71	0.9974
	25	112,4	0.00725	0.9899	0.27	0.71	0.9989
	35	181.8	0.0556	0.9942	0.467	0.77	0.9993
	45	222.3	0.00529	0.9916	0.645	0.804	0.9967
1 wt.% MWCNTs-PVDF-HFP	15	137	0.00618	0.9944	0.336	0.74	0.9995
	25	137	0.00626	0.994	0.324	0.732	0.9998
	35	217	0.00495	0.9967	0.534	0.79	0.9998
	45	256	0.00441	0.9898	0.583	0.79	0.9996
1 wt.% PAMAM-MWCNTs-PVDF-HFP	15	137	0.00619	0.994	0.338	0.74	0.9995
	25	166.7	0.00556	0.9969	0.394	0.76	0.9999
	35	212.8	0.00504	0.9961	0.53	0.79	0.9996
	45	323	0.00360	0.9909	0.604	0.79	0.9972
1.8 wt.% Ag-PAMAM-MWCNTs/ PVDFHFP	15	95.2	0.00752	0.9867	0.229	0.694	0.9975
	25	103.1	0.00733	0.9878	0.245	0.698	0.9983
	35	200	0.00510	0.9903	0.46	0.768	0.9994
	45	188.7	0.00601	0.9915	0.608	0.794	0.9965
2.5 wt.% Ag-MWCNTs-PVDF-HFP	15	94.3	0.00788	0.9946	0.26	0.709	0.9989
	25	95.2	0.00801	0.9916	0.269	0.709	0.9986
	35	149.3	0.00652	0.9944	0.452	0.766	0.9991
	45	175.4	0.00636	0.9926	0.607	0.794	0.9963

Figure 4.31 shows the linearized data during the adsorption of Cd(II) on PVDF-HFP, 1 wt.% MWCNTs-PVDF-HFP, 1 wt.% PAMAM-MWCNTs-PVDF-HFP, 1.8 wt.% Ag-PAMAM-MWCNTs-PVDF-HFP and 2.5 wt.% Ag-MWCNTs-PVDF-HFP composite membranes using Langmuir and Freundlich isotherm. The isotherm constants and their correlation coefficients (R^2) are listed in table 4.3.2. Based on the R^2 values, the results indicate that the adsorption processes of all composites membranes are well conformed to Freundlich model (R^2 = 0.999); which meets the heterogeneous

adsorption process [59,60]. The maximum adsorption capacity from Langmuir equation for PVDF-HFP, 1 wt.% MWCNTs-PVDF-HFP, 1 wt.% PAMAM-MWCNTs-PVDF-HFP, 1.8 wt.% Ag-PAMAM-MWCNTs-PVDF-HFP and 2.5 wt.% Ag-MWCNTs-PVDF-HFP are 112.3, 137, 167, 103.1 and 95.2 mg/g respectively; at room temperature. These results are higher than those reported in literature (table 4.3.3) using carbon and membrane based composite adsorbents. It is critical to note that 1 wt.% MWCNTs/PVDF-HFP composite membrane presented good desalination and fouling resistance properties in figure 4.16. It is therefore worth noting that the same composite membrane and the dendritic 1 wt.% PAMAM-MWCNTs/PVDF-HFP has also presented the best adsorption results at a low adsorbent dosage.

The separation factor, R_L, values were all below 1 indicating favourable adsorption as recorded previously [59-61] and the Freundlich constant, K_f, indicated the sorption capacity of the composite membrane. The K_f value of all composite membranes increased with an increase in temperature. According to Yang *et al*. [62] a higher value of n (n>1) indicates favourable adsorption for the Freundlich model. The calculated values of n for the adsorption of Cd(II) ions were all close to 1 showing good efficiency for Cd(II) ions on PVDF-HFP [63].

Table 4.3.3: Comparison of Cd(II) ions adsorption capacity by different materials

Adsorbent	**Experimental conditions**			**Adsorption capacity q_{max}(mg/g)**	**Reference**
	pH	**T (^oC)**	**Dosage**		
1 wt.% PAMAM-MWCNTs/ PVDFHFP	6.5	298	0.5 g/L	167	this study
Mesoporous silica nano-composite materials	5.5	298	1 g/L	148.32	43
Surfactant-modified chitosan beads	7.0	298	0.45 g/L	125	44

Aluminum Oxide-Impregnated Carbon Nanotube Membrane	7.0	298	Not specified	54.42	45
Poly(sodium 4-styrenesulfonate) -grafted polysulfone Porphyrin p-toluenesulfonate (PSF-PNaSS/ TMPyP)	8.0	298	Not specified	72.2	46
Graphene oxide/cellulose membranes	4.5	298	Not specified	26.8	47
Graphene oxide membranes	5.8	303	0.2 g/L	83.8	48
Graphene oxide nanosheets	4.99	298	0.5 g/L	44.64	49
PVDF/Graphene Oxide Nanofiber Composite Membranes	7	298	Not specified	1.11	50

4.3.1.5 Thermodynamic analysis

Figure 4.32 shows the linear plot of InK_o vs 1/T for Cd (II) on PVDF-HFP composite membranes at different concentrations. It was observed that Ink_o decreased as 1/T increased. The Arrhenius plot is obtained by plotting the logarithm of the rate constant, k, versus the inverse temperature, 1/T. The resulting negatively-sloped lines are useful in finding the missing components of the Arrhenius equation. The values of ΔH^o and ΔS^o were obtained from the slope and intercept of the plot of $\ln K_o$ versus 1/T. A similar trend was also reported in literature [57,64].

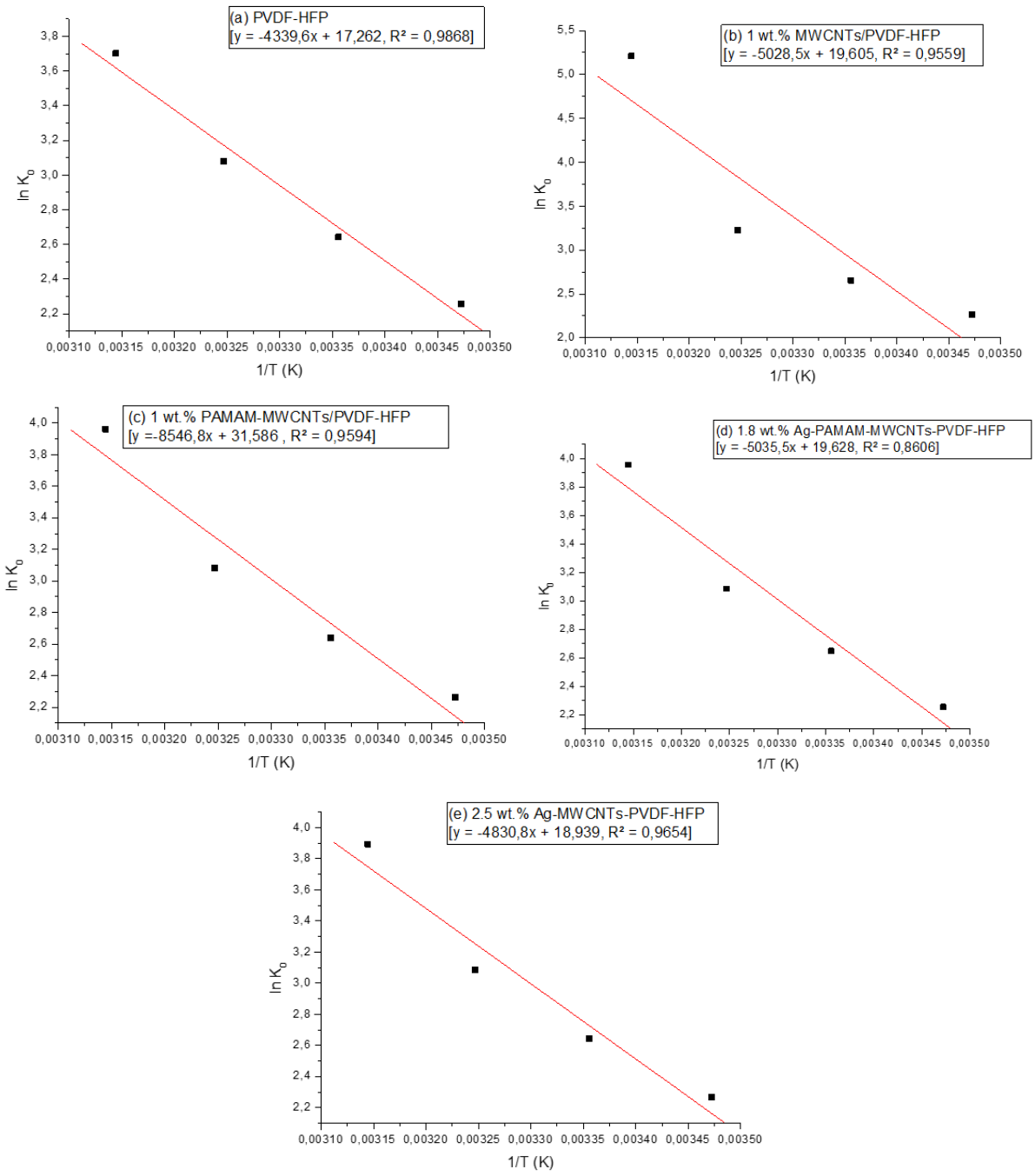

Figure 4.32: Thermodynamics parameters of Cd(II) ions onto (a) PVDF-HFP, (b) 1 wt.% MWCNTs-PVDF-HFP, (c) 1 wt.% PAMAM-MWCNTs-PVDF-HFP, (d) 1.8 wt.% Ag-PAMAM-MWCNTs-PVDF-HFP, (e) 2.5 wt.% Ag-MWCNTs-PVDF-HFP composite membranes

Table 4.3.4: Thermodynamic parameters for Cd(II) ions (100 ppm) adsorption by 1 wt.% PAMAM-MWCNTs-PVDF-HFP

Membrane	Thermodynamic parameters			
	Temperature (K)	ΔG (kJ.mol^{-1})	ΔH (kJ.mol^{-1})	ΔS (J.mol.K^{-1})
PVDF-HFP	288 298 308 318	-5,404 -6,545 -7,883 -9,789	36.07	143.5
1 wt.% MWCNTs-PVDF-HFP	288 298 308 318	-5,419 -6,543 -7,886 -10,47	41.81	162.99
1 wt.% PAMAM-MWCNTs-PVDF-HFP	288 298 308 318	-5,426 -6,577 -8,253 -13,77	71.06	262.6
1.8 wt.% Ag-PAMAM-MWCNTs-PVDF-HFP	288 298 308 318	-5,397 -6,559 -7,896 -10,45	41.87	163.19
2.5 wt.% Ag-MWCNTs-PVDF-HFP	288 298	-5,431 -6,552	40.16	157.46

	308 318	-7,903 -10,29		

Thermodynamics parameters including ΔG^o, ΔH^o, and ΔS^o for PVDF-HFP, 1 wt.% MWCNTs-PVDF-HFP, 1 wt.% PAMAM-MWCNTs-PVDF-HFP, 1.8 wt.% Ag-PAMAM-MWCNTs-PVDF-HFP and 2.5 wt.% Ag-MWCNTs-PVDF-HFP composite membranes were calculated from the slopes and intercept of the Van't Hoff plot as shown in figure 4.32 and are summarised in table 4.3.4. In general, the values of ΔG^o between 0 and -20 kJ/mol indicate that the adsorption process is physisorption, while the values in between -80 and -4000 kJ/mol correspond to chemisorption [64,65]. The adsorptive process will occur favourably and spontaneously at a given temperature if ΔG^o exhibits a negative quantity; and a positive quantity shows that the process is non-feasible and non-spontaneous [56]. The data indicates that the adsorption process of Cd(II) ions by 1 wt.% PAMAM-MWCNTs-PVDF-HFP composite membrane is spontaneous, endothermic and mainly physical in nature [57-58,64-64]. Furthermore, the higher temperature is favourable to the adsorption, which correlated with an increase in q_{max} values (Langmuir adsorption isotherm). A related trend was reported by Li *et al*., [57] while using PVDF nanofiber mat loaded with manganese dioxide.

The values of ΔH^o and ΔS^o were obtained from the slope and the intercept of the plots of $\ln K_d$ versus 1/T in figure 4.32. The positive values of ΔH^o confirmed that the adsorption process was endothermic in nature. A higher temperature is favourable to the adsorption, which may explain the increase in q_{max} on Langmuir isotherm as the temperature is raised. The positive values of ΔS^o reflects an increase in randomness at the adsorbent-solution interface during the Cd(II) ions adsorption process as observed in the literature [57,66].

4.3.1.6. Reusability studies

Reusability is one of the important aspects for the practical application of the adsorbent. The data in figure 4.33 shows the reusability studies of PVDF-HFP, 1 wt.% fMWCNTs-PVDF-HFP, 1 wt.% PAMAM-MWCNTs-PVDF-HFP, 1.8 wt.% Ag-PAMAM-

MWCNTs-PVDF-HFP and 2.5 wt.% Ag-MWCNTs-PVDF-HFP composite membranes. The adsorption capacity from the first adsorption to the fourth cycle decreased from 91 to 83%, 95 to 87%, 98 to 93 %, 94 to 88% and 92 to 85% for PVDF-HFP, 1 wt.% fMWCNTs-PVDF-HFP, 1 wt.% PAMAM-MWCNTs/PVDF-HFP, 1.8 wt.% Ag-PAMAM-MWCNTs-PVDF-HFP and 2.5 wt.% Ag-MWCNTs-PVDF-HFP respectively. The 1 wt.% PAMAM-MWCNTs/PVDF-HFP composite membrane showed the highest adsorption capacity loss as compared to the rest of the nanocomposite membranes. However, the adsorption capacity of the four composites remained above 80% after four cycles, which indicates that PVDF-HFP adsorbents can be recycled for Cd(II) ions adsorption. The adsorption loss for 1 wt.% PAMAM-MWCNTs/PVDF-HFP after 4 cycles was 5% compared to the adsorption loss of 12% observed by Wang *et al*. [38].

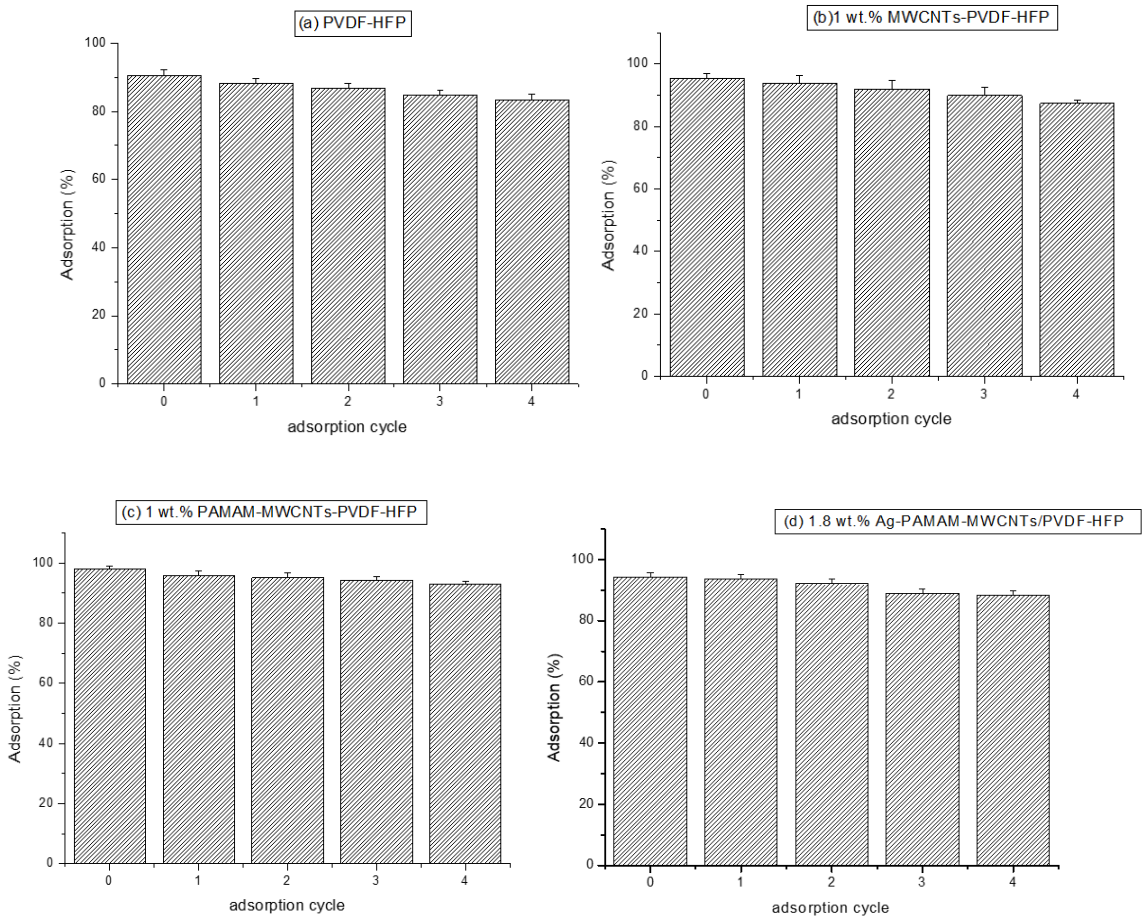

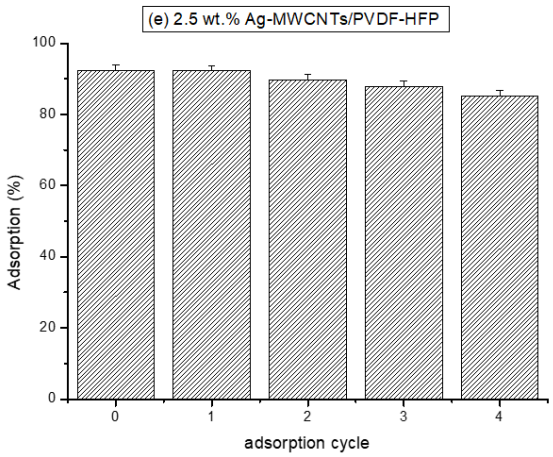

Figure 4.33: Reusability of (a) PVDF-HFP, (b) 1 wt.% MWCNTs-PVDF-HFP and (c) 1 wt.% PAMAM-MWCNTs-PVDF-HFP (d) 1.8 wt.% Ag-PAMAM-MWCNTs-PVDF-HFP, (e) 2.5 wt.% Ag-MWCNTs-PVDF-HFP composite membranes

The surface properties of the re-used best performing composite membrane (i.e., 1 wt.% PAMAM-MWCNTs/PVDF-HFP) was further studied by TGA, SEM, and Contact angle. Figure 4.33 shows the TGA profile of 1 wt.% PAMAM-MWCNTs/PVDF-HFP, after washing and reusing the membrane 4 times. The data indicates that the structure of all re-used 1 wt.% PAMAM-MWCNTs/PVDF-HFP remained stable up to 300 ^{o}C. However, a loss of 10% weight at 400 ^{o}C was observed. The data further shows the increase in the residual weights of the used composite, which indicate that Cd(II) ions remained strongly adsorbed with each successive run. To validate that some Cd(II) ions remained strongly adsorbed on the 1 wt.% PAMAM-MWCNTs/PVDF-HFP composite membrane, the re-used membranes were analysed by Inductively coupled plasma Optical Emission Spectroscopy (ICP-OES). The 1 wt.% PAMAM-MWCNTs/PVDF-HFP membrane samples were digested in 2% HNO_3 and analysed for Cd(II) ions. The analysis showed that about 1,8%, 2.5%, 2.7% and 4.75% Cd(II) ions remained strongly attached to membrane after reusing the membranes 4 times, respectively. This data supports the observed decrease in adsorption capacity as the cycle increases (figure 4.32), due to the loss of the adsorption sites.

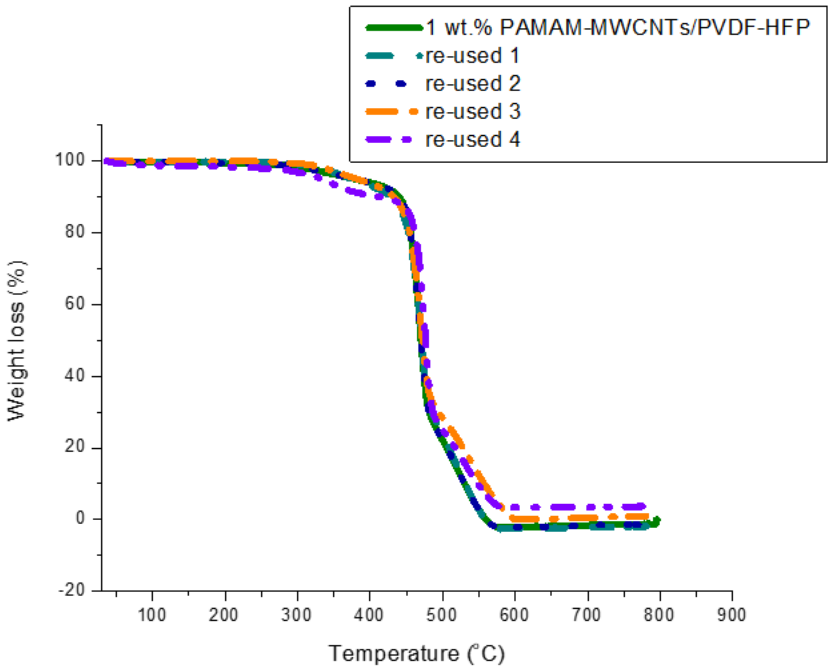

Figure 4.33: TGA of 1 wt.% PAMAM-MWCNTs-PVDF-HFP after reusing the membranes at least 4 times

The SEM data indicated that the morphology remained unchanged both before (figure 4.34a) and after reusing the membrane four times (figure 4.3.9e). The contact angles for membranes after Cd(II) ions adsorption were higher as compared to the contact angles of the membranes after cleaning them. This indicate that the membranes become less hydrophilic after absorbing the metal, the reduction in the contact angles after cleaning them show the effectiveness of membrane cleaning for reusability purposes. On average, the membranes hydrophilicity did not significantly change after reusing the membrane. EDX showed less percentage of Cd(II) ions on the surface of the membrane (most of it adsorbed within the membrane) after adsorption and no metal was detected on the surface after cleaning the membranes. Carbon, fluorine and oxygen which are the major constituents of PVDF-HFP were all retained on the membrane surface during the whole reusability process, further confirming the stability and good reusability of the 1 wt.% PAMAM/PVDF-HFP membrane.

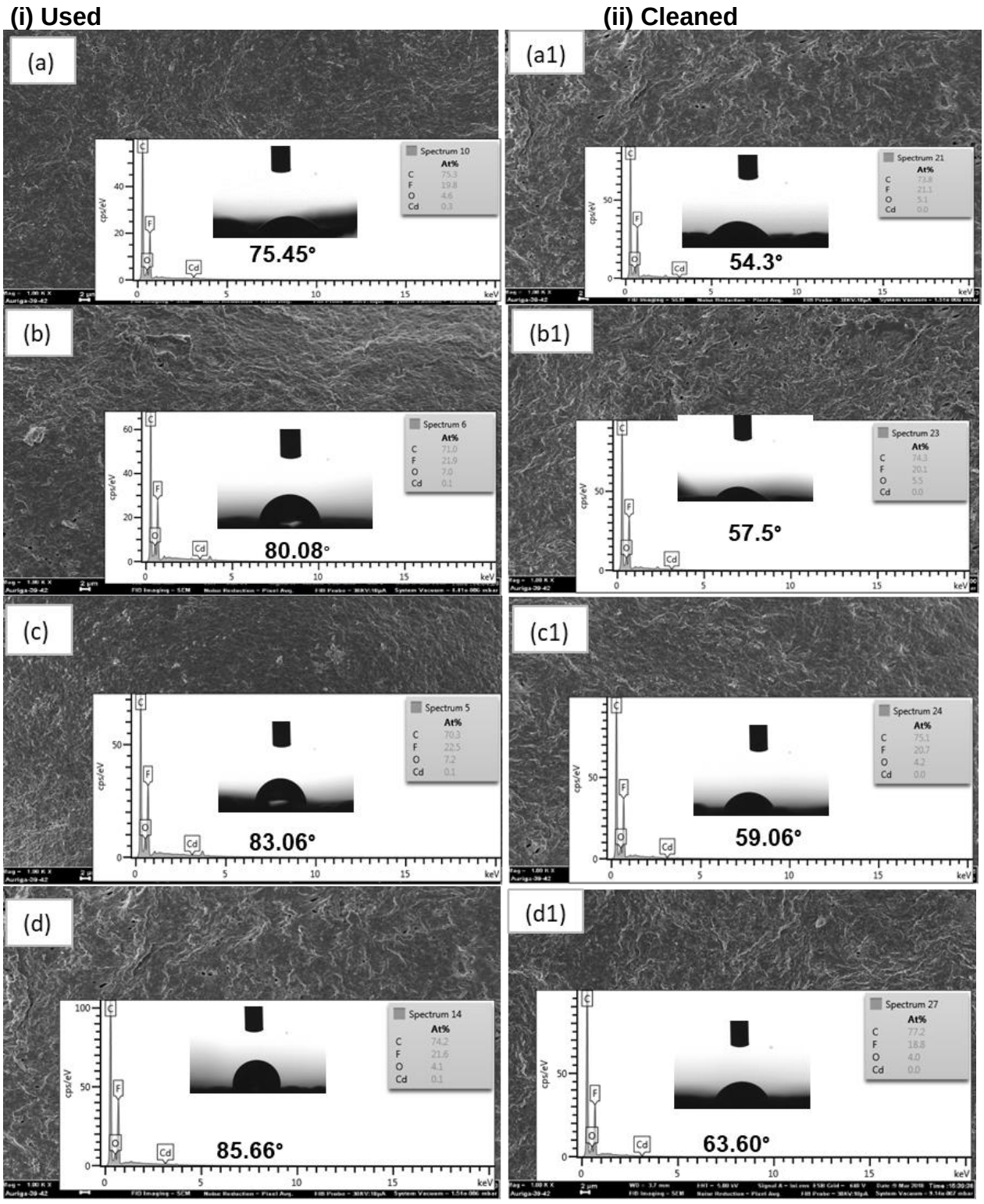

Figure 4.34: (a, b, c, & d) SEM, contact angle and EDX results of used and cleaned (a1, b1, c1, & d1) 1 wt.% PAMAM-MWCNTs-PVDF-HFP composite membrane

4.3.1.7 Selectivity studies

Figure 4.35 shows the selectivity studies of cadmium (II), copper (II), nickel (II) and zinc (II) in binary and quaternary metal adsorption on 1 wt.% PAMAM-MWCNTs-PVDF-HFP composite membrane. To examine the selectivity of the Cd(II) ions, competitive adsorption of Cd(II)/Cu(II), Cd(II)/Zn(II), and Cd(II)/Ni(II) ions from their binary mixtures was investigated. Compared with the Cd(II) ions single metal adsorptions, the adsorption capacity of Cd(II) ions in the binary solutions decreased slightly. However, the adsorption remained high (91%) as compared to that of copper (II) (56%), zinc (II) (51%) and nickel (II) (48%). Similar results were reported by Rahman *et al*. [61] and Kong *et al*. [67]. The membrane also exhibited high selectivity for Cd(II) ions in quaternary metal solutions.

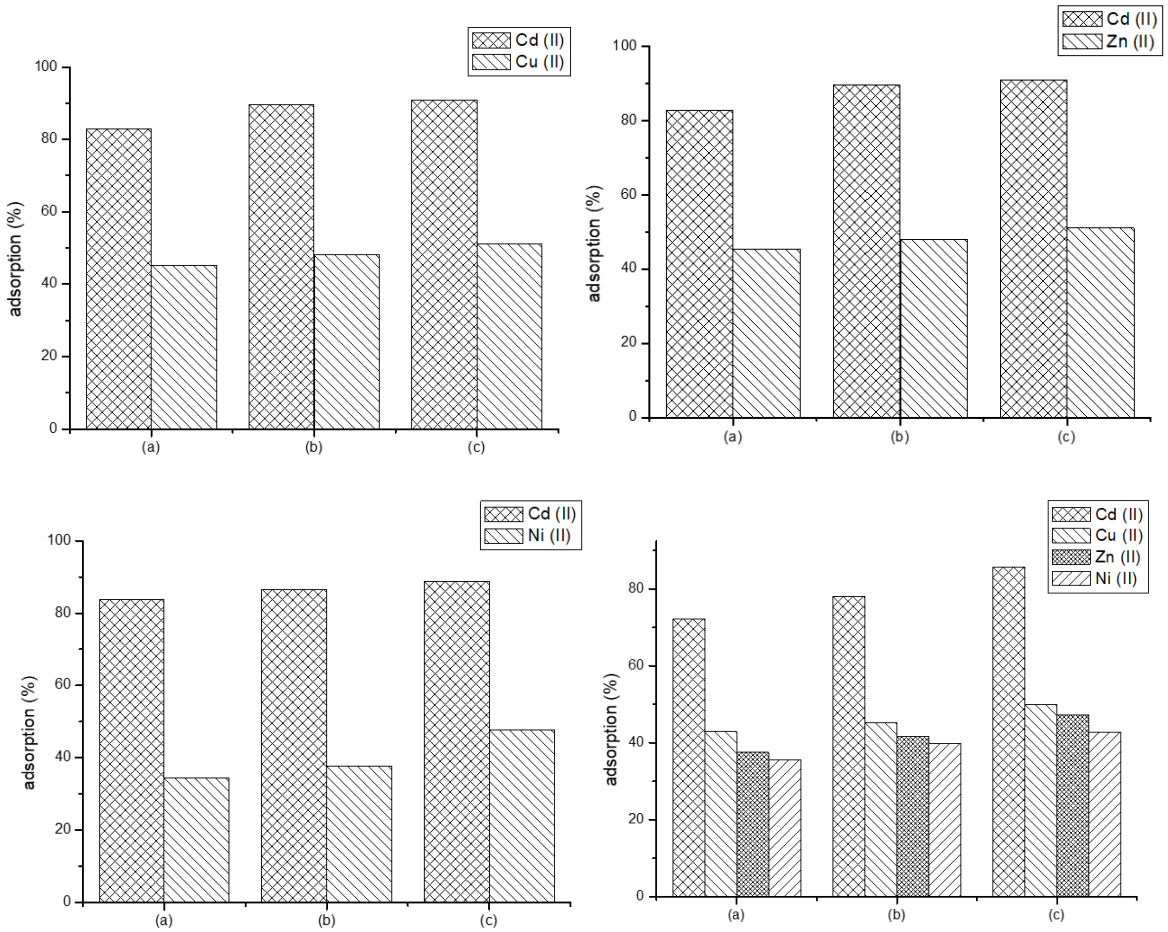

Figure 4.35: Selectivity studies of Cd(II)/Cu(II), Cd(II)/Zn(II), Cd(II)/Ni(II) ions in binary metal solutions and Cd(II)/Cu(II)/Zn(II)/Ni(II) quaternary metal solution on (a) PVDF-HFP, (b) 1 wt.% MWCNTs-PVDF-HFP and (c) 1 wt.% PAMAM-MWCNTs-PVDF-HFP membrane

The selectivity parameters of Cd(II) ions in the Cd(II)/Cu(II), Cd(II)/Zn(II) and Cd(II)/Ni(II) binary solution are given in table 4.3.5. Based on the distribution coefficient values (table 4.3.5), the adsorption by all composite membranes were more selective towards Cd(II) ions. The selectivity in the binary ionic pairs followed the following order: Ni(II) > Zn(II) > Cu(II), which is related to reported data in literature [67].

Table 4.3.5: Selectivity parameters for cadmium (II), copper (II), zinc (II) and nickel (II) adsorption in quaternary system for 1 wt.% PAMAM-MWCNTs/PVDF-HFP membrane

[a]Metals	$K_{d(Cd)}$	$K_{d(X)}$	k
(a) Cd(II)/Cu(II)	10.2	2.54	4.02
(b) Cd(II)/Zn(II)	9.5	2.09	4.55
(c) Cd(II)/Ni(II)	8.7	1.82	4.78

[a] All competitor ions have the same charge, more or less similar ionic radius with Cd(II) ion and adsorb at pH between 6 and 7.

4.3.2 Batch Adsorption studies of Chromium (VI) ions

4.3.2.1 Effect of adsorbent dosage

The adsorbent dosage is a key parameter for determining the adsorbent capacity for a given initial concentration. The effect of the adsorbent dosage on the adsorption of Cr(VI) ions (100 ppm) was studied by varying the membrane dosage from 0.5 g/L to 10 g/L at pH of 2.5.

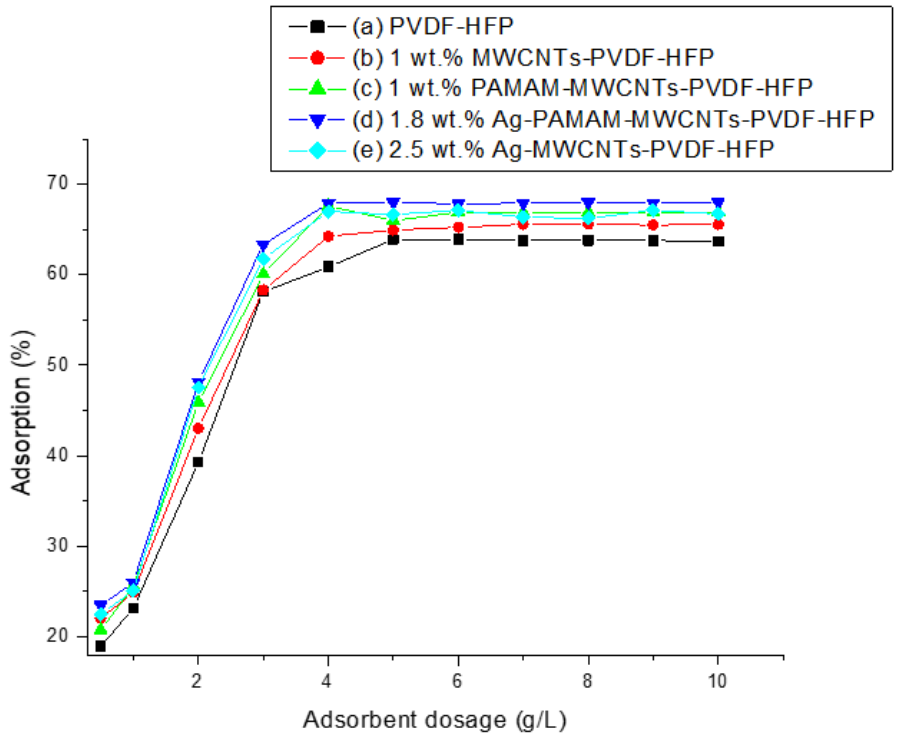

Figure 4.36: Effect of membrane adsorbent dosage on Cr(VI) ions adsorption

The effect of adsorbent dosage was plotted in figure 4.36. The result indicated that the adsorption performance increased as the adsorbent dosage is increased until it reached the optimum point. At higher membrane dosage beyond 5 g/L, a plateau was obtained probably due to the unavailability of the adsorbate in the solution for the incoming adsorbent. This point is where the maximum Cr(VI) ions is adsorbed at optimum dosage. This is attributed to the fact that as the mass of sorbent is increased, the total number of active sites on the sorbent surface also increases thereby resulting in an increase in a number of electrons which can be used for the removal of Cr(VI)

ions [68]. The optimum dosage for all membranes was at 5 g/L for all membranes and this dosage was used for all Cr(IV) ions adsorptions. The percentage adsorption of 1.8 wt.% Ag-PAMAM-MWCNTs/PVDF-HFP increased from 23.48% at 0.5 g/L membrane dosage to 68 % at 5 g/L membrane adsorbent dosage. The dosage is better than that of dolochar adsorbent were in only 65% of Cr(IV) ions adsorption was observed at a very high membrane dosage of 25 g/L [69].

4.3.2.2. Effect of pH on Cr(VI) ions removal by composites membranes

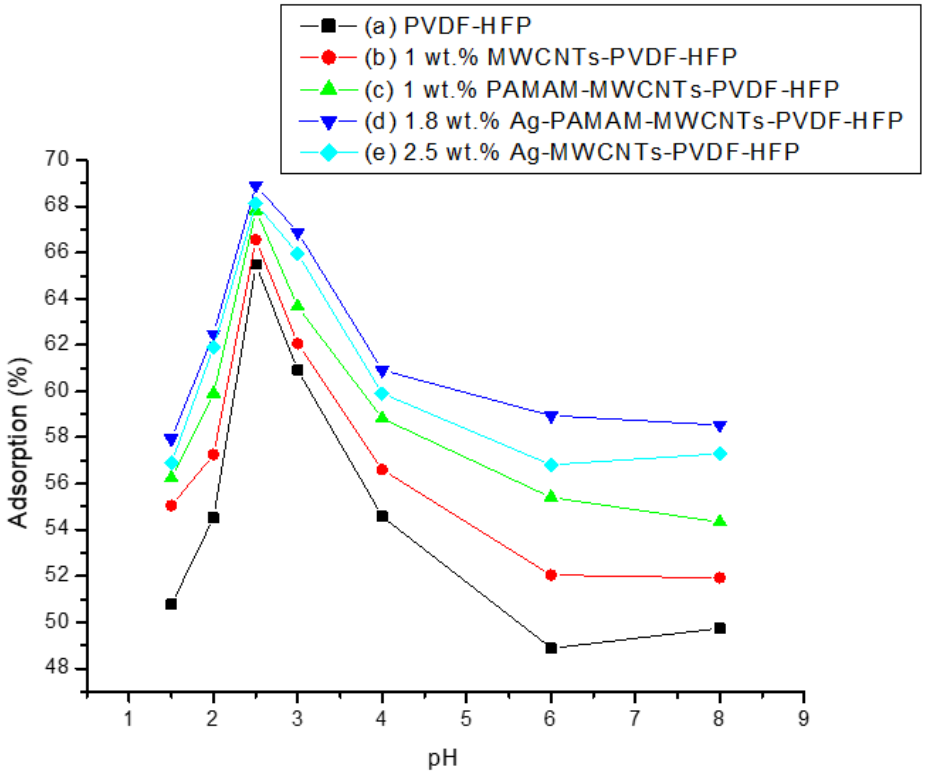

Figure 4.37: Effect of pH on the adsorption of chromium on (a) PVDF-HFP membrane. (b) 1 wt.% MWCNTs-PVDF-HFP. (c) 1 wt.% PAMAM-MWCNTs-PVDF-HFP. (d) 1.8 wt.% Ag-PAMAM-MWCNTs-PVDF-HFP. (e) 2.5 wt.% Ag-MWCNTs-PVDF-HFP

Figure 4.37 shows the effect of pH on the adsorption of chromium on PVDF-HFP, 1 wt.% MWCNTs-PVDF-HFP, 1 wt.% PAMAM-MWCNTs-PVDF-HFP, 1.8 wt.% Ag-PAMAM-MWCNTs-PVDF-HFP and 2.5 wt.% Ag-MWCNTs-PVDF-HFP composite

membranes. Optimising the pH is an important parameter while evaluating the adsorption capacity of an adsorbent in an aqueous solution. The pH of the solution had a significant influence on the adsorption of Cr(VI) ions for the composite nanofibers and the composite membranes exhibited much higher adsorption capacity under strong acidic condition rather than in neutral and alkaline conditions [70]. This is due to the predominate ionic species of Cr(VI) ions, hydrogen chromate ($HCrO_4$) and dichromate ($Cr_2O_7^{2-}$) which are negatively charged under the pH value from 2 to 5 at a pH of 2.5 [71]. $HCrO_4$ is the dominant species, consequently, electrostatic attraction between anionic chromate species and the positively charged surface can lead to a strong adsorption of Cr(VI) at low pH [71]. Similar results were also obtained by Mohamed *et al*. [64], were in the optimum pH of solution was observed at pH of 2 using PAN-CNT/TiO_2-NH_2 composite nanofibers. Sharma *et al*. [72] also showed the maximum adsorption of 74.3% at pH of 2.5 using riverbed sand as an adsorbent. In contrast, the decrease in adsorption at higher pH values was apparently due to the competitiveness of the Cr(VI) ions species (CrO_4^{2-}) and OH^- ions in the bulk [73].

4.3.2.3. Effects of contact time on adsorption efficiency of composite membranes

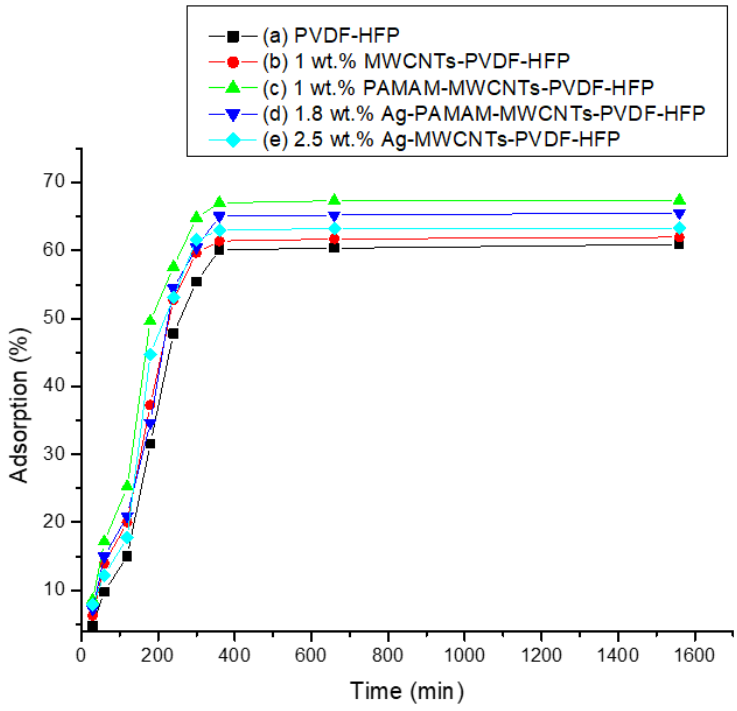

Figure 4.38: Effect of contact time on adsorption efficiency of Cr(VI) ions on (a) PVDF-HFP, (b) 1 wt.% MWCNTs-PVDF-HFP, (c) 1 wt.% PAMAM-MWCNTs/PVDF-HFP, (d) 1.8 wt.% Ag-PAMAM-MWCNTs/PVDF-HFP and (e) 2.5 wt.% Ag-MWCNTs/PVDF-HFP

Figure 4.38 shows the effect of contact time on the percentage removal of Cr(VI) ions (100 ppm) on PVDF-HFP based membranes. The results indicate that adsorption occurred rapidly during the first 3 hours, after which it became slow and then reach equilibrium after 6 hours. The highest adsorption of 67% was observed for 1 wt.% PAMAM/PVDF-HFP composite membrane. Similar results were observed by Khan *et al*. [74] on the adsorption of congo red dye by using anion exchange membrane. In order to describe adsorption kinetics, two commonly used kinetic models, the pseudo first-order kinetic model [75], and pseudo second-order kinetic model [76] were used to test the experimental data.

4.3.2.4 Adsorption kinetics of Cr(VI) ions removal by composites membranes

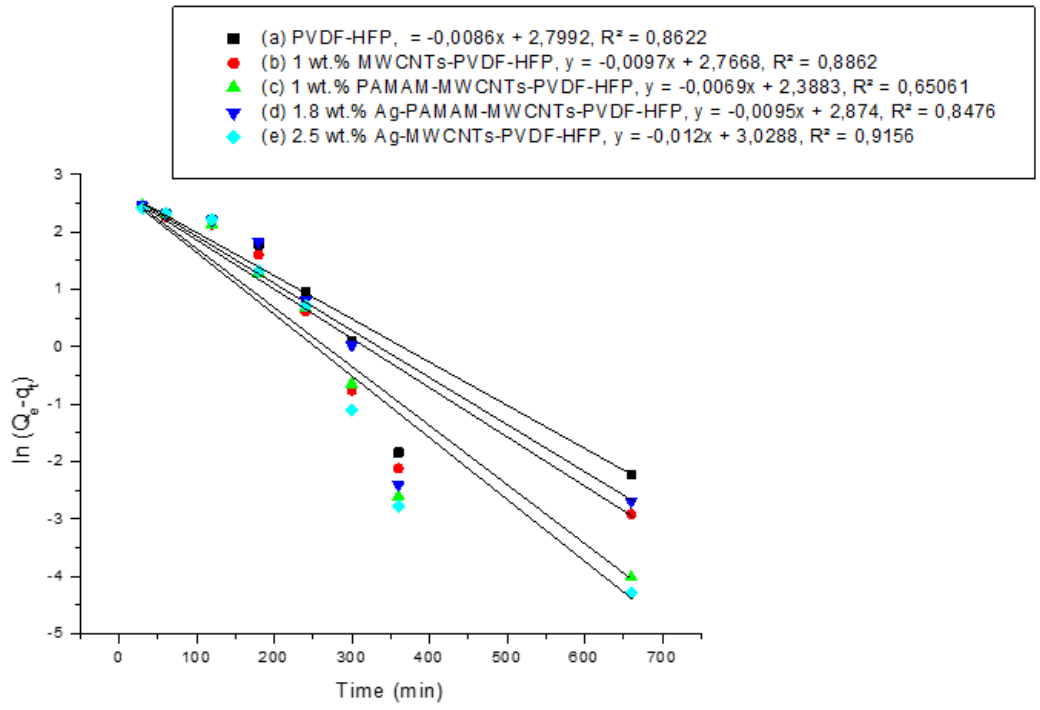

(i)

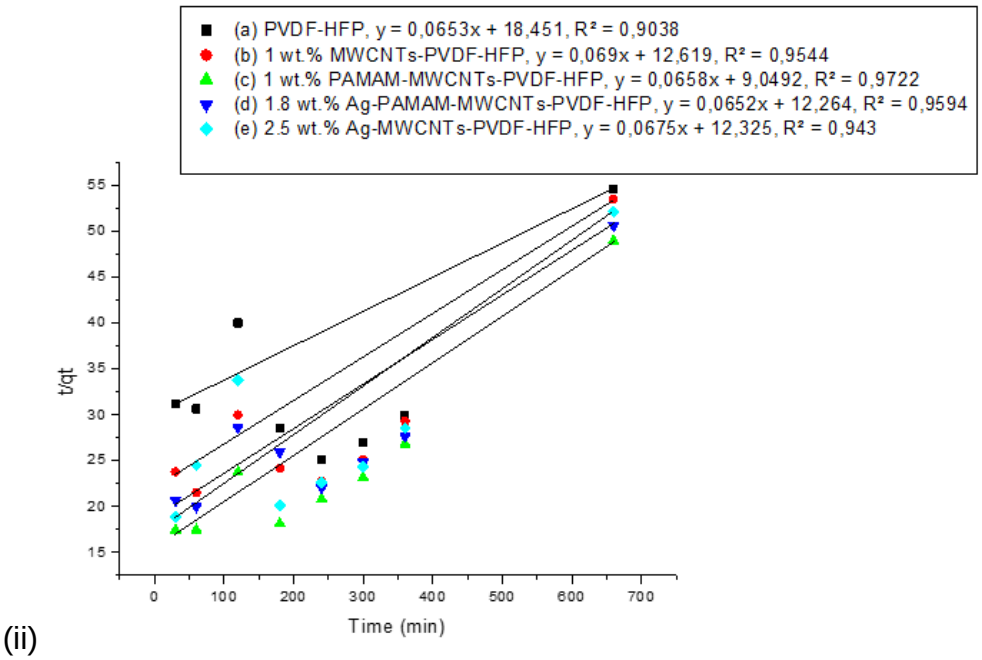

(ii)

Figure 4.39: Pseudo-first order and pseudo-second order kinetic model for adsorption of Cr(VI) ions on (a) PVDF-HFP, (b) 1 wt.% MWCNTs/PVDF-HFP, (c) 1 wt.% PAMAM-MWCNTs/PVDF-HFP, (d) 1.8 wt.% Ag-PAMAM-MWCNTs/PVDF-HFP, (e) 2.5 wt.% Ag-MWCNTs/PVDF-HFP composite membrane

Table 4.3.6: Kinetics parameters for Cr(VI) ions adsorption onto the PVDF-HFP membranes

Membrane	Experimental	Pseudo-first order kinetic model			Pseudo-second order kinetic model		
	q_e (mg g^{-1})	K_1 (min^{-1})	q_e (mg g^{-1})	R^2	K_2 (g.mg^{-1}.min^{-1})	q_e (mg g^{-1})	R^2
PVDF-HFP membrane	12.18	0.0086	16.43	0.862	2.31 x 10^{-4}	15.3	0.904
1 wt.% MWCNTs-PVDF-HFP	12.39	0.0097	15.91	0.886	3.75 x 10^{-4}	14.49	0.954

1 wt.% PAMAM-MWCNTs-PVDF-HFP	13.49	0.0069	10.89	0.651	4.78×10^{-4}	15.20	0.972
1.8 wt.% Ag-PAMAM-MWCNTs-PVDF-HFP	13.11	0.0095	17.71	0.848	3.47×10^{-4}	15.34	0.959
2.5 wt.% Ag-MWCNTs-PVDF-HFP	12.68	0.012	20.67	0.915	3.69×10^{-4}	14.81	0.943

Figure 4.39 shows the linearized forms of the pseudo-first and pseudo-second order models of Cr(VI) ions adsorption. K_1 and K_2 values were calculated from the slope of the graphs and given in Table 4.3.6. A comparison between experimental adsorption capacity values and calculated adsorption capacity showed that the adsorption follows a pseudo second-order model, which predicts the kinetic behaviour of biosorption, with chemical sorption being the rate-controlling step [76]. The values of the correlation coefficients (R^2 in table 4.3.6) also confirmed that the adsorption process follows a pseudo second-order process, which correlate with the behaviour reported in the literature [74,77-78].

4.3.2.5 Adsorption isotherms

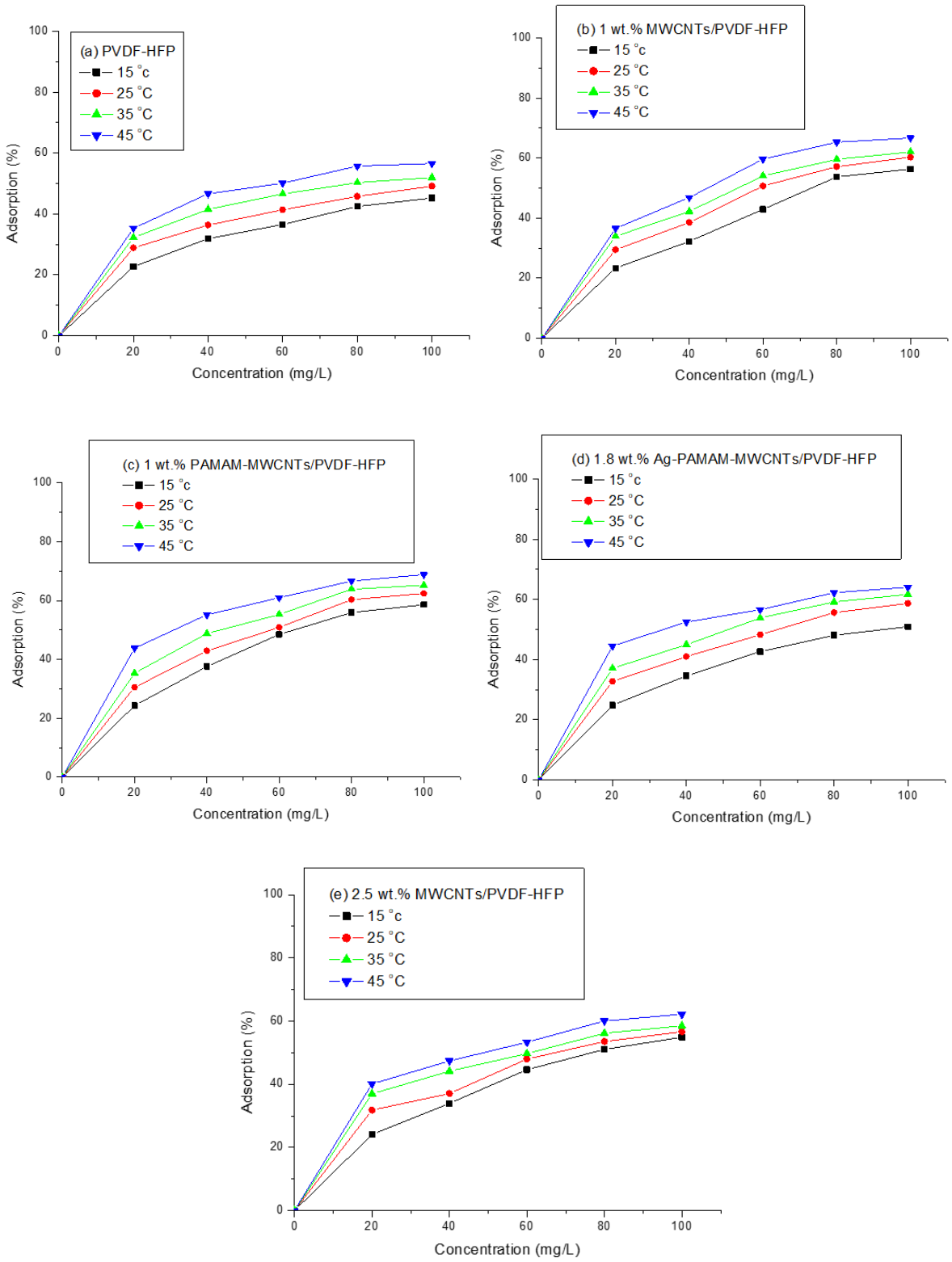

Figure 4.40: Effect of temperature on adsorption efficiency of Cr(VI) ions on (a) PVDF-HFP membrane, (b) 1 wt.% MWCNTs/PVDF-HFP, (c) 1 wt.% PAMAM-MWCNTs/PVDF-HFP, (d) 1.8 wt.% Ag-PAMAM-MWCNTs/PVDF-HFP and (e) 2.5 wt.% Ag-MWCNTs/PVDF-HFP

The effect of temperature of Cr(VI) ions at 15 ºC, 25 ºC, 35 ºC and 45 ºC is shown in figure 4.40. It was observed that the equilibrium adsorption capacities of PVDF-HFP based membranes increased as the temperature and concentrations of the Cr(VI) ions increased. The highest percentage adsorption of PVDF-HFP, 1% MWCNTs-PVDF-HFP, 1 wt.% PAMAM-MWCNTs/PVDF-HFP, 1.8 wt.% Ag-PAMAM-MWCNTs/PVDF-HFP and 2.5 wt.% Ag-MWCNTs/PVDF-HFP was 56, 67, 69, 64 and 62%, respectively. When the amount of Cr(VI) ions per unit volume of solution increased, the ratio amount of Cr(VI) ions to the available adsorption sites also increased and more Cr(VI) ions in solution were adsorbed by PVDF-HFP membranes, giving rise to the increase of the equilibrium adsorption capacity. Similar phenomena have been observed in the adsorption of Cr(VI) ions by magnetic carbon nanotubes [79]. This may be due to an increase in thermal energy of the adsorbing species, which leads to higher adsorption amount and faster adsorption rate as observed in literature [57,64].

Langmuir isotherm

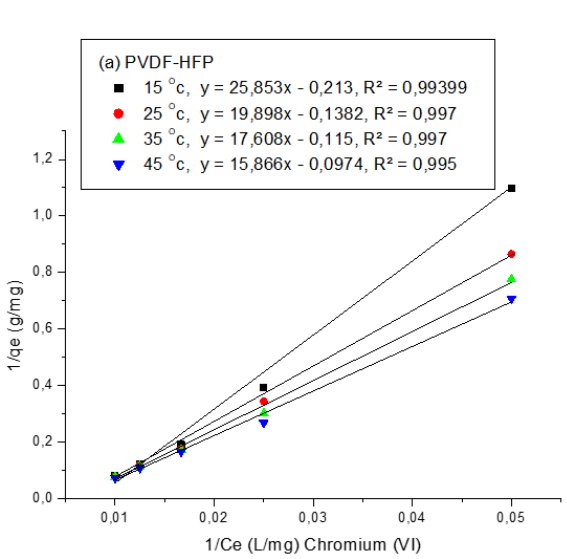

Freundlich isotherm

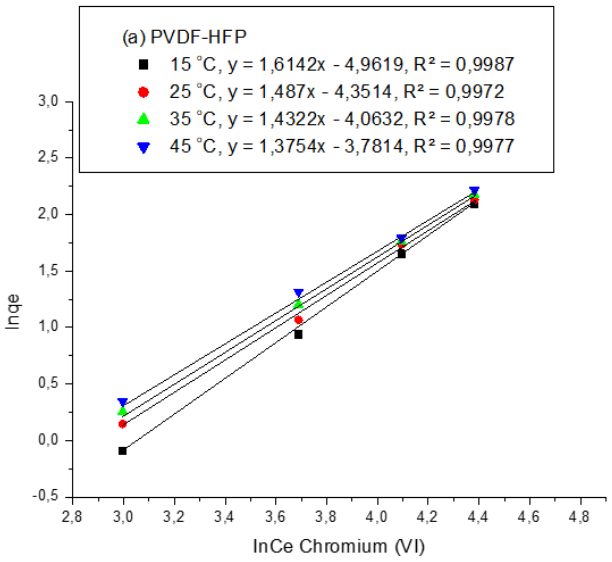

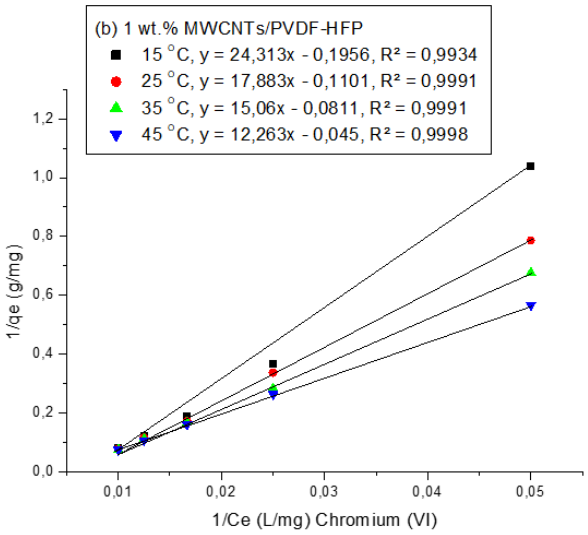
(b) 1 wt.% MWCNTs/PVDF-HFP
15 °C, y = 24,313x - 0,1956, R² = 0,9934
25 °C, y = 17,883x - 0,1101, R² = 0,9991
35 °C, y = 15,06x - 0,0811, R² = 0,9991
45 °C, y = 12,263x - 0,045, R² = 0,9998
1/qe (g/mg)
1/Ce (L/mg) Chromium (VI)

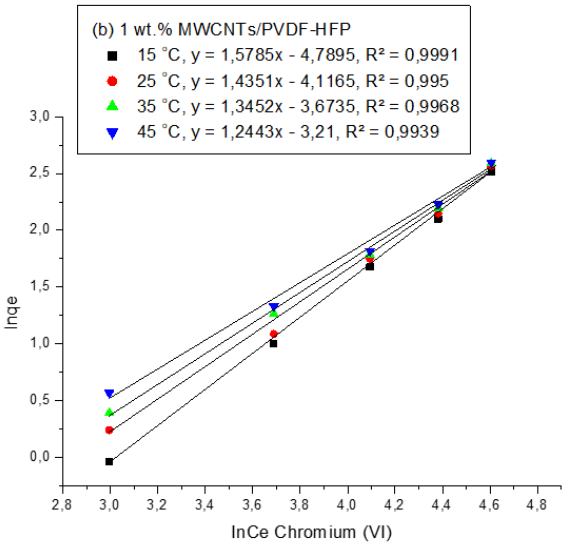
(b) 1 wt.% MWCNTs/PVDF-HFP
15 °C, y = 1,5785x - 4,7895, R² = 0,9991
25 °C, y = 1,4351x - 4,1165, R² = 0,995
35 °C, y = 1,3452x - 3,6735, R² = 0,9968
45 °C, y = 1,2443x - 3,21, R² = 0,9939
lnqe
lnCe Chromium (VI)

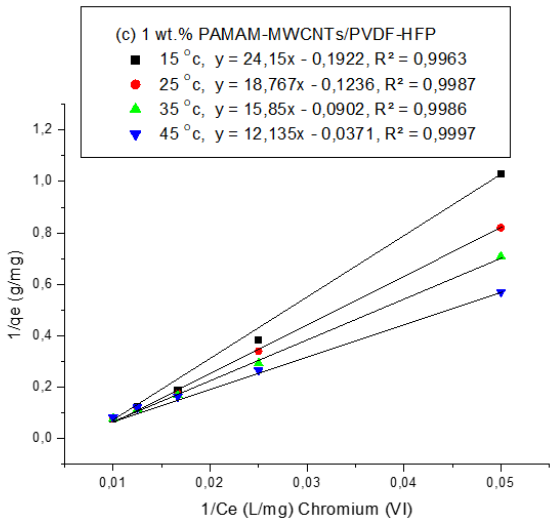
(c) 1 wt.% PAMAM-MWCNTs/PVDF-HFP
15 °c, y = 24,15x - 0,1922, R² = 0,9963
25 °c, y = 18,767x - 0,1236, R² = 0,9987
35 °c, y = 15,85x - 0,0902, R² = 0,9986
45 °c, y = 12,135x - 0,0371, R² = 0,9997
1/qe (g/mg)
1/Ce (L/mg) Chromium (VI)

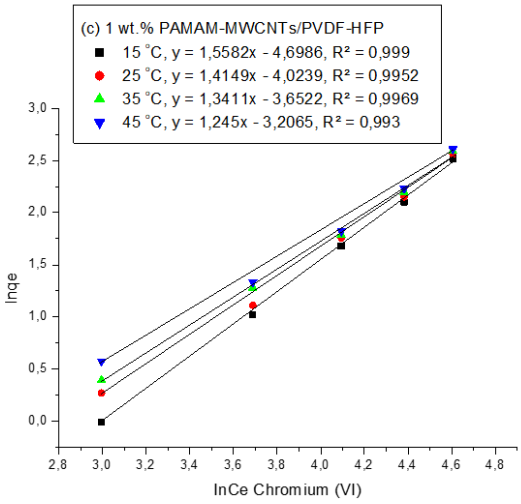
(c) 1 wt.% PAMAM-MWCNTs/PVDF-HFP
15 °C, y = 1,5582x - 4,6986, R² = 0,999
25 °C, y = 1,4149x - 4,0239, R² = 0,9952
35 °C, y = 1,3411x - 3,6522, R² = 0,9969
45 °C, y = 1,245x - 3,2065, R² = 0,993
lnqe
lnCe Chromium (VI)

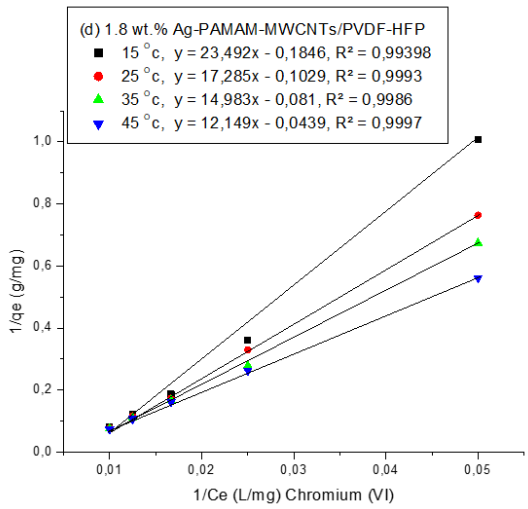
(d) 1.8 wt.% Ag-PAMAM-MWCNTs/PVDF-HFP
15 °c, y = 23,492x - 0,1846, R² = 0,99398
25 °c, y = 17,285x - 0,1029, R² = 0,9993
35 °c, y = 14,983x - 0,081, R² = 0,9986
45 °c, y = 12,149x - 0,0439, R² = 0,9997
1/qe (g/mg)
1/Ce (L/mg) Chromium (VI)

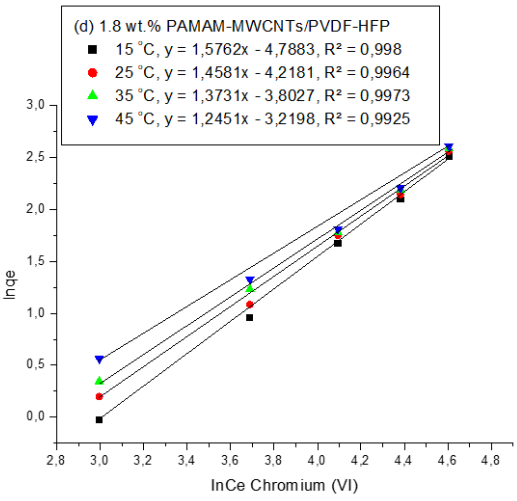
(d) 1.8 wt.% PAMAM-MWCNTs/PVDF-HFP
15 °C, y = 1,5762x - 4,7883, R² = 0,998
25 °C, y = 1,4581x - 4,2181, R² = 0,9964
35 °C, y = 1,3731x - 3,8027, R² = 0,9973
45 °C, y = 1,2451x - 3,2198, R² = 0,9925
lnqe
lnCe Chromium (VI)

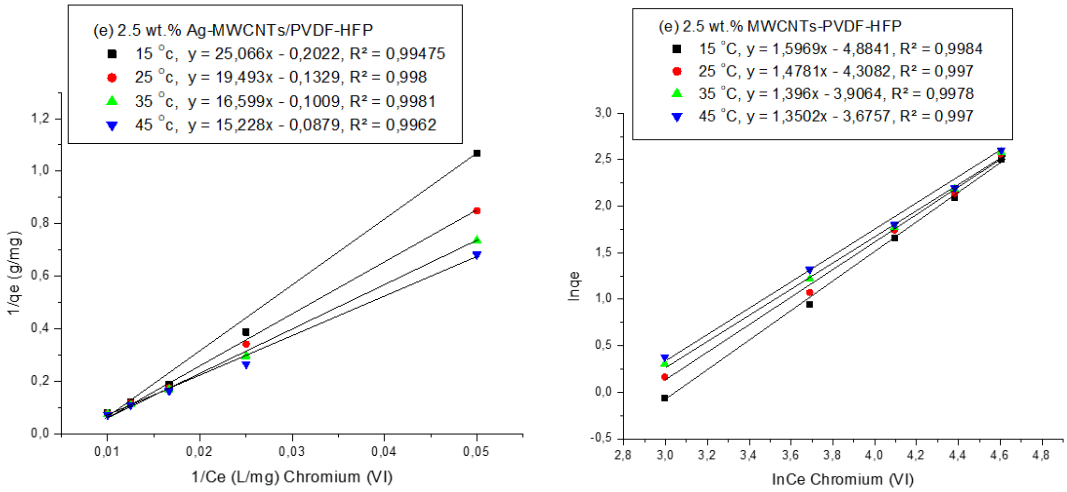

Figure 4.41: Langmuir and Freundlich isotherm adsorption of Cr(VI) ions on (a) PVDF-HFP, (b) 1 wt.% MWCNTs/PVDF-HFP, (c) 1 wt.% PAMAM-MWCNTs/PVDF-HFP, (d) 1.8 wt.% Ag-PAMAM-MWCNTs/PVDF-HFP and (e) 2.5 wt.% Ag-MWCNTs/PVDF-HFP composite membranes

Table 4.3.7: Parameters of Langmuir and Freundlich isotherm for Cr(IV) adsorption by PVDF based membranes.

Membrane	Temperature (°C)	Langmuir model			Freundlich model		
		q_m (mg/g)	b (L/mg)	R^2	K_f (mg/g)	n	R^2
PVDF-HFP	15	4.964	0.00824	0.994	0.0129	0.62	0.999
	25	7.24	0.00694	0.997	0.0129	0.67	0.997
	35	8.69	0.00654	0.997	0.0172	0.70	0.998
	45	10.27	0.00614	0.995	0.0228	0.73	0.998
1 wt.% MWCNTs-PVDF-HFP	15	5.112	0.00805	0.993	0.00832	0.63	0.999
	25	9.08	0.00616	0.999	0.0163	0.70	0.995
	35	12.33	0.00538	0.999	0.0254	0.74	0.997
	45	22.2	0.00367	0.999	0.0404	0.80	0.994
1 wt.% PAMAM-MWCNTs/PVDF-HFP	15	5.42	0.00785	0.994	0.00911	0.64	0.999
	25	9.72	0.00595	0.999	0.0179	0.71	0.995
	35	12.35	0.00540	0.999	0.0259	0.75	0.997
	45	22.78	0.00360	0.999	0.405	0.80	0.993
	15	5.2	0.00796	0.996	0.00833	0.63	0.998

1.8 wt.% Ag-PAMAM-MWCNTs/ PVDFHFP	25	8.09	0.00661	0.999	0.0147	0.69	0.996
	35	11.09	0.00569	0.999	0.0223	0.72	0.997
	45	26.95	0.00306	0.999	0.0399	0.80	0.992
2.5 wt.% Ag-MWCNTs-PVDF-HFP	15	4.96	0.00804	0.995	0.00757	0.63	0.998
	25	7.52	0.00682	0.998	0.0135	0.68	0.997
	35	9.91	0.00603	0.998	0.0201	0.72	0.998
	45	11.38	0.00577	0.996	0.0253	0.74	0.997

Figure 4.41 shows the linearized data using Langmuir and Freundlich isotherm of Cr(VI) ions on PVDF-HFP, 1 wt.% MWCNTs/PVDF-HFP, 1 wt.% PAMAM-MWCNTs/PVDF-HFP, 1.8 wt.% Ag-PAMAM-MWCNTs/PVDF-HFP and 2.5 wt.% Ag-MWCNTs-PVDF-HFP composite membranes. The isotherm constants and their correlation coefficients (R^2) are listed in table 4.3.7. The results indicate that the adsorption processes of PVDF-HFP membranes are well conformed to both Freundlich I (R^2 = 0.998) and Langmuir isotherm model (R^2 = 0.999) based on the R^2 values. This suggests that the sorption process meet both monolayer adsorption and heterogeneous adsorption process. The 1 wt.% MWCNTs/PVDF-HFP and 1 wt.% PAMAM-MWCNTs/PVDFHFP gave the highest value of q_{max} calculated from the Langmuir isotherm which gave the values of 9.08 and 9.72 mg/g, respectively. The q_{max} obtained in this study from the Langmuir isotherm was lower as compared to those reported in literature (table 4.3.8). The adsorbent dosage is inversely proportional to q_{max}, hence a low value of q_{max} resulted, since a high adsorbent dosage of 5 g/L was used to achieve a better adsorption.

For the Freundlich isotherm if the value of n lies between 1 and 10, it indicates good adsorption [80]. The calculated values of n for the adsorption of Cr(VI) ions were all above 0.6, showing moderate efficiency for Cr(VI) ions on PVDF-HFP in contrast to the work reported by Shi *et al*. [81].

Table 4.3.8: Langmuir constants for Cr(VI) ions adsorption by different adsorption

Adsorbent	Experimental conditions			Adsorption capacity q_{max} (mg/g)	Reference
	pH	T (ºC)	Dosage		
1 wt. % PAMAM-MWCNTs/PVDF-HFP	2.5	298	5 g/L	9.72	This study
Industrial waste (Dolochar)	2	303	20 g/L	0.904	56
Polyacrylonitrile (PAN) based nanofibers	3	308	2.5 g/L	23	69
Chitosan crosslinked with silicon materials NZ	5	298	4 g/L	5.54	68
Chitosan crosslinked with silicon material NM	5	298	4 g/L	6.35	68
La (III) encapsulated silica Gel/chitosan composite	4	303	2 g/L	6.127	70
Alumina/chitosan biocomposite	4	303	2 g/L	8.62	71
Wollastonite	2.5	303	20 g/L	0.686	72

4.3.2.6 Thermodynamic analysis

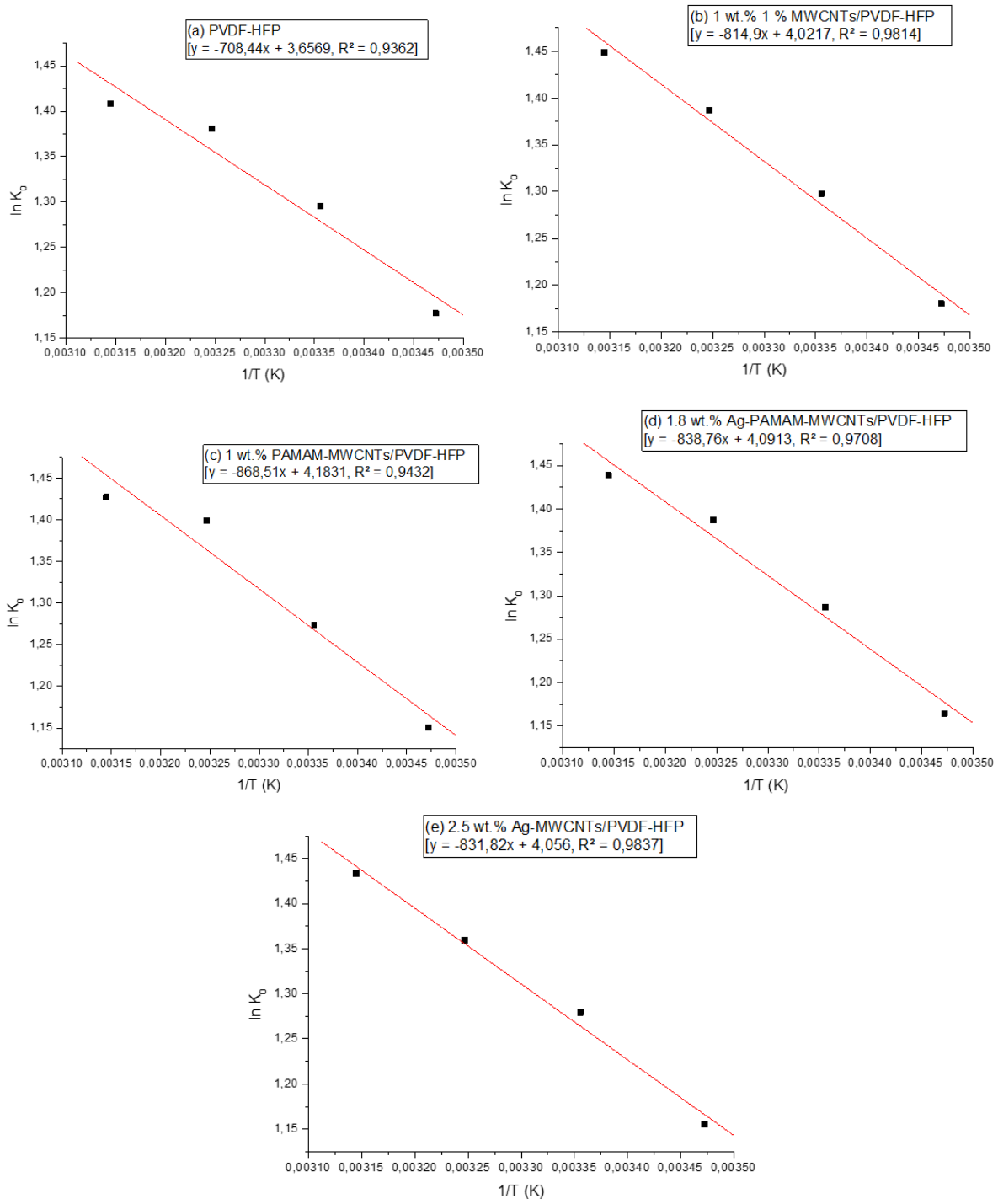

Figure 4.42: Linear plot of lnK_o verses 1/T for the adsorption of Cr(VI) ions onto (a) PVDF-HFP, (b) 1 wt.% MWCNTs/PVDF-HFP, (c) 1 wt.% PAMAM-MWCNTs/PVDF-HFP, (d) 1.8 wt.% Ag-PAMAM-MWCNTs/PVDF-HFP and (e) 2.5 wt.% Ag-MWCNTs/PVDF-HFP composite membrane

Figure 4.42 shows the linear plot of InK_o vs 1/T for Cr(VI) ions on PVDF-HFP based membranes. It was observed that Ink_o decreased as 1/T increased. The Arrhenius plot is obtained by plotting the logarithm of the rate constant, k, versus the inverse temperature, 1/T. The resulting negatively-sloped line is useful in finding the missing components of the Arrhenius equation. The values of ΔH^o and ΔS^o were obtained from the slope and intercept of the plot of ln K_o versus 1/T, as reported in the in literature [64,82].

Table 4.3.9: Thermodynamic parameters for Cr(VI) ions adsorption by PVDF-HFP based membranes

Membrane	**Thermodynamic parameters**			
	Temperature (K)	**ΔG^o (kJ.mol^{-1})**	**ΔH^o (kJ.mol^{-1})**	**ΔS^o (J.mol.K^{-1})**
PVDF-HFP	288 298 308 318	-2.819 -3.210 -3.535 -3.724	5.89	30.40
1 wt.% MWCNTs-PVDF-HFP	288 298 308 318	-2.826 -3.215 -3.551 -3.832	6.78	33.44
1 wt.% PAMAM-MWCNTs-PVDF-HFP	288 298 308 318	-2.755 -3.156 -3.583 -3.773	7.22	34.78

1.8 wt.% Ag-PAMAM-MWCNTs-PVDF-HFP	288 298 308 318	-2.788 -3.188 -3.494 -3.804	6.82	34.01
2.5 wt.% Ag-MWCNTs-PVDF-HFP	288 298 308 318	-2.766 -3.170 -3.480 -3.790	6.92	33.72

Table 4.3.9 show the thermodynamics parameters (ΔG^o, ΔH^o, and ΔS^o) for PVDF-HFP,1 wt.% MWCNTs/PVDF-HFP, 1 wt.% PAMAM-MWCNTs/PVDF-HFP, 1.8 wt.% Ag-PAMAM-MWCNTs/PVDF-HFP and 2.5 wt.% Ag-MWCNTs/PVDF-HFP composite membrane calculated from the slopes and intercept of the Van't Hoff plot in figure 4.3.2.5. The values of ΔG^o on average were negative suggesting that the adsorption process involved is feasible and spontaneous as reported by Huang *et al*. [79] and Shen *et al*. [83]. The experimental data shows that the adsorption process of Cr(IV) ions is mainly physical in nature. This means that the process of adsorption is accompanied by electrostatic attraction between sites and the adsorbed species and that is physical in nature [84]. Similar results were reported elsewhere during the adsorption of Cr(VI) ions on magnetic multi-wall carbon nanotubes [77].

The positive values of ΔH^o confirmed that the adsorption process was endothermic in nature. A higher temperature is favourable to the adsorption which may explain the increase in q_{max} in Langmuir isotherm as the temperature is raised. ΔS^o values on average decreased with an increase in concentration and were all positive suggesting that adsorption is spontaneous in nature [85]. The positive values of ΔS^o reflects the increased disorder and randomness of the Cr(VI) ions on the PVDF-HFP membranes and the solid-liquid interface during the adsorption process. This also indicate the affinity of the adsorbent material towards Cr(VI) ions [86].

4.4 REFERENCES

1. Tehrani, M.S., Azar, P.A. and Namin, P.E. 2013. Removal of lead ions from wastewater using functionalized multiwalled carbon nanotubes with Tris(2-Aminoethyl) Amine. *Journal of environmental protection*, 4, 529-536.

2. Mkhondo, N.B. and Magadzu, T. 2014. Effects of different acid-treatment on the nanostructure and performance of carbon nanotubes in electrochemical hydrogen storage. *Digest journal of nanomaterials and biostructures*, 9(4), 1331-1338.

3. Zhang, Y., Liu. X., Li. L., Guo. Z., Xue., Z. and Lu. X. 2016. An electrochemical paracetamol sensor based on layer-by-layer covalent attachment of MWCNTs and G4.0 PAMAM modified GCE. *Analytical methods*, 8, 2218-2225.

4. Fan., Y., Su, F., Li, K., Ke, C. and Yan, Y. 2017. Carbon nanotube filled with magnetic iron oxide and modified with polyamidoamine dendrimers for immobilizing lipase toward application in biodiesel production. *Scientific reports*, 7, 45643.

5. Rananga, L.E., Magadzu, T. 2015. Comparative studies of silver doped carbon nanotubes and β-cyclodextrin for water disinfection. *Digest journal of nanomaterials and biostructures,* 10, 831-836.

6. Sagar, S., Iqbal, N. and Maqsood, A. 2013. Dielectric, electric and thermal properties of carboxylic functionalized multiwalled carbon nanotubes impregnated polydimethylsiloxane nanocomposite. *Journal of physics: conference series*. 439.

7. Buang, N.A., Fadi, F., Majid, Z.A. and Shahir S. 2012. Characteristic of mild acid functionalized multiwalled carbon nanotubes towards high dispertion with low structural defects. *Digest journal of nanomaterials and biostructures,* 7 (1), 33-39.

8. Yuan, W., Giang, G., Che J., Qi, X., Xu, R., Chang, M.W., Chen, Y., Lim, S.Y., Dai, J, and Chan-Park, M.M. 2008. Deposition of Silver Nanoparticles on Multiwalled Carbon Nanotubes Grafted with Hyperbranched Poly(amidoamine) and Their Antimicrobial Effects. *Journal of physical chemistry C, 112,* 18754-18759.

9. Ma, P.C., Tang, B.Z. and Kima, J.K. 2008. Effect of CNT decoration with silver nanoparticles on electrical conductivity of CNT-polymer composites. *Carbon journal,* 46, 1497-1505.

10. Haider. A.J., Mohammed, M.R. and Ahmed. D.S. Preparation and characterization of multi walled carbon naotubes /Ag nanoparticles hybrid materials. *International journal of scientific & engineering research*, 5(3), 2229-5518.

11. Shi, Y., Liu, Z., Zhao, B., Sun, Y., Xu, F., Zhang, Y., Wen, Z., Yang, H. and Li, Z. 2011. Carbon nanotube decorated with silver nanoparticles via noncovalent interaction for a novel nonenzymatic sensor towards hydrogen peroxide reduction. *Journal of electroanalytical chemistry*, 656,29-33.

12. Forati-Nezhad, M., Sadeghi, G.M.M., Yaghmaine, F. and Alimohammadi, F. 2015. Affecting the morphology of silver deposition on carbon nanotube surface: From nanoparticles to dendritic (tree-like) nanostructures. *Materials science and engineering C,* 46, 232-238

13. Watts, PCP., Mureau, N., Tang, Z., Miyajima, Y., Carey, J.D. and Silva, SRP. 2007. The importance of oxygen-containing defects on carbon nanotubes for the detection of polar and non-polar vapours through hydrogen bond formation. Nanotechnology, 18, 175701

14. Park, H, S., Hwang, J.Y., Shin, U.S., Kim, H.W. and Gong, M.S. 2011. Positively charged silver nanoparticles threaded on carbon nanotube for the efficient delivery of negatively charged biomolecules. *Bulletin of the Korean chemical society journal*, 32, 10, 3581-3586.

15. Meng, Y., Su, F and Chen, Y. 2018. Effective lubricant additive of nano-Ag/MWCNTs nanocomposite produced by supercritical CO_2 synthesis. Tribology International 118 (2018) 180-188.

16. Salam, M.A. and Burk, R. 2017. Synthesis and characterization of multi-walled carbon nanotubes modified with octadecylamine and polyethylene glycol. *Arabian journal of chemistry*, 10, 921-927.

17. Malmonge, L.F., Langiano, SC., Cordeiro, M.M., Mattoso, L.H.C. and Malmonge, J.A. 2010. Thermal and mechanical properties of PVDF/PANI blends. *Material research*, 13(4), 465-470.

18. Zulfiqar, S., Zulfiqar, M. and Munir, A. 1994. Study of the thermal-degradation of polychlorotrifluoroethylene, poly(vinylidene fluoride) and copolymers of chlorotrifluoroethylene and vinylidene fluoride. *Polymer degradation and stability,* 43(3), 423-430.

19. Mehrizad, A., Aghaie, M., Gharbani, P., Dastmaichi, S.M, Monajjemi, M. and Zare, K. 2012. Comparison of 4-chloro-2-nitrophenol adsorption on single-walled and multi-walled carbon nanotubes. *Iranian journal of environmental health science & engineering,* 9, 5.

20. Ihsanullah., Patel, F., Khraisheh, M., Atieh, M.A. and Laoui, T. 2017. Novel aluminum oxide-impregnated carbon nanotube membrane for the removal of cadmium from aqueous solution. *Materials*, 10, 1144.

21. Ma, L., Dong, X., Chen, M., Zhu, L., Wang, C., Yang, F. and Dong, Y. 2017. Fabrication and water treatment application of carbon nanotubes (CNTs)-based composite membranes: A review. *Membranes*, 7, 16.

22. Kim, Y.A., Hayashi, T., Endo, M., Kaburagi, Y., Tsukada, T., Shan, J., Osato, K. and Tsuruoka, S. 2005. Synthesis and structural characterization of thin multi-walled carbon nanotubes with a partially facetted cross section by a floating reactant method. *Carbon journal*, 43. 2243-2245.

23. Larrude, D.G., Maia da Costa, M.E.H. and Freire Jr, F.L. 2014. Synthesis and characterization of silver nanoparticle-multiwalled carbon nanotube composites. *Journal of nanomaterials,* 1-7.

24. Guo, X., Fei, G.K., Su, G.T.H. Zhang, L.D. 2011. High-performance and reproducible polyaniline nanowire/tubes for removal of Cr(VI) in aqueous solution. *Journal of physical chemistry C*, 115 (5), 1608-1613.

25. Chen, J., Gu B., Leboeuf E., Pan, H. and Dai, S. 2002. Spectroscopic characterization of the structural and functional properties of natural organic matter fractions. *Chemosphere,* 48, 59-68.

26. Mohan, D. and Singh, K. P. 2002. Single- and multi-component adsorption of cadmium and zinc using activated carbon derived from bagasse – an agricultural waste. *Water research*, 36, 2304-2318.
27. Hayati, B., Arami, M., Maleki, A. and Pajootan, E. 2015. Thermodynamic properties of dye removal from colored textile wastewater by poly (propylene imine) dendrimer. *Desalination and water treatment*, 56, 97-106.
28. Maleki, A., Jebelli, M.A., Hayati, B., Daraei, H. and Gharibi, F. 2015. Antimicrobial effect of poly(amidoamine)-G2 and G4 dendrimers on some bacteria in water resources, *Journal of Mazandaran university of medical sciences*, 25.
29. Grossiord, N., Loos, J., van Laake, L., Maguey M, Zakri, C., Koning, CE., Hart, A.J. 2008. High-conductivity polymer nanocomposites obtained by tailoring the characteristics of the carbon nanotube fillers. *Advanced functional materials*, 18, 3226-3234.
30. Hamwi A, Alvergnat H, Bonnamy S, Beguin F. 1997. Fluorination of carbon nanotubes. *Carbon*, 35, 723-728.
31. Zhao, D., Yu, Y. and Chen, J.P. 2016. Treatment of lead contaminated water by a PVDF membrane that is modified by zirconium, phosphate and PVA. *Water research,* 101, 564-573.
32. Li, J.H., Shao, X.S., Zhou, Q., Li, M.Z., Zhang, Q.Q. 2013. The double effects of silver nanoparticles on the PVDF membrane: Surface hydrophilicity and antifouling performance. *Applied surface science*, 265, 663-670.
33. Badawi, N.E., Ramadan, A.R., Esawi, A.M.K. and El-Morsi, M. 2014. Novel carbon nanotube-cellulose acetate nanocomposite membranes for water filtration applications. *Desalination* 344, 79-85.
34. Shawky, H.A., Chae, S.R., Lin, S. and Wiesner, M.R. 2011. Synthesis and characterization of a carbon nanotube/polymer nanocomposite membrane for water treatment. *Desalination* 272, 46-50.
35. Li, M., Kim, I.-H Jeong, Y.G. 2010. Cellulose acetate/multiwalled carbon nanotube nanocomposites with improved mechanical, thermal, and electrical properties. Journal of applied polymer science. 118, 2475-2481.
36. Kahu, S.S., Shekhawat, A., Saravanan, D. and Jugade, R.M. 2016. Two fold modified chitosan for enhanced adsorption of hexavalent chromium from

simulated wastewater and industrial effluents. *Carbohydrate polymers*, 146, 264-273.

37. Ahmed, F., Santos, C.M., Vergara, R. and Tria, M.C.R. 2012. Antimicrobial applications of electroactive PVK-SWNT nanocomposites. *Environmental science & technology,* 46 (3), 1804-1810.

38. Wang, W.Y., Shi, J.Y., Wang, J.L., Li, Y.L., Gao, N.N., Liu, Z.X. and Lian W.T. 2015. Preparation and characterization of PEG-g-MWCNTs/PSf nano-hybrid membranes with hydrophilicity and antifouling properties. *RSC advances.* 5, 84746-84753.

39. Ho, C.C. and Zydney, A.L. 2000. A combined pore blockage and cake filtration model for protein fouling during microfiltration. *Journal of colloid and interface science*, 232, 389-399.

40. 36. Astaraee, R.S., Mohammadi, T. and Kasiri, N. 2015. Analysis of BSA, dextran and humic acid fouling during microfiltration, experimental and modelling. *Food and bioproducts processing,* 94, 331-341.

41. Park, S.J., Cheedrala, R.K., Diallo, M.S., Kim, C., Kim, I.S. and Goddard, W.A. 2012. Nanofiltration membranes based on polyvinylidene fluoride nanofibrous scaffolds and crosslinked polyethyleneimine networks. *The journal of nanoparticle research,* 14, 1884.

42. Zhu, H., Szymczyk, A. and Balannec, B. 2011. On the salt rejection properties of nanofiltration polyamide membranes formed by interfacial polymerization. *Journal of membrane science*, 379, 215-223.

43. Mericq, J.P., Mendret, J., Brosillon, S. and Faur, C. 2015. High performance PVDF-TiO_2 membranes for water treatment. *Chemical engineering science*, 123, 283-291.

44. Havelaar, A. and Bartram, J. 1996. World Health Organization: guidelines for drinking water quality, 2. *World health organization*, 29-31.

45. Stephan, A.M., Kumar, S.G., Renganathan, N.G. and Kulandainathan, M.A. 2005. Characterization of poly(vinylidene fluoride-hexafluoropropylene) (PVdF-

HFP) electrolytes complexed with different lithium salts. *European polymer journal*, 41, 15-21.

46. Leite, L., Stonkus, V., Edolfa, K., Ilieva, L., Andreeva, D., Plyasova, L., Sobckzak, J.W., Ionescu, S., Munteane, G. 2004. Active phases of supported cobalt catalysts for 2,3-dihydrofuran synthesis. *Journal of molecular catalysis a: chemical,* 215, 95-101.
47. Suhartono, J. and Tizaoui, C. 2015. Polyvinylidene fluoride membranes impregnated at optimised content of pristine and functionalised multi-walled carbon nanotubes for improved water permeation, solute rejection and mechanical properties. *Separation and purification technology* ,154, 290-300.
48. Phao, N., Nxumalo, E.N., Mamba, B.B. and Mhlanga, S.D. 2013. A nitrogen-doped carbon nanotube enhanced polyethersulfone membrane system for water treatment. *Physics and chemistry of the earth* 66, 148-156.
49. Kang, S., Herzberg, M., Rodrigues, D. F. and Elimelech, M. 2008. Antibacterial effects of carbon nanotubes: size does matter. *Langmuir*, 24, 6409-6413.
50. APHA 1992. Standard Methods for the Examination of Water and Waste Water, 18th Edition. American Public Health Association, American Water Works Association, Water Environment Federation. Published by the American public health association, Washington DC, USA.
51. SANS 241-1. 2015. Drinking water, Part 1: Microbial, physical, aesthetic and chemical determinants. South African bureau of standards (SABS), Pretoria.
52. https://www.filterwater.com/t-reverse-osmosis-water-and-ph.aspx
53. WHO. 2004. Guidelines for drinking-water quality, 3rd Ed. World health organization, Geneva.
54. Wu, S., Zhang, K., Wang, X., Jia, Y., Sun. B., Luo. T., Meng, F., Jin, Z., Lin, D., Shen, W., Kong, L. and Liu, J. 2015. Enhanced adsorption of cadmium ions by 3D sulfonated reduced graphene oxide. *Chemical engineering journal,* 262, 1292-1302.
55. Kumar, P.S., Ramalingam, S., Sathyaselvabala, V., Kirupha, S.D, Murugesan A. and Sivanesan S. 2012. Removal of cadmium(II) from aqueous solution by

agricultural waste cashew nut shell. *Korean journal of chemical engineering,* 29(6), 756-768.

56. Tran, H.N., You, S.J. and Chao, H.P. 2016. Thermodynamic parameters of cadmium adsorption onto orange peel calculated from various methods: A comparison study. *Journal of environmental chemical engineering,* 4, 2671-2682.

57. Li, Z., Kang, W., Wei, N., Qiu, J., Sun, C. and Chen, B. 2017. Preparation of a polyvinylidene fluoride tree-like nanofiber mat loaded with manganese dioxide for highly efficient lead adsorption. *RSC advances*, 7, 8220.

58. Snoussi, Y., Abderrabba, M. and Sayari, A. 2016. Removal of cadmium from aqueous solutions by adsorption onto polyethylenimine-functionalized mesocellular silica foam: Equilibrium properties. *Journal of the Taiwan institute of chemical engineers,* 66, 372-378.

59. Bhatt, A.S., Sakaria, P.L., Vasudevan, M., Pawar, R.R., Sadheesh, N., Bajaj, H.C. and Mody, H, M. 2012. Adsorption of an anionic dye from aqueous medium by organoclays: equilibrium modeling, kinetic and thermodynamic exploration. *RSC advances*, 2, 8663-8671.

60. Awwad, A.M. and Salem, N.M. 2012. Biosorption of copper(II) and lead(II) ions from aqueous solutions by modified loquat (Eriobotrya japonica) leaves (MLL). *Journal of chemical engineering and materials science*. 3(1), 7-17.

61. Rahman, M., Gul, S., Ajmal, M., Iqbal, A. and Achakzai, A.K.K. 2014. Removal of cadmium from aqueous solutions using excised leaves of quetta pine (pinus halepensis mill.). *Bangladesh journal of botany*, 43 (3), 277-281.

62. Yang, S., Zhao, Y., Chen, R., Feng, C., Zhang, Z., Lei, Z. and Yang, Y. 2013. A novel tablet porous material developed as adsorbent for phosphate removal and recycling. *Journal of colloid and interface science*, 396, 197-204.

63. Meroufel, B., Benali, O., Benyahia, M., Benmoussa, Y. and Zenasni, M.A. 2013. Adsorptive removal of anionic dye from aqueous solutions by Algerian kaolin: characteristics, isotherm, kinetic and thermodynamic studies. *Journal of material and environmental science,* 4 (3),482-491.

64. Mohammed, A., Nasser, W.S., Osman, T.A., Toprak, M.S., Muhammed, M. and Uheida, A. 2017. Removal of chromium (VI) from aqueous solutions using surface modified composite nanofibers. *Journal of colloid and interface science* 505, 682-691.

65. Salehi, E., Madaeni, S.S. and Heidary, F. 2012. Dynamic adsorption of Ni(II) and Cd(II) ions from water using 8-hydroxyquinoline ligand immobilized PVDF membrane: Isotherms, thermodynamics and kinetics. S*eparation and purification technology,* 94, 1-8.

66. Ganesan, V., Louis, C. and Damodaran, S.P. 2018. Graphene oxide-wrapped magnetite nanoclusters: A recyclable functional hybrid for fast and highly efficient removal of organic dyes from wastewater. J*ournal of environmental chemical engineering* 6, 2176-2190.

67. Kong, Q., Xe, B., Preis, S., Hu., Y. and Wu, H. 2018. Adsorption of Cd^{2+} by an ion-imprinted thiolfunctionalized polymer in competition with heavy metal ions and organic acids. *Royal society of chemistry*, 8, 8950-8960.

68. Karthikeyan, G., Anbalagan, K. and Muthulakshmi, A.N. 2004. Adsorption dynamics and equilibrium studies of Zn(II) onto chitosan. *Journal of chemical science*, 116,119-127.

69. Panda, H., Tiadi, N., Mohanty, M. and Mohanty, C.R. Studies on adsorption behavior of an industrial waste for removal of chromium from aqueous solution. *South African journal of chemical engineering*, 23, 132-138.

70. Argun, M.E., Dursun, S., Ozdemir, C. and Karatas, M. 2006. Heavy metal adsorption by modified oak sawdust: thermodynamics and kinetics. *Journal of hazardous materials*, 141 (1), 77-85.

71. Oladoja., N.A., Ololade, I.A., Olatujoye, V.O. and Akinnifesi, T.A. 2012. Performance evaluation of fixed bed of nano calcium oxide synthesized from a gastropod shell (Achatina achatina) in hexavalent chromium abstraction from aqua system. *Water, air, & soil pollution. An international journal of environmental pollution,* 223 (4),1861-1876.

72. Sharma, Y.C., Singh, B., Agrawal, A. and Weng C.H. 2008. Removal of chromium by riverbed sand from water and wastewater: Effect of important parameters. *Journal of hazardous materials*, 151, 789-793.

73. Das, D.D., Mahapata., J., Pradhan, S.N., Das. R.S. and Thakur J. 2000. *Colloids and interface science*, 232, 235-240.

74. Khan., M.I., Akhtar, S., Zafar, S., Shaheen, A., Khan, M.A., Luque, R. and Rehman A. 2015. Removal of Congo red from aqueous solution by anion exchange membrane (EBTAC): Adsorption kinetics and thermodynamics. *Materials*, 8, 4147-4161.

75. Lagergren, S., 1898. About the theory of so-called adsorption of soluble substances. Kungliga Svenska Vetenskapsakademiens. *Handlingar*, 24. 1-39.

76. Ho. Y.S. and McKay. G. 1999. Pseudo-second order model for sorption processes. *Process biochemistry*, 34(5), 451-465.

77. Hena, S. 2010. Removal of chromium hexavalent ion from aqueous solutions using biopolymer chitosan coated with poly 3-methyl thiophene polymer. *Journal of hazardous materials*, 181, 474-479.

78. Hu, X.J., Wang, J.S., Liu, Y.G., Li, X., Zeng, G.M., Bao, Z.L., Zeng, X.X., Chen. A.W. and Long, F. 2011. Adsorption of chromium (VI) by ethylenediamine-modified cross-linked magnetic chitosan resin: Isotherms, kinetics and thermodynamics. *Journal of hazardous materials*, 185. 306-314.

79. Huang, Z., Wang, X. and Yang, D. 2015. Adsorption of Cr(VI) in wastewater using magnetic multi-wall carbon nanotubes. *Water science and engineering*, 8(3), 226-232.

80. Goldberg, S. 2005. Equations and models describing adsorption processes in soils, Soil science society of America, 677 S. Segoe Road, Madison, WI 53711. USA.

81. Shi, T., Yang, D., Yang, H., Ye, J. and Chen, Q. 2017. Preparation of chitosan crosslinked modified silicon material and its adsorption capability for chromium (VI). *Applied clay science,* 142, 100-108.

82. Wang, K., Qiu, G., Cao, H., and Jin, R. 2015. Removal of Chromium(VI) from aqueous solutions using Fe_3O_4 magnetic polymer microspheres functionalized with amino groups. *Materials,* 8, 8378-8391.

83. Shen, F., Zhang, X., Zhang, K. and Qi, X. 2016. Chitosan-derived carbonaceous material for highly efficient adsorption of chromium (VI) from aqueous solution. *International journal of biological macromolecules,* 91, 443-449.

84. Horsfall, M., Abiba, A.A. and Spiff. A.I. 2006. Kinetic Studies on the adsorption of Cd^{2+}, Cu^{2+} and Zn^{2+} ions from aqueous solutions by cassava (Manihot sculenta Cranz) tuber bark waste. *Bioresource technology*, 97, 283-291.

85. Weng, C.H., Lin, Y.T. and Tzeng, T.W. 2009. Removal of methylene blue from aqueous solution by adsorption onto pineapple leaf powder. *Journal of hazardous materials*, 170 (1), 417-424.

86. Nasuha, N.H. and Hameed, B.H. 2011. Adsorption of methylene blue from aqueous solution onto NaOH-modified rejected tea. *Chemical engineering journal,* 166 (2), 783-786.

CHAPTER 5

CONCLUSIONS AND RECOMMENDATIONS

5.1 CONCLUSIONS

PVDF-HFP composite membranes were successfully prepared using a phase inversion method. The nanocomposite membranes prepared consisted of blends such as 1 wt.% MWCNTs/PVDF-HFP, 1 wt.% PAMAM-MWCNTs/PVDF-HFP, 5 wt.% Ag/PVDF-HFP, 2.5 wt.% Ag-MWCNTs/PVDF-HFP and 1.8 wt.% Ag-PAMAM-MWCNTs/PVDF-HFP. FTIR spectra confirmed the formation of functional groups such as COOH, OH, NCO, NH_2 on the nanocomposites and the characteristic of amide (-CO-NH-) I and II bonds on 1 wt.% PAMAM-MWCNTs/PVDF-HFP, indicating the presence of PAMAM dendrimer.

The X-ray diffraction peak of fMWCNTs at $2\theta = 26.01^{o}$ increased as compared to the raw MWCNTs, which was an indication of the carbon nanotubes purity after acid treatment. The diffraction patterns of fMWCNTs, Ag-MWCNTs, and Ag-PAMAM/MWCNTs all showed (111), (200) and (220) planes, indexed to a face-centred cubic symmetry, confirming the presence of Ag nanoparticles. The presence of Ag on PVDF-HFP composite membranes was also confirmed by EDX.

Transmission electron microscopy showed reduced thickness of amorphous carbon layer on the walls of the MWCNTs after functionalisation and the morphology of MWCNTs revealed both open and closed tubes. TEM of Ag containing nanoparticles showed homogeneous dark spherical spots corresponding to Ag nanoparticles.

Thermogravimetric analysis studies demonstrated that the functionalisation of PVDF-HFP with MWCNTs, Ag and PAMAM-MWCNTs affected the thermal stability of PVDF-HFP. The thermal stability of PVDF-HFP composite membrane was greatly enhanced by the addition of PAMAM-MWCNTs.

The surface structures of the composite membranes were significantly affected by the presence of MWCNTs and PAMAM nanocomposites as observed from the SEM structures. The cross sections of PVDF-HFP composite membranes showed a mixture of fingure-like microvoids with a membrane diameter of approximately 180 μm. The

modified PVDF-HFP composite membranes showed a decrease in the microvoids, with a high spongy surface which is good for heavy metal adsorption and desalination.

The Brunauer-Emmett-Teller results showed that the surface area, pore volume and pore sizes of PVDF-HFP composite membranes was improved by blending with fMWCNTs. The surface area for the composite membranes was as follows: 1 wt.% PAMAM-MWCNTs/PVDF-HFP > 1.8 wt.% Ag-PAMAM-MWCNTs/PVDF-HFP > 1 wt.% MWCNTs-PVDF-HFP > 2.5 wt.% Ag-MWCNTs/PVDF-HFP.

MWCNTs and PAMAM grafting was effective for improving membrane surface hydrophilicity, as demonstrated by swellability, water content, porosity and water contact angle changes. Contact angle measurements showed that the addition of fMWCNTs and PAMAM greatly improved the hydrophilicity of the PVDF-HFP composite membranes when compared to the addition of Ag-MWCNTs and Ag/PAMAM-MWCNTs due to fewer pores created on the surface.

PAMAM-MWCNTs blended PVDF-HFP greatly showed an improved flux rate and salt rejection during filtration studies. The 1 wt.% MWCNTs-PVDF-HFP and 1 wt.% PAMAM-MWCNTs/PVDF-HFP composite membranes which exhibited high surface area have also shown high fouling resistance with 95% NaCl salt rejection. High Cd(II) ions rejections were achieved by 1 wt.% MWCNTs/PVDF-HFP and 1 wt.% PAMAM-MWCNTs/PVDF-HFP composite membranes (approximately 91 and 93% respectively).

E. coli filtration studies indicated that 2.5 wt.% Ag-MWCNTs/PVDF-HFP and 1.8 wt.% Ag-PAMAM-MWCNTs/PVDF-HFP composite membranes displayed good microbial load reduction (100%), and excellent bactericidal effects, since no growth was observed on the surface of membrane. These membranes which had improved surface areas and hydrophilicity (observed from contact angle measurements); further displayed good non-leaching properties, as evidenced by bacterial growth on the edges of the membranes.

The microbial, physicochemical and heavy metal analysis of water samples from Sekhukhune area showed that the water was contaminated with *Enterobacteriaeceae* (89 CFU/mL), *E. coli* (4 CFU/mL), total coliform (125 CFU/mL) with high turbidity (21 NTU) and total suspended solids (28 mg/L) when compared with SANS 241 water

guidelines. The microbial and physicochemical quality of these water samples such as turbidity, total suspended solids, greatly improved to acceptable SANS 241 limits while *Enterobacteriaeceae, E. coli* and total coliform were all reduced to 0 CFU/mL after filtration with 1.8 wt.% Ag-PAMAM-MWCNTs/PVDF-HFP composite membrane.

Adsorption kinetic studies indicated that the adsorption process followed the pseudo second-order kinetic model during both Cd(II) ions and Cr(VI) ions adsorptions. It was also found that pH has an important effect on the adsorption of these metals; Cd(II) adsorption were optimum at pH of 6.5 while Cr(VI) adsorption was optimum at pH of 2.5. The highest adsorption capacity by Langmuir isotherm for Cd(II) ions and Cr(VI) ions was 166.7 and 9.72 mg/g respectively at 25 ^{o}C obtained using 1 wt.% PAMAM-MWCNTs/PVDF-HFP composite membrane.

According the thermodynamics data, the negative values of ΔG^{o} indicated that the adsorption process was physisorption and spontaneous. The positive values of ΔH^{o} indicated that the reactions were endothermic in nature, while the positive value of ΔS^{o} indicated randomness at solid/liquid solutions interface during adsorption process of Cd(II) and Cr(VI) ions.

Reusability studies showed that PVDF-HFP composite membranes can be reused at least 4 times with an adsorption loss of only 5% for 1 wt.% PAMAM-MWCNTs/PVDF-HFP composite membrane confirmed by TGA and ICP-OES analysis. Selectivity studies showed that the 1 wt.% PAMAM-MWCNTs/PVDF-HFP composite membrane was more selective towards Cd(II). The order of selectivity in the binary ionic pairs is as follows: Ni(II) > Zn(II) > Cu(II).

It can be concluded that functionalised MWCNTs-PAMAM modified PVDF-HFP composite membranes improved the mechanical and chemical properties of the polymeric membrane. Results from this study demonstrated potential utility of modified PVDF-HFP composite membrane which could be developed into a viable technology for disinfection of contaminated water by both inorganic and microbial contaminants.

5.2 RECOMMENDATIONS

The synthesised PVDF-HFP composite membranes have shown great potential for water purification. Since not much work has been done using PVDF-HFP polymer as a membrane material for water treatment, it is recommended that:

- The use of fMWCNTs, Ag nanoparticles and PAMAM-MWCNTs as PVDF-HFP modifying materials is extensively studied.
- Different ways of functionalisation, synthesis and doping nanomaterials into the polymer still needs to be investigated to further improve leaching and fouling.
- Long term testing is needed to assess the membrane stability.
- More filtration studies should be carried out using other major membrane foulants.
- Further investigations are needed to be done on the application of these membranes in water treatment including sea water and wastewater.
- Other heavy metal adsorption, selectivity and reusability studies should also be further investigated.
- The effects of different solvents, different coagulation temperatures and different membrane additives during membrane synthesis to improve the hydrophilicity of the membrane should be carried out to better understand the mechanism.

5.3 APPENDICES

1. Swellability was calculated as follows:

$$Q_t(\%) = \frac{(m_w / M_r)}{m_c} \; x \; 100$$

where m_c is the initial mass of the membrane in g, m_w is mass of water absorbed and M_r is the molar mass of water.

2. Water content was calculated as follows:

$$\text{water content } (\%) = \frac{(W_0 - W_1)}{W_0} \; x \; 100$$

3. Porosity was calculated as follows:

$$P(\%) = \frac{(W_o - W_1)}{Ahd} \; x \; 100$$

where A is the membrane surface area and h is the membrane thickness and d is the density of water

4. Water flux (J):

$$J = \frac{V}{At}$$

5. Membrane salt rejection was calculated as follows:

$$Salt \;\; rejection = 1 - \frac{(Conductivity_{permeate})}{(Conductivity_{feed})} \; x \; 100$$

6. Total suspended solids was calculated as follows:

$$TSS = \frac{(A-B)}{(C)}\ x\ 1000$$

- where A is the final weight of membrane after filtration (g)
- B is the initial weight of membrane before filtration (g)
- C is the volume of water sample filtered (mL)

7. Total dissolved solids was calculated as follows:

Calculation of TDS

$$TDS = \frac{(A-B)}{(C)}\ x\ 1000$$

- where A is the final weight of the beaker after evaporation (g)
- B is the initial weight of the beaker before evaporation (g)
- C is the volume of water sample evaporated (mL)

8. The Scherrer equation can be written as: $t = k\lambda / \beta \cos\theta$

where t is the crystallite size, λ is the wavelength of the X-ray radiation (CuK_α = 0.15406 nm), k is a constant taken as 0.94, θ is the diffraction angle and β is the line width at half maximum height.